Contribution of the potassium / chloride cotransporter KCC2 to hippocampal rhythmopathy

Marie Goutierre

Sorbonne Université

Ecole doctorale n°158
- Cerveau Cognition Comportement -
Institut du Fer à Moulin
Equipe « Plasticité des réseaux corticaux et épilepsie »

Contribution of the potassium / chloride cotransporter KCC2 to hippocampal rhythmopathy.

Implication du transporteur potassium / chlore KCC2 dans la rythmopathie hippocampique.

Par Marie GOUTIERRE

Thèse de doctorat de Neurosciences

Dirigée par Dr Jean-Christophe PONCER

Présentée et soutenue publiquement le 28 juin 2018

Devant un jury composé de :

Pr Ann LOHOF	Présidente du jury
Pr Claudio RIVERA	Rapporteur
Pr Andrew TREVELYAN	Rapporteur
Dr Lisa ROUX	Examinateur
Dr Corentin LE MAGUERESSE	Examinateur
Dr Jean-Christophe PONCER	Directeur de thèse

ABSTRACT

In the CNS, synaptic release of the neurotransmitter GABA is responsible for fast inhibitory transmission. This is predominatly mediated by chloride flow through GABAA receptors. Hence, tight control of chloride homeostasis is critical for maintaing the efficacy of GABAergic transmission. In mature neurons, this is primarily achieved by the activity of the potassium-chloride cotransporter KCC2, which usually acts to extrude intracellular chloride and potassium ions. Expression of KCC2 however is compromised in numerous neurological disorders including epilepsy, Rett syndrome or neuropathic pain. Subsequent defects in GABA signaling through alteration of transmembrane chloride gradients are thought to underlie the pathological symptoms associated with these conditions. However, KCC2 is also highly expressed in dendritic spines where it plays a major role in controling the efficacy and gating the long-term plasticity of glutamatergic synapses. Remarkably, these functions are independent of chloride transport but instead involve KCC2 interaction with several protein partners. Hence, KCC2 can be classified as a moonlightning protein with multiple functions at excitatory and inhibitory synapses, thereby complicating predictions of the overall effect of its suppression on network activity. During my PhD, I characterized the effects of a chronic downregulation of KCC2 in the rat dentate gyrus at the cellular and synaptic levels as well as on the hippocampal network activity *in vivo*. Unexpectedly, lack of KCC2 did not impact steady-state GABAergic transmission. In contrast, my work shed light on a novel critical role of KCC2 in controling neuronal excitability through interaction with the leak-potassium channel Task-3 (KCNK9). This in turn alters hippocampal rhythmogenesis independently of GABA signaling. My results thus reveal a novel mechanism through which KCC2 influences neuronal activity separately of its ion transport function. They predict that pathological conditions associated with KCC2 downregulation may be at least partly explained by altered neuronal excitability and point to Task-3 as a new potential therapeutic target in these disorders.

RÉSUMÉ

Dans le système nerveux central, la transmission inhibitrice est principalement assurée par la libération synaptique du neurotransmetteur GABA. La fixation du GABA aux récepteurs GABAA induit en effet un flux entrant d'ions chlorure, résultant en une hyperpolarisation du neurone. Le maintien d'une faible concentration intraneuronale en chlore est donc essentielle à l'action inhibitrice du GABA. Dans les neurones matures, cette fonction est principalement réalisée par l'activité du cotransporteur potassium-chlore KCC2, qui à l'état basal exporte les ions chlorure et potassium vers le milieu extracellulaire. De nombreuses affections neurologiques, telles que l'épilepsie, le syndrome de Rett ou encore les douleurs neuropathiques, sont associées à une diminution de l'expression de KCC2. Un déficit de transmission GABAergique dû à une altération des gradients transmembranaires d'ions chlorure sont généralement invoqués pour rendre compte des symptômes associés à ces affections. Cependant, KCC2 est également fortement exprimé dans les épines dendritiques des neurones corticaux. Sa présence à proximité de la densité postsynaptique influence l'efficacité mais également la plasticité à long terme des synapses glutamatergiques. Ces fonctions inattendues de KCC2 au niveau des synapses excitatrices ne reposent pas sur sa fonction de transport ionique mais impliquent au contraire des interactions avec divers partenaires protéiques. Ainsi, le transporteur KCC2 possède de multiple fonctions et régule différemment les transmissions excitatrice et inhibitrice. Ceci complique la prédiction de l'effet net d'une suppression de KCC2 sur l'activité d'un réseau neuronal dans la pathologie. Durant ma thèse, j'ai caractérisé les effets d'une suppression chronique de KCC2 dans le gyrus dentelé chez le rat adulte au niveau cellulaire, synaptique et de l'activité du réseau hippocampique *in vivo*. De façon inattendue, j'ai montré que la suppression de KCC2 n'entraînait pas de modifications majeures de la transmission GABAergique. En revanche, j'ai mis en évidence un nouveau mécanisme indépendant du transport ionique par lequel KCC2 contrôle l'excitabilité neuronale et la rythmogénèse hippocampique à travers son interaction avec le canal potassique de fuite Task-3 (KNCK9). Mes résultats prédisent que les déficits associés à une suppression de KCC2 dans la pathologie pourraient être en partie expliqués par cet effet sur l'excitabilité neuronale. Ils suggèrent également que Task-3 pourrait constituer une nouvelle cible thérapeutique dans le traitement des affections impliquant la suppression de KCC2.

ACKNOWLEDGMENTS

First of all, I would like to warmly thank all the members of my jury who agreed to review and evaluate my work : Andrew Trevelyan, Claudio Rivera, Lisa Roux, Ann Lohof and Corentin Le Magueresse. I'm looking forward to discussing it with you on the 28th of June.
I also want to thank Clément Léna, Jean-Antoine Girault and Etienne Audinat, who were part of my thesis committee and helped us shape this project through the years.

Mes plus profonds et plus sincères remerciements sont évidemment pour toi, Jean-Christophe.
Tu me pardonneras, je l'espère, mon caractère têtu, ma susceptibilité face aux remarques, mon côté "dernière minute" qui t'a causé bien des stress et une certaine tendance à faire passer les projets des autres avant les miens… En même temps, tu savais déjà à quoi t'en tenir lorsque tu m'as proposé de faire une thèse avec toi !
Ça fait, en effet, maintenant plus que 8 ans qu'on se connaît, 8 années pendant lesquelles tu m'as fait grandir à la fois scientifiquement et humainement.
Merci pour ta disponibilité, ta patience, ta confiance en moi. Ma thèse ne serait pas ce qu'elle est si tu ne m'avais poussé et encouragé comme tu l'as fait ! Au travers de nos (nombreuses) conversations scientifiques, tu m'as appris la rigueur du raisonnement et m'as montré comment on pense et construit un projet de recherche. Au-delà de la science, merci pour ton attention à l'humain et au bien-être de chacun. Combien de fois ne m'as-tu pas dit "fais attention à toi" lorsque tu notais une certaine fatigue ou "est-ce que tout va bien, que puis-je faire pour toi ?" dans des périodes un peu difficiles ! Un merci tout spécial pour ton soutien au cours de ces derniers mois si intenses.
Enfin, merci pour toutes ces discussions extra-scientifiques que nous avons pu avoir ensemble : elles ont été source d'enrichissement pour moi, et j'espère que la réciproque est un peu vraie !

Un petit mot également pour la responsable de la partie Nord de l'équipe. Sabine, merci pour ton enthousiasme scientifique et pour ton attention personnelle à chacun de nous. Scientifiquement, nos intérêts sont pour le moins éloignés mais cela ne nous a jamais empêchés d'échanger sur nos projets et je crois que c'est cette diversité qui fait la richesse de l'équipe.

Quatre années de thèse, c'est du temps partagé avec de nombreux collègues : pauses déjeuners / thé / bière, discussions autours de nos projets (scientifiques et personnels), autant de moments essentiels dans le quotidien.
Un merci particulier pour Quentin : finalement, c'est de ton observation qu'est né tout mon projet donc je te suis sacrément redevable ! Merci aussi à mes premiers voisins de bureau :

Martin (le calme et la sérénité incarné), Emmanuel (pour ton accueil et tes partages de chocolat noir) et Eric (l'expert en électrophysiologie).
Merci Ferran et Jessica (la team adénosine) pour votre gentillesse et votre simplicité, et aussi pour avoir su faire découvrir à l'équipe que, non, il n'y a pas que KCC2 dans la vie ! Marion, ma complice des pauses thé, merci pour tous ces temps de partage ensemble. Sana, merci pour ton rire magistral qui a le don de détendre l'atmosphère. Merci aussi pour toutes les conversations scientifiques que nous avons pu avoir et, en particulier, pour m'avoir fait découvrir les subtilités de la biochimie. Clémence, désolée de ne pas avoir été beaucoup plus disponible ces derniers mois pour te guider sur la partie KCC2 / rythmogénèse... Courage pour la fin de thèse, je suis sûre que tu vas gérer, comme d'habitude !
Merci à Yo et Marianne pour leur présence discrète mais toujours bienveillante. Merci Xavier et Floriane pour la bonne humeur que vous avez apportée à l'équipe depuis votre arrivée. A Etienne et Florian qui commencent / vont commencer une thèse (oui, parce que je suis sûre que tu l'auras ta bourse, Florian !), courage pour tout. J'ai une pleine confiance en vous pour mener vos projets avec brio, et pour entretenir l'esprit de l'équipe ! A last word for Manisha, welcome to the team again. I'm happy to leave you all of my Matlab scripts, I know they're in good hands !

Je ne peux pas oublier non plus ceux qui ne font pas directement partie de l'équipe mais qui ont contribué à rendre ma vie à l'IFM plus facile au quotidien. Je pense en particulier à l'ensemble du pôle laverie (Géraldine, Dominique et Emeline) et administratif (Christine, Jocelyne, Isabelle et Marianne) ainsi qu'à François et Gaël pour leur gestion de l'animalerie en ce moment. Merci également à tous les animaliers du 105, et spécialement Olivier, pour leur disponibilité durant le temps où j'ai travaillé là-bas.

Back to english to thank all the people in the institute who contributed to make these nearly 5 years fly so quickly. First of all, to our long-time neighbors of the first floor, the Mameli team. Manuel, Frank, Anna, Salvatore, Kristina and Massimo : it was amazing knowing you. Your passion and dedication to science really inspired me to give my best in my work and I won't forget either some of our drinking nights !
More generally, the IFM is a quite special institute in the world of research, filled with people willing to help each other and share more than just work. I cannot cite every member of the IFM but I really want to thank all of you for creating such atmosphere. A special thought to the regular members of the IFM Birretas group !

I was lucky during my PhD to spend some time in the lab of Liset Menendez de La Prida in the Cajal Institute. Thank you Liset, for your warm welcome, your support during my time there and your feedbacks on the *in vivo* part of my project ! Everybody in the lab made me feel like I belonged to the team but special thanks go to Dani (for teaching me EEG recording but mostly for our long tea-sessions while talking about everything and nothing), Manuel (for sharing such a passion for science, best of luck for your future in the Buzsaki lab !) and François (for taking care of introducing me to Madrid's nightlife during my first stay there).

Pendant ma thèse, j'ai aussi eu l'opportunité d'effectuer une mission à la Cité des Sciences : quelques jours par an pour déconnecter de la vie de laboratoire et apprendre à parler

sciences autrement. L'occasion surtout de faire de belles rencontres tant avec les médiateurs (Marlène, Valérie, Graziela, Isabelle, Nadège, Gilles…) qu'avec les autres doctorants (Elodie, Sandra, Batiste et tous les autres...). Au passage, vive la semaine du cerveau et vive le microbiote ;) !!

Je ne peux pas continuer mes remerciements sans un petit mot pour mon laboratoire de M2 et l'ensemble de l'équipe de Michaël Zugaro. Michaël, certes je ne suis pas restée en thèse chez toi (mais on ne va pas revenir encore une fois là-dessus, non ?), mais tu as su me donner le goût pour l'*in vivo* (et le code Matlab) au point que j'aie eu l'envie d'en rajouter dans mon projet de thèse ! De ces quelques mois au Collège de France, j'ai aussi gardé de belles amitiés. Nicolas, Céline, Virginie, Raly et Marco : merci pour tous ces moments partagés ! La bande ne va pas tarder à se disperser dans le monde (au grand regret des gérants du Village), mais je suis sûre que les liens resteront.

Que ce soit dans mes études, dans mon expérience de scoutisme, pendant mes années en Chine ou durant ma thèse, j'ai eu la chance de rencontrer de nombreuses personnes extraordinaires qui ont contribuées à me faire évoluer et à me donner envie de toujours donner le meilleur de moi-même. Certaines d'entre elles sont devenues de vrais amis et je ne serai pas qui je suis aujourd'hui sans eux. Alors merci Gaëlle, Cécile, Malo, Quentin, Kristell, Bénédicte, Aurélie, Viviane, Pauline, Léa, Mérie… et tous ceux que j'oublie certainement de citer ! Un mot tout spécial pour Quentin : merci d'avoir toujours su si bien me comprendre. Les relations seront forcément un peu différentes à partir de l'an prochain mais elles ne seront pas moins fortes pour autant !

Mon envie de faire de la recherche en biologie est très certainement venue en partie de l'exemple de mon parrain et ma marraine. Merci à eux de m'avoir transmis leur passion.
Un immense merci à toute ma famille pour son soutien au cours de ces années de thèse. Maman, je sais l'effort que c'était pour toi de prétendre t'intéresser à la biologie parce que c'est ce que je faisais. Merci pour ça ! Mais surtout merci pour la confiance que toi et papa me faites depuis des années et qui me porte. A mes frères et sœurs, merci pour votre présence et vos encouragements (même si c'était parfois surtout des encouragements à diminuer un peu le rythme !). On n'aime pas trop dire les choses directement dans la famille, mais j'espère que vous savez tous ce que je pense de vous !
Enfin, un grand merci à mes grands-parents, qui sont et ont toujours été des exemples pour moi dans la vie.

Je voudrais enfin terminer avec une pensée pour ceux qui m'ont accompagnée dans la préparation du futur lors de cette fin de thèse. Venceslas, merci pour ton écoute et tes conseils depuis tant d'années, et encore plus particulièrement sur ces derniers mois. A la communauté de Tibériade enfin, merci de m'avoir accueillie comme vous l'avez fait il y a un peu plus d'un an. Merci aussi d'avoir su délicatement vous mettre en retrait lorsqu'il a été nécessaire pour moi de d'abord me consacrer à ma fin de thèse. On se retrouve en octobre pour le début d'une nouvelle aventure !

TABLE OF CONTENTS

TABLE OF FIGURES

LIST OF ABBREVIATIONS

4-AP	4 Amino-pyridine
ACSF	Artificial Cerebro Spinal Fluid
AMPA	α-Amino-3-hydroxy-5-methyl-4-isoxazolepropionic acide
APP	Amyloid Precursor Protein
BDNF	Brain-derived neurotrophic factor
CA	Cornu Ammonis
CCC	Chloride co-transporter
CCK	Cholecystokinin
CIP1	CCC-interacting protein 1
CKB	Brain-type creatine kinase
ClC	Chloride channel
CNS	Central Nervous System
COPI	Coatomer protein I
CREB	C-AMP Response Element-binding protein
CSD	Current Source Density
CTD	C-terminal Domain
DF_{GABA}	Driving Force of GABAergic currents
DG	Dentate Gyrus
DMSO	Dimethyl sulfoxyde
DS	Dentate Spike
E/I	Excitatory / Inhibitory
EC	Entorhinal Cortex
EcoG	Electrocorticogram
EEG	Electroencephalogram
E_{GABA}	Reversal potential of GABAergic currents
Egr	Early growth response transcription factor
EPSC	Excitatory postsynaptic current
Erk	Extracellular signal-regulated kinase
FERM	Four.one, Ezrin,Radixin, Moesin
FRS	FGF receptor substrate
GABA	γ-Amino Butyric Acid
GABAAR	Receptor subtype A for GABA
$GABA_B$	Receptor subtype B for GABA
GC	Granule cell
GDP	Giant Depolarization potential
GFP	Green Fluorescent Protein
GluK2	Glutamate ionotropic receptor kainate type subunit 2
HEK	Human Embryonic Kidney
HPC	Hippocampus
ING	Interneuron Network of Gamma
IPSC	Inhibitory postsynaptic current

K2P	Two-pore potassium channel
KCC	K^+/Cl^- co-transporter
KO	Knockout
LFP	Local Field Potential
LIMK	Lin-11, Isl-1 and Mec-3 Kinase
mAchR	Metabotropic acetylcholine receptor
MI	Modulatory index
MQAE	(6-Methoxyquinolinio)acetic acid ethyl ester bromide
mRNA	Messenger Ribonucleic Acid
MS-DBB	Medial septum – Diagonal band of Broca
Neto2	Neuropilin and tolooid like-2 protein
NKCC	$Na^+/K^+/Cl^-$ co-transporter
NMDA	N-methyl-D-aspartate
NRSE	Neurn-restrictive silencing element
NTD	N-etylmaleimide-sensitive factor
OSR	Oxidative stress-responsive kinase
P	Postnatal day
PAK	p21-activated kinase
PING	Pyramidal Interneuron Network of Gamma
PKC	Protein kinase C
PLCγ	Phospholipase C gamma
PP1	Protein phosphatase 1
PTZ	Pentylenetetrazole
PV	Parvalbumin
Rac	Ras-related C3 botulinum toxin substrate
REM	Rapid-Eye Movement
SCI	Spinal Cord Injury
SE	Status Epilepticus
Shc	SRC homology 2 domain containing transforming protein
shRNA	Short hairpin Ribonucleic Acid
Slc	Solute carrier
SOM	Somatostatin
SPAK	Ste20p-related proline/alanine-rich kinase
SPW-R	Sharp-Wave Ripple
Src	Proto-oncogene tyrosine-protein kinase
TASK	Twik-related Acid-sensitive potassium channel
TBI	Traumatic Brain Injury
TLE	Temporal Lobe Epilepsy
TM	TransMembrane domain
TREK	Twik-related potassium channel
TrkB	Tropomyosin receptor kinase B
TTX	Tetrodotoxin
VGCC	Voltage-Gated Calcium Channels
VIP	Vasoactive intestinal polypeptide
WNK	With No Lysine kinase
βPix	Beta-PAK interacting exchange factor

INTRODUCTION

INTRODUCTION

GENERAL INTRODUCTION

In the central nervous system (CNS), information processing relies on synaptic connections, which enable information transfer between neurons. Following emission of an action potential by the presynaptic neuron, a neurotransmitter is released in the synaptic cleft. Depending on the identity of the neurotransmitter released, the activity of the postsynaptic neurons is either promoted or inhibited. In the mature CNS, excitatory transmission relies mainly on glutamate release while γ-Amino Butyric Acid (GABA) mostly inhibits the postsynaptic neurons.

Both synaptic inhibition and excitation are mediated by charge movements across the plasma membrane. Fast excitatory transmission resulting from glutamate receptor activation is mediated by a net influx of cations (Na^+, Ca^{2+}) through the membrane and subsequent depolarizing excitatory postsynaptic currents (EPSCs). On the other hand, ionotropic receptors subtype A for GABA (GABAAR) possess a mix permeability to chloride and bicarbonate ions with a relative permeability ratio of 4/1 (Kaila and Voipio, 1987). Hence, their activation classically mediates a net hyperpolarizing influx of chloride ions (inhibitory postsynaptic current, IPSC) (Fig 1b and c).

The directionality of ion fluxes through the receptors depends directly on the relationship between their reversal potential (determined by their electrochemical ionic gradient across the membrane of the neuron) and the resting membrane potential (V_m) of the cell. In neurons, the reversal potential of GABA (E_{GABA}) is close to V_m and small changes in chloride concentration may be sufficient to reverse the direction of chloride flow through the receptor. Hence, control of chloride homeostasis is crucial for neurons to maintain hyperpolarizing GABA transmission. This is mainly achieved through the combined action of two secondary active transporters, the Na/K/Cl cotransporter NKCC1 and the K/Cl cotransporter KCC2 which, under basal conditions,

use the Na^+ and K^+ electrochemical gradients generated by the Na/K ATPase to respectively load and extrude chloride ions from the cell (Fig. 1).

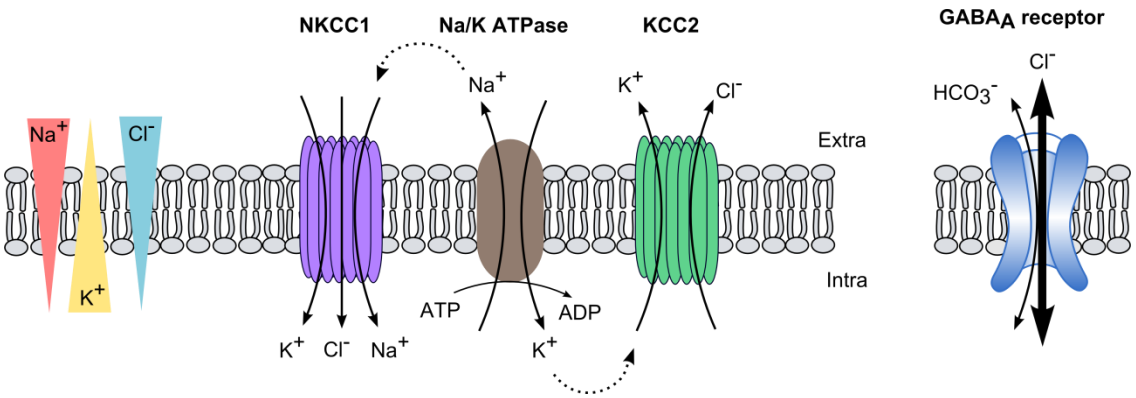

Figure 1 : CCC activity determines chloride flux through GABAARs
KCC2 extrudes chloride out of the cell using the electrochemical potassium gradient generated by the Na^+/K^+ ATPase. NKCC1, in contrast, transports chloride into neurons using the electrochemical gradient of sodium. Transmembrane chloride gradients and subsequently, the direction of chloride flux through GABAARs depend on the relative activity of the two transporters. In mature neurons, KCC2 activity dominates over NKCC1 leading to a high transmembrane gradient. Hence, GABAARs activation triggers hyperpolarizing influx of chloride ions.

Importantly, emission of action potentials by the postsynaptic neuron does not uniquely depend on the summation of both EPSCs and IPSCs but also on intrinsic properties of the cell such as its membrane potential, its membrane resistance (R_{in}) or its action potential threshold. Hence, modifications of both sodium (Ren, 2011) and potassium leak channels influence neuronal excitability by altering both V_m and R_{in} while voltage-gated sodium channels expression regulate action potential threshold (Fig 2).

At the network level, neurons tend to fire in a synchronous manner giving rise to oscillations that can be observed in electroencephalogram (EEG). Such neural oscillations, which require a tight control of both excitatory and inhibitory transmission as well as excitability, organize the information into coordinated patterns of activity. Various neural oscillations have been demonstrated as critical for cognitive processes such as perception, memory formation and consolidation but also consciousness. Hence, neural oscillations are believed to represent the intermediate link between cellular activity and behavior.

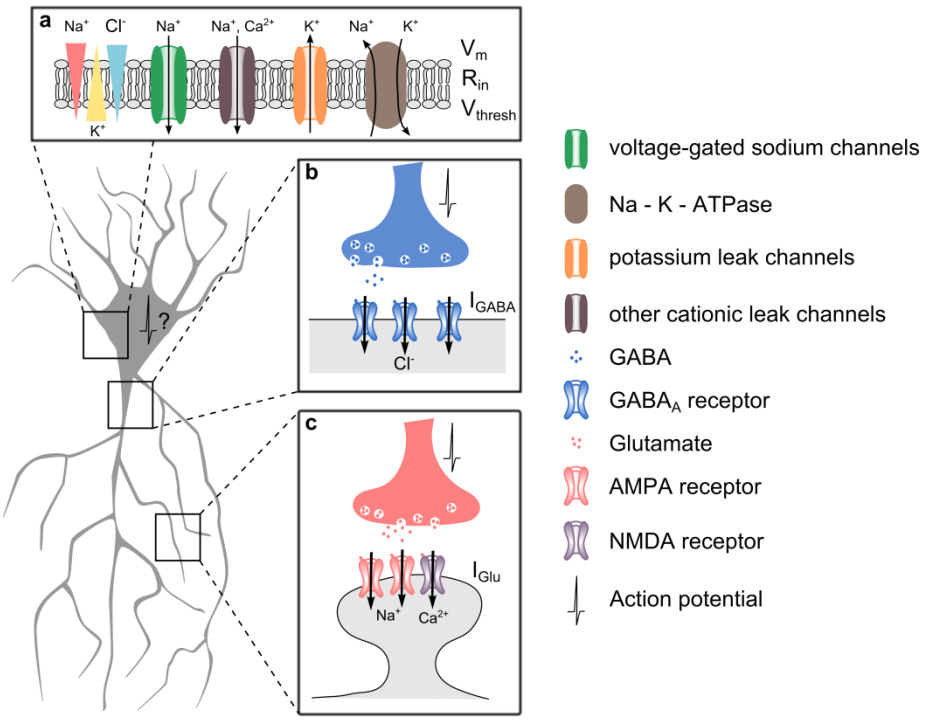

Figure 2 : Control of action potential emission
In the CNS, neurons need to constantly integrate stimuli from excitatory and inhibitory synapses. Synaptic GABA release classically triggers hyperpolarizing current (I_{GABA}) mediated by the influx of chloride through GABAARs (b). In contrast, glutamate mediates depolarizing currents (I_{Glu}) through AMPA and NMDA receptors (c). The emission of an action potential depends on postsynaptic integration of these synaptic inputs together with intrinsic properties of its membrane such as the membrane resting potential (V_m), the input resistance (R_{in}) and the action potential threshold (V_{thresh}) (a). In a simplistic reduction, the membrane of the neuron can be assimilated to a RC circuit. Hence, according to Ohm's law, an action potential will be triggered if $V_m - V_{thresh} = R_{in} * (I_{GABA} + I_{Glu})$

Altered activity of the K/Cl cotransporter KCC2 has been reported in numerous pathologies including epilepsy and neuropathic pain. Due to the close relationship between KCC2 activity and the polarity of GABAergic transmission, studies of KCC2 in the pathology have often focused on this aspect. However, KCC2 suppression was recently demonstrated to also alter glutamatergic transmission and plasticity through transport-independent mechanisms. Thus, the overall network effect of the loss of KCC2 is not so easy to predict.

During my PhD, I characterized the impact of KCC2 suppression on the hippocampal network. In particular, I focused on how the integration of the diverse cellular and synaptic modifications triggered by this suppression influences hippocampal physiological oscillations and I questioned their ability to favor the emergence of pathological activities. Before presenting these results in the form of a research article at the core of this thesis, I will introduce the function and regulation of KCC2 as well as the cellular and synaptic basis for hippocampal oscillations in health and disease.

I- KCC2, A PROTEIN WITH MULTIPLE FUNCTIONS AT BOTH EXCITATORY AND INHIBITORY SYNAPSES

1. Expression of KCC2 in the CNS

a. The CCC family

KCC2 is one of the nine members of the cation-chloride cotransporter (CCC) family, encoded by the genes slc12a1-9. Seven of them have been categorized as plasma membrane transporters (Gamba et al., 1993; Gillen et al., 1996; Hartmann and Nothwang, 2014; Hiki et al., 1999; Mercado et al., 2004; Payne et al., 1996). CCCs are widely expressed in all organs. They have been at first largely studied for their role in the control of cell volume upon osmotic challenges in epithelium and kidney in particular (Hoffmann and Dunham, 1995). In the CNS, special attention has been given to CCC function due to their key role in regulation of intraneuronal chloride homeostasis and, consequently, of the polarity of GABAergic transmission (Kaila, 1994; Payne et al., 2003). All CCCs cotransport Na^+ and/or K^+ ions coupled to chloride and are characterized by a transport stoichiometry of 1 cation for 1 chloride ion transported. Consequently, transport of chloride through the plasma membrane is accomplished without any net movement of charges across the membrane, which complicates the electrophysiological study of their activity, as we will discuss later (see I.2.a). Finally, all CCCs are secondary active transporters meaning they use the gradients of Na^+ and K^+ generated by the Na-K-ATPase to transport chloride.

The family of CCCs has been divided in two main branches (see Gagnon and Delpire, 2013 for review). The first branch corresponds to transporters using Na^+ gradient to import chloride into the cell. Specifically, this branch comprises two Na^+-dependent K^+/Cl^- cotransporters (NKCC1 and NKCC2) and one Na^+-dependent Cl^- cotransporter (NCC) which share about 55% conservation in amino acid sequence. The second branch comprises four K^+-dependent Cl^- cotransporter (KCC1, KCC2, KCC3 and KCC4). These transporters use the potassium gradient created by the Na-K-ATPase pump to extrude chloride from the cell and share more than 70% of homology in their sequence. The two remaining members of the CCC family, CIP1 and CC9 are less well characterized. They display relatively low identity with other CCCs (20-25%) and evidence for a chloride transport function is still lacking (Fig. 3A). CIP1 has been suggested to form heterodimers with other CCCs, thereby influencing their transport activity (Caron et al., 2000)

while CCC9 has been shown to influence polyamine transport in HEK-293 cells (Daigle et al., 2009). Based on these observations, whether CIP1 and CCC9 belong to the CCC family has been debated (Hartmann and Nothwang, 2014). From an evolutionary perspective, comparing gene sequences of putative CCC from Archeae and Eukaryota taxons suggests the existence of a single ancestral CCC gene in Archea (Hartmann et al., 2014). The diversity in the CCC family among and between species then emerged from consecutive duplication events.

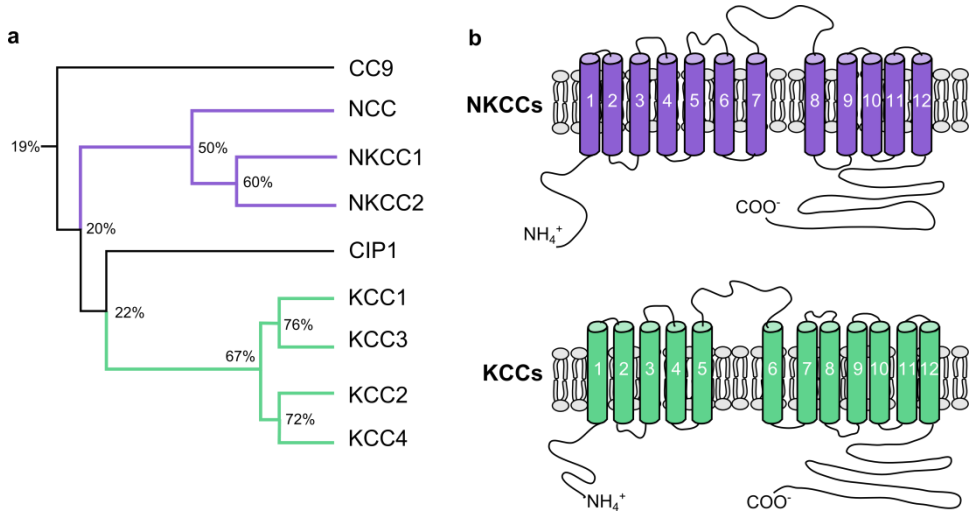

Figure 3 : Phylogeny and structure of the CCC family
(a) Phylogenic tree of the characterized CCC family members. Percent of sequence homology are indicated at each branching. (b) Proposed secondary structure for NKCCs (top) and KCCs (bottom) mainly differ in the position of the long extracellular loop. Adapted from (Gamba 2005)

CCCs are transmembrane proteins with an apparent molecular weight of 120-200 kDa. Even though no crystallographic structure of the CCC has been obtained to date, predictions of the molecular structure with hydrophobicity profiles were made and suggest the presence of 12 transmembrane domains (TM), and an intracellular localization of both N-terminal and C-terminal domains (Gamba 2005; Gerelsaikhan and Turner 2000; Payne et al., 1996). A notable difference between NKCC/NCCs and KCCs is the location of the large extracellular loop which is situated between TM7 and TM8 in NKCC/NCCs and between TM5 and TM6 in KCCs (Gamba 2005, Fig 3B). This extracellular loop contains several glycosylation sites (Hoover et al., 2003) which seem important for correct targeting at the membrane (Weng et al., 2013). A more detailed model of KCC2 structure has been recently proposed (Stödberg et al., 2015) based on its homology with the bacterial amino acid, polyamine, and organocation transporter (ApcT) (Shaffer et al., 2009). This model suggests a key role for the interaction of TM1 and TM6 for the transport function and proposes the putative substrate binding residues to be located in TM8.

b. NKCC1 and KCC2 are the main active CCC in the CNS

CCC show differential tissue expression patterns. While NKCC2 and NCC are mostly expressed in the kidney where they regulate salt reabsorption (Kahle et al., 2010; Russell 2000), NKCC1 is ubiquitously expressed (Plotkin et al., 1997). Hence, NKCC1 is the only chloride importer of the CCC family expressed in the CNS.

In contrast, all KCCs are expressed in the CNS, although at various levels. KCC1 and KCC4 exhibit low expression levels in the brain and, consequently, there is no obvious neurological phenotype in mice lacking one of these transporters (Boettger et al., 2002; Rust et al., 2007). Although KCC3 is expressed in the adult brain, its physiological relevance remains largely unknown but has been suggested to mainly contribute to volume homeostasis (Kahle et al., 2015).
Until its recent identification in some pancreatic cells (Kursan et al., 2017), KCC2 was believed to be uniquely expressed in the CNS. In contrast to other KCCs, KCC2 is constitutively active under isotonic conditions (Payne 1997). This feature is conferred by a short amino-acid sequence (1022-1037) called the ISO-domain, which lays in its carboxy-terminal domain (CTD) (Acton et al., 2012; Mercado et al., 2006). Interestingly the ISO-domain-lacking KCC2 transporter could still be activated under hypotonic conditions, indicating that two distinct domains are involved in the activation of KCC2 under isotonic *vs.* hypotonic conditions.

It should be mentioned that chloride anion exchangers, Na^+-dependent anion exchangers as well as calcium-gated and voltage-gated chloride channels also participate, to some extent, to neuronal chloride homeostasis. For instance, the voltage-gated channel ClC-2 contributes to background chloride conductance and influences GABAAR function (Staley et al., 1996). However, ClC-2 seems to be mostly active following transient chloride loading of the cell rather than in basal conditions (Rinke et al., 2010). Accordingly, ClC-2 knock-out mice do not present deficits of chloride homeostasis (Bösl et al., 2001). Hence, in the rest of this thesis, we will primarily focus on the role of KCC2 in the CNS.

c. Isoforms of KCC2

KCC2 is encoded by the *Slc12a5* gene. Two isoforms, KCC2a and KCC2b, were initially identified in the CNS, resulting from two alternative promoters (Uvarov et al., 2007). These isoforms only differ in their amino-terminal domain (NTD) which is 40 amino acids longer in KCC2a than in KCC2b and contains an additional putative Ste20p-related proline/Alanine-rich kinase (SPAK) /

oxidative stress-responsive kinase-1 (OSR1) phosphorylation site for KCC2a (de Los Heros et al., 2014). Both variants show similar ion transport properties when expressed in HEK cells (Uvarov et al., 2007) but KCC2a exhibits an increased sensibility to SPAK-dependent regulation due to this additional phosphorylation site (Markkanen et al., 2017). Furthermore, the two isoforms have different subcellular localization (Markkanen et al., 2014), suggesting a contribution of the NTD to the subcellular targeting of the transporter.

Originally, based on a study on its homologous protein KCC1 (Casula et al., 2001), the NTD of KCC2 had been proposed to be essential for the transport function of chloride (Li et al., 2007). Consequently, several groups have used a truncated form of KCC2, KCC2-ΔNTD, as a transport-deficient model in order to study ion-transport independent role of KCC2 (Fiumelli et al., 2013; Horn et al., 2010; Li et al., 2007). However, recent data from the group of Igor Medina in Marseilles revealed that the NTD domain of KCC2 is critical for the membrane insertion of the protein (Friedel et al., 2017). This study suggests KCC2-NTD influences primarily KCC2 trafficking, which is consistent with the difference in subcellular targeting of KCC2a *vs.* KCC2b.

A third isoform of KCC2 lacking the exon 25, KCC2a-S25, has recently been identified in pancreatic cells (Kursan et al., 2017) but is not expressed in the CNS. This isoform is characterized by the lack of 5 residues immediately after the ISO-domain and its functional properties remain to be determined.

d. Cellular and sub-cellular expression of KCC2 in the CNS

In the CNS, KCC2 expression is entirely neuron-specific due to the presence of neuron-restrictive silencing elements (NRSE), early growth response transcription factor 4 (Egr4) and upstream stimulating factors (USF1 and 2) binding sites in its promoter sequence (Uvarov et al., 2006; Markkanen et al., 2008; Yeo et al., 2009). Expression of KCC2 has been observed throughout the CNS (Fig. 4A,B) including spinal cord (Hübner et al., 2001) cerebellum (Williams et al., 1999), thalamus (Barthó et al., 2004), auditory brainstem (Blaesse et al., 2006) and cortical structures (Gulyás et al., 2001; Rivera et al., 1999). Although KCC2 seems ubiquitously expressed in the brain, differential values of E_{GABA} have been reported depending on brain structures and neuronal type. This could reflect differential levels of KCC2 expression. For instance, neurons of the reticular thalamic nucleus display low levels of KCC2 compared to adjacent brain structures

(Klein et al., 2018). However, changes in E_{GABA} may also reflect changes in the expression of NKCC1 as well as in the activity of other chloride channels or metabolism of bicarbonate.

At the subcellular level, KCC2 has been shown to be organized in clusters at the plasma membrane. In 2001, Gulyas and colleagues made the first surprising observation, using immunogold staining and electron microscopy, that KCC2 was highly enriched at the vicinity of excitatory synapses, within dendritic spines (Gulyás et al., 2001, Fig 4C). Data from our group later confirmed that not only is KCC2 enriched in dendritic spines, in close proximity to glutamatergic synapses, but also it seems to be excluded from the postsynaptic density (Chamma et al., 2012; Gauvain et al., 2011). Additionally, and perhaps more expectedly, KCC2 is also enriched near GABAergic synapses (Chamma et al., 2013). Interestingly, KCC2 is completely excluded from the axon, thereby leading to a higher intracellular concentration of chloride in axons compared to the somatodendritic compartment (Price and Trussell 2006, Fig 4D).

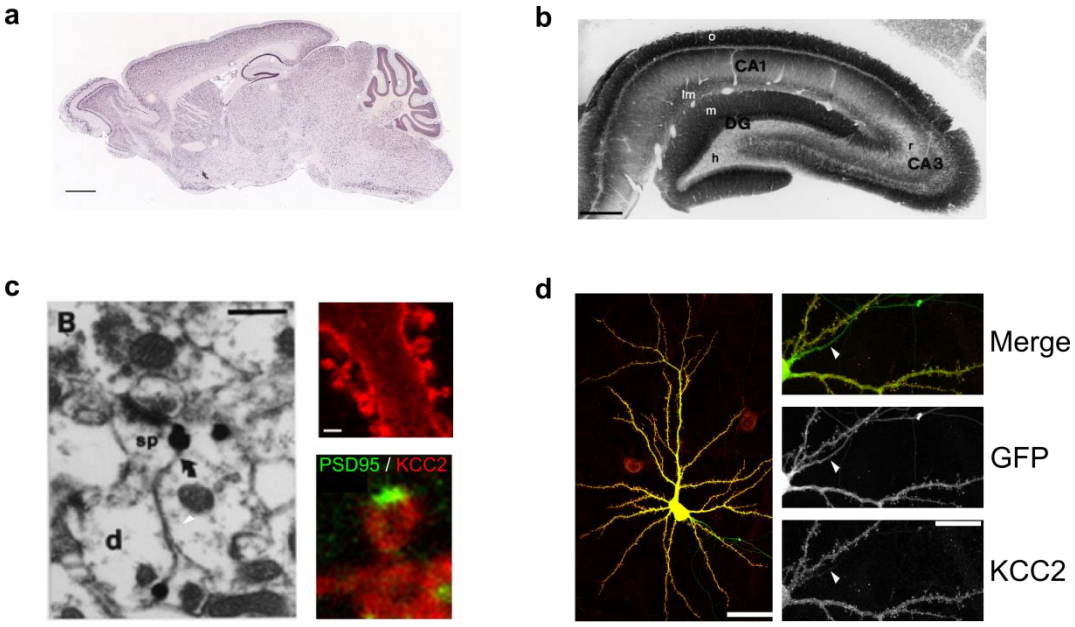

Figure 4 : Cellular and subcellular localization of KCC2
(a) *In situ* hybridization of KCC2 mRNA (Allen Brain Atlas, scale 1mm) indicate KCC2 is expressed in the whole brain
(b) Immunohistochemistry revealing KCC2 expression in the hippocampus (Gulyas et al. 2001, scale 0.6mm)
(c) KCC2 is expressed in dendritic spines. Left, electron microscopy revealed KCC2 presence in dendritic spines (Gulyas et al. 2001, scale 0.6µm). Right, immunocytochemistry showed KCC2 forms clusters in dendritic spines (top) and is excluded from the postsynaptic density as detected by PSD95 staining (bottom) (Gauvain et al. 2011, scale 2µm)
(d) KCC2 is excluded from the axons (white arrows) as revealed by immunocytochemistry on cultured hippocampal neurons. Scale 40µm for left image and 10µm for insets (Chamma et al. 2013)

As previously mentioned, the subcellular localization of the two isoforms of KCC2 has been recently described. It revealed only partial colocalization of KCC2a and KCC2b in mature neurons

(Markkanen et al., 2014). In general, KCC2b is more concentrated than KCC2a at the somatic membrane and the two isoforms are expressed in distinct dendritic compartments. Although the functional relevance of this observation is still unclear, such differences may indicate different roles for the two isoforms in the mature brain.

2. Transport function of KCC2

a. Control of the chloride homeostasis : setting the intraneuronal $[Cl^-]_i$

- **Thermodynamic considerations about KCC2 activity**

Historically, the first observation that intraneuronal concentration of chloride was lower than expected if due to passive distribution only was made in 1988 (Thompson et al. 1988) but the identification of the neuronal chloride extruder KCC2 occurred several years later (Payne et al. 1996).

In neurons, KCC2 operates close to its thermodynamic equilibrium (Payne 1997). Indeed, such equilibrium is obtained when reversal potential for chloride and potassium ions are equal. The reversal potential of an ion is calculated according to the Nernst equation:

$$E_{ion} = RT/zF * \ln([ion]_i / [ion]_o)$$

where R represent the ideal gas constant, T the temperature in Kelvin, F the Faraday constant and z the valence of the studied ion.

Hence, the equation $E_{Cl} = E_K$ is equivalent, after simplification, to $[Cl^-]_o * [K^+]_o = [Cl^-]_i * [K^+]_i$

Both extracellular chloride concentration and intracellular potassium can be considered as fixed and close to 140 mM. Such approximations indicate that if $[Cl^-]_i$ is higher than $[K^+]_o$, KCC2 extrudes both chloride and potassium. Conversely, KCC2 contributes to the influx of both ions when $[K^+]_o$ exceeds $[Cl^-]_i$. Physiological $[Cl^-]_i$ has been estimated to vary between 7 and 13 mM in a computational model (Doyon et al., 2011) while physiological $[K^+]_o$ ranges between 2 and 4 mM. However, intense neuronal activation induces a rise in $[K^+]_o$ which can reach values up to 8 mM (Branston et al. 1982) hence inducing a reversal in the directionality of KCC2-mediated transport (Fig 5A).

Thus, KCC2 is in an interesting position to reduce network excitability by two different means. Indeed, its activity is necessary to cope with the constant chloride load in the neurons due to GABAAR activation enabling the maintenance of a hyperpolarizing inhibitory GABAergic transmission. However, reverse transport through KCC2 also allows to buffer extracellular potassium in case of a transient rise, thereby reducing neuronal excitability (Fig 5B).

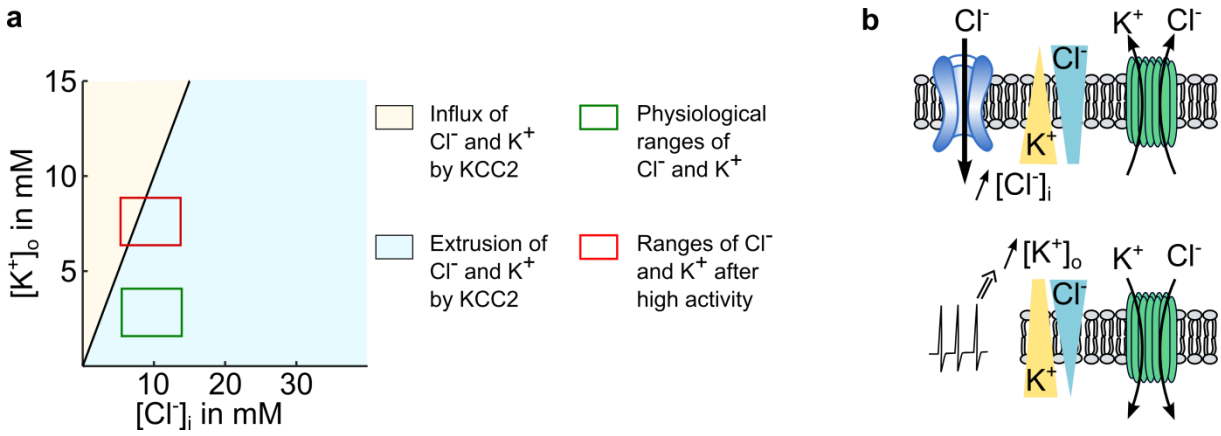

Figure 5 : KCC2 functions close to its thermodynamic equilibrium
(a) KCC2 thermodynamic equilibrium is achieved when $[Cl^-]_o * [K^+]_o = [Cl^-]_i * [K^+]_i$. Both $[Cl^-]_o$ and $[K^+]_I$ can be considered constant and close to 140 mM. Hence, KCC2 reaches its equilibrium when $[K^+]_o = [Cl^-]_i$ (as represented by the black line). Under physiological conditions, the intracellular chloride concentration is higher than the extracellular potassium concentration (green box). Hence, KCC2 classically extrudes chloride and potassium. However, following intense activity, extracellular potassium concentration increases (red box) and KCC2 might reverse if $[K^+]_o > [Cl^-]_i$.
(b) KCC2 can buffer both intraneuronal chloride following GABAARs activation (top) and extracellular potassium following intense activity (bottom).

- **Brief overview of methods for estimating KCC2 activity**

Since KCC2 activity is electroneutral, it is impossible to directly measure its activity by classical electrophysiological methods. A typical approach is then to use a radioactive potassium substitute such as $^{40}K^+$ or more frequently $^{86}Rb^+$ to evaluate KCC2 transport activity (Gamba 2005; Mount et al. 1998; Payne 1997). In addition to the obvious limitations of using radioactive elements, these techniques only estimate average KCC2 function at the population level and do not permit testing individual cells or subcellular compartments.

In contrast, electrophysiological techniques allow assessing KCC2 function for individual cells by using GABAergic currents as a proxy. Thus, in whole-cell patch clamp experiments, the extrusion capacity of KCC2 may be determined by measuring the recovery rate of GABAergic currents following intense chloride loading in neurons (Staley and Proctor 1999; Pellegrino et al. 2011). Alternatively, KCC2 activity may be derived from the somato-dendritic gradient of E_{GABA}

measured while imposing a fixed concentration of chloride through the patch pipette (Gauvain et al., 2011; Kelsch et al., 2001; Khirug et al., 2005). On the other hand, KCC2 activity can also be inferred from measures of steady-state chloride concentration. Since GABAARs are mostly permeable to chloride, measures of E_{GABA} provide a good estimation of the equilibrium potential of chloride ions and enable evaluation of chloride concentration. To this end, GABAergic currents can be measured in a gramicidin perforated-patch configuration which preserves intraneuronal chloride concentration (Akerman and Cline, 2006; Lee et al., 2011; Woodin et al., 2003).

Electrophysiological techniques of E_{GABA} measurements can be tedious thus preventing screening of large-scale populations. To counteract this inconvenience, several fluorescent indicators were developed to directly assess chloride concentration. Among these indicators, the organic dye chloride-sensitive MQAE (Doyon et al., 2011; Galeffi et al., 2004) has been largely due for its capacity to cross the plasma membrane. However, MQAE also shows a strong attenuation of its signal over time thus only allowing low frequency of acquisition (Inglefield and Schwartz-Bloom, 1997). Genetic ratiometric CFP - YFP sensors such as Clomeleon and Cl-Sensor do not show such limitation and have alternatively been used to estimate intraneuronal chloride concentration (Chamma et al., 2013; Kuner and Augustine, 2000; Markova et al., 2008). Yet, these ratiometric sensors are sensitive to pH, a parameter that can be affected by KCC2 function, which raises questions concerning the measures obtained by this method.

In conclusion, several techniques exist to estimate KCC2 activity. Each of them has their specific pros and cons and can be used to answer different questions. Hence, measures of chloride concentrations by fluorescence imaging or reversal potential of GABA by electrophysiological techniques inform on steady-state chloride homeostasis. In contrast, estimations of chloride extrusion capacity reflect the ability of the cell to cope with repetitive GABAergic stimulations in a more dynamic way.

- **Potential role of impermeant anions for setting chloride concentration**

In a much commented publication, the group of Kevin Staley proposed that chloride concentration may not be set by the activity of the CCCs but instead be primarily constrained by the relative concentration of extracellular and intracellular impermeant anions (Glykys et al., 2014). Indeed, impermeant anions may create a gradient of electrical charges across the membrane thereby influencing the transmembrane diffusion of permeable ions such as chloride.

Such effect is known as the Gibbs-Donnan effect. The most surprising observation of this study is that pharmacological blockade of the activity of CCCs did not affect chloride concentration when evaluated by chloride imaging, a result in complete contradiction with all prior publications on the topic (see, among many others, Dargaei et al., 2018; Doyon et al., 2011; Dzhala et al., 2005; Gauvain et al., 2011; Rivera et al., 1999; Zhu et al., 2005). Therefore, while impermeant anions may influence intraneuronal chloride concentration, as recently evidenced in reticular thalamic neurons (Klein et al., 2018), twenty years of research on the topic strongly argue for a primary role of CCC activity.

b. KCC2 transport function is critical for hyperpolarizing action of GABA.

- **Theoretical models reveal a critical role of KCC2 for maintenance of hyperpolarizing GABA transmission**

Given the critical role of KCC2 in chloride homeostasis, it is somehow not surprising that several computational models have revealed a direct relationship between KCC2 transport activity and GABAergic transmission (Doyon et al., 2011; Jedlicka et al., 2010; Lewin et al., 2012).

The main appeal of computational models is that they allow combination of various ions and electrical parameters as well as spatio-temporal integration of the signals to make predictions regarding KCC2 activity and GABA signaling. An interesting discovery of these models is that chloride extrusion capacity was already close to its maximum in neurons since increasing KCC2 activity had very little effects on E_{GABA} (Doyon et al., 2011).

Another consistent finding of all these models is to reveal a differential impact of GABA stimulation depending on the synapse position along the dendritic axis. More precisely, following GABAA receptor activation, chloride accumulates more rapidly in distal compared to proximal compartments. This indicates that distal synapses may be less robust for maintenance of hyperpolarizing GABA transmission when facing intense activation of GABAARs. However, all these models consider KCC2 activity to be equivalent along the dendritic axis. Yet, immunohistochemical studies revealed a higher density of KCC2 in distal dendrites (Báldi et al., 2010). This increased expression of the transporter could allow better coping with chloride accumulation in these compartments.

Finally, a mild KCC2 hypofunction was not sufficient to affect steady-state chloride homeostasis (Doyon et al., 2016). However, it resulted in less efficient coping of neurons upon repeated GABAergic stimulations as well as in an alteration of the neural code and information processing. Overall, these data indicate that even in the absence of changes in neuronal chloride concentration, information processing may be affected by both synapse localization and chloride extrusion capacity.

- **Developmental switch in the polarity of GABA transmission correlates with KCC2 developmental upregulation**

A striking example of the correlation between KCC2 activity and the polarity of GABAAR-mediated currents is observed during development. A few years before KCC2 was even identified, Ben-Ari and collaborators described the presence of giant depolarizing potentials (GDPs) as well as depolarizing responses to GABA in the immature brain (Ben-Ari et al., 1989; Cherubini et al., 1991). Around postnatal day 5 (P5), a switch in the polarity of GABA responses from depolarizing to hyperpolarizing occurs in hippocampal neurons and is closely followed by the disappearance of GDPs. The precise timing of this switch was later refined and placed around P13 in the hippocampus (Khazipov et al., 2004).

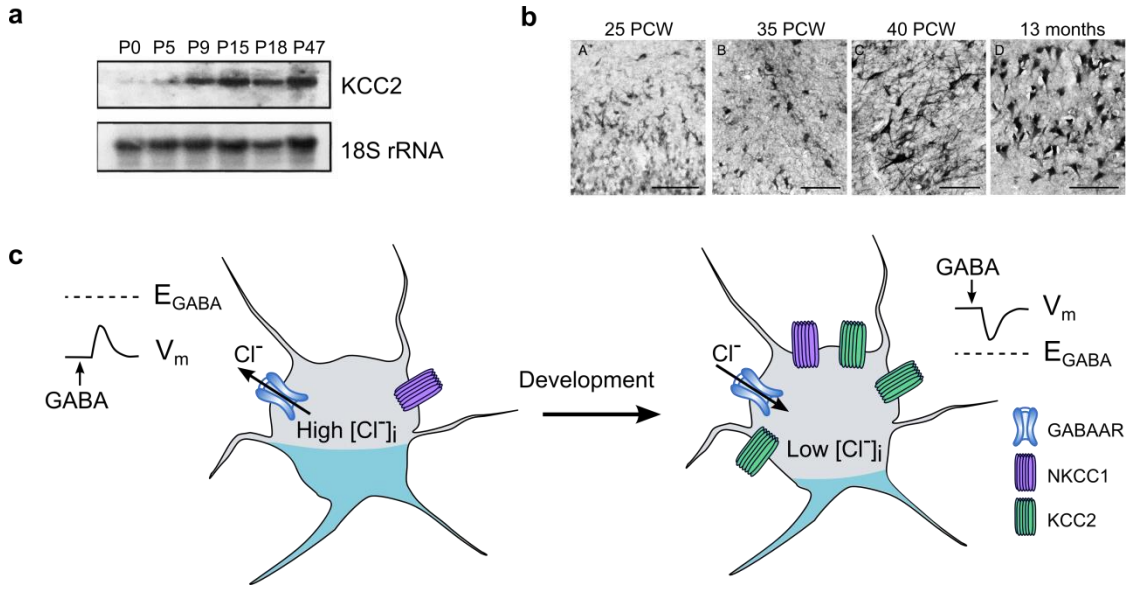

Figure 6 : Developmental upregulation of KCC2 is critical for GABAergic switch from depolarizing to hyperpolarizing
(a) Northern blot experiments revealed upregulation of mRNA levels of KCC2 through development in the rat hippocampus (adapted from Rivera et al. 1999)
(b) KCC2 protein levels are also upregulated in human hippocampus between 25 weeks post conception and 13 months. Scale : 100µm (adapted from Sedmak et al. 2016)
(c) Upregulation of KCC2 through development allow the establishment of a low intraneuronal chloride concentration, thus enabling hyperpolarizing GABA responses

Upregulation of KCC2 is observed throughout the forebrain in rodents (Rivera et al., 1999) from P5 - P7 before reaching its maximal level around P15 (Fig 6A). Inhibition of KCC2 expression by incubation of slices with antisense oligodeoxynucleotides against KCC2 mRNA was sufficient to prevent the switch of the polarity of GABAAR-mediated currents. Thus, KCC2 seems to be the main chloride extruder responsible for fast hyperpolarizing GABA transmission (Fig 6C). Several studies later revealed that the precise timing of this upregulation differs depending on brain regions but is highly correlated with the timing of switch of the polarity of GABAAR-mediated currents in each brain region (see Watanabe and Fukuda, 2015 for review). KCC2 developmental expression pattern is not restricted to the rodent brain but is also observed in the human brain between 25 weeks post conception and 13 months (Sedmak et al., 2016, Fig 6B). Similar to the observations made on rodent, the upregulation of KCC2 in the human brain coincides with a transition from depolarizing to hyperpolarizing GABA-mediated currents (Dzhala et al., 2005; Sedmak et al., 2016).

- **Physiological relevance of depolarizing GABA in immature brain**

In a controversial series of publications, the group of Yuri Zilberter argued that the depolarizing effect of GABA and the observation of GDPs in the immature brain were both experimental artifacts. They suggested that these observations arose from the absence of adequate energy substrates and showed that addition of ketone-bodies (Rheims et al., 2009), lactate or pyruvate (Holmgren et al., 2010) efficiently suppress the GDPs *in vitro*. Furthermore, slicing itself was suggested to be sufficient to render GABAAR-currents depolarizing at the surface of the slices due to unsatisfied energy requirements (Dzhala et al., 2012). However, the results published by the Zilberter's group failed to be reproduced by two independent groups (Ruusuvuori et al., 2010; Tyzio et al., 2011) who also demonstrated that actual levels of energy substrates in the pup brain are much lower than those used in the study from the Zilberter's group. Finally, GDPs have been observed both in intact hippocampal preparation (Khalilov et al., 1999) and *in vivo* (Sipilä et al., 2006) which refutes the hypothesis of a sole slicing artifact.

Instead, GDPs are thought to be essential for the neurotrophic action of GABA in the immature brain. Indeed, GABAergic synapses are formed and active prior to glutamatergic synapses. Depolarizing currents mediated by GABAARs lead to voltage-gated Ca^{2+} channels (VGCCs) activation as well as enhanced recruitment of N-methyl-D-Aspartate receptors (NMDARs) which in turn favors the development of glutamatergic synapses (Akerman and Cline, 2006). Early expression of KCC2 was also proven detrimental for interneuron migration (Bortone and Polleux,

2009) due to a lack of recruitment of VGCCs. Thus, KCC2 absence in the developing brain and subsequent depolarizing action of GABA is critical for its correct maturation.

c. Does E_{Cl} directly control the polarity of GABA transmission?

So far, I described a straightforward relationship through which KCC2 activity directly controls chloride homeostasis and consequently the reversal potential and polarity of GABAAR-mediated currents. Such affirmation needs to be partly moderated.

First, as I already mentioned, GABAARs also display a lesser conductance to bicarbonate ions. Reversal potential of bicarbonate-mediated currents is around -10 mV, sensibly more depolarized than membrane potential. Hence, activation of GABAARs leads to a depolarizing outward current of bicarbonate. Consequently, regulation of bicarbonate homeostasis may also influence GABA signaling. In particular, carbonic anhydrase, a catalytic enzyme of bicarbonate, is upregulated during development and participates in the regulation of E_{GABA} (Rivera et al., 2005). This importance of bicarbonate control for GABAergic transmission has been further highlighted in the context of febrile seizures. Indeed, in rat pups, hyperthermia triggers seizures through brain alkalosis, a mechanism which could be mimicked by bicarbonate injection (Schuchmann et al., 2006). In contrast, knock-out animals for the carbonic anhydrase VII show reduced susceptibility to hyperthermic seizures (Ruusuvuori et al., 2013). These seizures were mediated by GABAergic excitation since they were aggravated by diazepam, a positive allosteric modulator of GABAARs.

Second, it is important to distinguish between E_{GABA} and the driving force of GABA (DF_{GABA}). The latter reflects the difference between the reversal potential of GABAAR-mediated currents and the resting membrane potential and therefore determines the amplitude and polarity of GABAergic currents. Consequently, any changes in V_m will also affect GABA transmission. Thus, neuronal maturation has been associated with hyperpolarization of their resting membrane potential in hippocampal pyramidal cells (Spigelman et al., 1992), dentate gyrus granule cells (Ambrogini et al., 2004) as well as neurons derived from human stem cells (Johnson et al., 2007) but not striatal neurons (Deng et al., 2004). This indicates that the overall impact of development on GABA transmission may differ depending on cell types. Even more strikingly, Cre-mediated exon excision of KCC2 in the cerebellum modifies DF_{GABA} in Purkinje cells but not in cerebellar granule cells since changes in V_m exactly matches changes in E_{GABA} in the latest (Seja et

al., 2012). Therefore, as I will show later in this thesis, changes in KCC2 expression may be functionally masked by concomitant changes in resting membrane potential, thereby precluding changes in DF_{GABA}.

Finally, it should be highlighted that depolarizing GABA currents are not necessarily excitatory. Indeed, independently of the polarity of net ion flux through GABAARs, their activation leads to opening of a membrane conductance and therefore decreases the membrane resistance. This in turn hinders subsequent depolarization of the membrane by glutamatergic inputs by a shunting inhibitory effect (Staley and Mody, 1992). In particular, a recent *in vivo* study demonstrated that GABA transmission was depolarizing but inhibitory due to this shunting effect in neurons from the upper cortical plate during early postnatal development (Kirmse et al., 2015).

d. Osmotic regulation in neurons

In addition to its critical control of chloride homeostasis, KCC2 also plays an essential role in the osmotic regulation of neurons.

KCCs were first described in epithelial and red blood cells as swelling-activated transporters whose activity was critical for facing osmotic challenges (Dunham and Ellory, 1981; Lauf and Theg, 1980; Zeuthen and MacAulay, 2002). This is due to the fact that co-transport of potassium and chloride is indirectly or directly coupled to water transport (MacAulay and Zeuthen, 2010; Zeuthen and MacAulay, 2002). Notably, it has been estimated that up to 500 molecules of water may cross the membrane for each chloride ion transported by KCC2 or NKCC1, probably to partially equilibrate for osmotic changes due to the ion transport (MacAulay and Zeuthen, 2010).

In the CNS, activation of ionotropic GABAAR as well as glutamate receptors leads to net ion influx in the postsynaptic neuron. This influx is accompanied by water fluxes in order to maintain intracellular osmolarity. Thus, intense neuronal activity directly impacts cell volume and can lead to cell swelling and cell death in extreme cases. Since neurons lack aquaporins (Amiry-Moghaddam and Ottersen, 2003), other mechanisms may be necessary for coping with the activity-induced swelling. Hence, digital holographic microscopy revealed an important water influx through both NKCC1 and NMDARs following glutamate application (Jourdain et al., 2011) accompanied by cell swelling. This was counteracted by subsequent swelling-induced activation of KCC2 and water extrusion, which allowed recovery of cell volume. In one study, KCC2

transport - function was proven essential to neuronal survival following NMDA-induced excitotoxicity (Pellegrino et al., 2011). Although the authors did not fully explore the mechanisms underlying such neuroprotective effect, the role of KCC2 in coping with activity-induced swelling may be one of them.

Swelling-induced activation of KCC2 is most likely dependent on the inhibition of the With No Lysine Kinase (WNK) as well as SPAK / OSR1 pathway, which results in dephosphorylation of the threonine T906 and T1007 residues (Gagnon et al., 2006; Rinehart et al., 2009). Conversely, extracellular hyperosmotic challenges lead to activation of the WNK, SPAK / OSR1 pathway, phosphorylation of T906 and T1007 residues and inhibition of KCC2 membrane expression. Notably, NKCC1 is also regulated by this pathway in opposite direction thus also participating to the regulation of cell volume following osmotic challenges (Kahle et al., 2010).

In conclusion, KCC2 transport-function is essential in neurons both for maintenance of inhibitory GABAergic transmission and for coping with osmotic challenges associated in particular with synaptic activity. Thus, mechanisms influencing KCC2 expression and membrane stability are likely to also critically impact both of these physiological processes.

3. Regulation of KCC2 expression and membrane stability

a. Age-dependent regulation of KCC2 by the BDNF/TrkB pathway

The progressive upregulation of KCC2 during development is promoted by brain-derived neurotrophic factor (BDNF) release (Aguado et al., 2003). BDNF binding to the tropomyosin receptor kinase B (TrkB) leads to activation of the extracellular signal regulated kinases 1 and 2 (Erk1/2) pathway via its coupling with the Src homology 2 domain containing transforming protein (Shc) and FGF receptor substrate 2 (FRS-2) (Fig 7). This in turn enhances the activity of the Egr4 transcription factor, which favors the expression of KCC2 (Ludwig et al., 2011). Surprisingly, full knock-out mice for BDNF still present a developmental upregulation of KCC2 (Puskarjov et al., 2015). This could be explained by the presence of compensatory mechanisms to BDNF. Indeed, the neurturin trophic factor can also trigger Egr4 activity thereby regulating KCC2 expression (Ludwig et al., 2011). Interestingly, this upregulation is restricted to the KCC2b isoform (Yeo et al., 2009) resulting in different proportion of the two isoforms in the developing versus mature brain. Hence, whereas KCC2a contributes to about 20-50% of the total KCC2

mRNA expression in the neonatal brain, its contribution decreases to 5-10% in the adult brain (Uvarov et al., 2009). Surprisingly, the developmental upregulation of KCC2 also requires prior expression of neuroligin-2 (Sun et al., 2013) although the mechanisms underlying such regulation and whether it involves BDNF or neurturin signaling remains unknown.

Nevertheless, BDNF possesses completely opposite effects on KCC2 expression and membrane stability in the mature brain compared to its role in development. Indeed, BDNF incubation for 2 to 3 hours is sufficient to induce massive downregulation of KCC2 expression and mRNA levels (Rivera et al., 2002). This regulation is dependent on both Shc/FRS-2 and phospholipase Cγ (PLCγ) - cAMP response element-binding protein (CREB) signaling (Rivera et al. 2004). This shift in BDNF / TrkB signaling pathway during maturation could be explained by an age-dependent change of TrkB phosphorylation at its PLCγ binding site (Di Lieto et al., 2012).

Interestingly, BDNF also potentiates the maturation of GABAergic neurons in the developing brain (Yamada et al., 2002) but not at later developmental stages (Mizoguchi et al., 2003). Conversely, in immature but not mature hippocampal neurons, GABA increases BDNF mRNA levels (Berninger et al., 1995), indicating a possible synergistic effect of GABA and BDNF in the developing brain.

b. Activity-dependent regulation by synaptic transmission

- **Fast downregulation of KCC2 by excitatory transmission**

KCC2 expression and transport-function is rapidly downregulated by neuronal activity under physiological conditions (Kaila et al., 1997; Kitamura et al., 2008; Woodin et al., 2003). This effect was proposed to enable the maintenance of neuronal activity homeostasis (Wang et al., 2006) but also to participate in learning-related functions (Fiumelli and Woodin, 2007).

The group of Mu-Ming Poo was the first to show calcium-dependent downregulation of KCC2 in immature neurons (Woodin et al., 2003). This effect was dependent on both voltage-gated calcium channels (VGCCs) and protein kinase C (PKC) activity (Fiumelli et al., 2005). However, the action of PKC is likely to be indirect since the only known phosphorylation site targeted by PKC is the serine 940 (S940) whose phosphorylation stabilizes KCC2 membrane expression (Lee et al., 2007).

Raise of intracellular Ca^{2+} concentration and consecutive downregulation of KCC2 may occur upon activation not only of VGCC but also of NMDARs (Fig 7). Postsynaptic calcium influx through NMDARs induces protein phosphatase 1 (PP1) - dependent dephosphorylation of the S940 residue of KCC2 (Lee et al., 2011) which in turn reduces the membrane stability of the transporter. Furthermore, calcium recruits calpain protease leading to cleavage of the C-terminal domain of KCC2 and rapid endocytosis of the protein (Puskarjov et al., 2012; Zhou et al., 2012). Finally, a study from our group demonstrated that increased excitatory activity induces a rapid, NMDAR-dependent increase in KCC2 lateral diffusion. This effect was accompanied by a decrease of KCC2 function and clustering, involving both dephosphorylation of the S940 residue by PP1 and calpain cleavage of the CTD (Chamma et al., 2013).

- **Regulation of KCC2 by metabotropic receptors**

Stabilization and enhanced function of KCC2 has been demonstrated following activation of both group I metabotropic glutamate receptors (Banke and Gegelashvili, 2008), serotonin type 2A receptors (Bos et al., 2013) and metabotropic zinc-sensing receptors (Chorin et al., 2011). These receptors are all coupled to the $G\alpha_q$ protein and their activation ultimately leads to the recruitment of PKC and phosphorylation of the S940 residue.

On the other hand, intense activation of muscarinic acetylcholine receptors (mAchRs) lead to phosphorylation of the tyrosine Y903 and Y1087 by the proto-oncogene tyrosine-protein kinase Src and downregulation of the protein (Lee et al., 2010). Such observation is surprising since phosphorylation of these residues was previously shown to alter KCC2 activity in both heterologous systems (Strange et al., 2000; Watanabe et al., 2009) and neurons (Akerman and Cline, 2006; Chudotvorova et al., 2005; Pellegrino et al., 2011) without affecting its membrane expression. It is however possible that two independent mechanisms occur following intense mAchRs activation: one leading to phosphorylation of the tyrosine residues and the other resulting in destabilization of the protein, possibly through one of the previously described pathway.

- **Impact of inhibitory transmission on KCC2 membrane stability**

Recently, two different studies revealed new rapid regulation of KCC2 expression and function by inhibitory transmission (Fig 7). In a first study from our group, activation of GABAARs was shown to stabilize KCC2 at the plasma membrane while blockade of GABAergic transmission

increased diffusion and reduced clustering and membrane stability of the transporter (Heubl et al., 2017). These effects were mediated by chloride ions acting as secondary messengers to regulate the chloride-sensitive WNK1 activity and subsequently the phosphorylation levels of T906 and T1007 residues of KCC2.

In a second study, activation of $GABA_B$ receptors led to a rapid destabilization of KCC2 (Wright et al., 2017) which was unaffected by blockers of calcium signaling pathways or kinases and phosphatases implicated in KCC2 regulation. Instead, the authors described a new interaction between KCC2 transmembrane domain and $GABA_B$ receptors. The decrease of KCC2 expression correlated with the decrease in $GABA_B$ receptors expression, suggesting that stabilization of GABABRs at the plasma membrane was important for KCC2 stability. These results of Wright and colleagues somewhat contradict those of our group in which $GABA_B$ receptors activation had no effect on KCC2 diffusion and membrane stability (Heubl et al., 2017). Such discrepancy may reflect differences in the experimental models used. In fact, internalization of $GABA_B$ receptors following their activation had been previously reported in slices (Laffray et al., 2007), as used by Wright and collaborators, but not in dissociated neuronal cultures (Vargas et al., 2008), as used by our group.

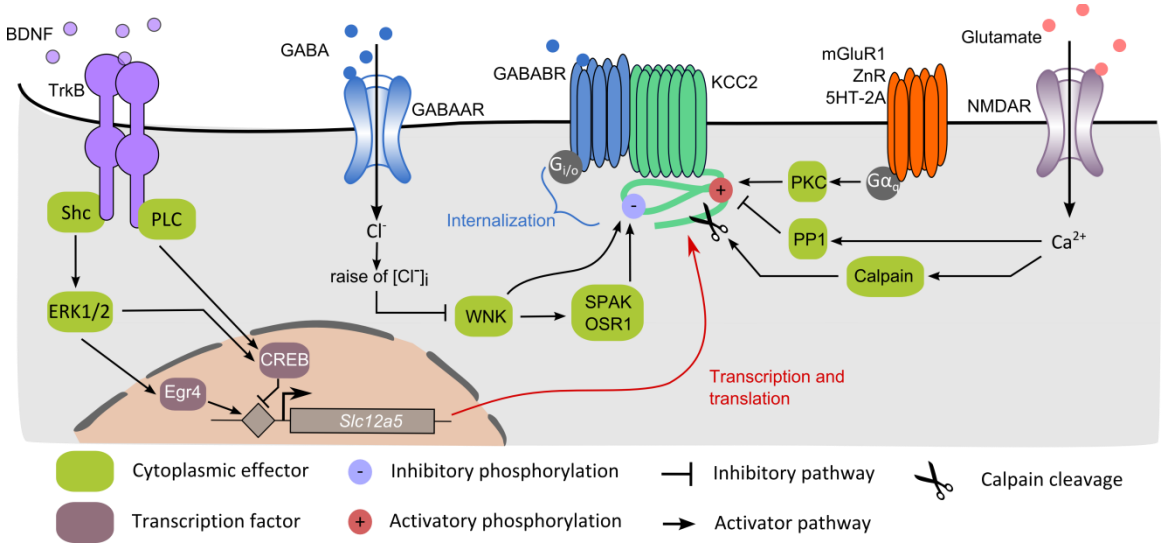

Figure 7 : Activity-dependent regulation of KCC2 expression and function
BDNF controls KCC2 expression in an age-dependent manner. During neuronal development, only Shc is stimulated leading to the transcription of KCC2 gene Slc12a5. On the contrary, in mature neurons, BDNF binding to TrkB induces the co-stimulation of Shc and PLC leading to the inhibition of KCC2 gene expression.
KCC2 is also highly regulated at the post-translational level. Both excitatory and inhibitory transmissions modulate its membrane expression and function through a variety of pathways.

We have previously shown that regulation of KCC2 stability and function in turn potently impacts GABA signaling. Hence, these discoveries on KCC2 fast regulation by both excitatory and inhibitory transmission reveal new mechanisms to rapidly controlling GABAergic transmission based on ongoing synaptic activity. Overall, these studies suggest KCC2 is ideally controlled to mediate a cross-talk between glutamatergic and GABAergic signaling.

c. Regulation of KCC2 expression through protein interaction

KCC2 is involved in numerous protein-protein interactions, mainly through its C-terminal domain but also through its transmembrane domains (Fig 8). Among KCC2 partners, several actin-related proteins expressed at glutamatergic synapses have been identified, including the protein 4.1N (Li et al., 2007) and βPix (Chevy et al., 2015; Llano et al., 2015). A recent native KCC2 interactome reveals that a large proportion of putative KCC2-interacting proteins is expressed at glutamatergic synapses (Mahadevan et al., 2017), indicating a potential role of KCC2 as a structural organizer of glutamatergic synapses. This study also identifies proteins involved in intracellular trafficking, such as 14-3-3 protein and Kif21B, as putative KCC2 interactors.

It is remarkable that several putative KCC2-interacting proteins are involved in regulation of either its membrane stability or function. We just described such reciprocal interaction with $GABA_B$ receptors (Wright et al., 2017). Additionally, KCC2 interaction with Neto2 and GluK2 seems to be required for its normal membrane expression and function (Ivakine et al., 2013; Mahadevan et al., 2014). Indeed, genetic ablation of either Neto2 or GluK2 results in decreased KCC2 expression and function. Interestingly, Neto2 is upregulated during the development with a timing similar to that of KCC2 upregulation (Michishita et al., 2004), suggesting a possible role of this interaction in the developmental upregulation of KCC2. A recent study from the Woodin group revealed that PKC-dependent phosphorylation of the GluK2 subunit is necessary to promote KCC2 recycling and enhance its function (Pressey et al., 2017).

Several other KCC2-interacting proteins were shown to affect the membrane stability of the transporter. Hence, interaction of KCC2 with the amyloid precursor protein (APP) is critical to limit both tyrosine-phosphorylation and ubiquitination of KCC2, thereby preventing subsequent degradation of the transporter (M. Chen et al., 2017). In contrast, interaction of the KCC2-CTD with the clathrin-binding adaptor protein-2 (AP-2), induces constitutive dynamin-dependent clathrin-mediated endocytosis of KCC2 (Zhao et al., 2008). KCC2 expression is also negatively

regulated by its interaction with the endocytic regulatory protein PACSIN1 (Mahadevan et al., 2017).

Lastly, activity of KCC2 was shown to be positively regulated in HEK-293 through its interaction with the CCC CIP1 (Wenz et al., 2009). However, the mechanism through which KCC2 function is enhanced by this interaction remains to be clarified. Similarly, KCC2 interacts with the the alpha2 subunit of the Na/K ATPase (Ikeda et al., 2004) as well as the brain-type creatine kinase (CKB), an enzyme which regenerates ATP using the energy contained in phosphocreatine (Inoue et al., 2004). CKB activity affects KCC2 transport function (Inoue et al., 2006), suggesting a phosphorylation of KCC2 by CKB. However, the target residue has not been identified yet.

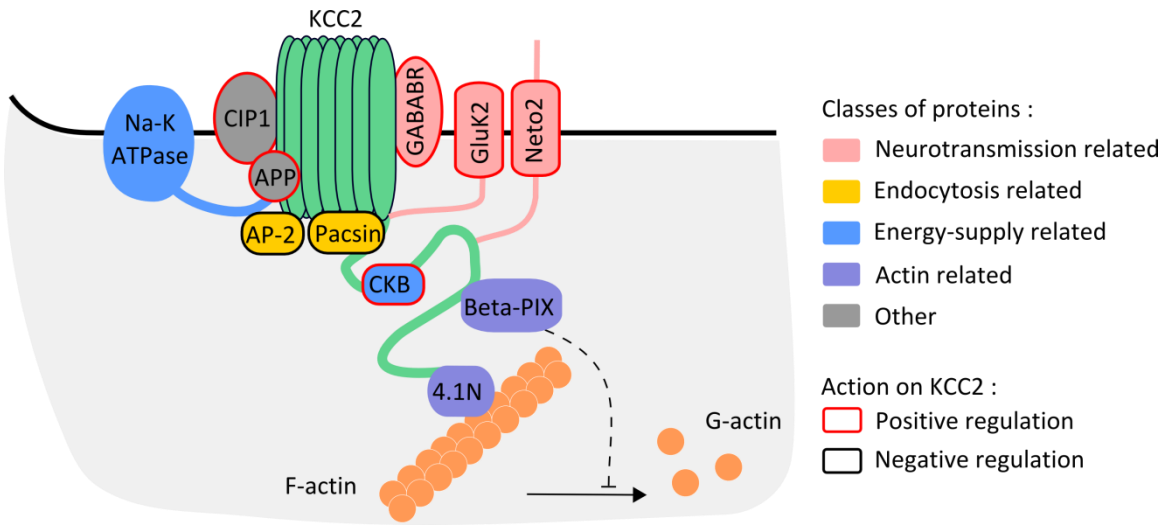

Figure 8 : KCC2 interactome
KCC2 is involved in several putative macromolecular complexes.
Several of these interactions positively regulate KCC2 membrane stability and / or function. Hence, near excitatory synapses, KCC2 interacts and is positively regulated by the kainate receptor GluK2 and its auxiliary protein Neto2. Similarly, the interaction with the GABAB receptors stabilizes KCC2 at the membrane. Furthermore, KCC2 function is positively regulated by its interaction with CIP1 and the amyloid precursor protein (APP). In contrast, the interaction of the transporter with several endocytic partners such as AP-2 and Pacsin favors its internalization.
KCC2 also interacts with proteins involved in energy supply such as the alpha2 subunit of the Na/K ATPase and with the brain-type creatine kinase (CKB). These interactions are thought to increase the energetic coupling between primary and secondary-types of active transporters as well as to promote ATP replenishment.
Finally, actin-related proteins such as 4.1N and βPix interact with the C-terminal domain of KCC2. The latest interaction has been shown to regulate actin polymerization (Llano et al. 2015, Chevy et al. 2015).

In conclusion, KCC2 is involved in macromolecular complexes composed of several proteins at the plasma membrane. Such complexes are critical for the regulation of KCC2 membrane stability and function. Identification of the components of these complexes reveals a variety of novel pathways through which KCC2 and ultimately GABA transmission may be regulated. Reciprocally, as we will see later in this thesis, these interactions may be lost upon KCC2 down-

regulation, in particular in the pathology. Fully understanding the functional impact of this down-regulation at the cellular and network levels then requires taking into account the various interactions KCC2 is normally engaged in.

d. Oligomerization and clustering of KCC2

Both oligomerization and clustering of KCC2 have been suggested to influence its function. Multimeric assembly has been demonstrated for a large number of members of the CCC family (Blaesse et al., 2006; Casula et al., 2001; Moore-Hoon and Turner, 2000; Simard et al., 2007; Starremans et al., 2003; Warmuth et al., 2009) and KCC2 oligomers were detected in the brain (Blaesse et al., 2006; Uvarov et al., 2009). However, a recently published study based on electron microscopy indicated that KCC2 in solution mostly forms dimers rather than oligomers (Agez et al., 2017). This dimerization involves disulfides bridges that may involve cysteine residues located in the extracellular loop, possibly together with interactions between the C-terminal domains.

Whether monomeric KCC2 is functional for chloride-transport is still an open question. The increase in KCC2 oligomerization during development (Blaesse et al., 2006) as well as the correlation between decreased oligomerization and reduced transport activity (Mahadevan et al., 2014; Watanabe et al., 2009) point in that direction. However, such observations are not sufficient to indicate causality. Furthermore, experimental limitations with studies of KCC2 oligomerization by western blot techniques were recently raised (Medina et al., 2014), which complicated the interpretation such experiments.

As mentioned previously, KCC2 protein has also been shown to form clusters at the plasma membrane (cf. I.1.d). Regulation and functional relevance of this clustering has been mainly investigated in three different studies. First, inhibition of tyrosine phosphorylation was shown to reduce KCC2 clustering and function with no apparent change in total surface expression of the transporter (Watanabe et al., 2009). Second, KCC2 clustering and function were demonstrated to be rapidly modulated by both excitatory and inhibitory through changes in diffusion properties of KCC2 (Chamma et al., 2013; Heubl et al., 2017).

Mechanisms controlling KCC2 clustering and oligomerization are still not fully understood. They may, however, represent important pathways for the regulation of chloride homeostasis through the control of KCC2 activity.

4. Emerging role of KCC2 at glutamatergic synapses

The identification of highly clustered KCC2 in dendritic spines, near the glutamatergic postsynaptic density, has prompted the study of the potential role of KCC2 in this unexpected location. In the original work from Gulyas and collaborators, the authors postulated that this localization of KCC2 could be a mechanism for neurons to cope with activity-induced swelling of the cell (Gulyás et al., 2001). Indeed, suppression of KCC2 induces a swelling of dendritic spines, as already mentioned above (Gauvain et al., 2011). However, further studies revealed other unexpected functions of KCC2 at excitatory synapses.

a. Maturation of dendritic spines

Initial studies on the role of KCC2 on the maturation of glutamatergic synapses were based on overexpressing KCC2 at early developmental stages. *In utero* electroporation of KCC2 in the developing retino-tectal circuit of Xenopus embryos reduced both the frequency and amplitude of mEPSCs (Akerman and Cline, 2006). This effect was indirectly dependent on KCC2 transport-function. Indeed, as mentioned previously (see I.2.b), the decrease in chloride concentration following KCC2 expression is sufficient to render GABA transmission hyperpolarizing in the developing brain. This, in turn, would prevent NMDA receptor activation and subsequent expression of AMPA receptors at silent synapses. Similar to previously published results on hippocampal neurons cultures (Chudotvorova et al., 2005), the authors found that early overexpression of KCC2 also promoted the maturation of GABA synapses (resulting in an increase of both the frequency and amplitude of mIPSCs). Interestingly, Chudotvorova and colleagues reported no change in glutamatergic transmission upon KCC2 overexpression. This discrepancy could be explained by the neuronal type (hippocampal *vs*. retino-tectal neurons) or by different mechanisms of regulation between the *in vitro* and the *in vivo* models.

The team of Claudio Rivera (Li et al., 2007) soon provided new insights into the role of KCC2 at glutamatergic synapses. Since full KCC2 knockout mice do not survive after birth (see I.5.c for more details), the authors used primary cultures of hippocampal neurons from $KCC2^{-/-}$ mice to investigate the effect of KCC2 suppression on excitatory synapses maturation. They showed that the absence of KCC2 impaired dendritic spine maturation, resulting in a higher proportion of filopodia-shaped dendritic spines and an overall reduction in the number of active glutamatergic

synapses. Unexpectedly, this effect was independent of KCC2 transport-function. Indeed, overexpression of the Δ-NTD KCC2 completely rescued the alterations of spine formation without restoring chloride homeostasis. Instead, control of dendritic spines maturation involved KCC2 interaction with the actin cytoskeleton. The authors described a novel interaction between the C-terminal domain of KCC2 and the FERM-domain of the cytoskeletal protein 4.1N. Disruption of this interaction by overexpression of KCC2-CTD or of a Myc-tagged FERM domain (both acting as dominant negative) was sufficient to mimic the phenotype of $KCC2^{-/-}$ neurons. Hence, interaction of KCC2 with the actin cytoskeleton through 4.1N is necessary for glutamatergic synapses maturation. Surprisingly, as I already mentioned (cf I.1.c), the Δ-NTD KCC2 was recently described as presenting deficits of membrane expression (Friedel et al., 2017). This questions the precise mechanism through which this mutant rescued the deficits in spinogenesis. Despite this unresolved issue, the work of Li and collaborators marked a breakthrough in the study of KCC2 role in the CNS since it was the first to highlight a non-canonical role of KCC2 through protein interaction independent of chloride transport.

Interestingly, this effect on dendritic spines morphology was not observed when KCC2 was suppressed after the period of spinogenesis. Thus, no change in either spine morphology or number of excitatory synapses were observed upon chronic suppression of KCC2 by RNA interference in mature hippocampal neurons in culture (Gauvain et al., 2011) or by Cre-mediated exon excision in the cerebellum in the weeks following birth (Seja et al., 2012). However, in line with the results from Li et al., *in utero* electroporation of KCC2 but also of the Δ-NTD KCC2 induces an increase in spine density in layer 2/3 of the somatosensory cortex (Fiumelli et al., 2013).

Altogether, these studies support a role of KCC2 in controlling the maturation of dendritic spines during development, through an interaction with the actin cytoskeleton.

b. Role of KCC2 at mature glutamatergic synapses

KCC2 interaction with the actin cytoskeleton is not only crucial for spinogenesis but also for basal excitatory transmission (Gauvain et al., 2011) and plasticity of glutamatergic synapses (Chevy et al., 2015). Thus, suppressing KCC2 in mature hippocampal neurons in culture leads to decreased amplitude of mEPSCs. This effect correlates with increased membrane diffusion of

these receptors and a reduction in GluA1-containing AMPARs in dendritic spines. Importantly, this effect is transport-independent as it is not reproduced by bath-application of the specific KCC2 antagonist, VU0240551 but can be mimicked by the expression of the CTD of KCC2. This study suggests KCC2 anchoring to the actin cytoskeleton could act as a physical barrier confining a pool of extrasynaptic AMPARs within dendritic spines (Fig 9).

KCC2 interaction with the actin cytoskeleton is not restricted to direct, physical interaction via the 4.1N protein. Thus, a novel interaction with the β isoform of the Rac/Cdc42 guanine nucleotide exchange factor β-Pix was recently identified (Chevy et al., 2015; Llano et al., 2015; see I.3.c). β-Pix is part of signaling pathway involving Rac1, PAK et LIMK that acts to inhibit cofilin-1, which binds and depolymerizes filamentous actin. Suppression of KCC2 then results in increased levels of phosphorylated cofilin and consequently in accumulation of polymerized F-actin in dendritic spines. In a study from our group in which I participated, we showed that this in turn impairs long-term potentiation of glutamatergic synapses by precluding activity-driven membrane delivery of AMPARs (Chevy et al., 2015; Fig 9). Again, this effect was independent of KCC2 ion transport function as these results were not mimicked by application of the KCC2 antagonist, VU0240551. Since long-term potentiation is thought to represent the cellular substrate for learning and memory (Whitlock et al., 2006), these observations predict KCC2 down-regulation may also result in cognitive deficits.

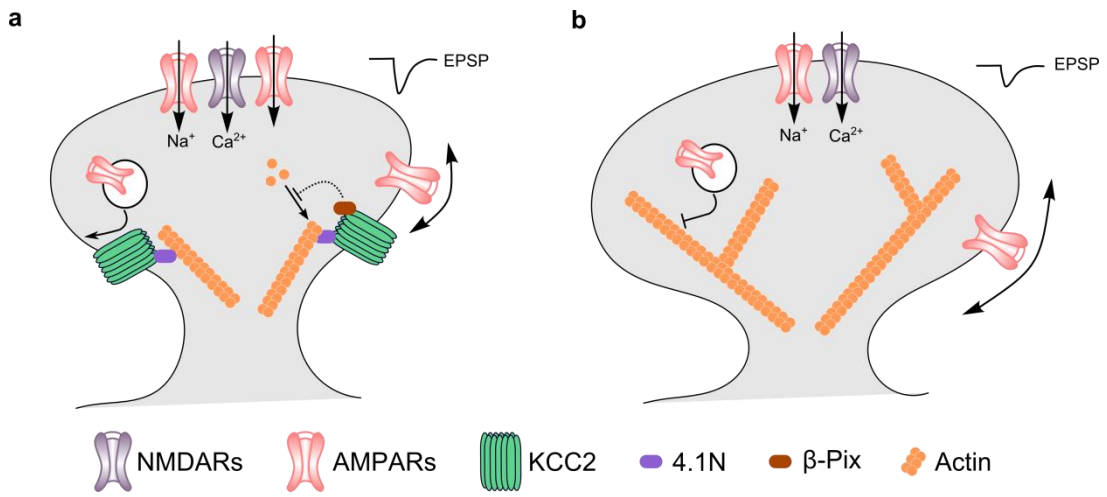

Figure 9 : Impact of KCC2 suppression on mature glutamatergic synapses
(a) In dendritic spines, KCC2 interacts with the actin cytoskeleton through 4.1N thus limiting AMPARs lateral diffusion. Its interaction with β-Pix also prevent accumulation of F-actin
(b) In absence of KCC2, spine volume increases due to loss of osmotic regulation via its transport function. AMPARs escape from the synapse thus decrease the efficacy of glutamatergic transmission. Finally, accumulation of F-actin precludes activity-dependent AMPARs exocytosis and long-term potentiation of the synapse.

This series of studies indicates a structural, transport-independent role of KCC2 in controlling both maturation, activity and plasticity of glutamatergic synapses. Thus, impairment of KCC2 expression is predicted to not only affect GABAergic but also alter glutamatergic signaling.

5. KCC2 in epilepsy

KCC2 is rapidly downregulated following seizure induction (Rivera et al., 2002). This in turn leads to accumulation of intraneuronal chloride and altered GABA signaling. Therefore, the loss of KCC2 has been proposed to not only be a consequence of seizures but also causal in epileptogenesis. However, evidence in support of the latter remains elusive.

a. Excitation / inhibition imbalance in epilepsy

The term *epilepsy* represents a complex disease with a variety of clinical characteristics and, consequently, a variety of underlying molecular mechanisms. One important distinction in this respect is between *epilepsy* and *seizure*. A seizure corresponds to a period of abnormal excitation and synchronization of a neuronal population. Epilepsy, on the other hand, represents a pathological condition characterized by the occurrence of seizures. Similarly, one should distinguish *epileptogenesis,* which refers to the process leading to epilepsy after an initial insult (a seizure, brain trauma, infection…), and *ictogenesis,* which refers to the mechanisms contributing to the generation of a seizure in an epileptic network.

One commonly proposed mechanism underlying seizures involves a dysregulation of the excitatory/inhibitory (E/I) balance. A failure in GABAergic inhibitory transmission has often been proposed as being at the basis of this E/I imbalance. Thus, several alterations in GABAergic networks have been associated (yet not always linked by causality) with epilepsy, including specific interneuron vulnerability (Cossart et al., 2001; de Lanerolle et al., 1989), dysfunction of GABAergic synapses (Thind et al., 2010) or reduced interneuron excitability (Martin et al., 2010; Sloviter, 1987).

In line with these observations, drugs acting to promote GABAergic transmission have been used for a long time in the treatment of epilepsy. For instance, sodium valproate which increases the

levels of GABA in the brain has been commonly used in many forms of epilepsy. Similarly, benzodiazepines, which act as positive allosteric modulators of GABAARs, have often been used as first-line treatment in case of status epilepticus (SE) (Alvarez et al., 2016). However, about 30% of epileptic patients do not respond to treatments by classical antiepileptic drugs (Picot et al., 2008). In the vast majority of cases, patients resistant to one type of treatment will not have their symptoms contained by any kind of medication, only leaving surgical resection of the epileptic focus as a potential therapeutic option (Engel, 2014). Hence, better understanding of the mechanisms explaining such pharmacoresistance is critical to provide new effective treatments.

b. KCC2 mutations and epileptogenesis

First evidence linking dysfunctions of KCC2 transporter, E/I imbalance and epileptogenesis arose from study of knockout (KO) lines.

- **Phenotype of KCC2 KO and mutant animal models**

Complete genetic deletion of a gene is often used to better understand the physiological role of a protein. In the case of KCC2, considering its developmental upregulation occurs around 9 days postnatal and its crucial role in both regulation of GABAergic transmission and synapses maturation (see I.2.b and I.4.a), severe deficits in $KCC2^{-/-}$ mice were expected to appear shortly after birth. Remarkably, these mice already suffered from drastic motor deficits at birth and die shortly after from respiratory failure (Hübner et al., 2001). In contrast, heterozygous animals were perfectly viable and the authors did not report any change in response to proconvulsant drugs.

A second model of KCC2 knockout targeted exon 1b of the Slc12a5 gene, leading to a specific deletion of KCC2b without affecting KCC2a and resulting in expression of approximately 5% of the protein level of KCC2 (Woo et al., 2002). These hypomorphic KCC2 mice survived for a couple of weeks after birth but exhibited spasticity, hyperexcitability in the hippocampus as well as frequent spontaneous generalized seizures. Surprisingly, in contrast to the full KCC2 KO described by Hübner and colleagues, heterozygous hypomorphic mice also displayed increased susceptibility to generalized seizure following pentylenetetrazol (PTZ) injection.

Finally, hypomorphic KCC2-deficient mice against KCC2a and KCC2b were raised (Vilen et al., 2001). These mice exhibit about 30% of the control protein level and did not display any obvious phenotype. From this strain, mice double heterozygous for the hypomorphic and null alleles of KCC2 were generated (Tornberg et al., 2005). Even though they expressed only about 17% of the control level of KCC2, these mice were viable and fertile. However, they exhibited a decreased body-weight, increased anxiety, impaired spatial learning and increased susceptibility to PTZ-induced seizures (Tornberg et al., 2005).

It should be noted that the phenotype observed in all these mice strains may not entirely be driven by changes in GABAergic transmission. As previously mentioned, suppression of KCC2 during the development also impairs the maturation of the dendritic spines, which could participate in the reported deficits.

In contrast, more subtle effects were observed with knock-in KCC2 phospho-mutants. *In vitro*, the activity of KCC2 is potentiated by the phosphorylation of serine 940 (Lee et al., 2007; see I.3.b). Mutants mice with constitutive dephosphorylation of this residue mutated in an alanine (S940A) were generated by the Moss lab (Silayeva et al., 2015). S940A mice do not exhibit changes in surface expression of KCC2 nor in basal E_{GABA}. However, they are more susceptible to epilepsy, as indicated by the decreased latency to SE and increased severity of SE in a kainate model. This observation was paralleled by a deficit in chloride homeostasis in neurons from S940A mice after transient glutamate exposure. Thus, phosphorylation of the serine 940 of KCC2 seems critical for stabilization of KCC2 following high excitatory activity and activation of NMDA receptors thus delaying the onset of pharmacologically- induced SE.

- **KCC2 mutations in human epilepsy**

Based on these observations from mutant mice, mutations in the *Slc12a5* gene encoding KCC2 have long been expected to be associated with inherited forms of epilepsy. However, the first reports of *Slc12a5* mutations linked to epilepsy only appeared in 2014. A first study identified the KCC2-R952H variant that co-segregated in an Austalian family with febrile seizures (Puskarjov et al., 2014; Fig 10). This variant displayed reduced membrane expression in heterologous cells and reduced chloride extrusion capacity when over-expressed in immature cortical neurons.

This variant was also nearly simultaneously identified in a second study in a family with idiopathic generalized seizures, along with another variant KCC2-R1049C (Kahle et al., 2014; Fig 10). The later was likewise characterized by an impaired maintenance of chloride homeostasis but had a normal membrane expression.

Three further recessive loss-of-function mutations in the Slc12a5 gene were later identified in patients suffering from epilepsy of infancy with migrating focal seizures (Stödberg et al., 2015; Fig 10). All these mutations resulted in decreased membrane expression of the protein, reduced glycosylation and impaired mechanism of chloride extrusion. Finally, biallelic mutations of KCC2 that reduce chloride transport without affecting surface expression of the transporter were identified in patients with migrating focal seizures (Saitsu et al., 2016, Fig 10).

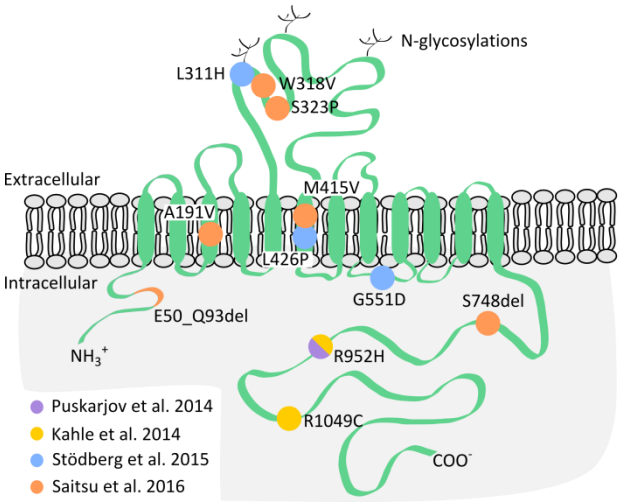

Mutation	Transport function	Membrane expression
R952H	Depolarized E_{GABA}	Decreased expression
R1049C	Depolarized E_{GABA}	Intact expression
L311H	Depolarized E_{GABA}	Decreased expression
L426P	Depolarized E_{GABA}	Decreased expression
G551D	Depolarized E_{GABA}	Decreased expression
E50_Q93del	Depolarized E_{GABA}	Intact expression
A191V	No changes in E_{GABA}	Intact expression
S323P	No changes in E_{GABA}	Intact expression
M415V	Depolarized E_{GABA}	Intact expression

Figure 10 : KCC2 mutations in epilepsy
Left, Overview of all variants and mutations described in the context of KCC2 and epilepsy with their localization. Note the diversity of residues affected. Right, Impact on KCC2 expression and function. Nearly all mutations impaired chloride homeostasis while only some of them were additionally associated with decreased membrane expression of the transporter.

Several conclusions may be drawn from the identification of these human mutations. First, contrasting with the drastic phenotype reported in knockout mice, the penetrance of these mutations was incomplete. Some of these variants were also reported in healthy controls (Kahle et al., 2014). Similarly, in the latest study (Saitsu et al., 2016), biallelic mutations of KCC2 were required for expression of the epileptic phenotype, while family members expressing only a single mutation did not suffer from epilepsy. Such observations dampen the hypothesis of direct causal link between KCC2 malfunction and epilepsy. In contrast, as often in epilepsy-related mutations, they suggest that mutations may represents susceptibility factors acting together with other environmental or genetic factors to promote epileptogenesis.

Second, it is worth noting that point mutations associated with epilepsy were identified in the NTD, but also in the transmembrane segment, the extracellular loop and the CTD of the protein. In particular, the identification of several mutations in the extracellular loop between TM5 and TM6 and inside TM6 pleads for an important role of these 2 regions in membrane expression and activity of KCC2. Overall, this suggests that a variety of mechanisms perhaps including conformational changes may be involved in regulating KCC2 expression and function.

Finally, whereas all identified mutations were characterized by impaired chloride extrusion, most of them also resulted in decreased membrane expression of the protein. KCC2 membrane expression and subsequent interaction with the actin cytoskeleton is critical for excitatory synapses maturation and maintenance. Hence, in addition to a deficit in the control of chloride homeostasis, patients expressing such mutations may also suffer from defects in glutamatergic synapse formation and maturation, which could then participate in the epileptic phenotype. In line with this idea, the KCC2-R952H variant was unable to rescue the aberrant spinogenesis in $KCC2^{-/-}$ neurons (Puskarjov et al., 2014).

c. Chloride homeostasis, GABA transmission and epilepsy

Well before KCC2 mutations were associated with inherited epilepsies, a pioneer series of experiments conducted by the team of Richard Miles shed new light on a possible role of KCC2 transport-function in the context of pharmacoresistant epilepsies.

Using hippocampal tissue resected from patients suffering pharmacoresistant temporal lobe epilepsy, they studied the pharmacology underlying the generation of spontaneous interictal activity in the subiculum (Cohen et al., 2002). Interictal events are short, spontaneous and recurrent bursts of activity that characterize an epileptic brain that can be recorded electrophysiologically but are clinically silent (refer to II.3.c for more details). As expected, the authors showed that interictal activity recorded *in vitro* from slices of human epileptic hippocampus was abolished by blockers of glutamatergic transmission. However, surprisingly, this was also the case with blockers of GABAergic transmission. Interestingly, some of the principal cells of the subiculum were excited during interictal events and displayed depolarizing responses to GABA. This led the authors to hypothesize that paradoxical excitatory GABA transmission may contribute to interictal activity. In a follow-up study, the authors revealed that

depolarizing, GABAAR-mediated currents partially correlated with a downregulation of KCC2, which was apparent in approximately 30% of the principal cells in the epileptic subiculum (Huberfeld et al., 2007; Fig 11). Restoring chloride homeostasis by blocking the chloride importer NKCC1 with bumetanide was then sufficient to suppress interictal activity.

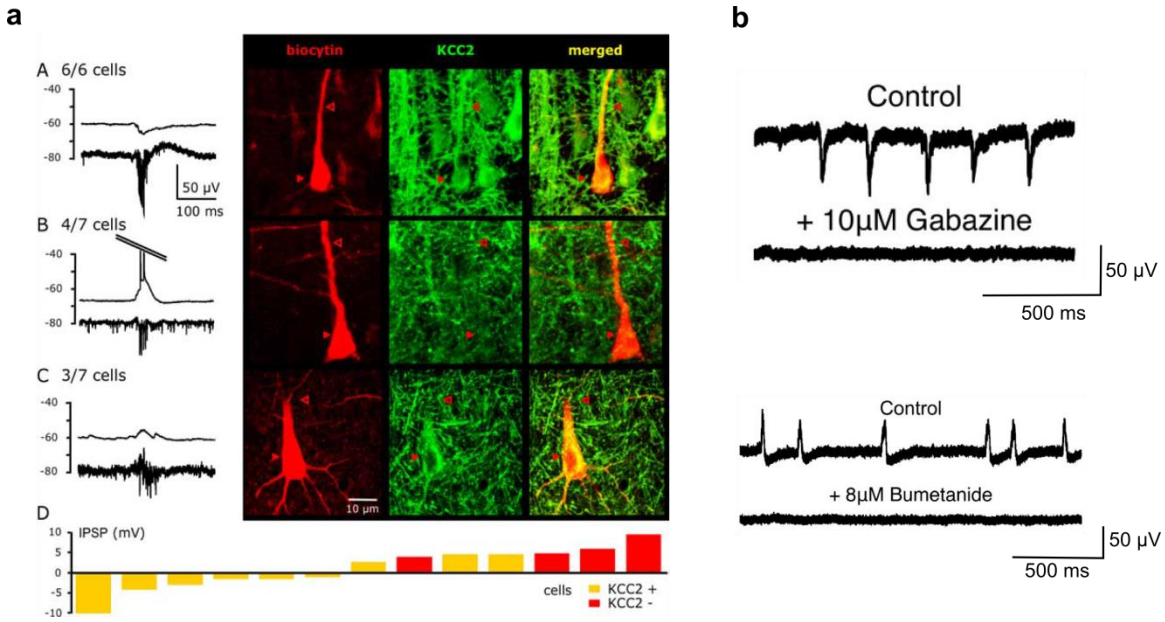

Figure 11 : Correlation between KCC2 expression, GABA transmission and interictal activities
(a) (A-C left) Simultaneous intracellular (top, thin traces) and extracellular (bottom, thick traces) recordings during interictal-like activity in resected hippocampus from a temporal lobe epilepsy patient. Immunostaining reveals the absence of KCC2 in 4 out of 7 recorded cells eliciting a depolarizing GABAergic transmission (A-C right). (D) Partial correlation between KCC2 protein expression and the polarity of GABAergic transmission (from Huberfeld et al, 2007). (b) In slices resected from patients with low-grade glioma, spontaneous interictal activity is suppressed by application of the GABAAR antagonist gabazine indicated an unexpected pro ictogenic action of GABA. Similar results were obtained by reducing intraneuronal chloride with the NKCC1 antagonist bumetanide. These results argue for a role of increased chloride concentration and subsequent depolarizing action of GABA in the appearance of interictal events (from Pallud et al. 2014)

Such a link between chloride homeostasis, GABA transmission and interictal activity is not limited to TLE patients. Indeed, a similar observation has recently been made in peri-tumoral human neocortex (Pallud et al., 2014). Low-grade glioma tissues spontaneously generate interictal activity *in vitro* that correlates with depolarizing GABA responses in some principal cells and can be abolished by bumetanide. It is worth noting that, in this study, bumetanide had no effect on either pre-ictal or ictal discharges. This may not be entirely surprising considering the different mechanisms leading to these different types of events. In fact, pre-ictal discharges have be shown to rely on glutamatergic transmission while interictal activity depends on both GABAergic and glutamatergic activity (Huberfeld et al., 2011).

In conclusion, the set of studies performed by the teams of Richard Miles and Gilles Huberfeld revealed an interesting correlation between the loss of KCC2 and the appearance of interictal activity in the epileptic brain. However, in the absence of control tissue, the specificity and thus physiological relevance of KCC2 downregulation remains unclear. It is also unclear whether the sole downregulation of KCC2 promotes interictal activity and whether it may contribute together with other factors to ictogenesis.

d. Transport-function of KCC2 and ictogenesis

In order to study the possible link between KCC2 expression and function and epilepsy, several teams took advantage of *in vitro* models of ictogenesis in slices, thus allowing easier use of pharmacology. Interictal and ictal events can be induced in both hippocampal and entorhinal cortex slices through a variety of models that all rely upon increased network excitability. Among the most commonly used models are an elevation of extracellular potassium levels (high $[K^+]_e$ model), a reduction in extracellular magnesium (0 Mg^{2+} model) or the blockade of potassium channels with 4-aminopyridine (4-AP model) or cesium (Cs-model). It should be noted that some models may themselves alter KCC2 activity and function. Indeed, as discussed above a high extracellular concentration of potassium could lead to reverse transport through KCC2 (cf I.2.a) while the 0 Mg^{2+} model will favor the activation of NMDA receptors thereby leading to destabilization of the transporter at the plasma membrane (see I.3.b).

- **KCC2 activity may aggravate pre-established ictal activity**

In a set of recently published papers, authors made the startling observation that pharmacological KCC2 blockade with the antagonists VU0240551 or furosemide nearly completely abolishes ictal activity in both piriform and entorhinal cortices in the 4-AP model (Hamidi et al., 2015; Hamidi and Avoli, 2015) and in hippocampal cortex in the Cs-model (Uwera et al., 2015). Conversely, potentiating KCC2 function with the newly identified drug CLP257 (Gagnon et al., 2013) increased the occurrence of ictal activity (Hamidi and Avoli, 2015). In contrast, interictal-like events were more frequent and of larger amplitude when KCC2 activity was blocked suggesting that impaired chloride homeostasis aggravates interictal activity. This is in line with previous observations in slices from human epileptic tissue where restoring chloride homeostasis by blocking NKCC1 activity suppresses interictal activity (Huberfeld et al., 2007;

Pallud et al., 2014). These results again highlight the different mechanisms underlying the emergence of ictal *vs.* interictal activity.

In order to understand this somewhat counterintuitive role of KCC2 in ictogenesis, it is worth noting that chloride accumulation and subsequent depolarizing GABA transmission play an important part in ictogenesis. Thus, in mouse hippocampal slices, ictal activity is preceded by an important firing of interneurons (Lillis et al., 2012). The resulting intense activation of GABAARs in pyramidal cells leads, at first, to intraneuronal chloride accumulation and, subsequently, to transiently depolarizing and excitatory GABAergic transmission. Hence, following ictal activity, interneurons can recruit and synchronize pyramidal neurons into clonic afterdischarges that maintain epileptiform activity (Ellender et al., 2014; Fig 12). Similar results were obtained in an *in vivo* model of optogenetic seizure induction in the cortex (Khoshkhoo et al., 2017). In this model, interneurons are rapidly recruited at the onset of the seizure, prior to principal cells. Inhibiting the interneurons once the seizure was established greatly reduced their duration, consistent with a transient excitatory action of GABA transmission during seizures. In these conditions, KCC2 activity may favor the increased excitability of the network. Indeed, following intense activation of GABAARs, KCC2 will be activated to cope with the increased $[Cl^-]_i$. This will be accompanied by a transient rise in the extracellular concentration of potassium, which, in turn, may act to further enhance neuronal excitability (Viitanen et al., 2010).

KCC2 function may however be important for the termination of an ictal event by promoting chloride extrusion back to basal concentration and restore hyperpolarizing GABA signaling. In line with this idea, pharmacological blockade of KCC2 with VU0463271, a more potent and specific antagonist of KCC2 function (Delpire et al., 2012), prolongs the duration of ictal activity in a 4-AP model in slices (Kelley et al., 2016). Furthermore, restoring chloride homeostasis using bumetanide in a kindling epilepsy model significantly reduced the duration and severity of induced seizures (Wang et al., 2017). Indeed, in slices, termination of ictal activity was accompanied by a recovery of hyperpolarizing GABA transmission (Ellender et al., 2014). Furthermore, KCC2 activity may be critical to maintain inhibitory GABAergic transmission in tissue surrounding the ictal tissue. This would be important to limit the spread of a seizure through inhibitory restraint (Trevelyan and Schevon, 2013).

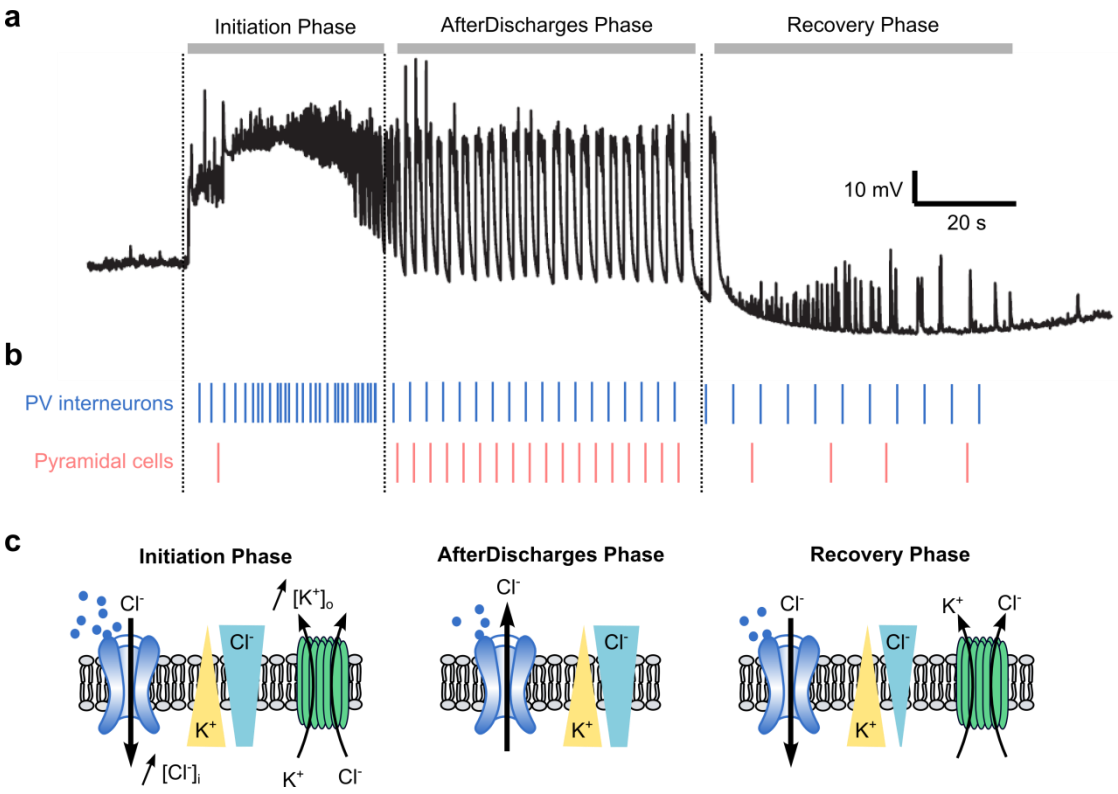

Figure 12 : Chloride homeostasis and KCC2 function during ictal phase
(a) Representative current-clamp recording from CA3 pyramidal neuron during epileptiform activity induced by 0 Mg^{2+} (adapted from Ellender et al. 2014).
(b,c) Firing pattern of PV interneurons and pyramidal cells during epileptiform activity (top) and suggested associated mechanism (bottom). During the initiation phase, interneurons massively fire thus leading to increased intraneuronal concentration. In turn, KCC2 activity generates extracellular potassium transients which increase neuronal excitability. During the afterdischarges phase, interneurons synchronize population of principal cells through depolarizing excitatory GABA-mediated currents. Finally, KCC2 activity allows recovery of low intraneuronal concentration and associated inhibitory action of GAB thus enabling termination of the epileptiform events. Model proposed based on Ellender et al. 2014, Viitanen et al. 2010, Khoshkhoo et al. 2017

Overall, the impact of KCC2 activity on pre-established ictal activity is mixed. Indeed, the activity of the transporter may facilitate the onset of seizures. Nevertheless, it could also favor termination of the event by enabling recovery of chloride concentration and may be necessary for inhibitory restraint preventing the spreading of the event.

- **Loss of KCC2 activity is not sufficient to trigger ictal activity**

A recent computational model claimed that KCC2 suppression in about 30% of principal cells was sufficient to trigger ictal activity in a modeled subicular network (Buchin et al., 2016). This model takes into account changes on GABA transmission as well as on extracellular potassium and subsequently on neuronal excitability. Nevertheless, the claim of a causal relationship between KCC2 suppression and ictal activity needs to be taken cautiously due to the high basal extracellular potassium concentration (8 mM) used by the authors in their model. Such

concentration is not quite physiological and results in increased excitability of the neurons, thus possibly priming the network to ictal activity. In addition, the model surprisingly lacks perisomatic inhibition - with all GABAergic synapses formed onto apical dendrites of principal cells - as well as GABAergic inhibition of interneurons. It is therefore difficult to extrapolate predictions from this model to the actual behavior of subicular (or any other) neuronal network.

Interestingly, in contrast to this computational study, complete pharmacological blockade of KCC2 in hippocampal slices was not sufficient to induce seizure-like events (Kelley et al., 2016) but reduced their latency in a 0 Mg^{2+} model (Sivakumaran et al., 2015). Similarly, massive chloride loading of pyramidal neurons using optogenetic tools induces a depolarizing shift in E_{GABA}, a hyperexcitability of the network and the appearance of high-frequency oscillations (HFOs) closely resembling those observed in the epileptic brain (see also II.3.c) but did not lead not full ictal activity (Alfonsa et al., 2015). Consistent with these observations, *in vivo* infusion of the KCC2 antagonist VU0463271 in the dorsal hippocampus of mice induces pathological epileptiform activity without ictal activity nor behavioral seizures (Sivakumaran et al., 2015). It should also be noted that this last study lacked important controls, including injections of vehicle (DMSO) only, which may be important considering the dose and volume of antagonist that was injected (0.5 µl, 100 µM, for an IC_{50} of 61 nM; Delpire et al., 2012).

All together, these data seriously dampens the hypothesis of a causal relationship of KCC2 downregulation in epilepsy through mechanisms solely involving control of chloride homeostasis. Additionally, they draw a special attention to a potential differential role of KCC2 function in the generation of interictal versus ictal events in the epileptic brain.

e. Is KCC2 downregulated in chronic epilepsy?

Since the demonstration that kindling induces a rapid decrease in KCC2 mRNA levels (Rivera et al., 2002), the idea of a downregulation of the protein in the epileptic brain has appeared as a consensus. Indeed, decreased KCC2 expression was reported in the hippocampus in a pilocarpine mouse model of epilepsy (Li et al., 2008) but also in the dentate gyrus in a kainate mouse model of TLE (Stamboulian-Platel et al., 2016). In human, similar observations were made in the subiculum of epileptic patients at both the RNA level (Palma et al., 2006) and the protein level (Huberfeld et al., 2007; Muñoz et al., 2007) as well as in peritumoral tissue of patients suffering from glioma (Pallud et al., 2014).

However, in contrast with these results, increase in KCC2 transcripts has been found in the inferior colliculus of a post-ischemic mouse model of audiogenic seizures (Reid et al. 2001). Most strikingly, a recent study also described an upregulation of KCC2 protein levels in the hippocampus of epileptic patients and of a pilocarpine mouse model of chronic epilepsy (Karlócai et al., 2016).

Two remarks could help solve this apparent discrepancy.
First, it is important to note the difference between seizure-induced downregulation of KCC2 and level of protein expression during the chronic phase of the pathology. Intense excitatory activity, which occurs for instance during SE, has been shown to induce rapid downregulation of KCC2 (see I.3.b). Thus, pilocarpine-induced SE leads to a rapid decrease of KCC2 expression accompanied by a depolarizing shift in reversal potential of GABAergic currents in dentate granule cells (Pathak et al., 2007), in all hippocampal subfields (Barmashenko et al., 2011) and in entorhinal cortex (Bragin et al., 2009). Similar decrease of KCC2 expression was also observed in mice in the subiculum following kindling (Wang et al., 2017). However, a return to control levels of KCC2 protein was observed during the chronic phase of epilepsy (Pathak et al., 2007).

Second, all the aforementioned studies indicating downregulation of KCC2 in human epileptic brain actually focused on epileptogenic regions (the subiculum and the peri-tumoral region). In particular, the decrease of mRNA levels of KCC2 in the subiculum was observed in comparison to the level measured in the rest of the hippocampus in the same patients (Palma et al., 2006) while the absence of KCC2 in about 20% of the principal cells was only observed in the subiculum and sclerotic CA1 but not in CA3 or the dentate gyrus (Muñoz et al., 2007). One could then argue that KCC2 downregulation in these regions may favor epileptic activity or, conversely, that these regions undergo frequent sustained excitatory activity which in turn downregulates KCC2.

In conclusion, the relationship between alteration of KCC2 expression and function, GABAergic transmission and epileptogenesis is not as straightforward as previously assumed. Data from both KCC2 knockout animal models and human mutations suggest a causal relationship between dysregulation of KCC2 and epilepsy. Notably, this effect could rely on alteration of both GABAergic transmission and glutamatergic synapse maturation. Furthermore, although complete blockade of KCC2-transport function seems pro-ictogenic *in vitro*, it now appears that these conditions are far from what actually happens in the epileptic brain. Indeed,

downregulation of KCC2 in the epileptic brain rather seems restricted to a small proportion of neurons located around the epileptic focus.

The hypothesis that KCC2 suppression upon a first seizure would, in turn, be sufficient to facilitate the emergence of further epileptic seizures remains to be demonstrated. The development of recent genetic tools allowing chronic suppression of KCC2 *in vivo* in an already mature brain (using viral-based ARN interference or viral expression of the Cre-recombinase in a floxed KCC2 mouse line) could help solve this query. In a recent publication, Chen and collaborators claimed that lentiviral-based suppression of KCC2 by ARN interference in the rat dentate gyrus was sufficient to induce seizures (L. Chen et al., 2017). This conclusion however needs to be taken cautiously since it is based only on 3 animals *vs.* 2 controls. Moreover, the authors reported spontaneous Racine stage III behavior (defined by unilateral forelimb clonus). However, they did not provide movie supporting this observation. Instead, they based their claim on short (< 1 second) abnormal activity observed in EEG recordings. Yet, classical Racine stage III seizures are usually lasting several seconds both at the behavioral and electrophysiological scale, as the authors themselves described in the first figure of the publication and in the supplementary video. Hence, the contribution of KCC2 regulation in the context of epilepsy clearly needs careful and unbiased examination.

6. Dysregulation of KCC2 expression and function in other pathologies

Given the critical implication of KCC2 expression and function in controlling GABA signaling as well as maturation, function and plasticity of glutamatergic synapses, it is not surprising that dysregulation of the transporter has now been implicated in a variety of neurological disorders beyond epilepsy.

a. Spasticity and neuropathic pain

Chronic pain and spasticity (hypertonia) are classical consequences of lesions affecting the sensory-motor system and the spinal cord. The sensory-motor system is severely affected in KCC2 knock-out mice which display severe motor deficits correlated with depolarizing responses to GABA and glycine in motoneurons of the ventral part of the spinal cord (Hübner et al., 2001).

Downregulation of KCC2 associated with a depolarizing action of GABA has been demonstrated in rodent spinal cord injury (SCI) models of chronic pain in spasticity. KCC2 downregulation is observed in both motoneurons in the case of spasticity (Boulenguez et al., 2010) and in neurons of the lamina I of the dorsal horn in chronic pain models (Coull et al., 2003), and appears to depend on the BDNF/TrkB pathway (Boulenguez et al., 2010).

A working hypothesis on neuropathic pain is based on the "gate control theory" which has been described in details in several reviews (Kaila et al., 2014; Price et al., 2005; Vinay and Jean-Xavier, 2008). Briefly, in basal conditions, nociceptive stimuli conducted by the pain-conductive C-fibers are gated by non-painful sensory inputs. Terminals of C-fibers are in fact contacted by GABAergic interneurons relaying tactile information from A-beta fibers, thus preventing transmission of the painful inputs to the CNS. Following SCI, the downregulation of KCC2 and subsequent effect on GABAergic signaling result in the loss of inhibition of neurons of the dorsal horn and in aberrant stimulation of pain-conducting fibers by tactile-conducting fibers, thus inducing hyperalgesia.

b. Psychiatric disorders

KCC2/NKCC1 imbalance has been suggested to be involved in several human neurological and psychiatric disorders characterized by perturbed network activity. Increased NKCC1 expression along with decreased KCC2 expression was observed in the brain of schizophrenic patients (Hyde et al., 2011; Kalkman, 2011) and suggested to contribute to autistic behavior (Lemonnier and Ben-Ari 2010). Quite consistently, dysregulated NKCC1 and KCC2 protein levels were found in the 22q11.2 deletion syndrome mouse model (Amin et al., 2017), a syndrome associated with higher risks for schizophrenia and autism. Low expression of KCC2 was also found in the cerebrospinal fluid (CSF) of Rett syndrome patients (Duarte et al., 2013). These results were paralleled by a decrease in KCC2 expression in MecP2 knockout mouse model of Rett syndrome (Banerjee et al., 2016). A recent study also described a reduced expression of KCC2 in the R6/2 mouse model of Huntington's disease (Dargaei et al., 2018). Finally, KCC2/NKCC1 imbalance was reported in Ts65Dn mouse model of Down's syndrome though it mainly relies on an upregulation of NKCC1 in this case (Deidda et al., 2015).

c. Therapeutic approaches in pathologies involving KCC2

Considering its major impact on GABAergic transmission, KCC2 is considered a promising therapeutic target, not only for the treatment of epilepsy but also in many of the aforementioned conditions. This idea was supported by *in vitro* studies demonstrating of positive effect of restoring chloride homeostasis on interictal activity in hippocampal slices from epileptic patients by blocking NKCC1 function (Huberfeld et al., 2007). Since then, a lot of emphasis has been put on the use of bumetanide as therapeutic treatment in pathologies with evidence for chloride homeostasis dysregulation. The fact that bumetanide is FDA-approved has certainly contributed to the interest for this compound.

The therapeutic potential of bumetanide was first illustrated by the team of Yezekhel Ben-Ari in autism (Lemonnier and Ben-Ari, 2010). In later work in rodents, the team showed that during delivery, maternal oxytocin release was suggested to lead to a transient hyperpolarizing shift in GABA responses in the fetal brain (Tyzio et al., 2006). This shift was not observed in fragile X and valproate models of autism due to KCC2 downregulation (Tyzio et al., 2014). Treatment of the dams with bumetanide to restore low intraneuronal chloride concentration was sufficient to attenuate autistic phenotype while inhibiting oxytocin signaling in wild-type dams triggered autistic characteristics in newborns (Tyzio et al., 2014). Intriguingly, this mechanism does not explain the beneficial effect of bumetanide in autistic children. In addition, the bioavailability of bumetanide in the brain is also debated, as bumetanide may not cross the blood brain barrier and may be >98% bound to plasmatic proteins (Brandt et al., 2010). Nevertheless, positive effects of bumetanide in autistic spectrum disorders is now well documented (Cellot and Cherubini, 2014; Grandgeorge et al., 2014; Lemonnier et al., 2012; Lemonnier and Ben-Ari, 2010).

Chronic treatments with bumetanide have now been shown to restore E_{GABA} in a Rett syndrome mouse model (Banerjee et al., 2016). Interestingly, it was also sufficient to rescue the cognitive deficits observed in both Down's syndrome (Deidda et al., 2015) and Huntington's disease (Dargaei et al., 2018), suggesting deficits underlying these disorders were primarily due to defects in chloride homeostasis and, likely, GABA signaling.

As promising as bumetanide currently appears, it may not fully rescue the phenotypes induced by the loss of KCC2 in many pathologies (Fig 13). Indeed, as described previously, in addition to

its transport function, KCC2 also plays a role in maturation, maintenance and plasticity of glutamatergic synapses in an ion transport-independent manner. Strategies aiming to restore KCC2 expression - not just function - may then prove advantageous. To this aim, a new stabilizer of KCC2, CLP 257, has been recently identified and proved to have a beneficial effects in the treatment of neuropathic pain (Gagnon et al., 2013). Prochlorperazine also increases KCC2 membrane expression and function and reduces spasticity after SCI (Liabeuf et al., 2017). 5-HT2A receptors have also been suggested as a potential therapeutic target in the treatment of spasticity following SCI since their stimulation leads to an increase in KCC2 expression (Bos et al., 2013). Finally, it was recently demonstrated that the insulin growth factor 1 (IGF-1) was sufficient to induce an upregulation of KCC2, which may explain some of the therapeutic effect of IGF-1 in the treatment of Rett syndrome (Tang et al., 2016).

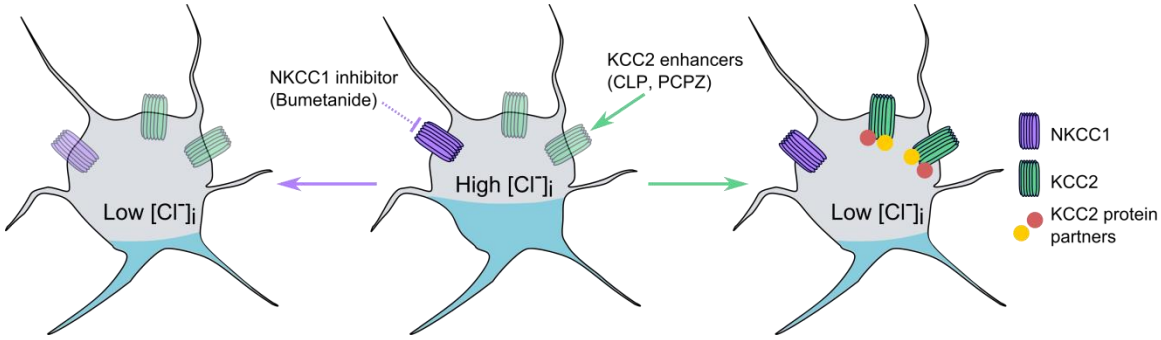

Figure 13 : Therapeutic strategies following KCC2 downregulation
In multiple pathologies, KCC2 is downregulated leading to increased intraneuronal chloride concentration and altered GABAergic transmission (middle). Two main therapeutic strategies are currently tested to rescue deficits induced by the loss of KCC2. In several studies, inhibiting the chloride importer NKCC1 with bumetanide restored GABAergic transmission as well as some of the pathological symptoms (left, Lemonnier and Ben-Ari 2010, Dargaei et al. 2018). In contrast, approaches aiming at enhancing KCC2 membrane stability or function have proven beneficial in spinal cord injury models (right, Gagnon et al. 2013, Liaboeuf et al, 2017). Notably, this strategy not only restores low intraneuronal concentration but also KCC2 interaction with protein partners.

In conclusion, suppression of KCC2 in a mature network triggers a variety of biological events affecting both GABAergic transmission through accumulation of intraneuronal chloride and glutamatergic transmission through structural changes at the dendritic spines. Whether such changes are sufficient to trigger the emergence of pathological, epileptiform activity remains unclear. Therefore, during my PhD, I asked how the multiple changes induced by the loss of KCC2 combined to affect hippocampal network dynamics. The following chapter of this manuscript will review the mechanisms leading to the emergence of various neural oscillations in the hippocampus, their physiological relevance and their alterations in the context of epilepsy.

II- THE HIPPOCAMPUS, A KEY STRUCTURE FOR COGNITION AND ITS INVOLVEMENT IN EPILEPSY

The hippocampus (HPC) is a structure located in the medial temporal lobe which belongs to the limbic system and has been extensively studied in the last 60 years. The case of Henry Molaison, (better known as patient H.M.) highly contributed to put the hippocampus in the spotlight for its key role in memory formation (Scoville and Milner, 1957). As a treatment to its intractable epilepsy, Henry Molaison underwent bilateral ablation of the hippocampal formation, following which he suffered from complete anterograde amnesia (that is the inability to form new memories). Since then, both the physiology and the circuitry of the HPC have been characterized in details, leading to several important breakthroughs such as the discovery of its role in spatial navigation (O'Keefe and Dostrovsky, 1971), the discovery of synaptic plasticity (Bliss and Lomo, 1973) or the importance of neural oscillations in cognition (Winson, 1978).

1. Overview of the hippocampal structure, connectivity and function

a. Anatomy and cellular physiology of the hippocampus

In mammals, the hippocampus is a highly conserved bilateral structure consisting of two interlocked folds of cortex, the *cornu Ammonis* (CA) which can be subdivided into areas CA1, CA2 and CA3, and the dentate gyrus (DG). Although the terminology varies among authors, the hippocampus *proper* usually refers to these four subregions. In a broader definition, the hippocampal formation also comprises the subiculum, the pre- and parasubiculum and the entorhinal cortex (Fig 14a). Here, I will focus on the anatomy and circuitry of the hippocampus *proper.* Since most of my PhD work focused on the dentate gyrus, I will put special emphasis on description of the properties of this region.

In contrast to the laminar organization of the neocortex, which consists of 5 or 6 layers, the HPC is a 3-layers structure referred to as 'archicortex'. Its configuration as well as its diversity in cell type and morphology was first thoroughly described by the original work of Santiago Ramón y Cajal (Cajal, 1909) and his student Rafael Lorente de Nó (Lorente De Nó, 1934). While in the

neocortex, principal cells are present in several different layers, the cell bodies of principal cells in the hippocampus are aligned in one thin layer (Fig 14b).

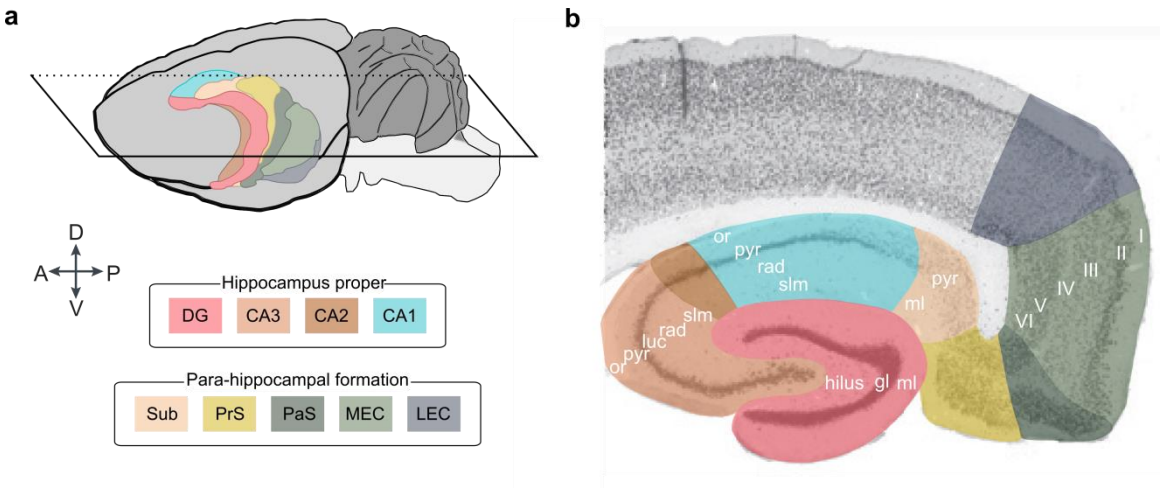

Figure 14 : Anatomy of the hippocampal formation
(a) Lateral view of the rat hippocampal formation inside the rodent brain. It consists of the hippocampus proper (DG; dentate gyrus; CA1-3, cornu ammonis 1-3); the subiculum (Sub), pre- and para-subiculum (PrS, PaS), medial (MEC) and lateral entorhinal cortices (LEC).
(b) Horizontal section of the area indicated by the plane on (a).
or, stratum oriens; pyr, pyramidal layer; luc, stratum lucidum; rad, stratum radiatum; slm, stratum lacunosum-moleculare; ml, molecular layer; gl, granular layer. The Roman numerals indicate cortical layers.
Adapted from (Strange et al., 2014; van Strien et al., 2009).

- **CA regions**

In the CA regions, principal cells are called pyramidal cells, due to the conic shape of their cell body. The layer formed by their somatas is the *stratum pyramidale*. Basal dendrites and most of axonal projections of pyramidal cells go through the deep, external layer called *stratum oriens,* while the apical dendrites extend within the *stratum radiatum.* The most superficial and internal part of the CA region is the *stratum lacunosum moleculare*. The lamination of the HPC is roughly similar in all the CA subregions with exception of an additional layer, the *stratum lucidum* above the pyramidal layer in CA3. Pyramidal cells of the hippocampus have long been considered as one homogenous population. However, several recent studies have revealed heterogeneity in both morphology and physiology between deep and superficial neurons of the CA1 region. This diversity leads to differential recruitment during oscillations and possibly a differential involvement in information processing (Danielson et al., 2016; Mizuseki et al., 2011; Valero et al., 2015).

- **The dentate gyrus**

The DG is a U-shaped structure formed of three layers: the *stratum moleculare* (most superficial), the *stratum granulosum* and the hilus. The principal cells of the DG are the dentate granule cells (GCs) whose cell bodies are densely packed in the *stratum granulosum*. GCs have a bipolar organization with spiny dendrites dispersed in the molecular layer while the axon emerges from the other pole and run through the hilus. Very sparse firing of the DG has been observed *in vivo* with only 10-20% of the cells active at a rate < 0.5 Hz while the animal is exploring its environment (Jung and McNaughton, 1993). It is likely that several intrinsic properties of the granule cells contribute to this low recruitment of the neurons. First, the resting membrane potential of GCs is particularly hyperpolarized (Spruston and Johnston, 1992). Although they possess a high membrane resistance, this is paralleled by a long time constant which reduces summation of synaptic inputs. Moreover, GCs display strong voltage attenuation of their inputs (Krueppel et al., 2011). Hence, GC recruitment requires large concomitant inputs due to a combination of membrane properties. Furthermore, GCs highly express a relatively rare type of GABAARs composed of $\alpha_4\beta\delta$ subunits (Chandra et al., 2006; Wei et al., 2003). These receptors are mostly located peri- and extra-synaptically and display a high affinity for GABA. Thus, they respond to ambient GABA and spillover from synapses and mediate strong tonic inhibition which further hinders GCs recruitment.

In rodents, the DG is one of the few regions able to undergo neurogenesis even in the adult brain, along with the subventricular zone and the olfactory bulb (Altman and Das, 1965). Neural stem cells are located at the limit of the hilus, in the subgranular zone of the DG (Eriksson et al., 1998). Consequently, there is a maturation gradient along the granule cell layer with older mature GCs located close to the molecular layer and newly generated GCs near the hilus. This ability of the DG to generate newborn GCs has been suggested to be essential for memory formation (Jessberger et al., 2009). However, the relevance of these observations in human is now debated since a recent study failed to detect hippocampal neurogenesis in the human adult brain (Sorrells et al., 2018).

Finally, the DG also contains a second type of excitatory glutamatergic cells : the mossy cells, which are located in the hilus.

- **Interneurons of the hippocampus**

While principal cells constitute approximately 80 to 90% of the hippocampal cells (Misgeld and Frotscher, 1986), the remaining 10-20% are GABAergic interneurons. In contrast to pyramidal cells which are restricted to the *stratum pyramidale,* interneurons can be found through all the layers of the hippocampus. GABAergic interneurons are extremely diverse with respect to their morphology, physiology, expression of neurochemical markers or axonal localization, which complicates their precise classification (Freund and Buzsáki, 1996; Parra et al., 1998; Somogyi and Klausberger, 2005)). Three main classes of interneurons can be distinguished based on their postsynaptic targets. First, some interneurons such as vasoactive intestinal peptide (VIP) positive interneurons show a particular specificity for targeting other GABAergic interneurons (Acsády et al., 1996). Principal cells, on the other hand, receive two main types of inhibitory inputs. Parvalbumin-containing (PV) and Cholecystokinin-expressing (CCK) interneurons mostly drive perisomatic inhibition while somatostatin-positive (SOM) interneurons – among others – mostly target dendritic compartments. This differential localization of inhibitory inputs has a profound effect on their functional role. Indeed, perisomatic inhibition effectively suppresses action potential firing while dendritic inhibition rather gates excitatory inputs by acting on dendritically generated calcium-mediated membrane depolarization (Miles et al., 1996).

Moreover, two main types of inhibition can be distinguished based on their circuitry. Hence, feedforward inhibition refers to the action of interneurons recruited by excitatory afferents on downstream neurons. This mechanism is thought to be essential to limit propagation of excitation and to temporally control spiking of principal cells. In contrast, feedback inhibition is a local recurrent network between principal cells and interneurons. Feedback perisomatic inhibition represents one of the system through which populations of principal cells can be synchronized. Therefore, as I will discuss in the second part of this chapter, it has been described as a key component favoring the emergence of rhythmic oscillations (see II.2.b-d).

b. Hippocampal intrinsic and extrinsic connectivity

- **The classical trisynaptic loop**

Unlike neocortical regions that mostly follow a reciprocal organization principle, the hippocampal network connectivity is mainly unidirectional. A simplified description of this circuit is the excitatory glutamatergic trisynaptic loop (Amaral and Witter, 1989; Andersen et al., 1971, 1966; Fig 15). The main input to the hippocampus originates from the layer II of the entorhinal cortex (EC) which connects onto the granule cells on the dentate gyrus through the perforant path (first synapse). Axons of the dentate granule cells, called mossy fibers, run through the hilus along the *stratum lucidum* where they contact CA3 pyramidal cells forming the second synapse (Claiborne et al., 1986). Finally, CA3 pyramidal cells project onto CA1 pyramidal cells apical dendrites through the Schaffer collaterals (Ishizuka et al., 1990). The loop is finally closed as the principal cells of CA1 connect to the deep layer V - VI of the entorhinal cortex either directly or through the subiculum (Köhler, 1986).

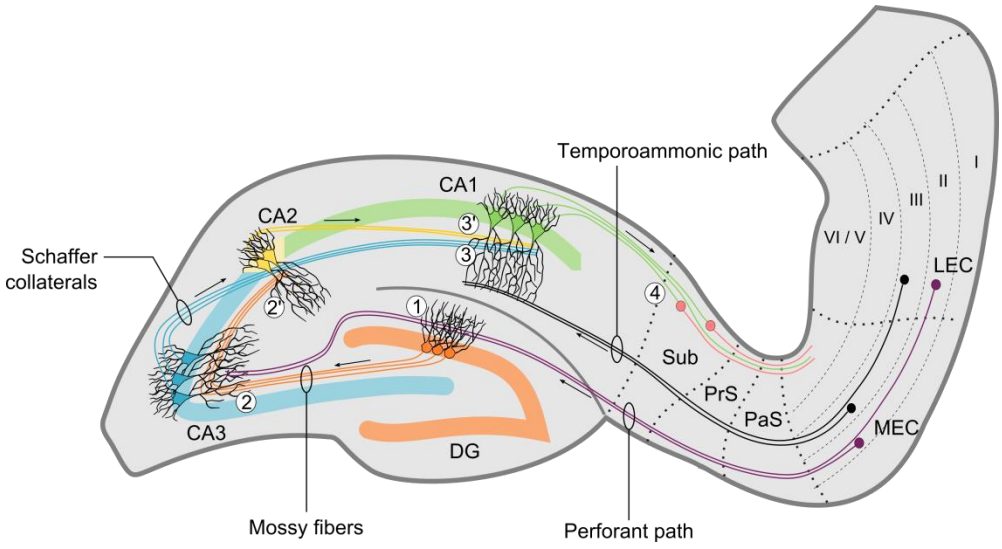

Figure 15 : Main intrinsic circuitry of the hippocampus. Horizontal section schema.
Representation of the classical trisynaptic loop :
The perforant path carries inputs from layer II entorhinal neurons (purple) to the DG (1). The DG projects to CA3 through the mossy fibers (2). Then CA3 pyramidal cells connect to CA1 region via the Schaffer collaterals (3). Finally, CA1 projects back to layers V/VI of the EC either directly or through the subiculum (4). Note the existence of an alternative loop through CA2 (2' and 3').
Note also the additional inputs from the entorhinal cortex with direct projections from layer III to CA1 via the temporoammonic path and connections from the perforant path to CA3.
CA1-3 cornu ammonis 1-3; DG dentate gyrus; Sub subiculum; PrS presubiculum; PaS parasubiculum; MEC, medial entorhinal cortex; LEC, lateral entorhinal cortex

During the last few years, the long-forgotten CA2 region started to be more extensively studied. A strong direct excitatory connection between CA2 and CA1 pyramidal cells was first identified (Chevaleyre and Siegelbaum, 2010). Later on, an optogenetic study revealed a direct synaptic connection from dentate granule cells onto CA2 principal cells (Kohara et al., 2014) leading to the idea of a secondary trisynaptic loop EC → DG → CA2 → CA1.

- **A more detailed view of the DG – CA3 network**

In addition to these two unidirectional circuits, a number of local interactions also regulate hippocampal activity through feedforward and feedback inhibition but also recurrent connections. I will here only focus on the circuits controlling activity in the DG and CA3 (Fig 16).

I previously mentioned that activity in the dentate gyrus is sparse due to a number of intrinsic properties of granule cells. Several networks characteristics also participate in setting this phenotype. Hence, both feedworard and feedback inhibition are strong in the DG (Freund and Buzsáki, 1996). Furthermore, dentate granule cells contact mossy cells of the hilus. Although mossy cells are glutamatergic neurons, the impact of their activation has been difficult to predict since they innervate both GABAergic interneurons of the DG and dentate granule cells (Buckmaster et al., 1996; Scharfman, 1995). A recent study described their role in both memory and epilepsy (Bui et al., 2018). The authors showed that optogenetic inhibition of mossy cells results in memory impairment in a spatial memory task while their activation in epileptic mice decreased the occurrence and duration of seizures. This suggests that the main output of mossy cells on dentate network is inhibitory through disynaptic inhibition. Finally, CA3 pyramidal cells project back onto mossy cells and dentate interneurons (Li et al., 1994) which ultimately results in inhibition of dentate granule cells (Scharfman, 1994).

The importance of feedforward inhibition is also evidenced at the DG – CA3 synapses. Indeed, mossy fiber terminals mostly contact CA3 interneurons (Acsády et al., 1998). Consequently, the main output of the DG onto CA3 is inhibitory. However, at high frequency (> 40 Hz), potentiation of mossy fibers terminals contacting CA3 pyramidal cells will favor their recruitment (Henze et al., 2002). Hence, only intense, repetitive dentate activity allows excitation of CA3 pyramidal neurons (Mori et al., 2007). CA3 region contains strong recurrent excitatory connectivity (Amaral and Witter, 1989). Thus, once pyramidal cells are recruited, amplification through recurrent connections allows the emergence of transient bursts of activity. These bursts are critical for the

emergence of synchronous activity such as ripples (see I.2.c) but may also favor mnesic processes such as pattern completion (see I.1.c).

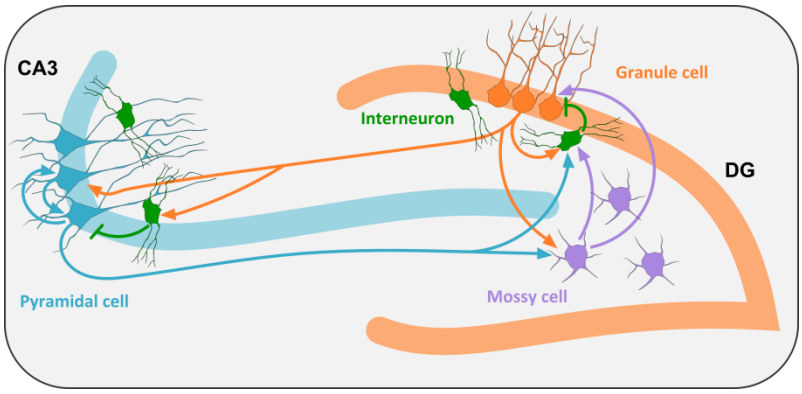

Figure 16 : Local connectivity in the DG - CA3 region
Various connections control the activity of the DG – CA3 region. While recurrent connections of CA3 region favor the emergence of bursts of activity, several mechanisms contribute to reduce network excitability. Hence, feedforward inhibition lowers recruitment of CA3 pyramidal cells while backprojections on hilar interneurons further silence dentate granule cells. Local circuitry in the hilus through mossy cells has more complex effect on DG activity since it mediates both direct excitation and disynaptic inhibition of granule cells.

The presence of such complex local networks forms the basis of specific activity patterns in each region. Moreover, it suggests a local processing of the information in individual hippocampal subfields in addition to its sequential treatment via the trisynaptic circuit.

- **Extrinsic hippocampal connectivity**

Although the perforant path represents the main afferent of the hippocampus, it is far from being the only one. It should first be noted that perforant path axons not only form synapses onto dentate granule cells but also onto CA3 pyramidal neurons (Yeckel and Berger, 1990). Furthermore, the layer III of the EC also projects directly onto the most distant part of the apical dendrites of CA1 through the temporoammonic path (Witter et al., 1988).

In addition to the inputs from the entorhinal cortex, the HPC receives modulatory afferents from many other cerebral structures among which cholinergic and GABAergic inputs from the medial septum, diagonal band of Broca (Freund and Antal, 1988; Swanson and Cowan, 1979) but also glutamatergic from the supramammillary nucleus (Haglund et al., 1984), noradrenergic from from the *locus coeruleus* (Jones and Moore, 1977), dopaminergic from the ventral tegmental area (Pasquier and Reinoso-Suarez, 1976) as well as serotoninergic from the raphe nuclei

(Moore and Halaris, 1975). All these afferents contribute to the fine tuning of hippocampal activity thereby influencing its function.

c. Linking physiology, connectivity and behavioral function

- **Different functions of ventral *vs.* dorsal hippocampus rely on distinct extrinsic connectivity**

Based on its internal circuitry, the HPC appears as a mostly homogenous structure. However, the extrinsic connectivity with the cortical and subcortical structures varies greatly along the dorso-ventral axis. In accordance with this observation, early lesions studies have suggested a differential role for dorsal and ventral hippocampus (Hughes, 1965; Stevens and Cowey, 1973). Thus, spatial learning impairment correlated tightly with the size of the lesion when it occurred in the dorsal hippocampus but was only mildly for lesions of the ventral hippocampus (Moser et al., 1993). In contrast, the ventral hippocampus controls the emotional behavior as ventral hippocampal lesions reduce anxiety in various unconditioned test (Kjelstrup et al., 2002; Pentkowski et al., 2006), an observation consistent with the more dense connectivity of the ventral hippocampus with the amygdala (Canteras and Swanson, 1992).
During my PhD, I only worked on dorsal hippocampus. Hence, from now on, I will only address the role of the dorsal hippocampus in episodic memory when referring to the cognitive functions of the HPC.

- **Subregion specific physiology of hippocampal network enables complementary functions in memory processes**

Episodic memory requires both the ability to distinguish between two relatively close contexts (pattern separation) and the capacity to interpolate from an incomplete set of information (pattern completion).

Sparse firing, such as that occurring in the DG (see I.1a), is considered to facilitate pattern separation by allowing recruitment of different subgroups of cells by similar incoming stimuli. Hence, the DG has long been hypothesized as the structure essential for pattern separation in the hippocampus (McNaughton and Morris, 1987) and several computational models have

supported this view (Treves et al., 2008). Indeed, *in vivo* recordings revealed that DG coding was strongly affected even by minimal modifications of the environmental cues (Leutgeb et al., 2007). Accordingly, alterations of the DG activity by suppression of the subunit NR1 of NMDARs resulted in impaired contextual memory (McHugh et al., 2007). Similarly, lesions of the DG induced by colchicine impair both contextual fear memory and drug-induced contextual place preference (Hernández-Rabaza et al., 2008).

In contrast, recurrent connectivity in the CA3 region is supposed to favor the emergence of an auto-associative network, thus enabling pattern completion. Indeed, CA3 cells maintain a rather stable spatial representation when small changes are made in the environment (Lee et al., 2004; Neunuebel and Knierim, 2014). Moreover, *in vitro* analysis of CA3 circuit revealed connectivity consistent with an auto-associative network (Guzman et al., 2016). Indeed, although the probability of connection between cells was low (1%), the efficacy of excitatory synapses was high. Thus, firing of one principal cell efficiently activates neuronal assemblies. Behaviorally, impairing CA3 activity by specific suppression of NMDARs led to impaired learning in the Morris water maze task specifically when part of cues are masked (Nakazawa et al., 2002). However, the view of CA3 as solely performing pattern completion seems simplistic and computational models suggested CA3 could perform both pattern completion for inputs of little intensity as well as pattern separation for inputs of higher intensity (Knierim and Zhang, 2012).

Finally, CA1 region receives inputs from both CA3 and the EC. It was hypothesized that these dual inputs onto CA1 would allow the region to compare sensory information (carried by EC afferents) to encoded memory (provided by CA3 afferents). Consequently, CA1 would act as a novelty detector. Indeed, the ability to perform novelty detection is impaired in rats upon disruption of the temporoammonic pathway (Vago and Kesner, 2008). Furthermore, in humans, CA1 activity correlates with match *vs.* mismatch detection (Duncan et al., 2012).

In conclusion, in a somewhat simplified view, the role of the DG can be ascribed to pattern separation in the HPC, while CA3 operates pattern completion and CA1 performs novelty detection.

d. Cellular substrate of memory in the hippocampus

A major advance in linking neuronal activity to hippocampal mnemonic function came from pioneer studies using *in vivo* recording techniques. This allowed identification of a most striking

feature of some neurons of the dorsal CA1 region of the HPC, namely their ability to discharge specifically when the animal is at a given location in the environment (O'Keefe and Dostrovsky, 1971). Consequently, such cells were called 'place cells' and their region of activity was named 'place field'. This particularity was suggested to form the basis for a 'cognitive map' that would support spatial memory (O'Keefe and Nadel, 1979). Although they were originally identified in the CA1 region, similar spatial selectivity was later found in both the CA3 region and the DG (Jung and McNaughton, 1993).

However, the HPC is not only involved in spatial memory but also in declarative memory, which is the conscious recollection of factual information and previous experience (Squire, 1986). Consistent with this more general function of HPC in memory, some hippocampal neurons respond specifically to sounds (Sakurai, 2002), odors (Eichenbaum et al., 1987), faces (Fried et al., 1997) but also to elapsed time (the 'time cells', MacDonald et al., 2011). Such observations prompted the team of David Tank to hypothesize that place cells are one example of a more general mechanism of task-relevant information encoding in the hippocampus (Aronov et al., 2017). To test this idea, they develop a task in which rats had to press a lever to manipulate sound along a continuous frequency axis and relieve it once a certain frequency was attained. To avoid misinterpreting 'time cells' as frequency cells, the task was rendered purely auditory by randomly varying the speed of sound streaming across trials. This paradigm revealed a complete mapping of the behavioral task with neurons displaying specificity to various sound frequencies in a manner closely resembling the characteristics of place cells. They also revealed that a same pyramidal neuron could both possess a spatial specificity and a sound specificity in two distinct tasks. Overall, this study suggests that similar hippocampal circuitry underlie various behavioral tasks and argue for a role of the hippocampus in all kind of attention-based tasks rather than spatial memory only.

In summary, the hippocampus is a structure highly connected with various cortical areas which play a key role in the formation and consolidation of episodic memory. Each hippocampal subregion shows specific connectivity and physiology which are believed to support the accomplishment of diverse mnemonic processes such as pattern separation in the DG, pattern completion in CA3 and novelty detection in CA1. The fundamental units of memory processing in the HPC are the principal cells, which display firing specificity relevant to the behavioral task.

How may memory be generated from sole neuronal activity ? Several types of neural oscillations can be recorded in the hippocampal formation. These network rhythmic activities are suggested to represent the link between unitary neural activity and cognition. Thus, in the following part, I will describe hippocampal rhythmic activities, how they participate in memory formation and consolidation and how they are affected in pathologies such as epilepsy.

2. Hippocampal oscillations and their behavioral correlates

a. In vivo electrophysiological recordings : what they are, what they say

Before describing the various neural oscillations in the hippocampus as well as their functional relevance, I will quickly introduce the concepts and methodology underlying this field of research.

Population activity in the brain is usually estimated through electrical measurements of local extracellular signals. When directly recorded in the brain, these signals are named *local field potentials* (LFP) in contrast to the term electroencephalogram (EEG) that is used for scalp recordings. Except for this distinction in the location of the probe, LFP and EEG fundamentally reflect the same concept (Fig 17a). The multiple ways through which neuronal activity contributes to the LFP have been expertly reviewed by Buzsáki and collaborators. They comprise mainly synaptic activity along with action potentials. However, other parameters such as calcium spikes, intrinsic currents or gap junctions also participate although to a lesser extent (Buzsáki et al., 2012).

An important notion in studying LFP is the distinction between sinks and sources. Influx of cations from the extracellular medium to the intraneuronal compartment - such as excitatory synaptic currents, for instance - gives rise to an extracellular *sink*. In order to maintain electroneutrality, such a sink is accompanied by an opposing flow of ions in the close vicinity, thus generating an extracellular *source* and creating an electrical dipole (Fig 17b). In the hippocampus, the laminar organization of the principal cells allow for the alignment of these various dipoles and the summation of the currents leading to the high magnitude of recorded LFPs as compared to other brain structures (Förster et al., 2006).

Another important property of the electrical field is that it can be *volume conducted*, thus leading to recording of potentials far away from their sources. The use of linear probes and current source density (CSD) analysis allow to distinguish the effect of volume conduction and to detect the location of sinks and sources accurately.

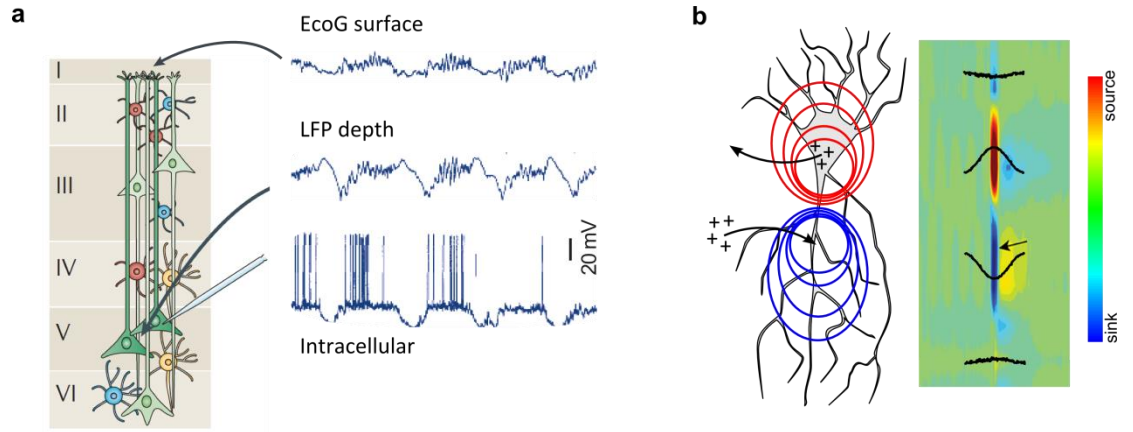

Figure 17 : LFP recordings and CSD analysis
(a) Simultaneous EcoG recording, LFP recordings from layer 5 of the visual cortex and intracellular recording from a layer-5 neuron in an anesthetized cat. EcoG recordings, LFP and intracellular recordings basically represent the same activity. Note that the bursts of firing of the neuron correspond to high frequency oscillations of both LFP and EcoG.
(b) CSD analysis allows identification of charges fluxes. Left : entrance of positive charges in the neuron forms a current *sink* compensated by an outward flow of charges, the current *source*. Blue and red lines represent isopotential lines (respectively negative and positive). Note that in proximity to the *sink* and *source*, potential varies quickly thus creating important variations in the CSD. Right : CSD signal corresponding to the charge fluxes represented in left. CSD is represented both by its value (black line) and by a color code.
Adapted from Buzsaki et al. 2012

Identifying sinks and sources however is not sufficient to provide direct information on neuronal activity. Indeed, dendritic excitation and somatic inhibition result in similar flow of currents hence displaying similar CSD maps. Discriminating between the two situations requires access to individual neuronal firing that can be achieved using tetrode recordings. This technique allows for subsequent spike clustering (Harris et al., 2000) and putative neuronal identification based on intrinsic properties such as frequency of firing, or action potential width (Barthó et al., 2004). Correlating firing of the different neuronal types with CSD analysis then allows differentiating between dendritic excitation and somatic inhibition.

b. Theta rhythm and memory encoding

During active exploration as well as rapid eye movement sleep (REM), the hippocampal LFP displays a regular oscillation at approximatively 8 Hz, called *theta rhythm* (Vanderwolf, 1969).

This oscillation is of largest amplitude in the *stratum lacunosum moleculare* and its phase reverses progressively across the layers. Before describing the mechanisms underlying theta oscillations in the hippocampus, it should be noted that this rhythm is not restricted to the hippocampus but is observed in several cortical structures (Steriade, 2000).

- **Mechanisms of theta generation**

Since lesions of the medial septum - diagonal band of Broca (MS-DBB) were shown to consistently abolish theta oscillations in all cortical structures (Petsche et al., 1962), the MS-DBB has long been considered as the main pacemaker of theta rhythm in the brain through its cholinergic and GABAergic afferents. In contrast to what have been shown in urethane-anesthetized animals, however, blockade of cholinergic transmission failed to suppress hippocampal theta in awake rats (Kramis et al., 1975). This indicates the existence of two types of theta-generating mechanisms, one visible under anesthesia and depending on cholinergic inputs from the MS-DBB ('atropine sensitive theta') while the other also requires GABAergic but not cholinergic transmission from the MS-DBB ('atropine resistant theta'). Since atropine-sensitive theta is mainly observed under anesthesia, I will rather focus on the mechanisms underlying the generation of atropine-resistant theta.

CSD analysis of theta oscillations reveals the presence of two distinct sources of currents in the *stratum pyramidale* and at the border between the *stratum radiatum* and the *stratum lacunosum moleculare* (Kamondi et al., 1998; Fig 18a). Based on this observation, a classical model of theta generation was proposed relying only on extrinsic afferents to the HPC (Buzsáki, 2002). In this model, the MS-DBB provides rhythmic inputs onto CA1 pyramidal cells through feedforward inhibition mediated by perisomatic interneurons. Concomitantly, the entorhinal cortex, which is known to also oscillate at theta frequency (Mitchell and Ranck, 1980), excites apical dendrites of the principal cells through the temporoammonic path (Fig 18b).

However, the idea of theta as a rhythm entirely generated outside of the HPC is now being challenged since theta oscillations can also spontaneously arise from intact hippocampal preparations *in vitro* (Goutagny et al., 2009). This preparation allowed identification of CA3 as an additional current generator for theta. The same group later took advantage of this intact hippocampal preparation to study in more detail the contribution of different types of interneurons to theta generation (Amilhon et al., 2015). They evidenced that PV interneurons are critical for the establishment of theta oscillations. In contrast, SOM interneurons activity

only affected theta when entorhinal afferents were stimulated. This suggests that SOM interneurons are mainly involved in gating entorhinal inputs. Finally, the picture is further complicated by the observation that activation of PV interneurons triggered theta frequency spiking (resonance) of pyramidal neurons (Stark et al., 2013), a characteristic driven by post-inhibitory rebound mediated by I_h conductance. Hence, CA1 pyramidal can also participate directly in the generation of theta oscillations.

Given the mechanisms that we just reviewed, it is not surprising that theta oscillations strongly modulate the firing of hippocampal cells. Hence, pyramidal cells preferentially discharge at the trough of the oscillation, whereas the various hippocampal interneurons display different preferred phases of firing depending on their type (Klausberger and Somogyi, 2008). In particular, PV interneurons discharge mostly at the peak of the oscillation, in alternation with pyramidal cells, while SOM interneurons are active at the trough (Figure 18c).

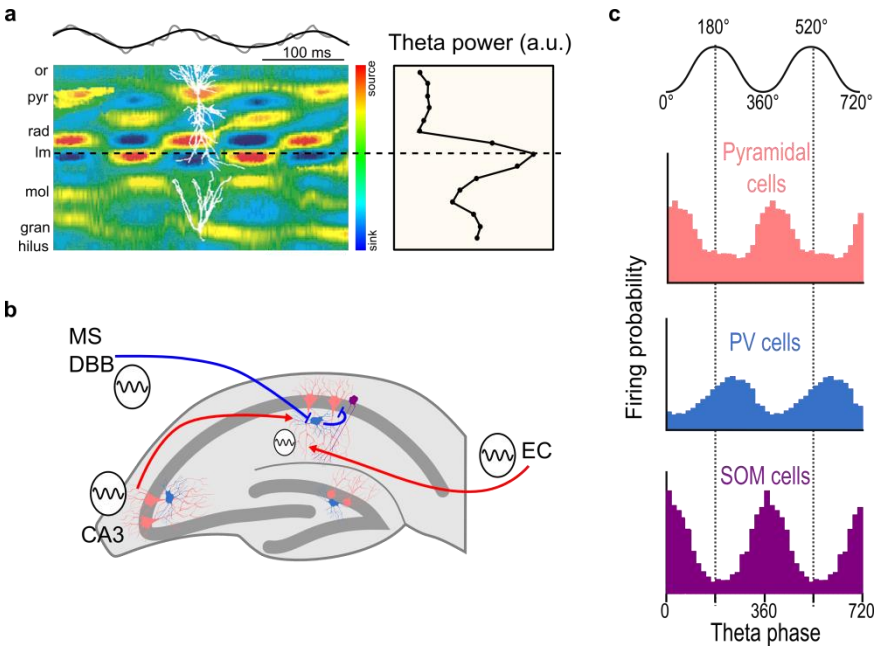

Figure 18 : Theta rhythm in the hippocampus
(a) Left : CSD profile across 3 cycles of oscillations revealing alternation of sink and sources in each layer. Right : Theta power is maximum in the stratum lacunosum moleculare. Adapted from Kamondi et al. 1998, Bragin et al. 1995
or : stratum oriens, pyr : stratum pyramidale, rad : stratum radiatum, lm : stratum lacunosum molecular, mol : stratum moleculare, gran : stratum granulare
(b) Theta is generated in CA1 through multiple inputs. The MS-DBB, the entorhinal cortex and the area CA3 are all theta generators. Additionally, CA1 pyramidal neurons display theta-frequency resonance.
(c) Different types of neurons discharge at various phases of theta cycle. Adapted from Klausberger and Somogyi 2008.

In summary, although the mechanisms underlying theta generation in the hippocampus are not fully understood yet, they clearly involve a delicate combination of extrinsic afferents as well as

internal properties of hippocampal cells and connections. Ultimately, theta oscillations arise from the rhythmic alternation of excitation and inhibition at different sites of pyramidal cells' dendritic tree. Consequently, regulation of theta activity necessitates a tight control of both excitatory and inhibitory transmission.

- **Function of theta oscillations**

The functional relevance of these theta oscillations in the process of memory formation has been suggested for a long time. Indeed, long-term potentiation of hippocampal synapses could be preferentially induced through stimulations at the theta frequency (Huerta and Lisman, 1993; Larson et al., 1986). Accordingly, several studies aiming to impair hippocampal theta oscillations also revealed memory deficits (McNaughton et al., 2006; Mitchell et al., 1982; Mizumori et al., 1990 among others). Further publications revealed that theta oscillations are critical for the formation of relevant neuronal ensembles. Thus, as an animal explores its environment, neurons fire sequentially as the animal enters their firing field, thereby creating a behavioral sequence of firing. Strikingly, similar sequences are compressed within each theta cycle, allowing simultaneous representation of past, present and future position of the animal in a few milliseconds timeframe (Skaggs et al., 1996). Such time compression was proposed to favor mechanisms of synaptic plasticity and to allow memory encoding of current experience. Indeed, altering theta sequences severely impaired spatial memory without affecting the specificity of place fields (Robbe and Buzsáki, 2009).

c. Sharp-Waves Ripples and memory consolidation

During periods of slow wave sleep as well as during quiet wakefulness, hippocampal LFP switches from theta to large amplitude irregular activity, characterized by the sporadic occurrence (0.01 - 3 per second) of transient field events called '*sharp wave-ripples'* (SPW-Rs, Buzsáki, 1986; Ylinen et al., 1995) in the CA1 region.

- **Mechanisms of SPW-Rs generation**

Sharp waves typically last 50 to 150 milliseconds. They show maximal amplitude in the *stratum radiatum* and reverse in the pyramidal layer. They arise from the transient bursts of collective firing in CA3 permitted by the high recurrent connectivity of this region (see II.1.b). This leads to

the massive depolarization of apical dendrites of CA1 pyramidal cells upon activation of Schaffer collateral inputs (Buzsáki et al., 1992). Concomitant to the sharp wave, a brief (50-150 ms) high-frequency (120-250Hz) oscillatory event can be observed in the pyramidal layer and is called a *ripple* (Fig 19a).

Activity in the hippocampus was shown to increase several-fold during SPW-R events (Csicsvari et al., 2000) with approximately 10 to 15% neurons emitting an action potential during the SPW-R (Buzsáki et al., 1992; Ellender et al., 2010). Interestingly, pyramidal neurons recruited during the event only fired at 10 Hz, thus usually generating a single action potential per ripple (Ylinen et al., 1995). In contrast, interneurons discharged at a frequency similar to the ripple. CSD analysis also revealed a rhythmic source of current located at the border between the *stratum pyramidale* and the *stratum radiatum* (Stark et al., 2014; Ylinen et al., 1995). Altogether, these observations led to the following model of ripple generation. At first, abundant recurrent connections in CA3 favor the emergence of intense bursts of activity in this region. In turn, interneurons are massively recruited and start firing at ripple frequency due to both their intrinsic properties and their reciprocal connections (Ellender et al., 2010; Schlingloff et al., 2014). Finally, the rhythmic activity of interneurons defines precise temporal window during which pyramidal cells can fire (Ylinen et al., 1995; Ellender et al. 2010). This model of ripple generation was mainly established based on *in vitro* experiments in the CA3 region (Ellender et al., 2010; Schlingoff et al., 2014). However, it is known that ripples in CA1 are not directly transferred from upstream regions but rather emerge from a local mechanism (Csicsvari et al., 2000; Sullivan et al., 2011). Based on the *in vitro* data in CA3, and the CSD analysis in CA1, perisomatic-targeting interneurons in the CA1 region were assumed to be directly excited by the depolarization of the sharp-wave and oscillate at ripple frequency due to reciprocal connections. However, optogenetic *in vivo* experiments revealed that small depolarization of CA1 pyramidal neurons was sufficient to trigger ripples. In contrast, rhythmic activation of interneurons while inhibiting pyramidal cells failed to generate ripples (Stark et al., 2014). This indicats that ripples in CA1 necessitate an initial activity of pyramidal neurons followed by massive recruitment of interneurons. The subsequent feedback loop, combined to reciprocal connections between interneurons, would finally generate ripples (Fig 19b).

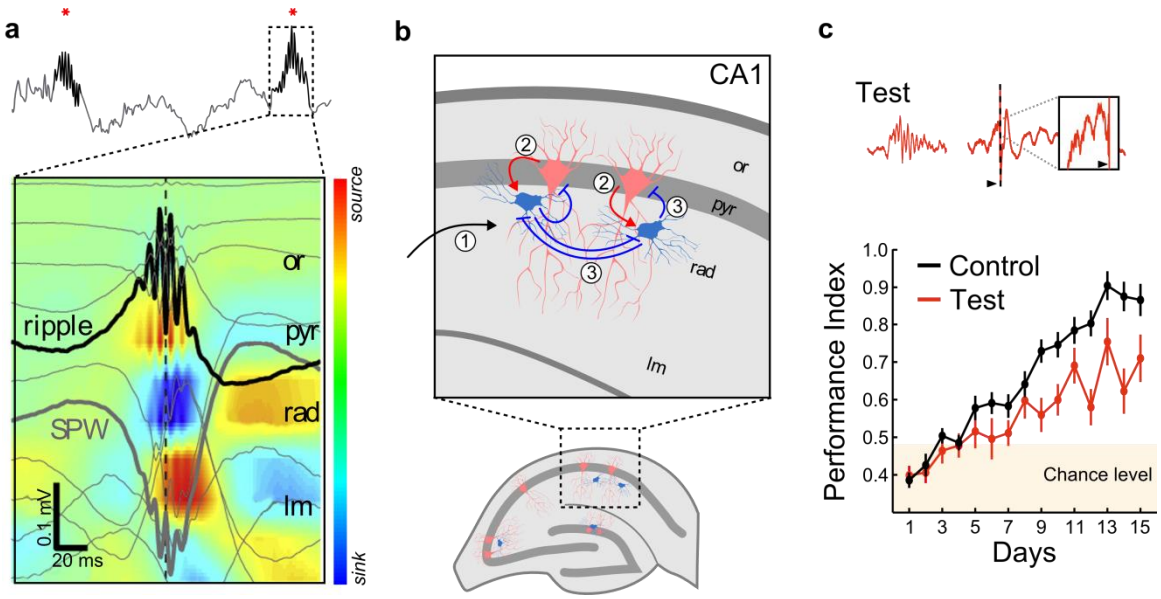

Figure 19 : Hippocampal ripples and their function

(a) Hippocampal LFP recorded in CA1 stratum pyramidale during sleep (Top, stars indicate ripples) and depth profile of a sharp-wave ripples superimposed on CSD map of the same events (bottom). Note the large sink in radiatum (sharp wave) and the fast alternation between sinks and sources in the pyramidal layer (ripple).

(b) Sharp waves in stratum radiatum reflect massive excitation of CA1 neurons by CA3 pyramidal cells via Schaffer collaterals (1). Activated CA1 pyramidal neurons (2) recruit interconnected network of interneurons (3) which synchronize at ~200Hz and control pyramidal cell firing through feedback inhibition thus generating a ripple in the pyramidal layer.

(c) Electrical stimulations during ripples effectively disrupt the ongoing oscillation (top) and subsequently impair spatial learning (bottom). Adapted from Girardeau et al. 2009

or : stratum oriens, pyr : stratum pyramidale, rad : stratum radiatum, lm : stratum lacunosum moleculare

- **Functions of SPW-Rs in memory**

Sleep SPW-Rs have long been suggested to play a critical role in memory consolidation (Fig 19c). Indeed they have been associated with the reactivation of spike sequences relevant to previous waking experiences in multiple studies (Kudrimoti et al., 1999; Lee and Wilson, 2002; Nádasdy et al., 1999; Wilson and McNaughton, 1994). First direct evidence for a causal role of SPW-Rs in memory came from two near-simultaneous studies (Ego-Stengel and Wilson, 2010; Girardeau et al., 2009). In both studies, animals were trained to complex spatial memory task over several consecutive days. Following each training sessions, animals were allowed to rest and ripples were detected online and subsequently suppressed by closed-loop electrical stimulations. Ripple disruption resulted in impaired learning, an effect which could not be attributed to the electrical stimulation only since delayed stimulations did not affect animal performance (Girardeau et al., 2009).

SPW-Rs also occur during waking in periods of immobility where they also coincide with reactivation of spike sequences (Diba and Buzsáki, 2007; Foster and Wilson, 2006). Interestingly, these reactivations usually occur in similar order as in behavior when happening at the beginning of a run (they are then called *forward replay*) but also in reverse order when occurring at the end of the run (*reverse replay*) (Diba and Buzsáki, 2007). Thus, it was suggested that forward replay could be associated to planning of the behavior and memory retrieval while reverse replay would be more linked to memory encoding. Similar to what was observed during sleep, electrical suppression of awake ripples impaired learning in a spatial memory task. However, the underlying mechanism of memory consolidation through ripple activity could be different during waking and sleep. Indeed, while sleep ripples may promote memory consolidation by favoring transfer of information to the neocortex (Maingret et al., 2016), awake ripples may rather favor the stabilization of spatial maps (Roux et al., 2017).

d. Gamma oscillations : not one but two distinct oscillations

The term *gamma oscillations* points to activities in a large frequency band ranging from 25 to 100 Hz. Activities in the whole range of gamma frequencies are observed in the hippocampus during both exploration and sleep (Bragin et al., 1995a). However, the amplitude of gamma oscillations is usually higher during waking and has therefore been better studied during that phase. Thus, I will solely focus on gamma during exploration.

- **Mechanisms of gamma generation in the HPC**

For a long time, gamma oscillations were analyzed as one unique rhythm in the HPC. CSD analysis first suggested the presence of two distinct generators, one in the DG that required an excitatory drive from the EC and another in CA3 that would entrain oscillations in CA1 (Csicsvari et al., 2003). However, this study assumed that these two generators triggered similar oscillations. In a groundbreaking study, Laura Colgin and colleagues demonstrated for the first time a clear distinction between slow (25-55 Hz) and fast (60-100 Hz) gamma (Colgin et al., 2009). Although both types of gamma activity are observed in the HPC in general and in CA1 in particular, they emerge from different pathways and rarely appear simultaneously. Hence, slow gamma in CA1 is directly entrained by CA3 afferents while fast gamma is generated by inputs from the medial EC.

Fast-spiking interneurons have long been hypothesized to be the key regulators of gamma oscillations due to their ability to discharge at gamma frequencies. Indeed, computational models suggest that gamma oscillations can arise from distinct mechanisms, both involving fast-spiking perisomatic inhibition (Whittington et al., 2000). The first proposed mechanism relies on an excitatory drive which recruits a feedback loop between interneurons and principal cells. This model has been called Pyramidal Interneuron Network of Gamma (PING). The second model depends only on interneuron activity and has thus been named Interneuron Network of Gamma (ING). It suggests that gamma oscillations arise from reciprocal connections between interneurons and subsequent rhythmic inhibition of principal cells (Fig 20a). Early *in vitro* studies on slices strongly argue for the PING model as carbachol-induced gamma oscillations required both PV interneurons and pyramidal cells activity (Fisahn, 2005; Gulyás et al., 2010). However, most recent *in vivo* studies suggest that, whereas slow gamma emerge from PING model, fast gamma is rather generated focally through an ING model (Lasztóczi and Klausberger, 2014; Strüber et al., 2017).

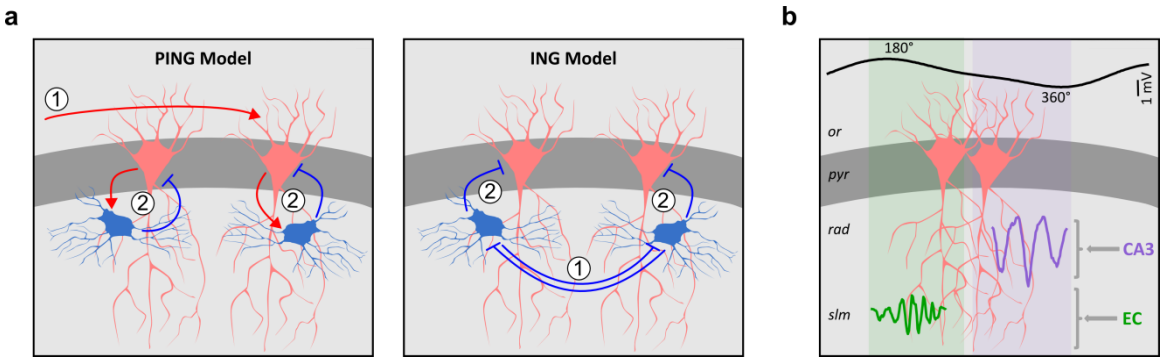

Figure 20 : Mechanisms of gamma oscillations and coupling to theta
(a) Gamma oscillations can arise through two distinct mechanisms. In the Pyramidal Interneuron Network of Gamma (PING), an excitatory drive is necessary to recruit a feedback loop between interneuron and principal cells. In contrast, in the Interneuron Network of Gamma (ING), oscillation emerges from reciprocally connected interneurons without requiring excitatory activity. PING model has been shown to underlie *in vitro* gamma and *in vivo* slow gamma while ING model explains fast gamma activity *in vivo.*
(b) In CA1, slow and fast gamma emerge from distinct afferents and couple differentially to theta. Hence, slow gamma (purple) is driven by CA3 and occurs at the trough of theta oscillation. In contrast, fast gamma (green) is generated by entorhinal inputs at the peak of theta. Adapted from Schomburg et al. 2014

One particularity of gamma oscillations is their coupling to theta rhythm. This means that gamma oscillations are not homogeneous across one theta cycle but instead preferentially appear with a specific phase with respect to the theta oscillation. Interestingly, both slow and fast gamma display a strong theta-phase coupling (Belluscio et al., 2012) although the actual coupling phase differs depending on the type of gamma. Thus, slow gamma is coupled to

descending phases of theta cycles while fast gamma emerges mostly at the troughs of theta cycles (Colgin et al., 2009; Schomburg et al., 2014; Fig 20b).

- **Functions of gamma oscillations in memory**

Since the identification of different types of gamma oscillations, attempts have been made to assign each rhythm with a specific role in memory. Advances towards this goal have been made through the study of how spike sequences are organized inside gamma oscillations. Indeed, two separate studies indicated that sequences during slow gamma reflected upcoming trajectories (Bieri et al., 2014; Zheng et al., 2016) as if the animal was planning its movement. Hence, this prospective coding during slow gamma suggested a role for memory retrieval. Consistent with this hypothesis, theta - slow gamma coupling increases in CA3 during retrieval (Tort et al., 2009). In contrast, the same studies showed that spike sequences during fast gamma rather represent past trajectories through retrospective coding, indicating a role in memory encoding.

However, other studies suggested different roles for both slow and fast gamma. Indeed, transient burst of fast gamma synchrony between CA1 and the EC appeared before correct choices in a working memory task, indicating a role of fast gamma in working memory rather than encoding (Yamamoto et al., 2014). Furthermore, pyramidal cells phase locking to slow gamma increases in relation with novelty but not during memory retrieval (Kitanishi et al., 2015). Hence, the specific functions of slow and fast gamma in memory processes still need to be clarified.

e. Dentate Spikes, the poor parent of hippocampal rhythms

More than 20 years ago, Bragin and colleagues described for the first time a novel population pattern arising specifically in the dentate gyrus of sleeping or immobile rats (Bragin et al., 1995b). They reported transient (< 30 ms), large amplitude positive deflections of the LFP associated with a decrease in the firing of CA3 pyramidal cells. CSD analysis indicated two types of DSs, both with a large sink in the molecular layer suggesting these events are triggered by entorhinal afferents through the perforant path (Fig 21a). Type-I DS had a sink in the outer molecular layer and e presumably triggered by lateral EC afferents while type-II DS displayed a sink in the inner molecular layer suggesting they resulted from medial EC activity. Consistently with this hypothesis, lesions of the entorhinal cortex led to complete disruption of the DS.

Further studies confirmed that dentate granule cells were depolarized and recruited during dentate spikes (Penttonen et al., 1997) and that stimulations of the perforant path would lead to similar population patterns (Braham, 1998). Thus, DS seem to arise from a transient increase in the excitatory drive from the entorhinal cortex to the DG.

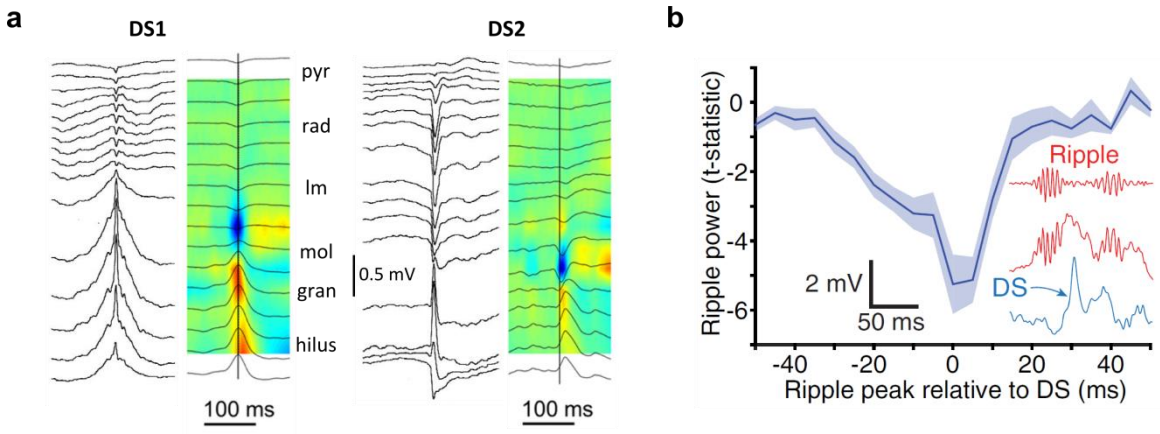

Figure 21 : Dentate spikes generation and their relationship to ripples
(a) Example traces and associated CSD profile of the two types of dentate spikes. Type I DS (left) display a sink in the outer molecular layer indicated they are generated by lateral entorhinal afferents. In contrast, type II DS (right) emerge from medial entorhinal inputs as evidenced by the localization of the sink close to the granular layer. Adapted from Bragin et al. 1995 and Laurent et al. 2015.
pyr : stratum pyramidale, rad : stratum radiatum, lm : stratum lacunosum molecular, mol : stratum molecular, gran : stratum granulare
(b) Dentate spikes influence downstream hippocampal activity. In particular, ripples occurring in close proximity to dentate spikes present reduced power. Adapted from Headley et al. 2017

Following this first set of publications, very little attention was given to the dentate spikes, their genesis or their physiological relevance. In 2013, a computational study revealed that LFP profiles similar to DS could be generated by the sole excitatory activity of the perforant path on the DG due to the particular U-shaped configuration of this region (Fernández-Ruiz et al., 2013). Although this study confirmed the hypothesis that DS emerge from brief burst of activity in the entorhinal cortex, it did not shed much light on their function. However, two studies published last year started to address this issue. The first one examined the relationship between DS and other patterns of activity appearing during sleep such as SPW-R (Headley et al., 2017). It demonstrated a clear interaction between DS and SPW-R. DS usually closely followed ripples. However, ripples preceded by a DS were of smaller amplitude (Fig 21b). Additionally, the authors reported increased gamma coherence across cortical regions specifically around the timing of DS. Although the functional impact of all these observations is not clear yet, it suggests that dentate spikes may participate in some way in the process of memory consolidation occurring during sleep. In accordance with this hypothesis, a second study showed that electrical

stimulations of the hippocampus during sleep retarded associative learning when precisely targeted at dentate spikes (Nokia et al., 2017).

In conclusion, oscillatory patterns in the hippocampus vary considerably depending on behavioral states. During exploratory behavior as well as REM sleep, the dominant oscillation is the theta rhythm along with superimposed gamma oscillations. In contrast, during slow-wave sleep, the hippocampal activity is mainly characterized by two transient events : the sharp wave - ripples in the CA fields and the dentate spikes in the DG. Except dentate spikes, which seem mostly dependent on glutamatergic inputs from the perforant path onto dentate granule cells, all others rhythms rely on a tight regulation of both excitatory and inhibitory inputs. Hence, alterations of synaptic transmission or intrinsic properties of hippocampal neurons are likely to severely impair network activity and oscillations. This in turn may result in memory deficits. Such changes often occur in pathologies affecting the hippocampus like epilepsy. In the following section, I will explore how hippocampal organization and neuronal activity are altered in temporal lobe epilepsy. I will specifically discuss how these modifications favor ictogenesis, impact rhythmogenesis and result in cognitive deficits.

3. The hippocampus in temporal lobe epilepsy

a. Cellular alterations of the hippocampus in mTLE

Temporal lobe epilepsy is the most common form of focal epilepsy. Mesial TLE (mTLE) possess a focus in the hippocampal formation. They are often pharmaco-resistant and are usually associated with memory deficits and mood disorders. Histological studies on both epileptic patients and animal models of mTLE revealed a number of important morphological alterations.

One major aspect of mTLE is the hippocampal sclerosis which can be observed in about 50% of the patients suffering of mTLE (Coras and Blümcke, 2015). The term sclerosis points to an atrophy of the hippocampal formation, which can reach from 30 to 50% of the hippocampal volume, due to a severe neuronal loss (Fig 22a). The magnitude of the sclerosis as well as the affected regions can vary across patients but several studies showed that it predominantly reflects degeneration of pyramidal cells in the CA1 and to a lesser extent the CA3 region (Blümcke et al., 2000; Mathern et al., 1997). Although most of the hippocampal shrinkage is due

to neuronal loss in these two regions, mossy cell and interneuron loss has also been extensively described and implicated in the pathogenesis of epilepsy (Blümcke et al., 2000; de Lanerolle et al., 1989; Maglóczky and Freund, 2005; Wittner et al., 2001). Finally, the entorhinal cortex sometimes undergoes neuronal loss, particularly in the layer III (Du et al., 1995; Jung et al., 2009). In contrast, the DG and CA2 are remarkably preserved from cell degeneration.

While the DG is relatively spared from hippocampal sclerosis, several morphological alterations were reported in these regions. First, epilepsy results in granule cells dispersion (Houser, 1990; Fig 22b). Hence, whereas the number of granule cells is unaffected, the granule cell layer is thicker in the epileptic DG. This is proposed to result from alteration of the local extracellular matrix and in particular decrease in reelin expression (Haas et al., 2002). Reelin is a secreted protein which has been proposed to critically control neuronal migration (Howell et al., 1997). In temporal epilepsy, the DG displays aberrant neurogenesis. Hence, *status epilepticus* induces a major increase in neurogenesis. Many of these newly generated cells have been shown to integrate abnormally in the local DG network (Kron et al., 2010; Parent, 2007) which could be at least partly linked to the deficits in reelin expression. In particular, numerous newborn cells migrate to ectopic locations within the hilus and displayed increased excitability and synchronization with CA3 pyramidal cells (Scharfman et al., 2003). Granule cell dispersion is also associated with a reorganization of their dendritic tree which are wider, show a redistribution of their dendritic spines (Freiman et al., 2011) and extend in the hilus (Kelly and Beck, 2017).

Another major alteration of the DG in epilepsy is the ectopic mossy fiber sprouting, which results in a recurrent excitatory circuit between dentate granule cells (Gabriel et al., 2004; Tauck and Nadler, 1985). As previously described, mossy fibers normally runs through the hilus and the *stratum lucidum* to contact CA3 interneurons and, to a lesser extent, principal cells (cf II.1.b). In TLE patients, mossy fibers sprout in the hilus, cross the granule cell layer and form characteristic giant mossy boutons in the molecular layer onto granule cells (Represa et al., 1993; Scharfman et al., 2003; Fig 22c). Activity of kainate receptors at these aberrant synapses contribute to shift granule cell firing mode from sparse to sustained (Artinian et al., 2011). A recent study implicated dysregulation of chloride homeostasis at the origin of mossy fibers sprouting in a pilocarpine mouse model of TLE (Kourdougli et al., 2017). Thus, decreasing intraneuronal chloride concentration by blocking NKCC1 activity with bumetanide in the days following epilepsy induction was sufficient to significantly reduce the sprouting of mossy fibers and ameliorates the epileptic phenotype.

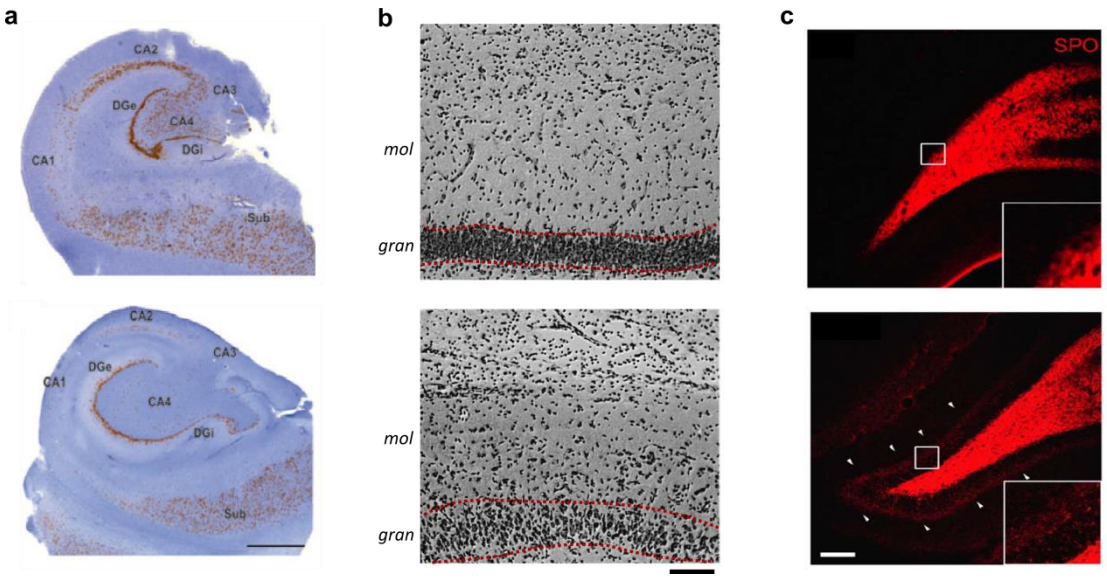

Figure 22 : Alterations of hippocampal anatomy in TLE patients
(a) Tissue from TLE patients suffering from hippocampal sclerosis. Neuronal loss can be mostly restricted to CA1 (top) or affect both CA1 and CA3 regions (bottom). Note that CA2 and the DG always remain preserved. Scale 1 mm. Adapted from (Blumcke et al., 2013)
(b) Non sclerotic patients present densely packed granule cell layer (top, delineated in red) while hippocampal sclerosis is often associated with granule cell dispersion (bottom). Scale 60 µm. Adapted from (Ying et al., 1998)
(c) Mossy fibers sprouting in a mouse model of epilepsy. In control animals (top), mossy fibers, as detected by synaptoporin staining, run exclusively through the hilus. Following *status epilepticus* (bottom), mossy fibers aberrantly form connexions in the molecular layer (white arrowhead). Scale 150 µm. Adapted from Kourdougli et al. 2017

Sparse DG firing is thought to be critical for restraining inputs to the hippocampus and preventing the spread of seizure (Heinemann et al., 1992; see also II.1.a-b). However, all the alterations that I presented combine to significantly increase DG excitability in epilepsy, thus lowering the gate to the HPC. In agreement with increased excitability of the DG, dentate spikes are more frequent in epileptic animals (Flynn et al., 2015). This alteration of dentate excitability and thereby dentate gate is critical in the pathophysiology of epilepsy. Indeed, optogenetic inhibition of granule cells in epileptic mice efficiently stopped spontaneous seizures while their activation aggravated seizures (Krook-Magnuson et al., 2015).

b. Alterations of theta rhythms in epilepsy

Given the extent of cellular and morphological changes that occur in the epileptic HPC, it is not surprising that many of the classical hippocampal oscillations undergo massive alterations. The most consistent modification observed throughout studies is a decrease in theta power, which is observed in both the pilocarpine model (Chauvière et al., 2009) and the kainate model of epilepsy in rodents (Dugladze et al., 2007; Inostroza et al., 2013). This is likely to be a direct

consequence of the hippocampal sclerosis that massively affects CA1, since theta oscillations mostly arise from the activity of CA1 pyramidal cells (Buzsáki, 2002, see also II.2.b). However, reduced theta power may also result from some molecular modifications and changes in intrinsic neuronal properties. For instance, the expression of HCN channels that underlie h-currents and contribute to theta generation, is reduced in a rat model of TLE (Marcelin et al., 2009). More subtle alterations of theta rhythm were also described such as altered theta coherence between the DG and the EC (Froriep et al., 2012), modified proximodistal coordination of theta rhythm (Laurent et al., 2015) or impairment of theta - gamma coupling reflecting a lesser phase locking of interneurons (Lopez-Pigozzi et al., 2016).

Given the importance of theta in memory encoding (as described previously in II.2.b), it is not surprising that these alterations of theta oscillations are accompanied by deficits in spatial learning (Chauviere et al., 2009) and episodic-like memory (Inostroza et al,. 2013). Consistently, theta sequences, which are assumed to constitute a cellular basis of memory encoding (Robbe and Buzsáki, 2009), are also altered in epileptic rats (Lenck-Santini and Holmes, 2008). This could be due directly to the sclerosis in CA1 or result from the loss of entorhinal neurons during hippocampal sclerosis (Du et al., 1993) since medial EC afferents are important for the establishment of theta sequences (Schlesiger et al., 2015).
Promisingly, restoring hippocampal theta activity has proven beneficial both in animal models and in epileptic patients. Indeed, deep brain stimulation of the entorhinal cortex of epileptic patients resets theta rhythm and improves learning in a spatial memory task (Suthana et al., 2012), while stimulations of the EC at theta frequency ameliorates learning in the Barnes maze in a pilocarpine rat model (Lee et al., 2017).

c. *Emergence of novel pathological oscillations around the epileptogenic zone*

Even in absence of seizures, the epileptic brain is characterized by the appearance of pathological events with constitute hallmarks of epilepsy. In particular, regular interictal discharges can be observed in the epileptic brain (Bragin et al., 2011; Schevon et al., 2009). These sharp events correspond to an intense recruitment of principal cells (Bragin et al., 2011). The function of interictal spikes in ictogenesis is currently debated (see Avoli et al., 2006 for review). Indeed, early studies indicated that interictal discharges rate increased prior to seizures suggesting a pro-ictogenic function (Dichter and Ayala, 1987). In contrast, *in vitro,* interictal

events in CA3 inhibit rather than promote ictal activity (Barbarosie and Avoli, 1997). Independently of their role in ictogenesis, it was recently suggested that interictal discharges contributed to memory deficits observed in temporal lobe epilepsy by inducing aberrant consolidation of memory traces (Gelinas et al., 2016). Indeed, in both animal model and epileptic patients, interictal discharges often triggered neocortical down-states. This temporal association of hippocampal and cortical rhythms has been shown to favor memory consolidation (Maingret et al., 2016). Thus, interictal discharges which do not convey any task-relevant information would compete with physiological ripples thereby preventing adequate learning.

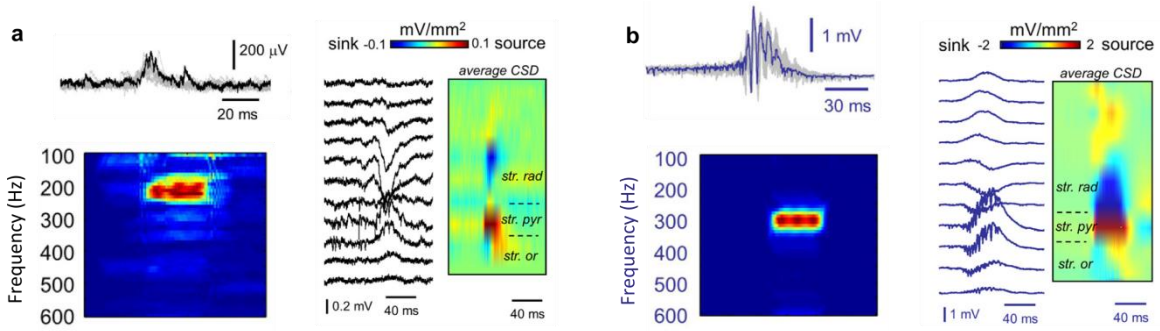

Figure 23 : Characteristics of fast ripples
(a) Left : *In vitro* recording of physiological ripple in 1 mM Ca^{2+} (top) and associated time-frequency spectrum revealing a band around 200Hz (bottom). Right : Linear recordings across CA3 layer and associated CSD analysis revealing a profile similar to *in vivo* SPW-R.
(b) Same as a for fast-ripples recorded in 3 mM Ca^{2+}. Note the higher amplitude of the event (left, top), the frequency of oscillation around 300 Hz (left, bottom) and the increased amplitude of currents revealed by the CSD profile (right)
Adapted from Aivar et al. 2014

In addition to interictal discharges, fast ripples (short oscillations of intrinsic frequency superior to 200 Hz, Fig 23) have been reported in the brain of epileptic patients and in animal epilepsy models (Bragin et al., 1999; Jefferys et al., 2012). In humans, the occurrence of fast ripples is usually limited to less than 1 mm^3 of the brain, close to the epileptic focus (Bragin et al., 2002). Intracerebral multi-electrode recordings in epileptic patients revealed that most of the fast ripples were restricted locally since they could usually only be detected by one electrode (Schevon et al., 2009). They can occur independently but also sometimes in close temporal proximity with interictal discharges (Schevon et al., 2009). Several groups investigated the mechanisms leading to the emergence of fast ripples *in vitro.* Fast ripples emergence could be favored in slices by increasing the excitability of the network either by acting on intrinsic properties of the neurons (with increased extracellular potassium or decreased extracellular magnesium) or by blocking inhibitory transmission (Karlócai et al., 2014). Interestingly, in all these models, the authors observed a clear transition from physiological ripples to fast-ripples. This indicates that these two events are fundamentally distinct. Analysis of cell activity during

fast ripples revealed an increased firing of principal cells due to a depolarizing block in interneurons. Another study came to quite similar conclusions (Aivar et al., 2014). There, decreasing extracellular potassium resulted in increased excitability of the neurons and altered disynaptic inhibition thus leading to the emergence of fast ripples.

How can these high-frequency oscillations arise from the activity of pyramidal cells that cannot sustain firing at such high frequency ? In slices from epileptic animals, enhanced synaptic activity in CA3 can lead to a less reliable timing of action potential firing (Foffani et al., 2007). This in turn could lead to out-of-phase firing of principal neurons. Hence, the high-frequency oscillation would result from several subgroups of neurons firing out of phase (Ibarz et al., 2010). Importantly, such loss of firing selectivity would be accompanied by a decrease in the information content, thereby resulting in memory impairment (Valero et al., 2017).

Finally, in epileptic patients, some ripples with spectral characteristics similar to physiological SPW-R may actually be pathological. Indeed, these high-frequency oscillations can occur in the dentate gyrus, where physiological SPW-Rs are never recorded (Bragin et al., 1999). Additionally, these events have been associated with the onset of seizures (Jacobs et al., 2009; Worrell et al., 2004). *In vitro*, these oscillations have been shown to directly reflect the pattern of inhibitory postsynaptic currents in pyramidal cells (Trevelyan, 2009). Strikingly, during the transition to ictal phase, the mechanisms underlying high-frequency oscillations changed. Indeed, the correlation between IPSCs in pyramidal neurons and LFP collapsed while excitatory synaptic actyivity became predominant. Hence, pathological high-frequency oscillations can emerge from diverse mechanisms that could evolve during seizure progression.

To summarize, in both temporal lobe epilepsy patients and animal models, the hippocampus undergoes vast morphological and physiological changes. All of these alterations combine to increase hippocampal excitability thereby favoring the emergence of seizures. Independently of seizure occurrence, the epileptic hippocampal circuitry is characterized by degradations of physiological rhythms and appearance of pathological interictal events. The mechanisms leading to this altered network activity are still not fully understood. During my PhD, I investigated how one specific event, the loss of KCC2, could participate in generating abnormal activities.

III- RATIONALE AND OBJECTIVE OF THE PROJECT

The expression and activity of the potassium-chloride cotransporter KCC2 critically regulate transmembrane chloride gradients in neurons. This, in turn, affects fast GABAergic transmission since GABAARs are primarily permeable to chloride and, to a lesser extent, bicarbonate ions. Thus, the progressive upregulation of KCC2 during development is accompanied by a gradual hyperpolarizing shift of the reversal potential of GABA-mediated currents (Rivera et al., 1999) by increasing transmembrane chloride gradient. Conversely, downregulation of KCC2, as observed in several neurological disorders (Rivera et al., 2002; Hyde et al., 2011; Duarte et al., 2013; Dargaei et al., 2018), is associated with reduced transmembrane chloride gradients which is often assumed to result in a depolarized reversal potential of GABAergic currents. This would results in altering the excitatory / inhibitory balance in neuronal networks, thereby leading to the emergence of pathological activities that underlie these disorders.

Over the last 20 years, KCC2 has been extensively studied in the context of epilepsy. Indeed, hypomorphic KCC2 mutant mice suffer from severe epilepsy (Woo et al., 2002). Furthermore, in slices resected from epileptic patients, pathological interictal activity can be suppressed by inhibition of GABAergic transmission, suggesting that GABA may have a paradoxical excitatory action in the epileptic brain (Cohen et al., 2002). This observation correlated with a depolarizing effect of GABA and the loss of KCC2 expression in a small subset of principal cells (Huberfeld et al., 2007). This series of experiments lay the ground for the hypothesis that downregulation of KCC2 could be causal to the epileptic phenotype, as recently suggested in a modeling study (Buchin et al., 2016). In line with this assumption, KCC2 expression is downregulated following traumatic brain injury (Bonislawski et al., 2007), a condition which often results in epileptogenesis. Similarly, loss of KCC2 following an initial seizure (Rivera et al., 2002) could favor the occurrence of further epileptic activity. However, in spite of a considerable literature on this topic, whether KCC2 suppression on its own is sufficient to trigger seizures remains unkonwn. In parallel, studies revealed a more complex role of KCC2 activity in epileptogenesis than previously expected. Although loss of KCC2 renders GABA transmission depolarizing and favors interictal activity (Huberfeld et al., 2007; Pallud et al., 2014), it exerts a paradoxical protective role on ictal activity (Hamidi and Avoli 2015). This could be due to a pro-excitatory impact of KCC2 activity on neuronal networks following intense GABAARs stimulations due to a rise of extracellular potassium (Viitanen et al., 2010).

A further level of complexity in exploring the role of KCC2 suppression in epileptogenesis and ictogenesis arises from the diversity of KCC2 functions. Thus, KCC2 is not just acting to regulate chloride and potassium homeostasis in neurons but also interacts with numerous protein partners involved in a wide range of cellular and synaptic processes. Several of these partners act as regulators of KCC2 membrane expression and function (M. Chen et al., 2017; Ivakine et al., 2013; Mahadevan et al., 2014). Conversely, KCC2 regulates the activity of some of its partners. In particular, KCC2 was shown to influence the organization and activity of glutamatergic synapses through its interaction with the actin-related proteins 4.1N and βPix. Thus, downregulation of KCC2 during development severely impairs dendritic spine maturation (Li et al., 2007) while its suppression in mature neurons decreases the efficacy of glutamatergic transmission (Gauvain et al., 2007) and precludes the long-term potentiation of the synapses (Chevy et al., 2015). These data suggest that the effects of KCC2 suppression should not considered solely in the context of altered GABAergic transmission and/or extracellular potassium clearance.

Hippocampal activity is characterized by the emergence of various oscillatory patterns associated with behavior. These oscillations, which have been shown essential for numerous cognitive processes, rely on an exquisite control of synaptic strength and connectivity as well as neuronal intrinsic properties. Since loss of KCC2 impacts both GABAergic and glutamatergic transmission, I predicted that it would also affects hippocampal rhythmogenesis.

In this context, I aimed at characterizing the consequences of a chronic downregulation of KCC2 on hippocampal network activity. In particular, I asked whether suppression of KCC2 in a mature network might affect hippocampal rhythmogenesis and whether it could be sufficient to favor the emergence of pathological, epileptiform activities. I examined the mechanisms underlying the observed changes and questioned their dependence on KCC2 transport-function. To address these questions, I combined *in vitro* and *in vivo* electrophysiological techniques to investigate in detail the impact of KCC2 suppression on both cellular physiology, synaptic transmission and network activity.

MATERIALS AND METHODS

MATERIALS AND METHODS

Most methods are described in detail in the research manuscript presented in the Result section of this thesis. Therefore, I will only present here methods relevant to the additional experiments presented in the result section but not in the manuscript.

Slice preparation

Methods for slicing and tissue preservation are critical for keeping neurons healthy, especially when preparing slices from older animals.

When I arrived in the lab, the classical method for these preparations was the following. Animals were deeply anesthetized with ketamine / xylazine (115/15 mg/kg) and transcardially perfused with an ice-cold choline-based solution containing (in mM) : 110 Choline Cl, 25 Glucose, 25 $NaHCO_3$, 11.6 Ascorbic acid, 3.1 Pyruvic acid, 1.25 NaH_2PO_4, 2.5 KCl, 0.5 $CaCl_2$, 7 $MgCl_2$ saturated with 95% O_2/5% CO_2. Rats were then decapitated and 350µm parasagittal sections were prepared using a vibratome (Microm, Thermofisher). Slices were then kept for ~30 minutes at 37°C in the cutting solution before being transferred in a submerged chamber containing bicarbonate-buffered ACSF oxygenated with 5% CO_2 in O_2, containing (in mM) : 126 NaCl, 26 $NaHCO_3$, 10 Glucose, 2.5 KCl, 1.25 NaH_2PO_4, 3 $CaCl_2$, 2 $MgCl_2$.

However, although neurons seemed healthy with this preparation, this technique yielded a very low rate of spontaneous activity. In a first series of experiments, I was interested in recording sharp wave-ripple activity in slices, which requires strong basal activity. Hence, I decided to improve our protocol. Based on interactions with the team of Attila Gulyas in Budapest, who commonly record sharp-wave ripples in slices, I realized that conserving slices in an interface chamber rather than submerged considerably increases slice survival and spontaneous activity. I also slightly modified the composition of ACSF to increase cellular excitability by raising the concentration of extracellular potassium to 3.5 mM and decreasing the amounts of divalent cations while keeping similar ratios of calcium and magnesium (1.6 $CaCl_2$, 1.2 $MgCl_2$).

Network activity such as sharp wave-ripples is more likely to occur when neuronal connections are well preserved. In the hippocampus, these connections are mostly transversal. Parasagittal

slicing allows recovering transverse hippocampal sections from the dorsal hippocampus. However, the number of perfectly transverse sections is quite low (~2 per hemisphere) with this technique. I therefore decided to dissect out each hippocampus and make transverse sections using a guiding agar block to immobilize the hippocampus. Finally, network activity is also more prominent in thicker slices so I used 450µm thick slices for this set of experiments

Therefore, I used the following slicing protocol. After transcardiac perfusion with ice-cold choline-based cutting solution, rats were decapitated, hippocampi were rapidly dissected and 450µm transverse sections (400µm for patch clamp experiments) were prepared using a vibratome. Slices were then transferred and allowed to recover for 1 hour in a humidified interface chamber filled with bicarbonate-buffered ACSF pre-heated at 37°C and oxygenated with 5% CO_2 in O_2, containing (in mM) : 126 NaCl, 26 $NaHCO_3$, 10 Glucose, 3.5 KCl, 1.25 NaH_2PO_4, 1.6 $CaCl_2$, 1.2 $MgCl_2$.

Extracellular *in vitro* recordings

For recordings, slices were transferred in a submerged-style recording chamber equipped with a dual superfusion system to improve metabolic and oxygen supply to the slice (Hajos et al. 2009). In this design, slices were placed on a nylon mesh and two separate inlets allowed ACSF to flow both above and below the slices at a rate of 5 ml/min, at 34°C. A bubble trap was added right before the chamber to avoid degassing of ACSF under the slices which could impair the stability of recordings.

A recording pipette of 2-3 MΩ resistance was filled with ACSF and inserted in the pyramidal layer of the CA3 region. Signals were acquired with a Multiclamp 700B amplifier (Molecular Devices), band-pass filtered (0.1 Hz - 10 kHz), and digitized at 20 kHz.

To test the effect of complete blockade of KCC2 function, the specific KCC2 blocker VU0463271 (10µM in DMSO, Tocris) was bath applied for 15 minutes on the slice. Similar amount of DMSO (0.01%) was added in ACSF for baseline condition. Since spontaneous activity can slowly build-up in slices over time, drug application was only performed if pattern of activity was stable for at least 10 minutes prior to application, as checked by visual observation of the recordings.

Analysis of *in vitro* extracellular recordings

Methods for detection and analysis of ripples were adapted based on classical standards used for *in vivo* recordings (Csicsvari et al., 2000, Girardeau et al., 2009). Ripple detection was ;performed by band-pass filtering (100–600 Hz), squaring and normalizing, followed by thresholding of the signal. SPW-Rs were defined as events starting at 2-fold the standard deviation (s.d.) of the baseline signal, peaking above 5 s.d., and remaining above 2 s.d. for more than 30 ms and less than 300 ms. Event amplitude was determined as the positive deflection of the recorded local field potential. For average spectrogram of the events, ripples were aligned on their peak (defined as the maximum of the filtered signal). Spectrograms were then computed using a multi-taper method with 50 ms window and 5 ms step

Spike detection was performed by high-pass filtering above 500 Hz. Events exceeding 4 s.d. and lasting less than 2.5 ms were considered as spikes.

Bursts were defined as series of minimum 3 spikes separated by less than 30 ms each. The inter-spike interval used for burst consideration was arbitrarily defined based on the distribution on these intervals through the whole recordings.

To study the effect of KCC2 blockade on slices, analyses were performed on 5 minutes of recordings either just preceding VU0463271 application, at the end treatment or 10-15 minutes following treatment.

***In vivo* recordings and analysis**

For *in vivo* intrahippocampal recordings methods, please refer to the method section of the manuscript.

All analyses were performed offline using Matlab built-in functions, Chronux (http://chronux.org/), the FMAToolbox (http://fmatoolbox.sourceforge.net/) as well as custom-written scripts.

Power spectra and spectrograms were computed using multi-tapers estimates on the raw LFP with 5 seconds window and 2.5 seconds step. Gamma band was defined as 25-90 Hz. Slow and fast gamma ranges (respectively 25 - 55 and 60 – 90 Hz) were determined according to Colgin et al. 2009. Theta-gamma coupling was estimated using the measure of modulatory index as described in (Tort et al., 2008). Briefly, this index allows to estimate the modulation of the amplitude of an oscillation (here, in the gamma band) by the phase of the other oscillation (here theta). A modulatory index (MI) of 0 indicates lack of phase to amplitude modulation while increased value of MI reveal stronger amplitude-phase coupling.

Ripple detection was performed by band-pass filtering (100–600 Hz), squaring and normalizing, followed by thresholding of the field potential recorded in CA1 pyramidal layer. SPW-Rs were defined as events starting at 4 s.d., peaking at more than 6 s.d., and remaining above 4 s.d. for more than 15 ms and less than 150 ms. To estimate the strength of ripples recorded *in vivo*, the amplitude of the raw LFP signal cannot be used since it depends on the precise layer localization of the electrode, which cannot be controlled. Hence, different approaches were developed. One option is to calculate the power of the ripple based on its spectrogram (Headley et al., 2017). Alternatively, strength can be estimated as the peak of the *z*-score filtered signal (Peyrache et al., 2011), or as the envelope amplitude measured using the Hilbert transform of the band-pass filtered signal (Girardeau et al., 2009). I tested the last two methods and obtained similar results with both. I then decided to only estimate strength of the ripples by measuring the envelope amplitude of the signal.

RESULTS

RESULTS

I- *IN VITRO* STUDY OF THE IMPACT OF KCC2 SUPPRESSION ON HIPPOCAMPAL RHYTHMOGENESIS

In a first set of experiments, I aimed at investigating the impact of KCC2 suppression on hippocampal rhythmogenesis *in vitro.* Our initial hypothesis was that the loss of KCC2 expression in a small subset of neurons, as reported in epilepsy (Huberfeld et al., 2007), could be sufficient to favor the emergence of epileptiform activity such as interictal discharges or fast ripples, as suggested by a recent computational model (Buchin et al., 2016).

To test this hypothesis *in vitro*, I first set up conditions for reliable recordings of ripple activity in the CA3 region of rat hippocampal slices (see Methods). Even after improvement of slicing and conservation techniques, basal activity remained highly variable among slices (Fig 24A). One third of the recorded slices (7 out of 21) did not show any pattern of organized activity and only displayed regular multi-unit activity. I analyzed the characteristics of the ripples events recorded in the remaining slices. Consistent with data published from other groups (Aivar et al., 2014; Hájos et al., 2009), ripples were typically accompanied by depolarization of the local field potential (LFP) of ~ 100 to 200 µV, lasted 50 to 80 ms and occurred at a rate of ~0.3 Hz. I noticed that in some slices (5/16), these events, although of similar amplitude, were accompanied by a high multi-unit activity. I wondered whether this difference in neuronal activity could coincide with different spectral properties of the two types of events. Indeed, classical ripples displayed a frequency of oscillation around 150 Hz. In contrast, in slices with high multi-unit activity, an additional frequency of oscillation between 200 and 300 Hz was revealed (Fig 24B,C), suggesting these events may be reminiscent of pathological fast-ripples (see Introduction II.3.c).

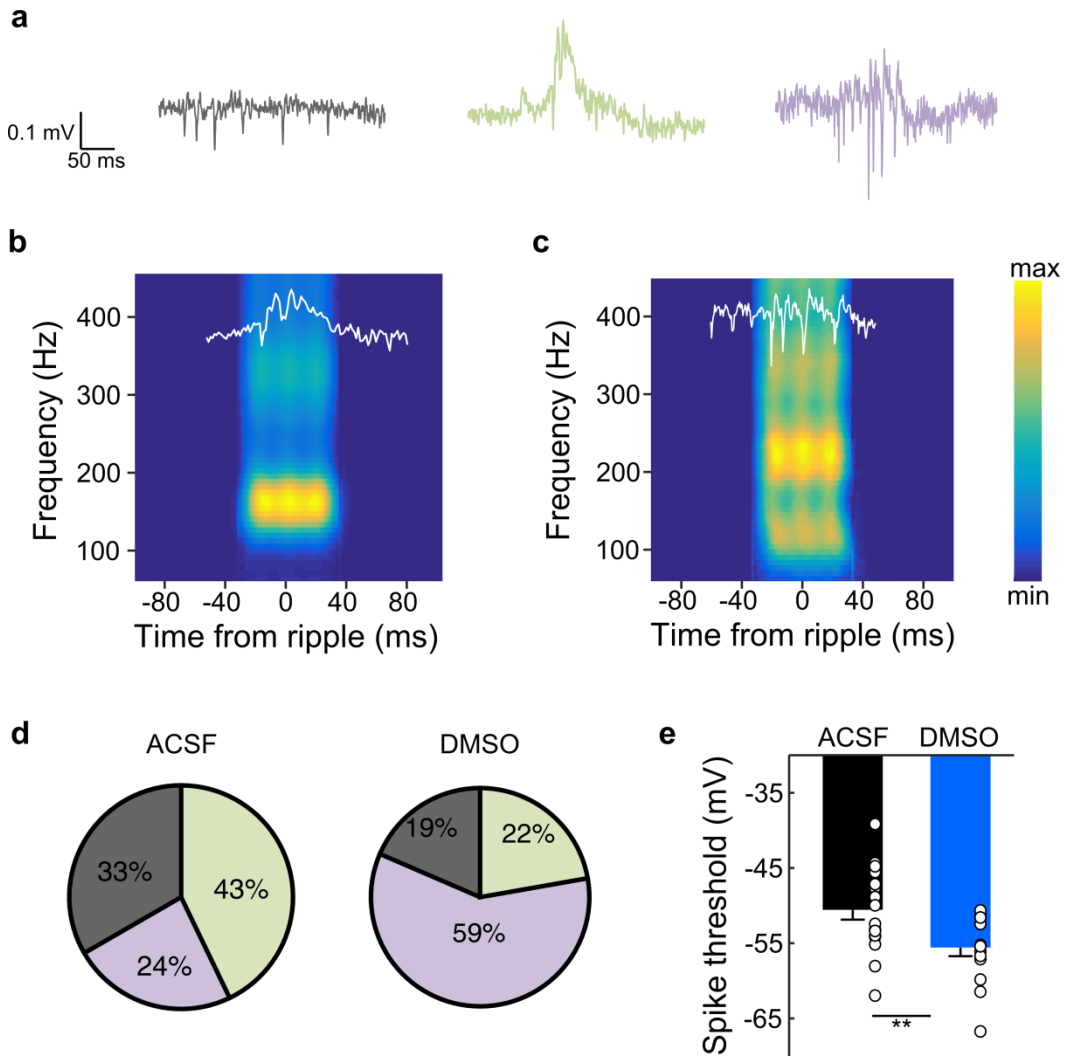

Figure 24 : High variability of rhythmic activity in area CA3 of rat hippocampal slices

(a) Representative 300ms traces of extracellular recording from slices without organized activity (grey, left), with typical ripples (green, middle) or with multi-unit activity superimposed on ripples (purple, right)

(b,c) Average time-frequency spectrograms of all detected events in a slice showing typical ripples (b) and ripples with associated spiking (c). Note the appearance of a band between 200 – 300 Hz in the latter case.

(d) Proportion of the different patterns of activity in ACSF and in 0.01% DMSO. In DMSO, higher proportion of slices presented ripples with superimposed spikes.

(e) Summary data for action potential threshold in dentate granule cells in ACSF (n = 13 cells) and in 0.01 % DMSO (n = 15 cells). ** $p < 0.01$

Since basal conditions were already highly variable, I reasoned that suppression of KCC2 in a subset of neurons as in Buchin et al. (2016) may not be sufficient to uncover differences in network activity. I therefore decided to first examine the effects of complete KCC2 blockade by using the specific antagonist of KCC2 VU0463271 (Delpire et al., 2012). VU0463271 is only soluble in DMSO. Hence, I added 0.01% DMSO to the ACSF for control conditions. Even low concentrations of DMSO may alter neuronal excitability and cell membrane properties (Sawada and Sato, 1975; Tamagnini et al., 2014). Indeed, the presence of 0.01% of DMSO modified the type of recorded events by increasing the proportion of spike-containing ripples (ACSF, n = 21

slices, DMSO, n = 27 slices, Fig 24D). In whole-cell patch clamp recordings, I observed DMSO application induced a hyperpolarizing shift of action potential threshold in dentate granule cells (Fig 24E, -55.55 ± 1.15 vs -50.56 ± 1.30 mV, n = 13 and 15 cells, t-test, p <0.01) thus increasing their excitability. This could explain the higher proportion of pathological fast-ripples in the presence of DMSO since fast-ripples are associated with a combination of altered inhibition and increased excitability (Aivar et al., 2014).

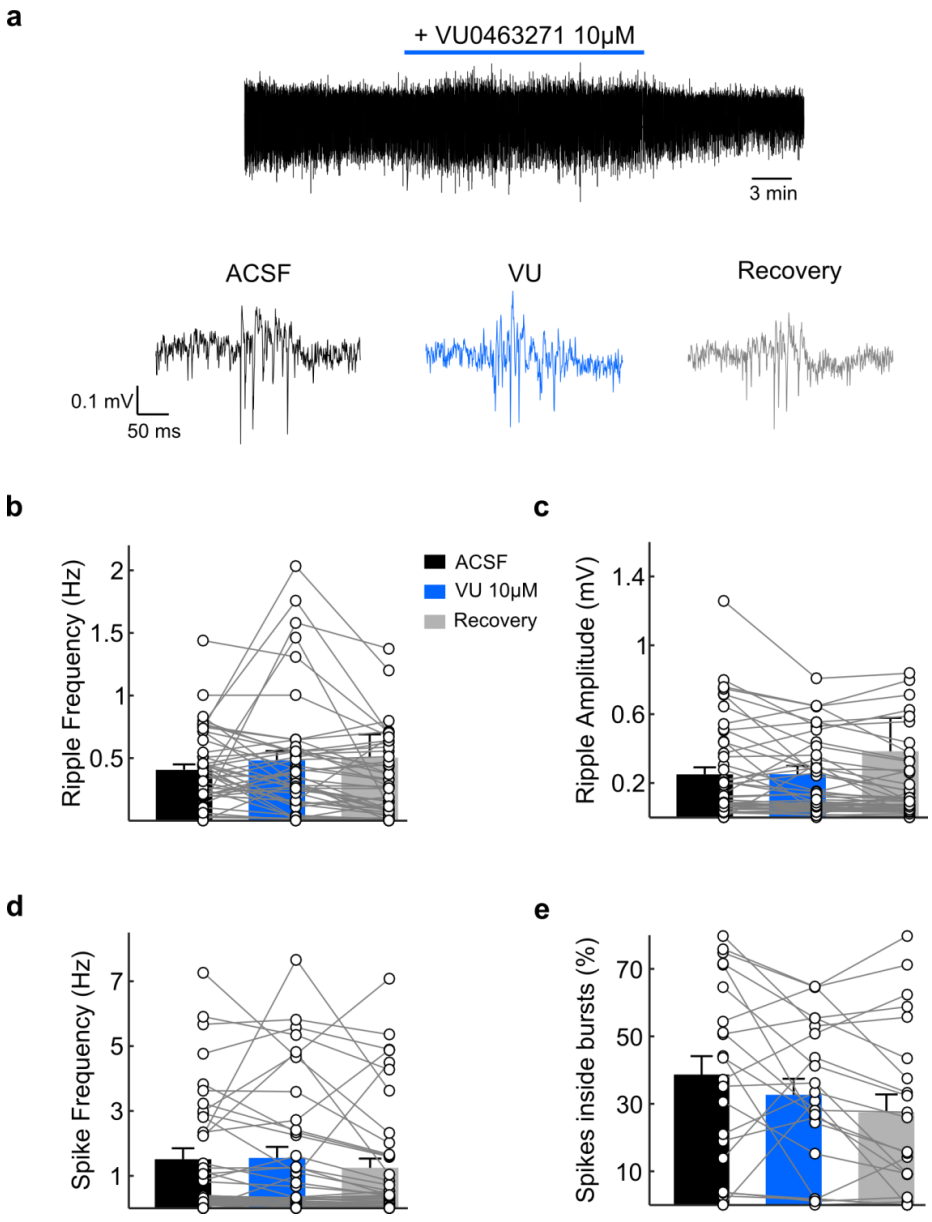

Figure 25 : Pharmacological blockade of KCC2 function does not affect *in vitro* rhythmogenesis
(a) Top, representative LFP recordings in the CA3 pyramidal layer. The blue line indicates the timing of application of the KCC2 antagonist VU0463271. Bottom, typical examples of the recorded events before (black, left), during (blue, middle) and after (grey, right) pharmacological blockade of KCC2
(b,c) Analyses of ripples rate (b) and amplitude (c) during the 5 minutes preceding the drug application, the last 5 minutes of treatment by KCC2 antagonist and 10 to 15 minutes following treatment for every slice.
(d) Frequency of action potential firing during the same periods as for ripple analysis
(e) Percentage of action potential belonging to a burst during the same periods as for ripple analysis

Bath application of the KCC2 antagonist for 15 minutes did not alter rhythmogenesis *in vitro* (Fig 25). Thus, neither the frequency of occurrence (0.34 ± 0.07 vs 0.29 ± 0.05 Hz, paired t-test, p = 0.38) or the amplitude of the events (113.5 ± 13.8 vs 141.0 ± 48.3 µV, paired t-test, p = 0.18) were affected by the loss of KCC2 transport-function. Additionally, I did not detect any differences in the action potential rate upon VU0463271 application compared with DMSO (2.97 ± 0.69 vs 0.91 ± 0.68 Hz, paired t-test, p = 0.86). I also wondered whether loss of KCC2 could affect the firing mode of neurons by favoring the emergence of bursts. However, the proportion of spikes belonging to a burst was unchanged between conditions (20.86 ± 0.03 vs 25.44 ± 0.04 Hz, paired t-test, p = 0.09).

Overall, I did not detect any change in hippocampal rhythmogenesis *in vitro* following complete blockade of KCC2 transport function. Similar observations were later reported in two papers published during my PhD (Sivakumaran et al., 2015; Kelley et al., 2016). The method used in these experiments possesses two main disadvantages. First, as reported, the variability of the activity recorded in control conditions remains high, which hinders the possibility to detect tenuous differences. Furthermore, as described in my introduction, blocking KCC2 function does not replicate well the effect of suppressing KCC2 expression as observed in the pathology, since only ion transport function is affected, but not interactions with protein partners.

These observations highlighted the need for a better model of KCC2 suppression to study its impact on hippocampal rhythmogenesis and epileptogenesis. Therefore, I decided to use a viral-based shRNA-mediated approach to chronically suppress KCC2 in a mature hippocampal network. Thus, the main part of my thesis was dedicated to the characterization of the effect of KCC2 suppression in the dentate gyrus on hippocampal activity. The results of this study are presented in the following part of this manuscript.

II- MAIN ARTICLE : KCC2 REGULATES NEURONAL EXCITABILITY AND HIPPOCAMPAL RHYTHMOGENESIS VIA DIRECT INTERACTION WITH TASK-3 CHANNELS

Preface

Patients suffering from temporal lobe epilepsy often present massive hippocampal sclerosis (Coras and Blümcke 2015). Noticeably, CA1 and CA3 regions are mostly affected by neuronal loss while the dentate gyrus, CA2 and the subiculum are relatively spared. This led to hypothesize that the latter regions may be essential to the process of ictogenesis. Indeed, studies on slices resected from temporal lobe epilepsy patients revealed spontaneous interictal activities emerging from the subiculum (Cohen et al., 2002), CA2 (Wittner et al., 2009) and the dentate gyrus (Eugène et al., 2014). Traumatic brain injury highly correlates with later development of epilepsy (Jennett, 1975). In this context, epileptogenesis has been associated with an increased excitability of the dentate gyrus (Lowenstein et al., 1992). Since traumatic brain injury also results in a decrease in KCC2 mRNA level in the dentate gyrus, loss of KCC2 has been suggested to underlie epileptogenesis in these conditions (Bonislawski et al., 2007). To test this hypothesis, I decided to chronically suppress KCC2 in the dorsal dentate gyrus using viral-based shRNA extinction. Since in epileptic patients, only a minority of neurons presents a downregulation of KCC2 expression (Cohen et al., 2002; Huberfeld et al., 2007), I decided to use lentiviral vectors rather than AAV to better control for the rate of neuronal transduction. Using a combination of *in vitro* and *in vivo* electrophysiological techniques, I showed that :

- Chronic KCC2 extinction in the dentate gyrus is not sufficient to generate seizures or epileptiform activities
- GABAergic transmission at rest is unaffected in KCC2 knockdown neurons, due to a regulation of their intrinsic properties which act to increase their excitability and their synaptic recruitment by excitatory afferents
- This effect is mediated by regulation of the leak-potassium channel Task-3 (KCNK9) through its interaction with KCC2
- Hippocampal rhythmogenesis is altered primarily due to increased excitability of the granule cells, not defect GABA signaling

KCC2 regulates neuronal excitability and hippocampal rhythmogenesis via interaction with Task-3 channels

Marie Goutierre[1,2,3], Sana Al Awabdh[1,2,3], Emeline François[1,2,3], Daniel Gomez-Dominguez[4], Theano Irinopoulou[1,2,3], Liset Menendez de la Prida[4], Jean Christophe Poncer[1,2,3*]

[1] Inserm UMR-S 839, 75005 Paris, France.; [2] Sorbonne Université, F75005, Paris, France ; [3] Institut du Fer à Moulin, F75005, Paris, France; [4] Instituto Cajal, Consejo Superior de Investigaciones Científicas (CSIC), Madrid, E-28002, Spain

* Corresponding author: Jean Christophe Poncer, Institut du Fer à Moulin, INSERM/Sorbonne Université UMR-839, 17 rue du Fer à Moulin, 75005 Paris, France

Author contributions

M.G., L.M.P. and J.C.P. designed the research. L.M.P. and J.C.P. supervised the research. M.G. performed all experiments involving animal surgery, *in vitro* and *in vivo* electrophysiology, immunohistochemistry and imaging. S.A.A. performed all biochemical assays, immunocytochemistry and imaging of heterologous cells. E.F. and J.C.P. performed experimental epilepsy assays. D.G.D. and L.M.P. helped set up *in vivo* electrophysiological recordings and data analysis, T.I. contributed confocal imaging and quantification. M.G., S.A.A. and E.F. analyzed the data. M.G. and J.C.P. wrote the paper.

Competing interests

The authors declare no competing interests.

Materials & Correspondence

Requests for materials and correspondence should be addressed to Jean Christophe Poncer.

Abstract

The K^+/Cl^- co-transporter KCC2 *(SLC12A5)* regulates neuronal transmembrane chloride gradients and thereby controls GABA signaling in the brain. KCC2 downregulation is observed in several neurological and psychiatric disorders including epilepsy, neuropathic pain and autism spectrum disorders. Paradoxical, depolarizing GABA signaling is usually assumed to contribute to abnormal network activity underlying the pathology. We tested this hypothesis and explored the functional impact of chronic KCC2 downregulation in the rat dentate gyrus. Although the reversal potential of GABAA receptor currents was depolarized in KCC2 knockdown neurons, this shift was fully compensated by depolarization of their resting membrane potential. This effect was due to downregulation of Task-3 leak potassium channels that we show is controlled via interaction with KCC2. Increased neuronal excitability upon KCC2 suppression altered dentate gyrus rhythmogenesis that could be rescued by chemogenetic hyperpolarization. Our data reveal KCC2 downregulation engages complex synaptic and cellular alterations beyond GABA signaling that concur to perturb network activity, thus offering novel targets for therapeutic intervention.

Introduction

Fast synaptic inhibition in the brain is primarily mediated by GABAA receptors (GABAAR), which are ligand-gated receptors associated with an anion-permeable conductance. GABAAR currents are carried by fluxes of chloride and, to a lesser extent, bicarbonate ions[1]. Consequently, the polarity of the net ion flux through GABAAR channels relies on both the transmembrane gradients of these ions as well as the neuronal resting membrane potential, which thereby determine the driving force of GABAAR currents. In mature neurons, transmembrane chloride gradients are predominantly regulated by the opposing actions of the two cation-chloride co-transporters (CCCs) KCC2 and NKCC1, which respectively mediate outward and inward co-transport of chloride and potassium ions[2]. Thus, postnatal upregulation of KCC2 expression is associated with a progressive hyperpolarizing shift in the reversal potential of GABAAR-mediated currents (E_{GABA})[3].

In mature neurons, KCC2 expression and function is rapidly regulated by neuronal activity via multiple posttranslational mechanisms[4,5]. Thus, Ca^{2+} influx through postsynaptic NMDA

receptors or during prolonged postsynaptic firing[6] rapidly reduces KCC2 membrane expression and function through protein phosphatase 1-dependent dephosphorylation of its Ser940 residue and protein cleavage by the calcium-activated protease calpain[7,8,9]. Conversely, chloride influx through GABAA receptors stabilizes KCC2 at the plasma membrane via Cl^--mediated inhibition of the serine/threonine WNK1 kinase and its downstream effectors SPAK/OSR1, which phosphorylate KCC2 on Thr906 and Thr1007 residues[10,11,12]. Finally, KCC2 expression is also regulated by several neuromodulators acting on G-protein couples receptors[13] as well as neurotrophins such as BDNF acting via TrkB signaling[14].

KCC2 dysregulation has been associated with numerous neurological and psychiatric disorders involving synaptic alterations[15,16]. These include epilepsy[17,18,19,20,21,22,23], neuropathic pain[24,25], posttraumatic spasticity[26], Huntington disease[27], schizophrenia[28] and Rett syndrome[29,30,31]. In most cases, reduced KCC2 expression was associated with a depolarizing shift in E_{GABA} that could be partly reversed using NKCC1 antagonists or drugs acting to enhance KCC2 function[18,25,27,30,32]. Since these drugs also ameliorated the pathological symptoms, those were generally assumed to primarily reflect defect neuronal chloride transport and altered GABAergic neurotransmission.

However, KCC2 functions in neurons extend beyond the mere control of chloride transport. Through interactions with multiple transmembrane and intracellular partners, KCC2 was shown to regulate dendritic spine morphology[33,34] and actin cytoskeleton[35,36], as well as the strength and long-term plasticity of glutamatergic synapses[33,35]. Recent functional proteomics data revealed additional putative KCC2 partners, including some involved in the recycling and trafficking of various transmembrane proteins and receptors[37]. Those may then either influence KCC2 function or, conversely, be regulated by KCC2. Thus, dysregulation of KCC2 expression may affect a variety of neuronal intrinsic and synaptic properties and thereby contribute to abnormal activity patterns that underlie neurological and psychiatric disorders. Deciphering the relative contribution of the various perturbations upon KCC2 downregulation may then help predict the most effective rescue strategies.

In the present study, we therefore explored the functional impact of chronic KCC2 downregulation in the rat dentate gyrus at the cellular, synaptic and network activity levels. We found that KCC2 knockdown had no significant effect on the driving force of GABAAR currents

but instead enhanced neuronal excitability and EPSP/spike coupling through membrane depolarization and increased resistance. Pharmacological and biochemical evidence suggest this reflected downregulation of a leak potassium conductance carried by TWIK-related acid-sensitive 3 (Task-3) channels, the expression of which was regulated via interaction with KCC2. KCC2 knockdown was not sufficient to promote epileptiform activity but altered hippocampal rhythmogenesis, which was fully rescued by restoring granule cell membrane properties. Our results show that KCC2 downregulation affects network activity primarily through enhanced neuronal excitability, suggesting novel targets for therapeutic strategies.

Results

We investigated the impact of a chronic KCC2 suppression in the dentate gyrus using *in vivo* RNA interference. Young adult rats (P30) were stereotaxically injected in the dorsal dentate gyrus with lentiviruses expressing previously validated KCC2-directed or non-target small hairpin RNA sequences together with GFP[33,35]. Suppression of KCC2 expression in transduced neurons was confirmed by immunohistofluorescence imaging two weeks after infection (Fig 1A, B). We first analyzed GABAAR-mediated transmission using gramicidin perforated-patch recordings. GABAAR-mediated currents were evoked by somatic laser uncaging of Rubi-GABA (15µM) while varying holding potentials (Fig 1C-D). As expected, the reversal potential of GABAAR currents (E_{GABA}) was significantly more depolarized in neurons with suppressed KCC2 expression (-73.26 ± 2.57 mV) compared to control granule cells (-82.10 ± 2.26 mV, t-test, $p< 0.05$, Fig 1E). However, neurons transduced with lentivirus expressing KCC2-directed shRNA also displayed more depolarized resting membrane potential (V_{rest}, -83.6 ± 1.52 *vs* -89.77 ± 0.82 mV, t-test, $p<0.01$). The shift in E_{GABA} and V_{rest} was of similar magnitude such that the driving force of ion flux through GABAARs at rest was unaffected by KCC2 knockdown (10.34 ± 2.37 *vs* 7.66 ± 2.38 mV, t-test, p=0.44). Additionally, neither the amplitude (14.12 ± 1.24 *vs* 14.78 ± 0.72 pA, Mann-Whitney, p=0.42) or mean frequency (0.91 ± 0.13 *vs* 1.17 ± 0.16 Hz, Mann-Whitney, p=0.27) of miniature inhibitory post-synaptic currents (mIPSCs) was affected by chronic KCC2 down-regulation (Fig S1). Therefore, KCC2 suppression in dentate granule cells does not affect steady-state GABAergic transmission, due to an unexpected depolarizing shift in resting membrane potential.

We further explored the mechanisms underlying changes in membrane potential upon KCC2 suppression in granule cells. We recorded infected neurons in whole-cell configuration while blocking synaptic transmission with bicuculline (20 μM), NBQX (20 μM) and APV (50 μM). In these conditions, depolarized resting membrane potential in KCC2 knockdown granule cells (-80.79 ± 1.61 *vs* -87.67 ± 1.06 mV, t-test, p<0.01) was accompanied by a ~30% increase in input resistance (662.70 ± 47.14 vs 513.38 ± 47.85 MΩ, t-test,p<0.05, Fig 2A; Table 1). These changes in intrinsic membrane properties resulted in higher excitability of KCC2 knockdown neurons following current injection (Fig 2C, repeated measures ANOVA, p<0.001). Changes in the input/output relationship primarily reflected changes of membrane properties since no difference was observed in action potential threshold upon KCC2 knockdown (Fig 2D -50.7 ± 1.92 vs -50.56 ± 1.30 mV, t-test, p = 0.95). Additionally, action potential waveform and amplitude were also unchanged in KCC2 knockdown *vs* control neurons (Fig 2E-2F, see Table 1 for details).

Increased neuronal excitability upon KCC2 down-regulation was cell-autonomous since neighboring uninfected cells had similar properties in slices from animals infected with viruses expressing non-target or KCC2-directed shRNA (Fig S2). In addition, acute application of the KCC2-specific antagonist VU0463271[38] (6 □M) for more than 30 min did not affect membrane resistance in granule cells from uninjected animals (298.95 ± 26.16 vs 356.14 ± 35.73 MΩ, Fig S2), indicating that KCC2-mediated ion transport *per se* does not significantly contribute to input resistance. Finally, these modifications were not specific of dentate granule cells, since KCC2 knockdown in CA1 pyramidal cells also resulted in depolarized resting membrane potential (-66.59 ± 1.04 vs -72.06 ± 1.53 mV, t-test, p<0.01), increased input resistance (213 ± 25.38 vs 134.45 ± 10.21 MΩ, Mann-Whitney, p<0.01) and shifted input/output curve (repeated measures ANOVA, p<0.001, Fig S3).

Depolarized membrane potential and increased input resistance likely reflect a reduction in potassium currents operating at rest. We tested this hypothesis by recording potassium currents upon voltage ramps from -120 to -50 mV at 0.03 mV/ms while blocking synaptic transmission. In KCC2 knockdown granule cells, potassium conductance was reduced throughout the range of potentials tested (Fig 2G-H). This reduction however was of higher magnitude for outward than inward currents, as evidenced by reduced rectification index (I_{-60} / I_{-120}) in KCC2 knockdown *vs* control granule cells (0.46 ±0.05 vs 0.82 ± 0.08, t-test, p<0.001, Fig 2I). This suggests that

outwardly rectifying leak potassium channels might be down-regulated upon KCC2 suppression. Two-pore-domain potassium channels (K2P) are a large family of leak potassium channels comprising both inward and outward rectifiers[39,40]. We therefore tested whether currents carried by K2P channels may be reduced in KCC2 knockdown neurons. Bath application of bupivacaine (200µM), a non-specific antagonist of K2P channels significantly reduced potassium currents in neurons expressing non-target shRNA but had very little effect in neurons expressing KCC2-directed shRNA (Fig 2G). Moreover, bupivacaine abolished the difference in resting membrane potential (-77.31 ± 1.86 vs -81.03 ± 1.48 mV, Mann-Whitney test with Bonferroni correction, p = 1, Fig 2J) and input resistance (998.7 ± 118.6 vs 1343.1 ± 207.4 MΩ, Mann-Whitney test with Bonferroni correction, p = 1) between KCC2 knockdown and control granule cells. Together, these results demonstrate that chronic KCC2 suppression increases neuronal excitability primarily through regulation of an outwardly rectifying leak potassium conductance.

Trek-2 and Task-3 are the most prominent outward-rectifier K2P in dentate gyrus granule cells[41,42,43]. Immunohistofluorescence imaging of Trek-2 however revealed a predominant expression in mossy fibers (Fig. S4A) with little or no expression in somato-dendritic compartments, suggesting Trek-2 may not prominently contribute to granule cell resting membrane potential and membrane conductance. Conversely, Task-3 expression was primarily observed in granule cell somata and dendrites (Fig. S4B). We therefore examined whether Task-3 protein expression in granule cells might be affected by chronic KCC2 suppression. Immunohistofluorescence confocal imaging indeed revealed a reduced expression of Task-3 in granule cells expressing KCC2-directed shRNA compared to non-target shRNA (Fig 3A). We then investigated the mechanisms underlying Task-3 down-regulation upon KCC2 silencing. KCC2 has been shown to interact with a variety of proteins, including transmembrane proteins such as GluK2[44], Neto2[45] and $GABA_B$ receptors[46] that regulate KCC2 membrane expression or the intracellular guanylyl exchange factor βPIX which is regulated through direct interaction with KCC2[35,36]. We therefore asked whether KCC2 might also interact with Task-3 channels and thereby influence their membrane expression and/or function. In order to test whether KCC2 interacts with Task-3 channels *in vivo*, we performed a co-immunoprecipitation assay from adult rat hippocampal homogenates. We observed that anti-KCC2 antibodies pulled down KCC2 and Task-3 complexes, indicating an interaction between the endogenous proteins in hippocampal neurons (Fig 3B). In order to characterize KCC2-Task-3 interaction further, we co-immunoprecipitated exogenously expressed Flag-tagged KCC2 and HA-tagged Task-3 in HEK293T cells. In lysates from double-transfected cells, anti-HA antibodies pulled down Flag-KCC2

together with Task-3 while anti-Flag antibodies pulled down HA-Task-3 and Flag-KCC2 (Fig 3C). Importantly, this interaction was specific of Task-3 since overexpressed HA-tagged GFP failed to interact with KCC2 in a similar assay (Fig. 3C). We then asked whether interaction with KCC2 may influence the expression of Task-3 channels. To test this hypothesis, we expressed HA-Task-3 in Neuro2A cells either alone or together with Flag-KCC2 and analyzed Task-3 expression by immunostaining and confocal imaging. In the absence of KCC2, Task-3 expression at plasma membrane was reduced and accumulated in an intracellular compartment (Fig. 3D-E). Line scans of immunofluorescence across the cell membrane and cytoplasm therefore revealed a reduced membrane to intracellular intensity ratio in cells lacking KCC2 (0.74 ± 0.08 vs. 2.47 ± 0.34, Mann-Whitney, $p<0.001$, Fig 3E). Together, our results show that KCC2 interacts with Task-3 and regulates its membrane expression in dentate gyrus granule cells, thereby regulating their intrinsic excitability.

We next asked how reduced leak conductances and enhanced excitability upon KCC2 suppression might affect EPSP/spike coupling in granule cells. Previous work showed that loss of KCC2 expression in hippocampal neurons led to reduced synaptic strength at glutamatergic inputs due to enhanced lateral diffusion of AMPA receptors[33]. Enhanced intrinsic excitability may then act as a homeostatic compensatory mechanism for reduced synaptic excitation[47]. To test this hypothesis, we first compared synaptic strength at glutamatergic inputs onto granule cells by recording miniature excitatory postsynaptic currents (mEPSCs). As previously reported, KCC2 knockdown granule cells showed a ~30% decrease in mEPSC amplitude (5.06 ± 0.43 vs 6.54 ± 0.28 pA, Mann-Whitney, $p<0.001$, Fig 4B) with no change in their mean frequency (1.60 ± 0.42 vs 1.82 ± 0.41 Hz, Mann-Whitney, $p = 0.09$, Fig 4B) compared to control cells. From these recordings, waveforms of quantal currents were derived, fitted, and used as a current command in current-clamp recordings from KCC2 knockdown *vs* control granule cells. Thus, neurons were recorded in whole-cell configuration and maintained at their resting membrane potential while somatically injecting multiples of quantal current waveforms to mimic synchronous excitatory inputs (Fig 4C). Although the efficacy of excitatory inputs was reduced in KCC2 knockdown neurons compared to control, enhanced intrinsic excitability overcompensated this reduction, leading to enhanced EPSP/spike coupling. Thus, KCC2 knockdown neurons fired action potentials from ~40 simultaneous quanta whereas firing of control neurons expressing non-target shRNA required at least 60 quanta (Fig 4D, repeated measures ANOVA, $p < 0.001$). In addition, synaptic integration during high frequency (>50 Hz) trains of EPSCs was also facilitated in KCC2

knockdown granule cells, owing to increased membrane resistance compared to control cells (Fig. 4E).

Perforant path input to the dentate gyrus provides synaptic excitation to granule cells as well as feedforward inhibition that contributes to their sparse activation by entorhinal afferents[48]. In order to explore EPSP/spike coupling of perforant path inputs in a more physiological setting, we recorded evoked fEPSP and population spike upon stimulation of perforant path inputs. The recording electrode was positioned in a densely infected area of the granular layer and stimulus intensity was set such as amplitude of the population spike was about half of its maximum amplitude (see Methods). In slices infected with viruses expressing KCC2-directed shRNA, fEPSP/population spike coupling was increased by ~47% compared to control slices expressing non-target shRNA (2.00 ± 0.25 vs 1.36 ± 0.15 ms^{-1}, t-test, $p < 0.05$, Fig 4F,G). This result further supports that increased excitability upon KCC2 knockdown is not homeostatic but instead acts to promote granule cell recruitment by entorhinal afferents. Importantly, bath application of the GABAAR blocker picrotoxin (100µM) increased the amplitude of population spike similarly in slices expressing either non-target shRNA (1.12 ± 0.15 mV *vs* 0.88 ± 0.13 mV, paired t-test, $p< 0.01$) or KCC2-directed shRNA (1.21 ± 0.17 mV *vs* 0.79 ± 0.11 mV, paired t-test $p < 0.001$; Fig 4H). These results suggest that GABAergic transmission, although depolarizing in dentate granule cells[49] (Fig. 1E), remains shunting and inhibitory independent of KCC2 expression. Therefore, KCC2 suppression in dentate granule cells promotes their recruitment by entorhinal afferents primarily through enhanced excitability and EPSP/spike coupling rather than altered GABA signaling.

The dentate gyrus is often considered as a filter or a gate for activity propagation from the entorhinal cortex to the hippocampus[50], in particular owing to dentate granule cells' sparse firing. These properties allow for pattern separation[51] and may prevent runaway excitation in the hippocampal[52]. Enhanced EPSP/spike coupling in dentate granule cells upon KCC2 suppression may then act to increase their excitatory drive by entorhinal afferents and thereby alter hippocampal rhythmogenesis. We explored this hypothesis using chronic intrahippocampal recordings from rats injected with lentivirus expressing either KCC2-directed or non-target shRNA (n=7 and 5, respectively, Fig 5A-B). Unlike a recent study using a similar approach[53], we did not observe spontaneous seizures in any of these animals. Susceptibility to pilocarpine-induced seizures was also unaffected by KCC2 knockdown in the dorsal dentate gyrus (Fig S5 A-C). Chronic, intrahippocampal recordings using linear silicon probes did not reveal interictal

spikes or fast ripples (Fig S5 D-E) that could represent hallmarks of an epileptic hippocampal network even in the absence of behavioral symptoms[54]. These results indicate that KCC2 suppression in the dentate gyrus is not sufficient to trigger or promote epileptiform activity.

Further analysis of hippocampal rhythmogenesis during various behavioral states however revealed significant alterations upon KCC2 knockdown in the dentate gyrus. Thus, while theta-band activity recorded during exploration and rapid-eye movement (REM) sleep was not significantly affected (Fig S6), we observed a specific increase in both the amplitude (Kolmogorov-Smirnov, $p < 0.001$, Fig 5E) and frequency (Kolmogorov-Smirnov, $p < 0.001$, Fig 5E) of dentate spikes during slow-wave sleep (SWS). Dentate spikes are sharp hilar LFP events associated with rest[55] that arise from a transient increase in the excitatory drive from the entorhinal cortex, as revealed by current source density analysis[55]. Our results suggest these changes in dentate spike activity resulted primarily from increased excitability of dentate granule cells. Restoring granule cell excitability independently of chloride export and GABA signaling was then predicted to rescue dentate spike activity. We tested this prediction by co-injecting animals with adeno-associated viruses (AAV2.1) expressing the inhibitory receptor hM4D(Gi)[56] and either non-target or KCC2-directed shRNA with GFP (Fig S5F-G). Using this approach, all granule cells expressing GFP also expressed hM4D(Gi), thereby enabling specific silencing of neurons expressing shRNA sequences (Fig. 5G). We first verified that hM4D(Gi) activation was sufficient to hyperpolarize transduced granule cells *in vitro*. Indeed, in whole cell recordings from transduced neurons, bath application of the hM4D(Gi) ligand CNO (10µM) induced a hyperpolarizing shift of V_{rest} by -5.66 ± 1.42 mV (paired t-test, $p < 0.01$, Fig S7). As in lentivirus-infected animals, AAV-mediated KCC2 suppression in the dorsal dentate gyrus increased the amplitude of dentate spikes during SWS ($n = 3$ rats per condition, Kolmogorov-Smirnov, $p < 0.001$, Fig 5H). Following systemic injection of CNO (1 mg/kg, i.p.), the amplitude of dentate spikes in animals injected with KCC2-directed shRNA was reduced to levels below those of saline-treated control animals (Fig 5H). Similarly, CNO injection reduced the frequency of dentate spikes in both KCC2-knockdown and control animals (Kolmogorov-Smirnov, $p < 0.001$, Fig 5F). Together, our data demonstrate that KCC2 suppression in dentate granule cells leads to altered hippocampal rhythmogenesis through a reduced Task3-mediated potassium conductance and a subsequent increase in neuronal excitability, independent of GABA signaling.

Discussion

Cation-chloride cotransporters (CCCs) are essential to neuronal chloride homeostasis. Thus, changes in their expression level in the developing brain are associated with changes in the polarity of GABA transmission[3] and altered CCC function or expression is observed in a variety of neurological and psychiatric conditions[15,16]. In the pathology, KCC2 downregulation has often been assumed to primarily affect GABA signaling and thereby promote hyperexcitability[17,18,25,26,27,57]. However, this hypothesis was not tested in isolation from other, potentially confounding pathological factors. Here we directly tested the impact of a chronic suppression of KCC2 both on the cellular and synaptic properties of hippocampal neurons as well as on network activity associated with behavior. We demonstrate that KCC2 knockdown in dentate granule cells has little effect on GABA signaling at rest but instead increases their excitability via interaction with the leak potassium channel Task-3. We establish that this increased excitability strengthens EPSP/spike coupling in dentate gyrus granule cells thereby acting to enhance their recruitment by entorhinal afferents. This in turn results in altered local rhythmogenesis that was fully rescued by restoring granule cell intrinsic excitability. Thus, KCC2 downregulation affects a variety of synaptic and intrinsic properties in hippocampal neurons beyond the mere control of GABA transmission and concur to perturb hippocampal rhythmogenesis.

KCC2 interacts with a variety of transmembrane as well as intracellular partners, including postsynaptic receptors[44,45,46], actin-related proteins[34,35,36] and others involved in protein trafficking and recycling[37]. Although these interactions are most often considered with regard to KCC2 expression or function, they also influence the function of KCC2 partners. For instance, loss of βPIX-KCC2 interaction increases the activity of βPIX effectors of the Rac1/PAK/LIMK pathway, likely through subcellular relocation[35,36]. Here, using immunoprecipitation assays, we identified the leak potassium channel Task-3 (*KCNK9*) as a novel KCC2 interactor in hippocampal neurons. We show Task-3 expression and function in neurons are reduced upon KCC2 downregulation and demonstrate that Task-3 membrane targeting requires KCC2 expression in heterologous cells. Thus, in cells lacking KCC2, Task-3 was sequestered intracellularly and its membrane expression was reduced (Fig. 3). We did not attempt to fully identify the molecular determinants of this interaction or the mechanism involved in KCC2-dependent trafficking of Task-3 channels. However, it is remarkable that whereas Task-3 was not found among KCC2 interactors by functional proteomics, several members of the *YWHA* family encoding 14-3-3 proteins were identified as putative partners[37]. 14-3-3 are adaptor proteins involved in a variety of biological

functions that include masking phosphorylated or interaction sites of their targets or altering their subcellular localization[58]. In particular, 14-3-3 proteins were shown to bind to and influence the membrane traffic of both Task-1 and Task-3 channels[59]. This effect is mediated through a KRR retention signal in the carboxy-terminal domain of the channels that is masked by 14-3-3 binding. Thus, phosphorylation-dependent binding of 14-3-3 suppresses coatomer protein I (COPI)-mediated retention of Task channels in the endoplasmic reticulum[59,60]. We therefore propose that KCC2 binding to both 14-3-3 and Task-3 may somehow influence the interaction between the two proteins, thereby preventing COPI-mediated sequestration of the channels in the endoplasmic reticulum. We cannot exclude, however, that KCC2-Task-3 interaction may also occur at the plasma membrane and act to stabilize Task-3 channels.

In mature neurons, KCC2 plays a prominent role in maintaining transmembrane chloride gradients, thereby influencing ion flux through the chloride-permeable GABAA receptor channels. Thus, KCC2 pharmacological blockade[45,46], genetic ablation[61,62] or suppression[63], or activity-dependent modulation[6,11,46,64] all result in a depolarization of the reversal potential of GABAAR-mediated currents (E_{GABA}). Consistent with these observations, we found that chronic KCC2 knockdown in dentate granule cells resulted in a depolarizing shift of E_{GABA} by about 9 mV. This effect was, however, almost fully compensated by a depolarization of their resting membrane potential (V_{rest}) of about the same magnitude (Fig. 1), resulting in a driving force of GABAAR currents that was virtually unaffected. This effect was not specific of dentate gyrus granule cells as it was observed also in CA1 pyramidal neurons (Fig. S3). Despite the importance of the membrane potential in setting the efficacy and polarity of GABA signaling, only one study investigated the effect of KCC2 suppression on V_{rest} in cerebellar neurons[61]. Thus, conditional KCC2 ablation resulted in a depolarization of V_{rest} that also compensated the shift in E_{GABA} in granule cells but not Purkinje cells. Interestingly, hippocampal and cerebellar granule cells as well as CA1 pyramidal cells strongly express Task-3 channels[42,65] whereas in Purkinje cells predominantly express Task-1 and Task-5[65,66]. Thus, differential expression of leak potassium channels may underlie cell-specific effects of KCC2 knockdown on resting membrane potential and the driving force of GABAAR currents.

KCC2 downregulation has often been linked to epileptogenesis. Thus, KCC2 expression is reduced in several animal models of experimental epilepsy including kindling[67], traumatic brain injury[68] and pilocarpine-induced *status epilepticus*[20]. Moreover, genetic studies identified loss of

function mutations in the *Slc12a5* gene encoding KCC2 in families with idiopathic epilepsy[19,22,69]. Finally, lack of KCC2 expression was associated with depolarized E_{GABA} in 20-30% principal neurons in the subiculum resected from temporal lobe epilepsy patients[18,70] as well as in human peritumoral neocortical slices[71]. This work suggested that KCC2 downregulation may be causal to the pathological, interictal activity recorded *in vitro* and a modeling study supported such conclusion[17]. Our experiments allowed us to test this hypothesis experimentally for the first time. Despite a high density and wide spread of infection in most of the dorsal dentate gyrus, we did not however find any sign of epileptiform activity in rats with suppressed KCC2 expression (Fig. S5). Thus, these animals did not show spontaneous seizures and intrahippocampal recordings around the infected area failed to reveal interictal discharges or fast ripples that occur between seizures both in patients and in animal models of focal epilepsy[72,73]. Susceptibility to pilocarpine-evoked *status epilepticus* was also unaffected by KCC2 knockdown. Our data therefore argue against a causal link between KCC2 downregulation and the emergence of epileptiform activity, at least in the dentate gyrus. Several arguments may help resolve this apparent discrepancy between our results and data from human epileptic tissue and animal models. First, epileptic networks undergo a number of physio-pathological alterations that may contribute to or promote epileptiform activities, including cell death, axonal sprouting, inflammation, as well as changes in synaptic and intrinsic neuronal membrane properties[74]. Thus, it is interesting to note that KCC2 suppression failed to produce epileptiform activity in a subicular model network unless extracellular potassium was raised to a non-physiological range, thereby increasing neuronal excitability[17]. In addition, our data show that depolarized E_{GABA} upon KCC2 suppression is fully compensated by depolarized V_{rest}, such that KCC2 knockdown neurons are more excitable although GABA signaling remains inhibitory. Depolarizing GABAergic responses may then require further depolarization of E_{GABA}, for instance through concomitant upregulation of the NKCC1 transporter, as observed in temporal lobe epilepsy models[20,75] as well as in the cortex and hippocampus from epileptic patients[71,76].

Our results show that KCC2 downregulation in the dentate gyrus is nevertheless sufficient to alter local rhythmogenesis. Thus, we report a specific increase in the amplitude and frequency of dentate spikes upon KCC2 knockdown (Fig. 5). Dentate spikes are population activities that occur in the dentate gyrus during sleep and immobility and are thought to represent synchronous activation of granule cells by entorhinal afferents[55]. This phenotype is therefore consistent with the cellular impact of KCC2 knockdown we observed in dentate granule cells, i.e. membrane depolarization and increased excitability due to Task-3 downregulation. We showed

these effects combined to promote EPSP/spike coupling, despite a reduced synaptic strength at glutamatergic inputs onto granule cells, as previously observed in hippocampal neurons[33,35]. Although granule cells fire sparsely under physiological conditions, KCC2 suppression and subsequent increased excitability promote their recruitment by entorhinal afferents. Thus, less simultaneous glutamatergic quantal EPSCs are required for firing KCC2 knockdown granule cells and they fire more action potentials than control cells during high frequency trains of afferent inputs (Fig. 4C-D). Several arguments support that these effects were mostly independent of KCC2-induced alterations in GABA transmission. First, GABA transmission was still inhibitory upon KCC2 suppression, as indicated by the unchanged driving force of GABAAR-mediated currents (Fig. 1) and the excitatory effect of picrotoxin on evoked population spikes (Fig. 4G). Second, increased dentate spike amplitude was fully compensated by chemogenetic hyperpolarization of KCC2 knockdown neurons (Fig. 5). Since GABAAR activation is depolarizing in dentate granule cells[49], hM4D(Gi)-induced hyperpolarization rescued V_{rest} in infected granule cells but further enhance the depolarizing nature of GABA transmission. If GABA signaling was involved in the increased dentate spike amplitude and frequency, hM4D(Gi) silencing would then be expected to worsen, not rescue this phenotype.

Together, our work reveals for the first time the effects of a chronic downregulation of KCC2 expression in an intact network. We show these effects are diverse but primarily involve increased neuronal excitability, not reversed GABA signaling. They lead to altered network activity without however promoting seizures. Thus, KCC2 suppression in the dentate gyrus primarily affects dentate spike activity with no detectable effect on theta-band activity throughout the hippocampal formation (Fig. S6). This rather subtle phenotype may still be of physiopathological relevance for disorders associated with KCC2 downregulation. Dentate spikes coincide with periods of stronger gamma-band activity coherence between hippocampus and cortex and are temporally correlated to the power of sharp-wave ripples[77]. Since both dentate spikes[78] and sharp-wave ripples[79] have been associated with memory consolidation in hippocampal-dependent learning, we predict KCC2 suppression in the pathology may impact cognitive performances through a combination of GABA-dependent and -independent mechanisms. Our results suggest therapeutic strategies aiming to either restore neuronal chloride homeostasis by blocking NKCC1 function[57] and neuronal excitability by targeting leak potassium channels[80], or to stabilize KCC2 membrane expression[25,32] may best compensate for altered network activity and associated behavioral or cognitive deficits.

Figures

Table 1. Overview of membrane and firing properties in infected dentate granule cells

	shNT	shKCC2	p.value (t-test)
N (cells / slices / rats)	18 / 9 / 5	21 / 12 / 7	
Series resistance (MΩ)	7.28 ± 0.33	6.57 ± 0.50	0.2634
Membrane potential (mV)	-87.67 ± 1.06	-80.79 ± 1.61	0.0014
Membrane resistance (MΩ)	513.38 ± 47.85	662.70 ± 47.14	0.0332
AP threshold (mV)	-50.56 ± 1.30	-50.70 ± 1.92	0.9524
AP amplitude (mV)	89.59 ± 1.82	88.31 ± 3.31	0.5636
AP width (ms)	0.89 ± 0.030	0.74 ± 0.026	0.0008
AHP (mV)	15.19 ± 1.04	19.70 ± 1.73	0.0390

Figure 1. KCC2 suppression in dentate granule cells does not alter steady state GABA signaling

A, Top, Experimental timeline. P30 Wistar rats were injected with lentiviral vectors (LV) expressing either non-target (shNT) or KCC2-directed (shKCC2) shRNA sequences and EGFP. *In vitro* electrophysiological recordings were performed 10 to 20 days post-injection. Bottom, maximal intensity projection of confocal micrographs showing infected cells (GFP, green) and DAPI (blue) staining in a parasagittal hippocampal slice 2 weeks after injection. Arrowhead indicates mossy fibers from infected granule cells. Scale bar, 500 µm. **B,** Maximal intensity projection of confocal micrographs of infected dentate gyrus areas, showing massive extinction of KCC2 expression in KCC2 knockdown neurons. Dotted line delimitates *st. granulosum*. Neurons expressing non-target but not KCC2-directed (arrows) show pericellular KCC2 immunostaining, as do neighboring uninfected cells (arrowheads). Scale bar, 50 µm. **C,** Representative currents following Rubi-GABA somatic uncaging (Flash, dotted line) recorded in gramicidin perforated-patch configuration during incremental voltage steps. **D,** I-V curve of GABA-induced currents corresponding to the examples shown in C. E_{GABA} is interpolated from the two points around reversal. E, Summary data (shNT n = 12 cells, 6 rats, shKCC2 n = 14 cells, 6 rats) show depolarized E_{GABA} upon KCC2 suppression (* $p<0.05$). The resting membrane potential (V_{rest}) is also depolarized (** $p<0.01$), resulting in no significant change in the driving force of GABAergic currents.

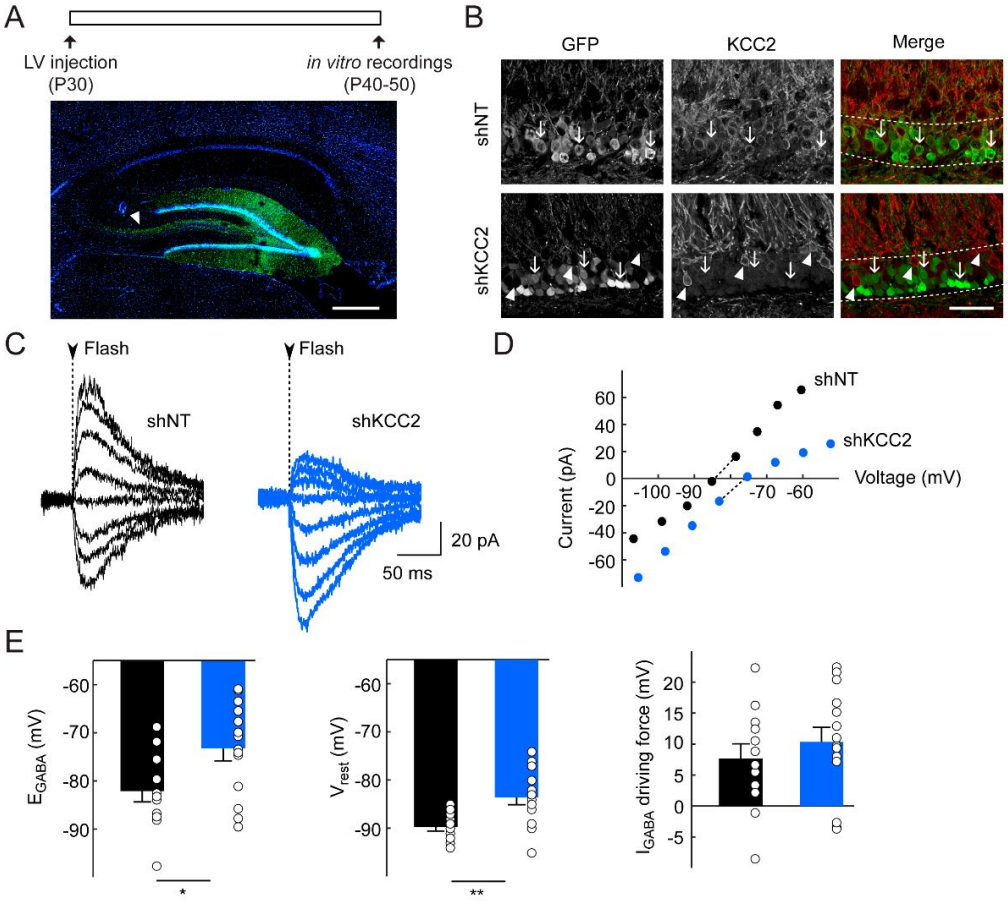
A
LV injection
(P30)
in vitro recordings
(P40-50)
B
GFP
KCC2
Merge
shNT
shKCC2
C
Flash
shNT
Flash
shKCC2
20 pA
50 ms
D
shNT
shKCC2
Current (pA)
Voltage (mV)
60
40
20
0
-20
-40
-60
-100 -90
-70 -60
E
E_{GABA} (mV)
V_{rest} (mV)
I_{GABA} driving force (mV)
-60
-70
-80
-90
20
15
10
5
0
-5
*
**

Figure 2. Increased excitability upon KCC2 extinction reflects downregulation of a leak potassium conductance

A, Summary graphs of membrane properties of granule cells expressing non-target (n = 18 cells, 5 rats) or KCC2-directed (n = 21 cells, 7 rats) shRNA recorded in whole-cell patch clamp mode in the presence of synaptic transmission blockers. KCC2 knockdown resulted in depolarized membrane potential (** $p<0.01$) and increased input resistance (* $p<0.05$). **B,** Individual traces in both conditions for a depolarizing current pulse of 50 pA. **C,** Input/output curve for all cells representing the firing frequency as a function of the injected current (*** $p<0.001$). **D,** Action potential threshold was determined as the voltage for which derivative of the signal exceeded 15 mV/ms and was not different between conditions. **E,** Individual phase plots of action potentials (insets) recorded in neurons expressing either shRNA sequence, showing no change in the shape of action potentials upon KCC2 suppression. **F,** The amplitude of action potentials was also unchanged in KCC2-knockdown cells. **G,** Representative individual traces for potassium currents recorded in voltage-clamp mode with a voltage ramp ranging -120 to -50 mV at 0.03 mV/ms, in the presence of synaptic transmission blockers and TTX. **H,** Summary plots of mean currents in cells expressing non-target (shNT n = 18 cells, 5 rats) vs. KCC2-directed (shKCC2 n = 21 cells, 7 rats) shRNA. Bath application the leak-potassium channel blocker bupivacaine (100 µM) reduced potassium currents only in control cells (shNT n = 16 cells, 3 rats, shKCC2 n = 19 cells, 5 rats). **I,** Rectification index plot, defined as the ratio of potassium-mediated currents at -60 mV vs. -120 mV. KCC2 knockdown resulted in reduced rectification (*** $p<0.001$). **J,** Bath application of bupivacaine (100µM) rescues resting membrane potential in KCC2-knockdown neurons (* $p<0.05$).

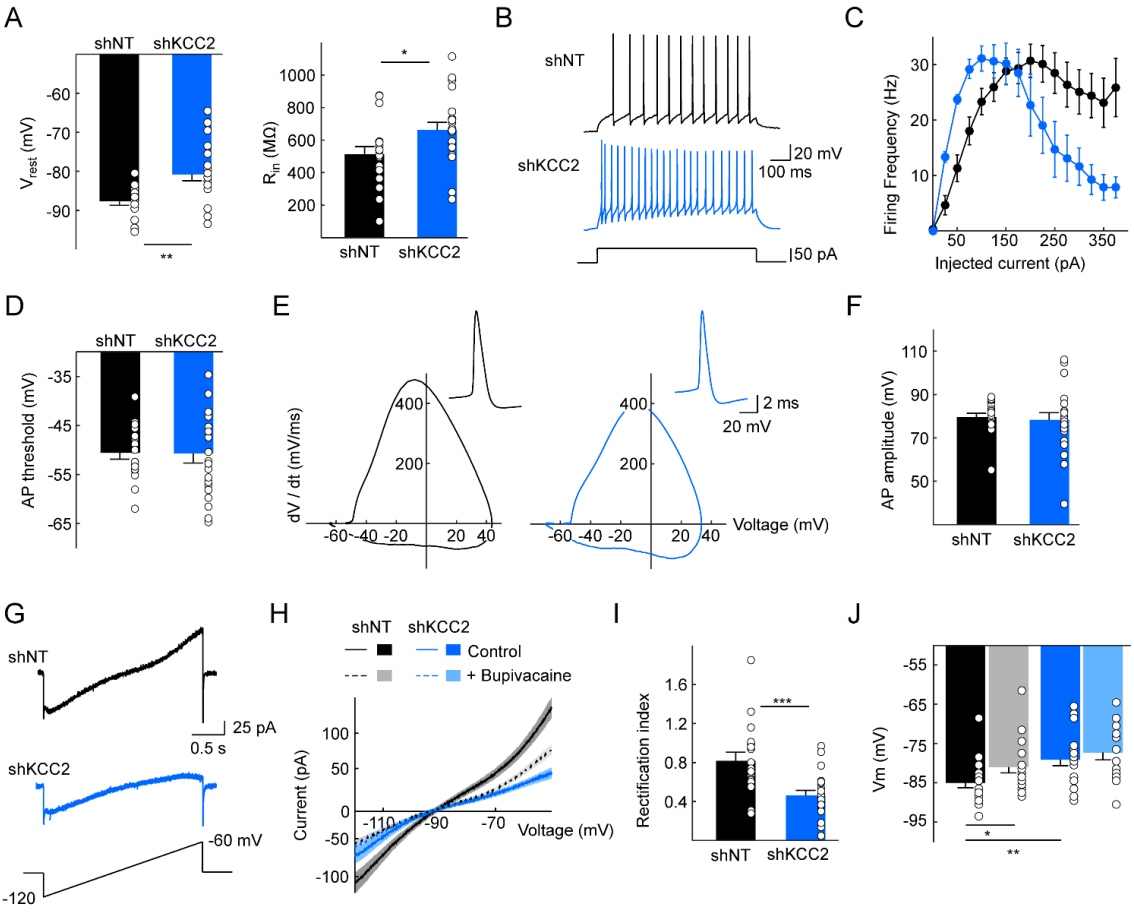
A
shNT
shKCC2
V_{rest} (mV)
-60
-70
-80
-90
**
R_{in} (MΩ)
1000
800
600
400
200
*
shNT
shKCC2
B
shNT
shKCC2
20 mV
100 ms
50 pA
C
Firing Frequency (Hz)
30
20
10
50
150
250
350
Injected current (pA)
D
shNT
shKCC2
AP threshold (mV)
-35
-45
-55
-65
E
dV / dt (mV/ms)
400
200
-60 -40 -20
20 40
2 ms
20 mV
Voltage (mV)
F
AP amplitude (mV)
110
90
70
50
shNT
shKCC2
G
shNT
25 pA
0.5 s
shKCC2
-60 mV
-120
H
shNT
shKCC2
Control
+ Bupivacaine
Current (pA)
100
50
0
-50
-100
-110
-90
-70
Voltage (mV)
I
Rectification index
1.6
1.2
0.8
0.4
***
shNT
shKCC2
J
Vm (mV)
-55
-65
-75
-85
-95
*
**

Figure 3. KCC2 interacts with Task-3 and promotes its membrane expression

A, Maximal intensity projection of confocal micrographs (4 focal planes, 0.2 µm z-step) of infected dentate gyrus, showing decreased Task-3 pericellular immunostaining in KCC2 knockdown *vs.* control granule cells. Scale, 10 µm. **B,** Immunoblot of co-IP samples of endogenous proteins extracts from adult rat hippocampi. Solubilized membrane homogenates (input) were immunoprecipitated with either Task-3, KCC2 or control IgG antibodies. Eluates resulting from immunoprecipitations (IP fractions) were then probed for both Task-3 and KCC2. Task-3 IP pulled down KCC2, therefore demonstrating KCC2 interaction with Task-3 in adult hippocampus. KCC2 IP however did not reveal detectable Task-3 protein level in these samples. Representative example of three independent replicates. **C,** Immunoblot of the immunoprecipitates from HEK293T cell homogenates coexpressing recombinant, Flag-tagged KCC2 and HA-tagged GFP (left) or HA-tagged Task-3 (right). Immunoprecipitation using Flag antibodies pulled down Task-3 (right) but not GFP (left). Conversely, immunoprecipitation with HA antibodies precipitated Flag-KCC2 only in HA-Task-3 expressing cells. Each immunoblot is a representative example of three independent experiments. **D,** Focal plane from confocal micrographs of HEK293T cells transfected with either HA-Task-3 alone (top) or HA-Task-3 together with Flag-KCC2 (bottom). Note the accumulation of HA immunostaining in an intracellular compartment in absence of Flag-KCC2 (arrowhead). Scale, 20µm. Fluorescence intensity of HA staining across the cell membrane and cytoplasm was analyzed along the white line shown on the micrographs and plotted in dotted insets (right). Scale, 5 µm. **E,** Averaged, scaled line scan intensity plots from all cells (HA-Task-3, n = 12 ; HA-Task-3+Flag-KCC2, n =15) reveal intracellular accumulation of Task-3 in absence of KCC2 as evidenced by the averaged HA intensity across line scans and the decreased ratio of membrane to intracellular intensity (inset, *** $p<0.001$).

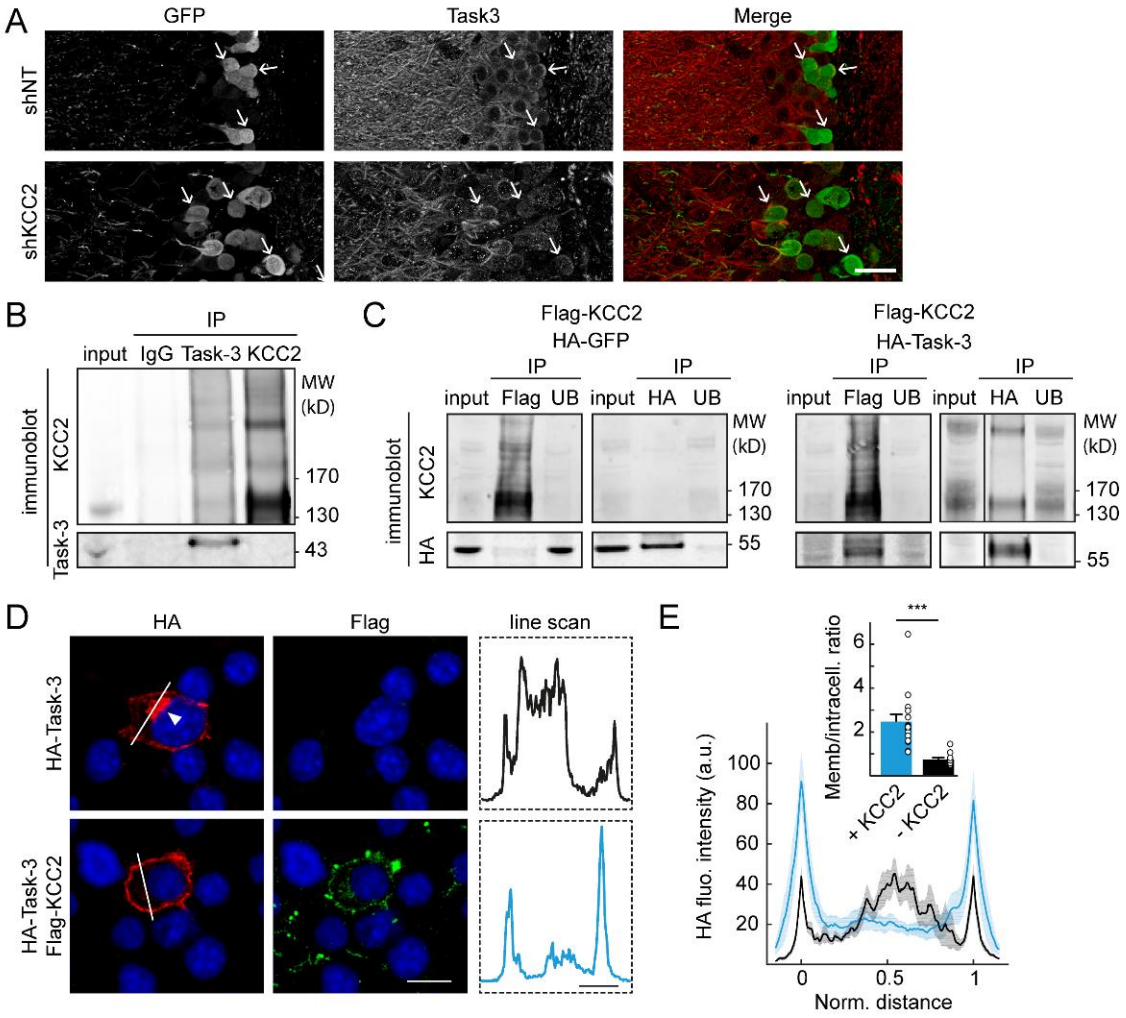
A
GFP
Task3
Merge
shNT
shKCC2
B
IP
input IgG Task-3 KCC2
immunoblot
KCC2
Task-3
MW (kD)
170
130
43
C
Flag-KCC2
HA-GFP
Flag-KCC2
HA-Task-3
IP
input Flag UB input HA UB
immunoblot
KCC2
HA
MW (kD)
170
130
55
D
HA
Flag
line scan
HA-Task-3
HA-Task-3 Flag-KCC2
E
***
Memb/intracell. ratio
+ KCC2
- KCC2
HA fluo. intensity (a.u.)
Norm. distance

Figure 4. KCC2 suppression increases EPSP/Spike coupling in dentate granule cells

A, 4 s-recordings of mEPSCs from infected granule cells expressing non-target (shNT, black, n = 13 cells, 3 rats) or KCC2-directed (shKCC2, blue, n = 15 cells, 3 rats) shRNA. **B,** Summary data of mEPSC showing reduced amplitude (left) but not frequency (right). **C,** Left, representative recordings of current clamp recordings (top) from granule cells kept at their resting membrane potential upon somatic injection of multiples of scaled, mEPSC waveforms of increasing amplitude (bottom). Right, summary plots of all data (shNT, n = 13 cells, 2 rats, shKCC2, n = 15 cells, 2 rats) showing enhanced EPSP/spike coupling in KCC2 knockdown neurons. **D,** Neurons were kept at -87 mV in current clamp mode and trains of 120 pA amplitude mEPSCs (about 20x quantal size) were injected as in C at various frequency. Left, representative traces for trains of 10 EPSC waveform at 10, 50 and 100 Hz. Right, for trains delivered at 50 or 100 Hz, firing probability was enhanced in KCC2 knockdown granule cells (* $p < 0.05$, shNT, n = 13 cells, 2 rats, shKCC2, n = 15 cells, 2 rats). **F,** Left, experimental paradigm to test EPSP/spike coupling for synaptically evoked responses in slices. A bipolar electrode was located in the molecular layer to stimulate entorhinal afferents while field PSPs and population spikes were recorded with a glass electrode located in the granule cell layer (top). fEPSP and population spike amplitudes were measured as shown (bottom). Right, average of 10 consecutive responses recorded at 0.1 Hz. **G,** Data from n = 15 slices infected with non-target shRNA (shNT, 6 animals,) and 16 slices infected with KCC2-directed shRNA (shKCC2, 6 animals) confirmed increased coupling of fEPSP to population spike (* $p<0.05$). **H,** Bath application of the GABAAR pore blocker picrotoxin resulted in increased amplitude of the population spike in both conditions, indicating GABA transmission was functionally inhibitory.

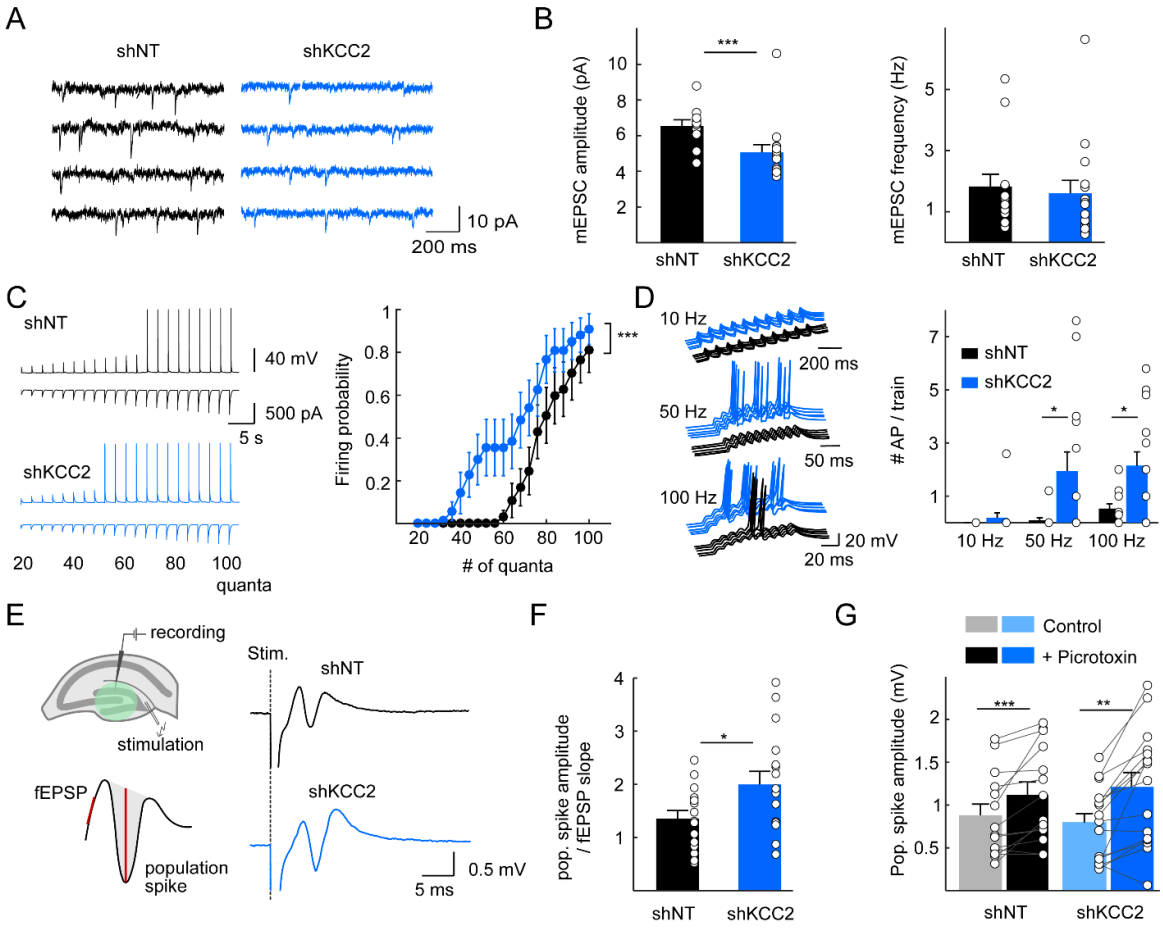
A
shNT
shKCC2
10 pA
200 ms
B
mEPSC amplitude (pA)
***
shNT
shKCC2
mEPSC frequency (Hz)
C
shNT
40 mV
500 pA
5 s
shKCC2
20 40 60 80 100
quanta
Firing probability
# of quanta
D
10 Hz
200 ms
50 Hz
50 ms
100 Hz
20 mV
20 ms
AP / train
10 Hz 50 Hz 100 Hz
E
recording
stimulation
fEPSP
population spike
Stim.
shNT
shKCC2
0.5 mV
5 ms
F
pop. spike amplitude / fEPSP slope
G
Control
+ Picrotoxin
Pop. spike amplitude (mV)

Figure 5. KCC2 suppression alters dentate gyrus rhythmogenesis primarily through increased neuronal excitability

A, Experimental timeline. P30 Wistar rats were injected with shRNA-expressing lentiviral vectors. A week later, 16-channels linear silicon probe were implanted at the same coordinates. *In vivo* recordings were performed starting from 3 days post-implantation. **B,** Longitudinal spread of the viral infection was determined at the end of each experiments and was similar between groups (shNT n= 5 rats, shKCC2 n = 7 rats; p= 0.45). **C,** Macroscope DIC micrograph revealing probe localization (vertical scar). Scale, 250 µm. **D,** Top, the 16-channels silicon probe allow simultaneous recording of all hippocampal layers. Examples of recordings during non-REM sleep showing dentate spikes (highlighted in grey: shNT or blue : shKCC2). **E,** Dentate spikes were automatically detected for each animal. Cumulative amplitude (left) and inter-event intervals (right) histograms from 140 randomly selected events per animal, showing increased amplitude and frequency of dentate spike upon KCC2 knockdown in the dentate gyrus (*** $p<0.001$) **F,** Experimental timeline for rescue experiments with DREADD silencing as above, except that each animal was after either saline or CNO (1 mg/kg) i.p. injection. **G,** Single plane confocal micrographs confirmed most granule cells were co-infected with shRNA+GFP and hM4D(Gi)-mCherry (stars). Scale, 20 µm. **H,** Dentate spikes were automatically detected for each animal (3 per group). Cumulative amplitude (left) and inter-event intervals (right) histograms from 185 randomly selected events per animal. Injection of CNO significantly reduced dentate spike amplitude ($p < 0.001$) and frequency ($p < 0.001$) in both groups of animals.

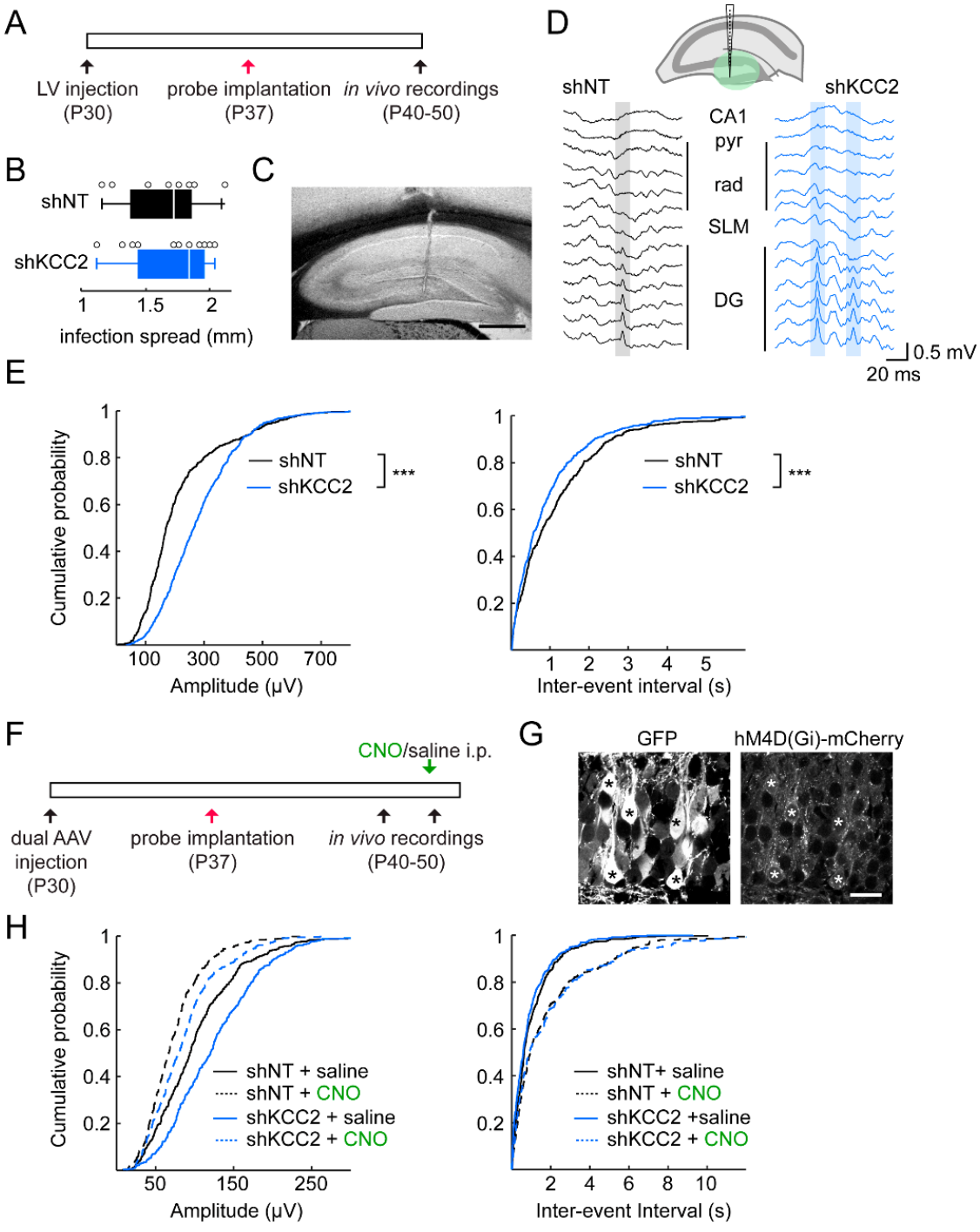
A
LV injection
(P30)
probe implantation
(P37)
in vivo recordings
(P40-50)
B
shNT
shKCC2
1
1.5
2
infection spread (mm)
C
D
shNT
shKCC2
CA1
pyr
rad
SLM
DG
0.5 mV
20 ms
E
Cumulative probability
shNT
shKCC2
***
Amplitude (μV)
Inter-event interval (s)
F
CNO/saline i.p.
dual AAV
injection
(P30)
probe implantation
(P37)
in vivo recordings
(P40-50)
G
GFP
hM4D(Gi)-mCherry
H
shNT + saline
shNT + CNO
shKCC2 + saline
shKCC2 + CNO
shNT+ saline
shKCC2 +saline
Inter-event Interval (s)

Supplementary Figures

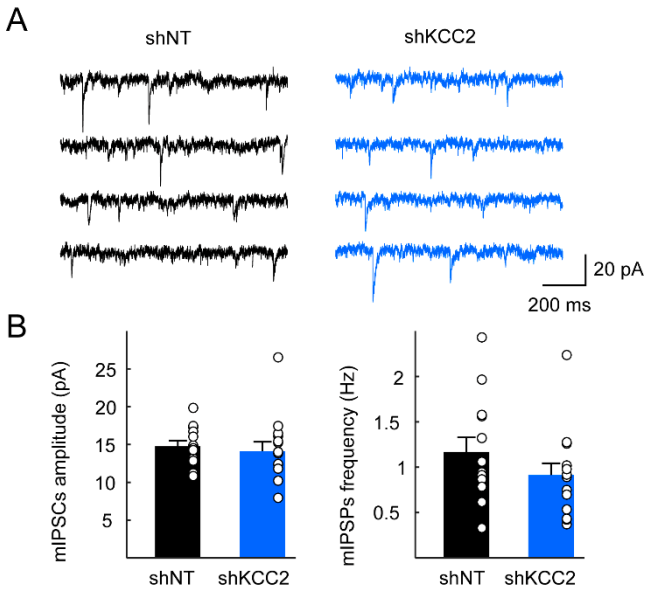

Figure S1. KCC2 suppression does not affect the efficacy of GABAergic synapses

A, 4 s-recordings of mIPSCs from granule cells expressing non-target (shNT, black) or KCC2-directed (shKCC2, blue) shRNA. **B,** Summary data from shNT (n = 13 cells, 2 rats) and shKCC2 (n = 14 cells, 2 rats) showing no changes in mIPSCs amplitude (left, p=0.42) or frequency (right, p=0.27).

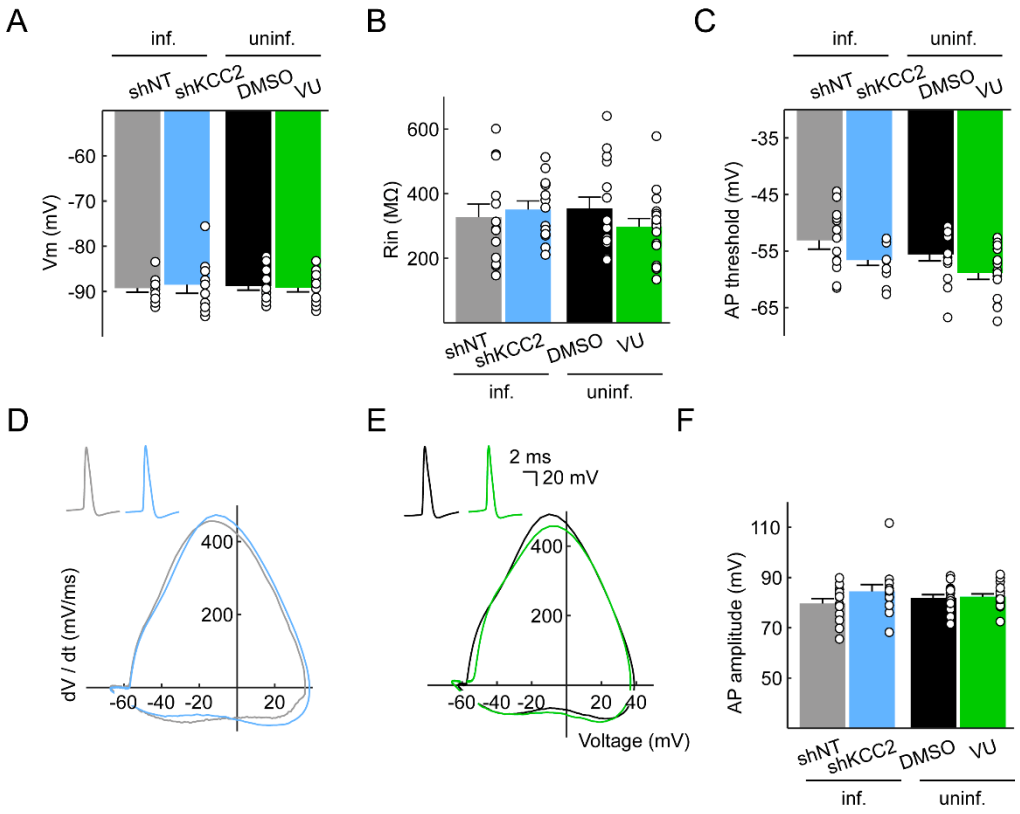

Figure S2. Increased excitability upon KCC2 knockdown is cell-autonomous and independent of KCC2-mediated ion transport.

Membrane and spike properties were analyzed for uninfected cells from slices infected with lentiviral vectors expressing non-target (grey, n = 13 cells, 5 rats) or KCC2-directed (light blue, n = 13 cells, 7 rats) shRNA sequences. Effect of KCC2 blockade for >30 min with its specific antagonist VU0463271 was also analyzed (green, n = 17 cells, 5 rats) and compared to DMSO treatment (black, n = 15 cells, 4 rats). No differences were observed in membrane potential (**A,** shNT *vs* shKCC2 p = 0.83, DMSO *vs* VU p =0.75), input resistance (**B,** shNT *vs* shKCC2 p = 0.63, DMSO *vs* VU p =0.20) was well as AP threshold (**C,** shNT *vs* shKCC2 p = 0.063, DMSO *vs* VU p =0.055), waveform (**D-E**) and amplitude (**F,** shNT *vs* shKCC2 p = 0.24, DMSO *vs* VU p =0.77).

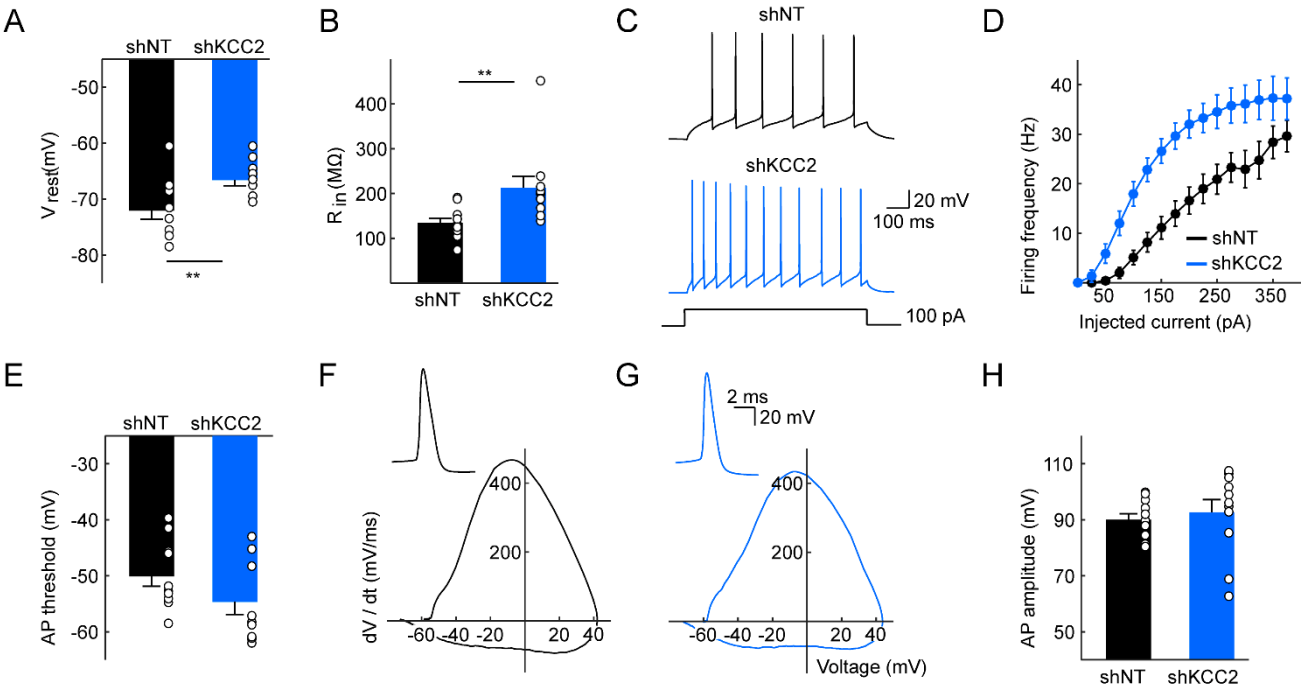

Figure S3. Increased excitability in CA1 pyramidal cells upon KCC2 suppression

A-B, Membrane properties of CA1 superficial pyramidal cells expressing non-target (n = 11 cells, 3 rats) or KCC2-directed (n = 11 cells, 3 rats) shRNA, as detected in whole-cell patch clamp recordings while blocking synaptic transmission. KCC2 knockdown resulted in depolarized membrane potential (A, ** $p<0.01$) and increased input resistance (B, ** $p<0.01$). **C,** Individual traces in both conditions for a depolarizing current pulse of 100 pA. **D,** Mean input/output relationships representing the frequency of APs as a function of injected current (*** $p<0.001$). No difference was observed between shNT and shKCC2-expressing CA1 pyramidal cells with regard to action potential threshold (**D**, $p=0.13$), spike waveform (**E**) or spike amplitude (**F**, $p=0.59$).

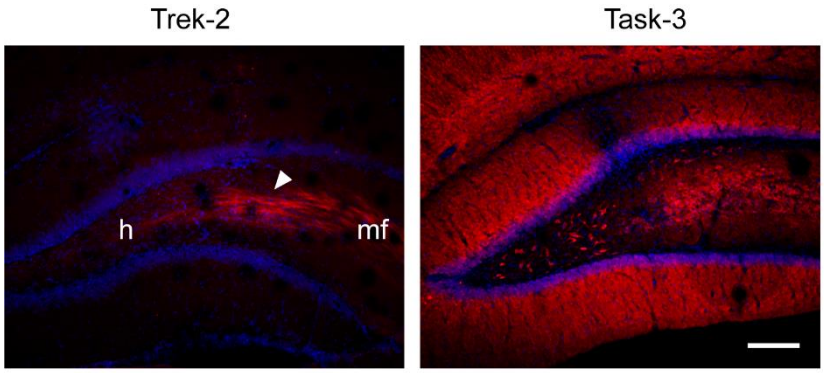

Figure S4. Differential subcellular localization of leak-potassium channels in the dentate gyrus

Left**,** Average intensity projection of confocal micrographs of dentate gyrus immunostained with Trek-2 antibody. Note the massive expression of Trek-2 in mossy fibers (arrowhead) and its relative absence in the granular and molecular layers of the dentate gyrus. h : hilus, mf : mossy fibers. Right**,** Average intensity projection of confocal micrographs of dentate gyrus immunostained with Task-3 antibody revealing a strong expression in both granular and molecular layers as well as in hilar mossy cells. Scale, 200 µm.

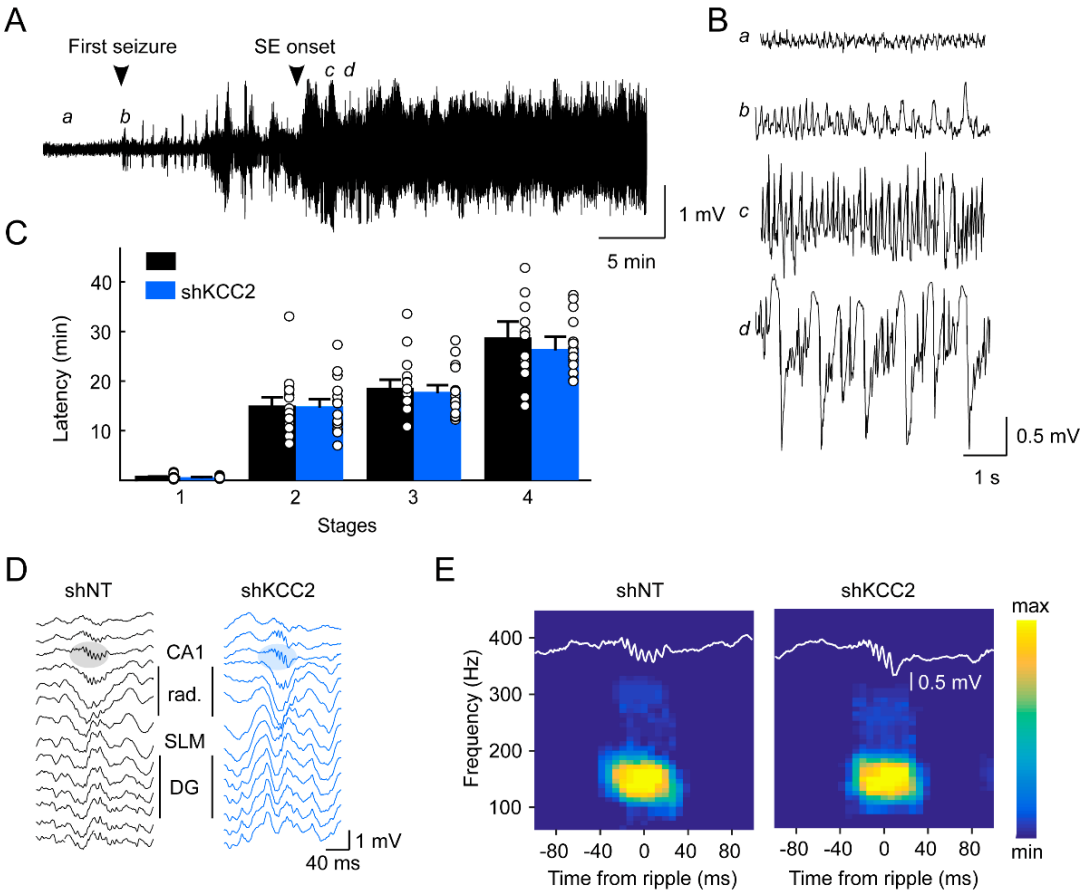

Figure S5. KCC2 suppression in the dentate gyrus does not induce or promote epileptiform activity

A, Example trace of an EcoG recording during epilepsy induction with a pilocarpine protocol. Arrowheads indicate the timing of the first seizure and the onset of the *status epilepticus*. **B**, Expanded sections of the recording shown in A, showing the evolution of the EcoG signal at different time points of ictogenesis. **C**, Behavioral state was classified according to modified Racine's scale as follows: stage 1, immobility and chewing; stage 2, neck and body clonus; stage 3, forelimb clonus and rearing; stage 4, *status epilepticus*, uninterrupted seizures. The onset of *status epilepticus* was assessed based on EcoG recordings. Latency to different stages was similar between groups (n = 15 animals each). **D**, Traces of ripple events recorded in CA1 during sleep for rats implanted with 16-channels silicon probes as in **Fig. 5**. **E**, Ripples were automatically detected and 100 events per animal were randomly selected (shNT n= 5 rats, shKCC2 n = 7 rats). Suppression of KCC2 in the dentate gyrus did not lead to pathological fast ripples as evidenced by the absence of band around 300 Hz in the average time-frequency spectra.

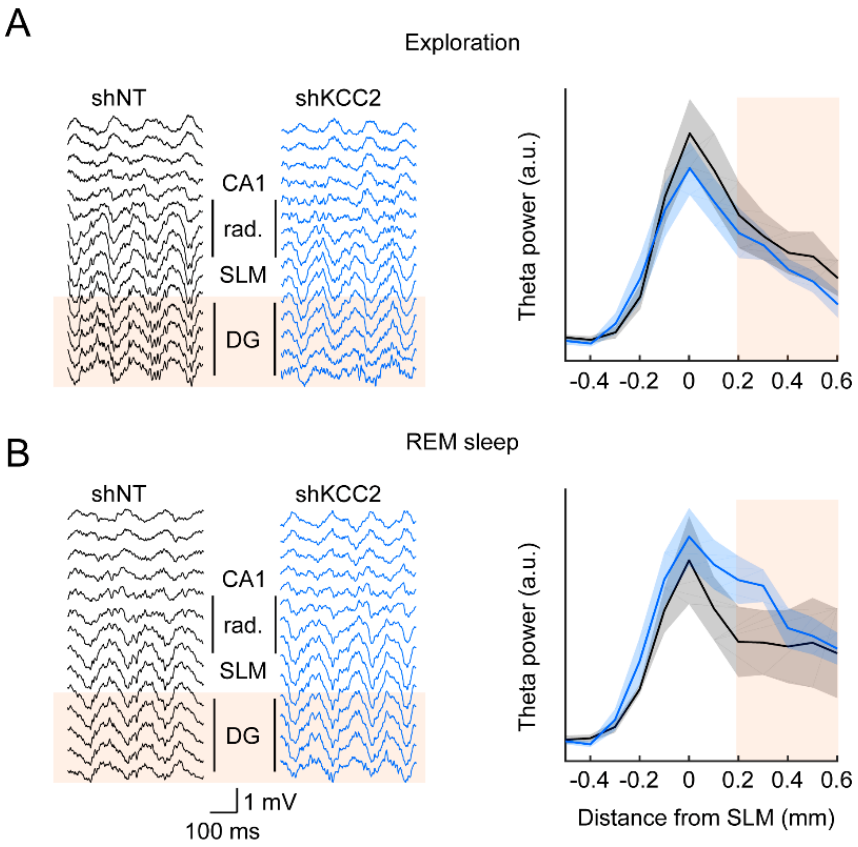

Figure S6. KCC2 suppression in the dentate gyrus does not affect hippocampal theta rhythm

A, Left, 500 ms stretches of intrahippocampal recordings (as in **Fig. 5**) during exploratory behavior in rats expressing non-target shRNA (left, black) or KCC2-directed shRNA (blue, right) in the dentate gyrus. Note the prominent theta oscillation in all channels. The localization of the *stratum lacunosum moleculare* was defined by the highest power of theta and CA1 was identified by the presence of action potentials and of ripples during sleep. Localization of the dentate gyrus is highlighted in orange. Right, theta power in the 5-10 Hz frequency band measured over > 1 min of recording using multi-tapers estimates. Power is represented as a function of the electrode localization. Depth of the electrode is expressed as the distance from *stratum lacunosum moleculare* (SLM). Two-way ANOVA $p = 0.15$. **B,** Similar as A, but during REM sleep. Depth profile was slightly different between groups (2-way ANOVA $p = 0.024$). However, comparisons for each layer individually did not yield any significant difference (Mann-Whitney, $p > 0.05$ for all layers).

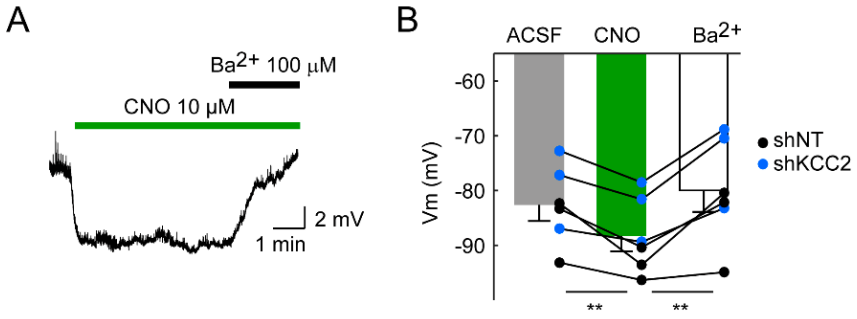

Figure S7. CNO application hyperpolarizes hM4D(Gi)-expressing dentate granule cells

A, Example current clamp recording of a dentate granule cell expressing non-target shRNA and hM4D(Gi) receptor, showing hyperpolarization of the membrane potential upon CNO (10 µM) bath application. Application of Ba^{2+} (100 mM $BaCl_2$) completely blocks CNO-induced hyperpolarization. **B,** Summary data from 3 cells expressing non-target shRNA and 3 cells expressing KCC2-directed shRNA, together with hM4D(Gi). All cells were hyperpolarized following CNO application (** $p<0.01$) and repolarized upon Ba^{2+} application

Methods

Animals

Juvenile male Wistar rats were obtained from Janvier Labs (Le Genest Saint Isle, France). All procedures conformed to the International Guidelines on the ethical use of animals, the French Agriculture and Forestry Ministry guidelines for handling animals (decree 87849, licence A 75-05-22) and were approved by the Charles Darwin ethical committee (APAFIS2015111011588776v3).

Virus and constructs

Rat *slc12a5*-specific and non-target shRNA sequences[33] were introduced in pTrip vector under U6 promoter and used to produce purified lentiviral particles (titer 7-9 x 10^9 TU/ml, UNC Vector Core Facility)[35]. For some experiments, these same sequences were introduced in pAAV vector under U6 promoter and used to produce purified AAV particles (AAV2.1-shRNA-GFP, titer 10^{13} TU/ml, Atlantic Gene Therapy, Nantes). AAV particles expressing inhibitory DREADD under synapsin promoter were obtained from the Viral Vector Facility of Zurich University (AAV2.1-hM4D(Gi)-mCherry, titer 10^{13} TU/ml).

Stereotaxic viral injection and EcoG electrodes implantation

30-days Wistar rats were anesthetized by intraperitoneal injection of ketamine / xylazine (75/10 mg/kg) and subcutaneous injection of buprenorphine (0.05 mg/kg) for analgesia. Animals were then head-fixed in a stereotaxic apparatus. 1 µl of lentivirus (concentrated at 10^9 TU/ml) was injected bilaterally in the dentate gyrus (AP -4.0 mm, ML +/- 2.5 mm, DV -3.1 mm) at 125 nl/min. For DREADD experiments, 500nL of mix AAV2.1-shRNA-GFP and AAV2.1-hM4D(Gi)-mCherry (ratio 2/3:1/3) was injected bilaterally in the dentate gyrus. For experiments in CA1, animals were injected bilaterally with 1 µl of AAV2.1-shRNA-GFP (AP -4.0 mm, ML +/- 2.5 mm, DV -2.35 mm).

For pilocarpine experiments, animals were also implanted with EcoG electrodes soldered to stainless steel screws. Two electrodes were placed above each hippocampus, at the same coordinates as the injection sites. A third screw was placed above the cerebellum and used as reference.

Intracerebral probe implantation

For intra-hippocampal recordings, animals were anesthetized with isoflurane one week following viral injection, and injected subcutaneously with 0.05 mg/kg of buprenorphine for

analgesia. One 16-channels silicon probe was implanted in the right hemisphere, at the site of the injection. Signals were monitored during the insertion of the probe to ensure correct localization of the probe in the hippocampus. One stainless steel screw was placed above the cerebellum and connected to the probe as a reference. Four additional screws were placed above the prefrontal cortex and the contralateral hemisphere to secure the dental cement adhesion. During the recovery period (minimum 3 days), rats were daily monitored and additional injection of buprenorphine (subcutaneous, 0.05 mg/kg) were made in case of detectable pain.

Electrophysiology

Slice preparation

10 to 20 days after viral injection, animals were deeply anesthetized with ketamine / xylazine (115/15 mg/kg) and transcardially perfused with an ice-cold choline-based solution containing (in mM) : 110 Choline Cl, 25 Glucose, 25 $NaHCO_3$, 11.6 Ascorbic acid, 3.1 Pyruvic acid, 1.25 NaH_2PO_4, 2.5 KCl, 0.5 $CaCl_2$, 7 $MgCl_2$ saturated with 95% O_2/5% CO_2. Rats were then decapitated, hippocampi were rapidly dissected and 400µm transverse sections were prepared using a vibratome (Microm, Thermofisher). Slices were then transferred and allowed to recover for 1 hour in a humidified interface chamber filled with bicarbonate-buffered ACSF pre-heated at 37°C and oxygenated with 5% CO_2 in O_2, containing (in mM) : 126 NaCl, 26 $NaHCO_3$, 10 Glucose, 3.5 KCl, 1.25 NaH_2PO_4, 1.6 $CaCl_2$, 1.2 $MgCl_2$. For recordings, slices were transferred in a submerged recording chamber and superfused with ACSF maintained at 32°C.

Patch clamp recordings

Electrophysiological recordings were made with 4-5 MΩ borosilicate glass pipettes. Signals were acquired with a Multiclamp 700B amplifier (Molecular Devices), low-pass filtered at 10 kHz, and digitized at 20 kHz. All cells were recorded in the suprapyramidal blade of the dentate gyrus.

For perforated-patch recordings, internal solution contained (in mM) 140 KCl and 10 HEPES (pH adjusted to 7.4 with KOH). Gramicidin was added in the pipette solution to reach a concentration of 60 µg/ml. Rubi-GABA was added in ACSF (15 µM, Tocris) together with NBQX (20 µM, HelloBio), APV (50 µM, HelloBio), CGP54626 (10 µM, Tocris) and TTX (1 µM, Latoxan). Rubi-GABA was photolyzed using a digital modulated diode laser beam at 405 nm (Omicron Deepstar, Photon Lines, Marly Le Roi, France) delivered through a single path photolysis head (Prairie Technologies, Middleton, USA). The laser beam diameter was set to a diameter of 3-5 µm and was directed onto the soma of the recorded neuron. Photolysis was induced by a 5 ms/30 mW pulse. Once access resistance was stabilized, cells were held at a potential of -70 mV

and 3.5 s voltage steps ranging from -100 to -30 mV were applied to the cell. Laser pulses were delivered at 2.2 s after the onset of the voltage step to allow for stabilization of the holding current. Currents were analyzed offline using Clampfit software (Molecular Devices). Voltages were corrected for liquid junction potential (4.1 mV) and for the voltage drop through the series resistance

For all other patch clamp experiments, cells were recorded in whole-cell configuration and maintained at -70 mV. All voltages were corrected offline for liquid junction potential (of 14.5 mV).

Intrinsic properties were evaluated using an internal solution containing (in mM) 120 K-Gluconate, 10 KCl, 10 HEPES, 0.1 EGTA, 4 MgATP, 0.4 Na_3GTP (pH adjusted to 7.4 with KOH) and blocking synaptic transmission with NBQX, APV and picrotoxin (10µM, HelloBio). Resting membrane potential was measured using I=0 current clamp mode one minute after break-in. Input resistance was measured in current-clamp mode with -50 pA current steps. Input/output curves were derived from series of 800 ms current steps (ranging from -100 to 375 pA, 25 pA step increment). For potassium currents measurements, TTX (1 µM) was added to the bath. Currents were recorded in voltage-clamp mode between -120 mV and -60 mV with a continuous ramp at 0.03 mV/ms. For EPSP/spike coupling recordings, artificial waveforms derived from mEPSC recordings were used as a current command applied to the patch pipette. Effect of CNO application on membrane potential was estimated by whole-cell recordings in current-clamp mode with no current injection.

For miniature excitatory postsynaptic current (mEPSCs) recordings, pipettes were filled with internal solution containing (in mM) 115 Cs-Methylsulfonate, 20 CsCl, 10 HEPES, 0.1 EGTA, 4 MgATP, 0.4 Na_3GTP (pH adjusted to 7.4 with CsOH) and currents were isolated by adding TTX and bicuculline to the extracellular solution. For miniature inhibitory postsynaptic currents (mIPSCs), pipettes were filled with (in mM) 135 CsCl, 10 HEPES, 10 EGTA, 4 MgATP, 0.4 Na_3GTP, 1.8 $MgCl_2$ (pH adjusted to 7.4 with CsOH) and currents were isolated by adding TTX, NBQX and AP-V in the bath. Series and input resistance were regularly monitored with -5 mV voltage steps and recordings were interrupted if either value varied by more than 20 Miniature synaptic currents were detected and analyzed offline using Detectivent software[81].

Extracellular field recordings

For extracellular recordings, a recording pipette of 2-3 MΩ resistance was filled with ACSF and inserted within the granular layer, in a densely infected area of the dentate gyrus. A tungsten

bipolar electrode (0.5 MΩ) was used to stimulate perforant path inputs. Stimulation intensity was adjusted to induce a population spike of about half its maximum amplitude. Field EPSP (fEPSP) slope was determined over a 1ms window preceding the population spike. Population spike amplitude was assessed as the distance between its peak and the baseline extrapolated from its initiation and termination points using a routine written under Matlab (The MathWorks, Inc., Natick, MA, USA).

Biochemistry

Co-immunoprecipitation assays from HEK293T cells

HEK293T cells were grown in DMEM GlutaMAX (Invitrogen) supplemented with 5 g/l glucose and 10% fetal bovine serum. Cells (60-70% confluent) were co-transfected using transfectin (Biorad) according to the manufacturer's instructions with plasmids expressing Flag-tagged rat KCC2 (Chamma et al., 2013) and HA-tagged mouse Task3 (kindly provided by Guillaume Sandoz, Nice Univ., France) or HA-tagged GFP (Addgene) as control (with a 1:1 ratio). 48 hours after transfection, cells were homogenized by sonication in co-immunoprecipitation buffer containing (in mM): 50 Tris-HCl pH 7.4, 150 NaCl, 1 EDTA, as well as 0.5 % triton X-100 and protease inhibitors. Cells were then solubilized by rotation for 2 hours at 4°C and centrifuged at 20,000 g for 30 minutes at 4°C. Supernatants were transferred into a microtube with 20 µl of pre washed anti-HA coupled beads (Cell signaling) or EZview™ Red anti-Flag M2 Affinity Gel (Sigma). Samples were incubated overnight at 4°C under rotation. Complexes were precipitated with 20 µl protein-G magnetic beads (Invitrogen) for 2 hours at 4°C. Beads were then washed twice with 1ml of co-immunoprecipitation buffer and once with triton-free co-immunoprecipitation buffer. Bound complexes were eluted in 4X sample buffer (Invitrogen) for 1 hour at 37°C. Samples were analyzed by SDS-PAGE and western blot.

Co-immunoprecipitation assays from rat hippocampal homogenates

Hippocampi were dissected from adult Sprague Dawley female rats and homogenized by sonication in co-immunoprecipitation buffer as above (1 ml/100 mg of tissue) and solubilized by rotation for 2 to 4 hours at 4°C. After centrifugation at 20,000 g for 40 minutes at 4°C, protein content of the supernatant was measured by BCA protein assay (Pierce). 6.5 mg of proteins were transferred into microtube and 5 µg of primary antibody (Rabbit anti-KCC2, Millipore, and Rabbit anti-Task3, Alomone) or nonimmune IgG control antibody of the same species (Jackson Immunoresearch) were added. Samples were then incubated overnight at 4°C under rotation and processed as above.

Western blotting

Proteins were separated on a 4-12% SDS polyacrylamide gradient gel (Invitrogen) and transferred onto a nitrocellulose membrane (GE Healthcare). For co-immunoprecipitation assays from rat hippocampal homogenate, blots were probed with antibodies against KCC2 (1/1000, Millipore) and Task3 (1/250, Santa Cruz). For co-immunoprecipitation assays from HEK293T cells, blots were probed with HA (1/3000, Cell signaling) and KCC2 or FlagM2 (1/1000, Sigma). The primary antibodies were detected with fluorescent secondary antibody (1/1000-1/3000, DyLight 700 or 800, Rockland) using Odyssey infrared imaging system (LI-COR Bioscience). All biochemical assays were repeated at least 3 times on independent hippocampal extracts or cultures.

Immunocytochemistry

Neuro-2a cells were grown on glass coverslips in DMEM GlutaMAX (Invitrogen) supplemented with 1 g/l glucose and 10% fetal bovine serum. Cells at 60-70% confluence were co-transfected using Transfectin (Biorad) according to manufacturer's instructions with plasmids expressing Flag-tagged rat KCC2[7,11] and either HA-tagged mouse Task-3 (kindly provided by Guillaume Sandoz, Nice Sophia Antipolis Univ., France) or a pCAG empty vector as control (with a 3:1 ratio). 48 hours after transfection, cells were washed with PBS, fixed with paraformaldehyde (4%) supplemented with 4% sucrose in PBS and permeabilized with 0.25% Triton X-100 in PBS. After 3 x 10 min washes in PBS, cells were incubated for 30 min in blocking buffer (10% normal goat serum in PBS). Incubation with primary antibodies, HA (rabbit, 1/2000, Chemicon) and FlagM2 (mouse, 1/2000, Sigma) was then performed in blocking buffer for 2 hours at room temperature. After 3 x 10 min washes in PBS, cells were incubated with secondary antibodies for 1 hour (donkey anti-rabbit Alexa 647, 1/1000, Jackson Immunoresearch and goat anti-mouse CY3, 1/2000, Jackson Immunoresearch). Coverslips were washed 3 times in PBS and mounted in Mowiol/Dabco (25 mg/ml) solution. Immunofluorescence images were acquired using an upright confocal microscope (Leica TCS SP5), using a 63x 1.40-N.A. objective with 2.5X electronic magnification and an Ar/Kr laser set at 561 and 633 nm for excitation of Cy3 and Alexa 647, respectively.

Immunohistochemistry

At least 2 weeks following viral injections, rats were anesthetized by intraperitoneal ketamine / xylazine injection (110/15 mg/kg) and perfused transcardially with ice-cold cutting solution of choline as above. Brain were removed, postfixed in PFA 4% for 48 hours and stored at 4°C in

30% sucrose PBS. Parasagittal sections (40 µm thick) were obtained using a cryotome. After washes, brain slices were preincubated 3 hours with 0.5% Triton and 10% goat serum in PBS and then 48 hours at 4°C with primary antibodies: GFP (chicken, 1:1000, Millipore), KCC2 (rabbit, 1:400, Millipore), Prox1 (rabbit, 1:10000, Millipore), Task3 (rabbit, 1:400, Alomone), Trek2 (rabbit, 1:400, Alomone). After rinsing in PBS, slices were incubated 3 hours with secondary antibody (Cy3-coupled goat anti-rabbit and FITC-coupled goat anti-chicken) and mounted with Mowiol/Dabco (25 mg/mL). Images were acquired on an upright confocal microscope (Leica TCS SP5), using a 63X 1.40-N.A. objective with 2X electronic magnification and Ar/Kr laser set at 491 and 561 nm for excitation of Cy3 and FITC, respectively. Stacks of 4 to 6 µm optical sections were acquired at a pixel resolution of 1024 x 1024 with a z-step of 0.2 µm. Individual sections were then analyzed with Imaris (Bitplane). For images of the entire dentate gyrus, images were acquired using a 10X objective and stacks of 10 to 20 µm optical sections were acquired at a pixel resolution of 1024 x 1024 with a z-step of 1 µm.

Behavior and recordings

All recordings took place in a dimly-lit area enclosed by black curtains. Animals were handled for at least 3 days for habituation and to ensure stability of the recordings (location of the probe, power of the signal) before experiments started. A 80 cm x 80 cm arena with 50 cm high black plastic walls was used for exploration phase. A white card on one of the wall was used as spatial cue. For sleep recordings, animals were put in a white cylinder box (20 cm of diameter, 40 cm high). During the habituation phase, animals were placed in the cylinder box then in the empty arena for 10 min each, twice a day.

For recordings of awake behavior, new objects were placed in the open-field to stimulate exploration. All sleep recording sessions took place during the 2 hours following exploration of novel objects. For DREADD experiments, saline or CNO (1 mg/kg) was injected in i.p. 30 minutes before starting recording. All recordings took place less than 3 hours after i.p. injection.

Data were acquired at 20 kHz using an Intan recording controller (Intan Technologies, Los Angeles, USA) and Intan Recording Controller software (version 2.05).

Data analysis

All analyses were performed offline using Matlab built-in functions and custom-written scripts as well as Chronux (http://chronux.org/) and the FMAToolbox (http://fmatoolbox.sourceforge.net/). Power spectra and spectrograms were computed using multi-tapers estimates on the raw LFP. Theta power was determined in the 5 – 10 Hz band. Dentate spikes detection was performed after high-pass filtering (> 30Hz), squaring and

normalizing the field potential in the dentate gyrus. DS were defined as events of positive deflection peaking at > 8 s.d. and remaining above 4 s.d. for less than 30 ms.
Ripple detection was performed by band-pass filtering (100–600 Hz), squaring and normalizing, followed by thresholding of the field potential recorded in CA1 pyramidal layer. SPW-Rs were defined as events starting at 4 s.d., peaking at >6 s.d., and remaining at >4 s.d. for <150 ms and >15 ms

Electrocorticogram (EcoG) recordings and epilepsy induction

EcoG data were acquired at 20 kHz using Epoch Wireless recording system (Ripple, Salt Lake City, USA) and Clampex software (Molecular Devices). Video recording (29 frames/s) was synchronized to data acquisition to enable offline analysis.
For epilepsy induction, animals received intraperitoneal injection of 127 mg/kg of lithium 24 hours before treatment. The following day, animals received i.p. injection of 1 mg/kg of methylscopolamine in order to prevent peripheral effects of pilocarpine. 30 min later, 40 mg/kg of pilocarpine was injected i.p. Both video and EcoG data were acquired for one hour following pilocarpine injection. Status epilepticus was then interrupted by i.p. injection of 5 mg/kg diazepam. Animals were then sacrificed and brain were recovered and processed for visualization of the infected area.

Rat behavior was scored according to the following modified Racine's scale : stage 1, immobility and chewing; stage 2, neck and body clonus; stage 3, forelimb clonus and rearing; stage 4, *status epilepticus*, uninterrupted seizures. The onset of *status epilepticus* was assessed based on EcoG recordings.

Statistics

All statistical tests were performed using Matlab functions (Statistics and Machine Learning Toolbox). Data are presented as mean ± sem unless stated otherwise. All tests are two-tailed tests. Comparison of means was performed using Student's t-test for normally distributed variables (as tested with Shapiro-Wilk test) of equal variances (tested with Bartlett test). Otherwise, comparison of mean was performed using the non-parametric Mann-Whitney test. Kolmogorov-Smirnov test was used for comparison of distributions. Significance was determined as $p < 0.05$.

Acknowledgements

We are grateful to Quentin Chevy for sharing original observations related to the present work. We also thank Richard Miles and Kai Kaila for critical reading of the manuscript. This work was supported in part by Inserm, Sorbonne Université, as well as the Fondation pour la Recherche Médicale (Equipe FRM DEQ20140329539 to J.C.P.), the Human Frontier Science Program (RGP0022/2013 to L.M.P. and J.C.P.) and the Fondation Française pour la Recherche sur l'Epilepsie - Fédération pour la Recherche sur le Cerveau (research grant to J.C.P.). M.G. was the recipient of fellowships from Sorbonne Université and Fondation pour la Recherche Médicale as well as an IBRO-InEurope Short Stay Grant. The Poncer lab is affiliated with the Paris School of Neuroscience (ENP) and the Bio-Psy Laboratory of excellence.

References

1. Bormann J, Hamill OP, Sakmann B. Mechanism of anion permeation through channels gated by glycine and gamma-aminobutyric acid in mouse cultured spinal neurones. *The Journal of physiology* **385**, 243-286 (1987).

2. Blaesse P, Airaksinen MS, Rivera C, Kaila K. Cation-chloride cotransporters and neuronal function. *Neuron* **61**, 820-838 (2009).

3. Rivera C*, et al.* The K+/Cl- co-transporter KCC2 renders GABA hyperpolarizing during neuronal maturation. *Nature* **397**, 251-255 (1999).

4. Chamma I, Chevy Q, Poncer JC, Levi S. Role of the neuronal K-Cl co-transporter KCC2 in inhibitory and excitatory neurotransmission. *Frontiers in cellular neuroscience* **6**, 5 (2012).

5. Medina I*, et al.* Current view on the functional regulation of the neuronal K(+)-Cl(-) cotransporter KCC2. *Frontiers in cellular neuroscience* **8**, 27 (2014).

6. Fiumelli H, Cancedda L, Poo MM. Modulation of GABAergic transmission by activity via postsynaptic Ca2+-dependent regulation of KCC2 function. *Neuron* **48**, 773-786 (2005).

7. Chamma I*, et al.* Activity-dependent regulation of the K/Cl transporter KCC2 membrane diffusion, clustering, and function in hippocampal neurons. *The Journal of neuroscience : the official journal of the Society for Neuroscience* **33**, 15488-15503 (2013).

8. Lee HH, Deeb TZ, Walker JA, Davies PA, Moss SJ. NMDA receptor activity downregulates KCC2 resulting in depolarizing GABAA receptor-mediated currents. *Nature neuroscience* **14**, 736-743 (2011).

9. Puskarjov M, Ahmad F, Kaila K, Blaesse P. Activity-dependent cleavage of the K-Cl cotransporter KCC2 mediated by calcium-activated protease calpain. *The Journal of neuroscience : the official journal of the Society for Neuroscience* **32**, 11356-11364 (2012).

10. Caraiscos VB*, et al.* Tonic inhibition in mouse hippocampal CA1 pyramidal neurons is mediated by alpha5 subunit-containing gamma-aminobutyric acid type A receptors. *Proceedings of the National Academy of Sciences of the United States of America* **101**, 3662-3667 (2004).

11. Heubl M*, et al.* GABAA receptor dependent synaptic inhibition rapidly tunes KCC2 activity via the Cl−-sensitive WNK1 kinase. *Nature communications* **8**, 1776 (2017).

12. Kahle KT*, et al.* Inhibition of the kinase WNK1/HSN2 ameliorates neuropathic pain by restoring GABA inhibition. *Science Signaling* **9**, ra32 (2016).

13. Mahadevan V, Woodin MA. Regulation of neuronal chloride homeostasis by neuromodulators. *The Journal of physiology* **594**, 2593-2605 (2016).

14. Rivera C*, et al.* BDNF-induced TrkB activation down-regulates the K+-Cl- cotransporter KCC2 and impairs neuronal Cl- extrusion. *The Journal of cell biology* **159**, 747-752 (2002).

15. Kaila K, Price TJ, Payne JA, Puskarjov M, Voipio J. Cation-chloride cotransporters in neuronal development, plasticity and disease. *Nature reviews Neuroscience* **15**, 637-654 (2014).

16. Kahle KT*, et al.* Roles of the cation-chloride cotransporters in neurological disease. *Nature clinical practice Neurology* **4**, 490-503 (2008).

17. Buchin A, Chizhov A, Huberfeld G, Miles R, Gutkin BS. Reduced Efficacy of the KCC2 Cotransporter Promotes Epileptic Oscillations in a Subiculum Network Model. *The Journal of neuroscience : the official journal of the Society for Neuroscience* **36**, 11619-11633 (2016).

18. Huberfeld G*, et al.* Perturbed chloride homeostasis and GABAergic signaling in human temporal lobe epilepsy. *The Journal of neuroscience : the official journal of the Society for Neuroscience* **27**, 9866-9873 (2007).

19. Kahle KT*, et al.* Genetically encoded impairment of neuronal KCC2 cotransporter function in human idiopathic generalized epilepsy. *EMBO reports* **15**, 766-774 (2014).

20. Kourdougli N*, et al.* Depolarizing GABA contributes to glutamatergic network rewiring in epilepsy. *Annals of neurology* **81**, 251-265 (2017).

21. Puskarjov M*, et al.* A variant of KCC2 from patients with febrile seizures impairs neuronal Cl- extrusion and dendritic spine formation. *EMBO reports* **15**, 723-729 (2014).

22. Saitsu H*, et al.* Impaired neuronal KCC2 function by biallelic SLC12A5 mutations in migrating focal seizures and severe developmental delay. *Scientific reports* **6**, 30072 (2016).

23. Stodberg T*, et al.* Mutations in SLC12A5 in epilepsy of infancy with migrating focal seizures. *Nature communications* **6**, 8038 (2015).

24. Coull JA*, et al.* Trans-synaptic shift in anion gradient in spinal lamina I neurons as a mechanism of neuropathic pain. *Nature* **424**, 938-942 (2003).

25. Gagnon M*, et al.* Chloride extrusion enhancers as novel therapeutics for neurological diseases. *Nature medicine* **19**, 1524-1528 (2013).

26. Boulenguez P*, et al.* Down-regulation of the potassium-chloride cotransporter KCC2 contributes to spasticity after spinal cord injury. *Nature medicine* **16**, 302-307 (2010).

27. Dargaei Z*, et al.* Restoring GABAergic inhibition rescues memory deficits in a Huntington's disease mouse model. *Proceedings of the National Academy of Sciences of the United States of America*, (2018).

28. Hyde TM*, et al.* Expression of GABA signaling molecules KCC2, NKCC1, and GAD1 in cortical development and schizophrenia. *The Journal of neuroscience : the official journal of the Society for Neuroscience* **31**, 11088-11095 (2011).

29. Deidda G, Parrini M, Naskar S, Bozarth IF, Contestabile A, Cancedda L. Reversing excitatory GABAAR signaling restores synaptic plasticity and memory in a mouse model of Down syndrome. *Nature medicine* **21**, 318-326 (2015).

30. Banerjee A*, et al.* Jointly reduced inhibition and excitation underlies circuit-wide changes in cortical processing in Rett syndrome. *Proceedings of the National Academy of Sciences of the United States of America*, (2016).

31. Tang X*, et al.* KCC2 rescues functional deficits in human neurons derived from patients with Rett syndrome. *Proceedings of the National Academy of Sciences of the United States of America* **113**, 751-756 (2016).

32. Liabeuf S*, et al.* Prochlorperazine Increases KCC2 Function and Reduces Spasticity after Spinal Cord Injury. *J Neurotrauma*, (2017).

33. Gauvain G*, et al.* The neuronal K-Cl cotransporter KCC2 influences postsynaptic AMPA receptor content and lateral diffusion in dendritic spines. *Proceedings of the National Academy of Sciences of the United States of America* **108**, 15474-15479 (2011).

34. Li H*, et al.* KCC2 interacts with the dendritic cytoskeleton to promote spine development. *Neuron* **56**, 1019-1033 (2007).

35. Chevy Q*, et al.* KCC2 Gates Activity-Driven AMPA Receptor Traffic through Cofilin Phosphorylation. *The Journal of neuroscience : the official journal of the Society for Neuroscience* **35**, 15772-15786 (2015).

36. Llano O*, et al.* KCC2 regulates actin dynamics in dendritic spines via interaction with beta-PIX. *The Journal of cell biology* **209**, 671-686 (2015).

37. Mahadevan V*, et al.* Native KCC2 interactome reveals PACSIN1 as a critical regulator of synaptic inhibition. *eLife* **6**, (2017).

38. Delpire E*, et al.* Further optimization of the K-Cl cotransporter KCC2 antagonist ML077: development of a highly selective and more potent in vitro probe. *Bioorg Med Chem Lett* **22**, 4532-4535 (2012).

39. Lesage F, Lazdunski M. Molecular and functional properties of two-pore-domain potassium channels. *American journal of physiology Renal physiology* **279**, F793-801 (2000).

40. Ketchum KA, Joiner WJ, Sellers AJ, Kaczmarek LK, Goldstein SA. A new family of outwardly rectifying potassium channel proteins with two pore domains in tandem. *Nature* **376**, 690-695 (1995).

41. Aller MI, Wisden W. Changes in expression of some two-pore domain potassium channel genes (KCNK) in selected brain regions of developing mice. *Neuroscience* **151**, 1154-1172 (2008).

42. Marinc C, Derst C, Pruss H, Veh RW. Immunocytochemical localization of TASK-3 protein (K2P9.1) in the rat brain. *Cell Mol Neurobiol* **34**, 61-70 (2014).

43. Talley EM, Solorzano G, Lei Q, Kim D, Bayliss DA. Cns distribution of members of the two-pore-domain (KCNK) potassium channel family. *The Journal of neuroscience : the official journal of the Society for Neuroscience* **21**, 7491-7505 (2001).

44. Mahadevan V*, et al.* Kainate receptors coexist in a functional complex with KCC2 and regulate chloride homeostasis in hippocampal neurons. *Cell reports* **7**, 1762-1770 (2014).

45. Ivakine EA*, et al.* Neto2 is a KCC2 interacting protein required for neuronal Cl- regulation in hippocampal neurons. *Proceedings of the National Academy of Sciences of the United States of America* **110**, 3561-3566 (2013).

46. Wright R*, et al.* Neuronal Chloride Regulation via KCC2 Is Modulated through a GABAB Receptor Protein Complex. *The Journal of neuroscience : the official journal of the Society for Neuroscience* **37**, 5447-5462 (2017).

47. Turrigiano GG. Homeostatic plasticity in neuronal networks: the more things change, the more they stay the same. *Trends in neurosciences* **22**, 221-227 (1999).

48. Witter MP. The perforant path: projections from the entorhinal cortex to the dentate gyrus. In: *The Dentate Gyrus: A Comprehensive Guide to Structure, Function, and Clinical Implications* (ed^(eds) (2007).

49. Staley KJ, Mody I. Shunting of excitatory input to dentate gyrus granule cells by a depolarizing GABAA receptor-mediated postsynaptic conductance. *Journal of neurophysiology* **68**, 197-212 (1992).

50. Hsu D. The dentate gyrus as a filter or gate: a look back and a look ahead. **163**, 601-613 (2007).

51. Rolls ET. The mechanisms for pattern completion and pattern separation in the hippocampus. *Front Syst Neurosci* **7**, 74 (2013).

52. Heinemann U, Beck H, Dreier JP, Ficker E, Stabel J, Zhang CL. The dentate gyrus as a regulated gate for the propagation of epileptiform activity. *Epilepsy research Supplement* **7**, 273-280 (1992).

53. Chen L*, et al.* KCC2 downregulation facilitates epileptic seizures. *Scientific reports* **7**, 156 (2017).

54. Bragin A, Engel J, Jr., Wilson CL, Vizentin E, Mathern GW. Electrophysiologic analysis of a chronic seizure model after unilateral hippocampal KA injection. *Epilepsia* **40**, 1210-1221 (1999).

55. Bragin A, Jando G, Nadasdy Z, van Landeghem M, Buzsaki G. Dentate EEG spikes and associated interneuronal population bursts in the hippocampal hilar region of the rat. *Journal of neurophysiology* **73**, 1691-1705 (1995).

56. Roth BL. DREADDs for Neuroscientists. *Neuron* **89**, 683-694 (2016).

57. Ben-Ari Y. NKCC1 Chloride Importer Antagonists Attenuate Many Neurological and Psychiatric Disorders. *Trends in neurosciences* **40**, 536-554 (2017).

58. Cornell B, Toyo-Oka K. 14-3-3 Proteins in Brain Development: Neurogenesis, Neuronal Migration and Neuromorphogenesis. *Front Mol Neurosci* **10**, 318 (2017).

59. Zuzarte M*, et al.* Intracellular traffic of the K+ channels TASK-1 and TASK-3: role of N- and C-terminal sorting signals and interaction with 14-3-3 proteins. *The Journal of physiology* **587**, 929-952 (2009).

60. Kilisch M, Lytovchenko O, Arakel EC, Bertinetti D, Schwappach B. A dual phosphorylation switch controls 14-3-3-dependent cell surface expression of TASK-1. *J Cell Sci* **129**, 831-842 (2016).

61. Seja P*, et al.* Raising cytosolic Cl- in cerebellar granule cells affects their excitability and vestibulo-ocular learning. *The EMBO journal* **31**, 1217-1230 (2012).

62. Hubner CA, Stein V, Hermans-Borgmeyer I, Meyer T, Ballanyi K, Jentsch TJ. Disruption of KCC2 reveals an essential role of K-Cl cotransport already in early synaptic inhibition. *Neuron* **30**, 515-524 (2001).

63. Pellegrino C*, et al.* Knocking down of the KCC2 in rat hippocampal neurons increases intracellular chloride concentration and compromises neuronal survival. *The Journal of physiology* **589**, 2475-2496 (2011).

64. Lee HH, Jurd R, Moss SJ. Tyrosine phosphorylation regulates the membrane trafficking of the potassium chloride co-transporter KCC2. *Molecular and cellular neurosciences* **45**, 173-179 (2010).

65. Ramadoss J, Lunde ER, Ouyang N, Chen WJ, Cudd TA. Acid-sensitive channel inhibition prevents fetal alcohol spectrum disorders cerebellar Purkinje cell loss. *Am J Physiol Regul Integr Comp Physiol* **295**, R596-603 (2008).

66. Karschin C*, et al.* Expression pattern in brain of TASK-1, TASK-3, and a tandem pore domain K(+) channel subunit, TASK-5, associated with the central auditory nervous system. *Molecular and cellular neurosciences* **18**, 632-648 (2001).

67. Rivera C*, et al.* Mechanism of activity-dependent downregulation of the neuron-specific K-Cl cotransporter KCC2. *The Journal of neuroscience : the official journal of the Society for Neuroscience* **24**, 4683-4691 (2004).

68. Bonislawski DP, Schwarzbach EP, Cohen AS. Brain injury impairs dentate gyrus inhibitory efficacy. *Neurobiology of disease* **25**, 163-169 (2007).

69. Merner ND*, et al.* Regulatory domain or CpG site variation in SLC12A5, encoding the chloride transporter KCC2, in human autism and schizophrenia. *Frontiers in cellular neuroscience* **9**, 386 (2015).

70. Cohen I, Navarro V, Clemenceau S, Baulac M, Miles R. On the origin of interictal activity in human temporal lobe epilepsy in vitro. *Science* **298**, 1418-1421 (2002).

71. Pallud J*, et al.* Cortical GABAergic excitation contributes to epileptic activities around human glioma. *Science translational medicine* **6**, 244ra289 (2014).

72. Levesque M, Salami P, Shiri Z, Avoli M. Interictal oscillations and focal epileptic disorders. *The European journal of neuroscience*, (2017).

73. Menendez de la Prida L, Trevelyan AJ. Cellular mechanisms of high frequency oscillations in epilepsy: on the diverse sources of pathological activities. *Epilepsy research* **97**, 308-317 (2011).

74. Goldberg EM, Coulter DA. Mechanisms of epileptogenesis: a convergence on neural circuit dysfunction. *Nature reviews Neuroscience* **14**, 337-349 (2013).

75. Wang F*, et al.* NKCC1 up-regulation contributes to early post-traumatic seizures and increased post-traumatic seizure susceptibility. *Brain structure & function* **222**, 1543-1556 (2017).

76. Sen A, Martinian L, Nikolic M, Walker MC, Thom M, Sisodiya SM. Increased NKCC1 expression in refractory human epilepsy. *Epilepsy research* **74**, 220-227 (2007).

77. Headley DB, Kanta V, Pare D. Intra- and interregional cortical interactions related to sharp-wave ripples and dentate spikes. *Journal of neurophysiology* **117**, 556-565 (2017).

78. Nokia MS, Gureviciene I, Waselius T, Tanila H, Penttonen M. Hippocampal electrical stimulation disrupts associative learning when targeted at dentate spikes. *The Journal of physiology* **595**, 4961-4971 (2017).

79. Girardeau G, Benchenane K, Wiener SI, Buzsaki G, Zugaro MB. Selective suppression of hippocampal ripples impairs spatial memory. *Nature neuroscience* **12**, 1222-1223 (2009).

80. Loucif AJC*, et al.* GI-530159, a novel, selective, mechanosensitive two-pore-domain potassium (K2P) channel opener, reduces rat dorsal root ganglion neuron excitability. *Br J Pharmacol*, (2017).

81. Ankri N, Legendre P, Faber DS, Korn H. Automatic detection of spontaneous synaptic responses in central neurons. *Journal of neuroscience methods* **52**, 87-100 (1994).

III- DOWNSTREAM EFFECTS OF KCC2 SUPPRESSION IN THE DENTATE GYRUS ON HIPPOCAMPAL RHYTHMOGENESIS

I previously showed that KCC2 suppression in the dentate gyrus specifically alters dentate spikes during sleep (manuscript Fig 5). This effect was rescued by chemogenetically hyperpolarizing neurons with an inhibitory DREADD. This indicates that the alteration of dentate spikes relies on increased neuronal excitability. The dentate gyrus represents the main entry point to the hippocampus. Its activity therefore influences both CA3 and CA1 activity via the classical trisynaptic circuit.

I questioned whether the enhanced recruitment of dentate granule cells by entorhinal afferents would have downstream effects on hippocampal rhythmogenesis in the CA1 region. I showed that theta-band activity was unaffected during exploration and REM sleep (manuscript Fig S5). However, the two main generators of theta activity in the hippocampus are inhibitory inputs from the medial septum diagonal band of Broca onto CA1 interneurons and excitatory inputs from the entorhinal cortex onto distal dendrites of CA1 pyramidal neurons (see Introduction II.2.b). These two inputs are unaffected by the suppression of KCC2 in dentate granule cells. In contrast, gamma rhythm emerges from local networks and is more likely to be affected by the alteration of the dentate firing pattern. Gamma power (25-90 Hz) was not affected in the dentate gyrus during exploration or REM sleep (Fig 26A-B). However, somewhat surprisingly, KCC2 suppression in the dentate gyrus induced a decrease in gamma power in the *stratum radiatum* of area CA1 during awake exploration (n = 6 rats for controls, 7 for KCC2 suppression).

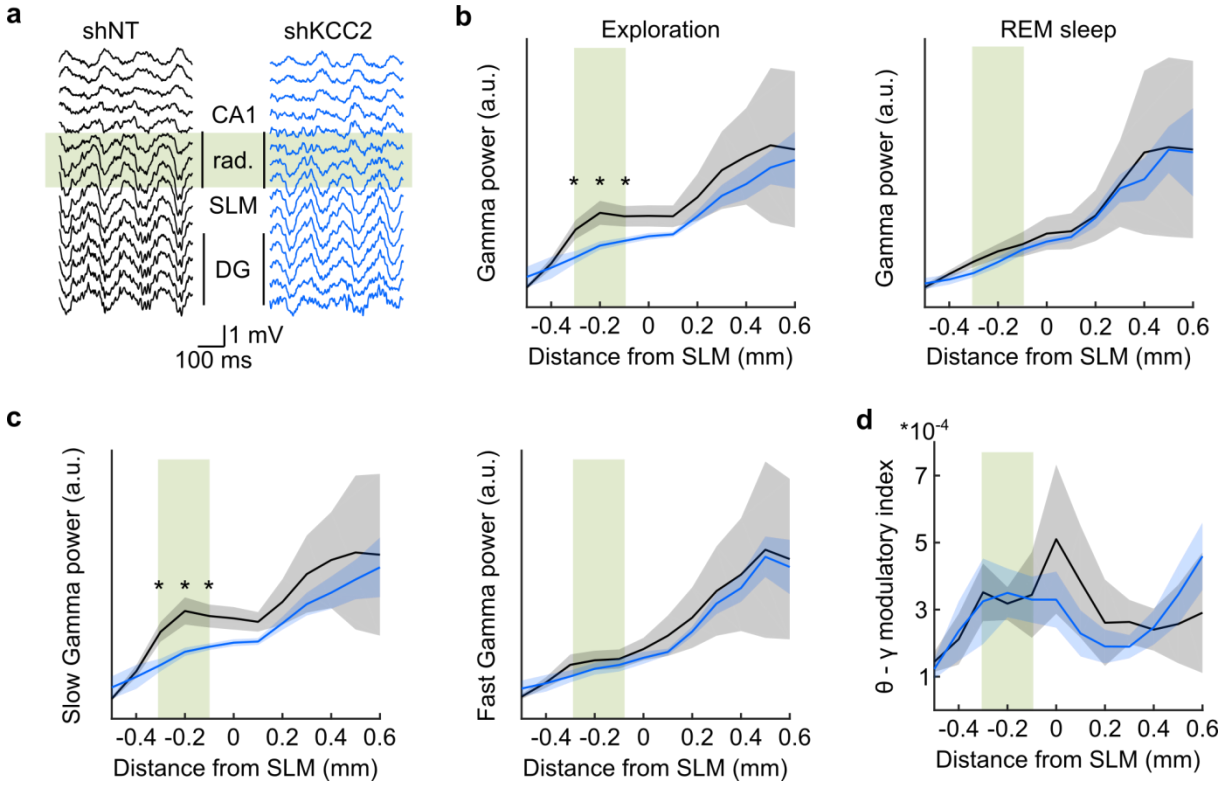

Figure 26 : Reduction of slow-gamma power in CA1 following KCC2 suppression in the dentate gyrus
(a) Example traces of 500 ms of LFP recordings with 16-channels silicon probes during awake exploration from rats infected in the dentate gyrus with a non-target shRNA (black, left) or KCC2-directed shRNA (blue, right). The localization of the *stratum lacunosum molecular* was defined by the highest power of theta and CA1 was identified by the presence of action potentials and of ripples during sleep. Localization of the *stratum radiatum* is highlighted in green.
(b) Gamma power in the 25-90 frequency band was measured during exploration (left) and REM sleep (right) using multi-tapers estimates. Power is represented as a function of the electrode localization. Depth of the electrode is expressed as the distance with the *stratum lacunosum molecular* (SLM). * $p < 0.05$
(c) Gamma power during exploration was further subdivided into slow gamma power (left, 25-55 Hz) and fast gamma power (right, 60-90 Hz). * $p < 0.05$
(d) Theta-Gamma coupling during exploration was estimated using the measure of modulatory index described by Tort et al. 2008 and represented as a function of the electrode localization

Gamma-band activity can be separated in two distinct oscillations: the slow (25-55 Hz) and fast gamma (60-90 Hz). In CA1, whereas slow gamma is entrained by CA3, fast gamma is generated by entorhinal afferents (Colgin et al., 2009, Introduction II.2.d). Interestingly, the decrease in gamma power observed in the whole gamma range could be explained solely by a decrease in slow gamma power (Fig 26C). Finally, although slow gamma power was decreased in CA1, its modulation by theta activity was unaffected as indicated by the absence of changes in its modulatory index (Fig 26D).

Due to the positioning of our electrodes, I could not record from the CA3 region in our experiments. However, my data indicate that increased excitability in the dentate gyrus may result in decrease slow gamma power in CA3 and subsequently in CA1. This observation is

consistent with the synaptic physiology of the hippocampal network. Indeed, activation of the dentate gyrus mostly results in inhibition of the CA3 region due to a strong feedforward inhibition (Acsády et al., 1998; Mori et al., 2007).

To further characterize the downstream effects of KCC2 suppression in the dentate gyrus, I analyze in more details the sharp-wave ripples during slow-wave sleep. KCC2 suppression in the dentate gyrus was not sufficient to promote pathological fast-ripples (see Results II- Fig S3). I then analyzed the features of the ripples recorded in CA1 (Fig 27A).

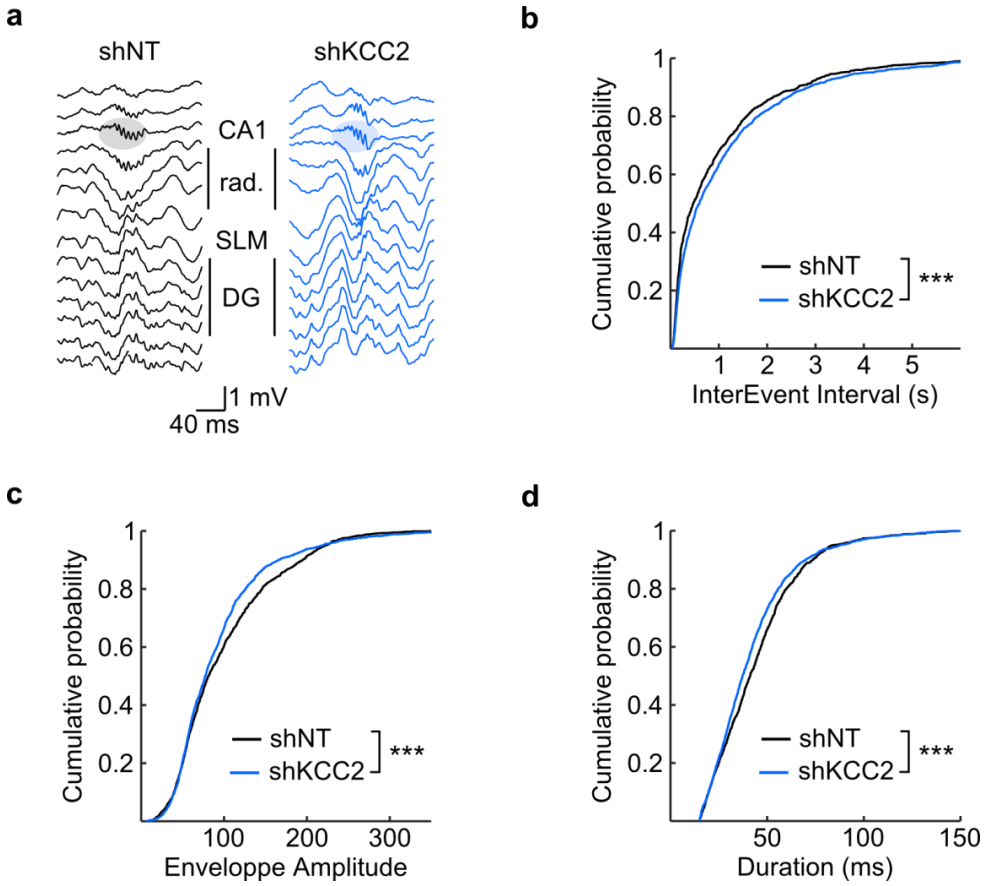

Figure 27 : Suppression of KCC2 in the dentate gyrus alters CA1 ripples
(a) Example traces of 200 ms of LFP recordings with 16-channels silicon probes during slow-wave sleep from rat infected in the dentate gyrus with a non target shRNA (black, left) or KCC2-directed shRNA (blue, right). Note the presence of the fast ripple oscillation in the CA1 pyramidal layer (highlighted in black and blue respectively) and the associated sharp-wave in the radiatum.
(b) Cumulative distributions were performed from 185 events per rats (n = 5 and 7 rats) to compare inter-event intervals (b), the strength of the ripples as evaluated by their envelope amplitude (c) and their duration (d). Distributions are compared using Kolmogorov-Smirnov test. *** $p < 0.001$

Although the differences between the two groups are relatively small, I found that ripples tended to be less frequent (Fig 27B), smaller (Fig 27C) and shorter (Fig 27D) following extinction

of KCC2 expression in the dentate gyrus. My results are consistent with a recent study demonstrating that ripples immediately following dentate spikes are smaller (Headley et al., 2017). The authors did not propose a mechanism for their observation. However, ripples are elicited by a strong excitatory drive from CA3 while dentate gyrus output on CA3 is mostly inhibitory (Mori et al., 2007). The combination of these two observations could explain the inverse relationship between dentate spikes and CA1 sharp-wave ripples.

To test whether the alterations of slow gamma and ripples indeed depend on increased excitability of dentate gyrus neurons, I analyzed these two activity patterns in recordings from animals co-infected with either non-target shRNA or KCC2-directed shRNA together with the inhibitory DREADD hM4D(Gi) following saline or CNO injection (Fig 28).

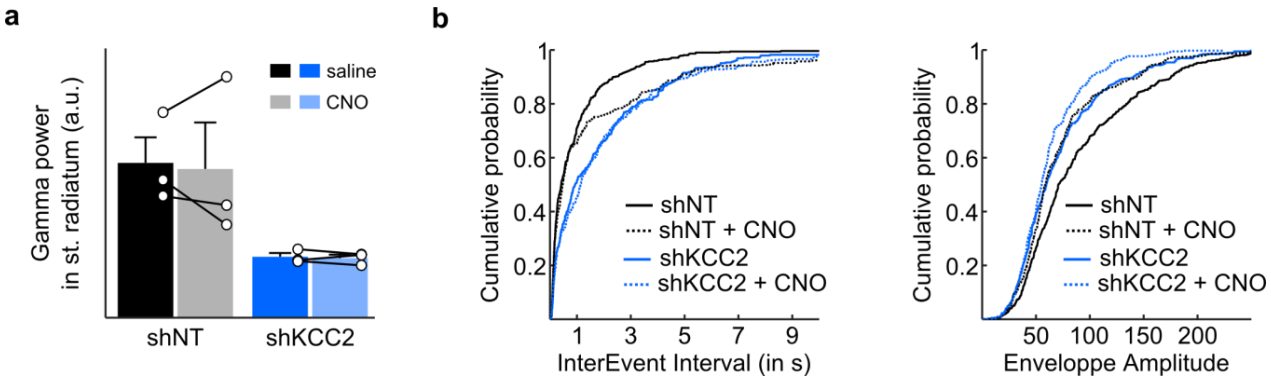

Figure 28 : Chemogenetic silencing of dentate gyrus neurons does not rescue deficits in gamma and ripples upon KCC2 suppression
(a) Slow gamma (25-55 Hz) power was measured in the *stratum radiatum*, 200 µm above the *stratum lacunosum molecular* after saline and CNO injection. N = 3 rats per group
(b) Cumulative distributions were realized from 130 events per rats to quantify the inter-event interval and the envelope amplitude of the ripples.

Surprisingly, CNO injection did not rescue slow gamma power in the stratum radiatum in rats with suppressed KCC2 expression in the dentate gyrus (n = 3 rats, paired t-test, p = 0.40, Fig 28A). Gamma power in control rats was equally unaffected (n = 3 rats, paired t-test, p = 0.75). Similarly, ripples features (frequency, envelope amplitude) were not rescued by inhibiting granule cells via CNO injection (Fig 28B). Animals lacking KCC2 in the dentate gyrus did not exhibit any changes in rate of ripples (n = 3 rats, 130 events per rats, Kolmogorov-Smirnov, p = 0.29) and displayed slightly smaller ripples (Kolmogorov-Smirnov, $p < 0.01$). Strikingly, inhibition of the dentate gyrus by CNO injection considerably degraded ripples in control rats as evidenced by an increased inter-event interval (n = 3 rats, 130 events per rats, Kolmogorov-Smirnov, $p < 0.001$) and decreased envelope amplitude (Kolmogorov-Smirnov, $p < 0.001$).

Overall, our results indicate that the modifications of dentate gyrus activity upon chronic KCC2 suppression have downstream consequences on CA1 rhythmogenesis. In particular, slow gamma power is decreased, and ripples are smaller and shorter. However, our experiments suggest these effects do not arise from the sole increased excitability of KCC2 knockdown neurons since they were not rescued by their silencing with hM4D(Gi) activation.

DISCUSSION

DISCUSSION

During my PhD, I have characterized the functional impact of a chronic KCC2 suppression in the dentate gyrus. I discovered a previously unreported interaction between the transporter and the leak-potassium channel Task-3 that regulates the membrane expression of Task-3. Although I did not fully elucidate the mechanisms underlying this effect, I showed that downregulation of KCC2 results in reduced expression and function of Task-3 channels in both heterologous cells and hippocampal neurons. This in turn increases neuronal excitability through membrane depolarization and increased resistance and favors the recruitment of dentate granule cells by entorhinal afferents. In addition, I discovered that KCC2 suppression in hippocampal neurons unexpectedly preserves steady-state GABAergic transmission. Indeed, the depolarization of the resting membrane potential in KCC2 knockdown neurons fully compensated their depolarized reversal potential of GABAergic currents. Overall, increased excitability of dentate granule cells was sufficient to alter local rhythmogenesis and in particular to increase the amplitude and frequency of occurrence of dentate spikes during sleep. Together, these observations shed light on a novel role of KCC2 in controlling neuronal activity through regulation of Task-3 channels.

My results also raise several questions. In particular, I will discuss in this section i) the possible mechanisms of Task-3 regulation by KCC2 and the relevance of this interaction in the pathology, ii) the involvement of KCC2 in hippocampal rhythmopathies and iii) the impact of KCC2 suppression on epileptogenesis.

I- A NOVEL NON-CANONICAL ROLE OF KCC2 AS A REGULATOR OF TASK-3 ACTIVITY

In my study, I demonstrated that KCC2 suppression was accompanied by a strong decrease in the currents mediated by the leak potassium channel Task-3. Task-3 is one of the 15 members constituting the family of two-pore domain (K2P) potassium channels (Goldstein et al., 2001). In contrast to most voltage-gated potassium channels wich possess one pore allowing ion flow and

6 transmembrane domains, the structure of K2P channels consists of 2 pores and 4 transmembrane domains.

Although the existence of leak-potassium conductance has been postulated for a long time (Hodgkin and Huxley, 1947), the molecular bases of these currents were only discovered in the 1990s with the identification of the K2P family (Ketchum et al., 1995; Lesage et al., 1996a, 1996b). Following studies revealed that the K2P family can be further divided in several subfamilies with various properties in terms of expression patterns, electrophysiological properties and regulation (see Table1). The three main subfamilies of K2P are TWIK (Tandem two-pore Weakly Inwardly rectifier potassium channel), TREK (Twik-related potassium channel) and TASK (Twik-related Acid-Sensitive Potassium channel).

Family name	Members (gene)	Electrophysiological properties	Pharmacology (inhibitor / activator)	Expression In the CNS
TWIK (two-pore Weakly Inwardly rectifier)	Twik1 (KCNK1) Twik2 (KCNK6) KCNK7	Inward rectifier	G_i-coupled receptor Acid pH_i PKC	Absent from hypothalamus
TREK (Twik-related)	Trek1 (KCNK2) Trek2 (KCNK10) Traak (KCNK4)	Outward rectifier	Acid pH_i Mechanical stretch G_q protein	Cortical regions and cerebellum
TASK (Twik-related Acid-Sensitive)	Task1 (KCNK3) Task2 (KCNK5) Task3 (KCNK9) Task5 (KCNK15)	Outward rectifier	Volatile anesthetics G_q protein Acid pH_o	Ubiquitous
TALK (Twik-related Alkaline-activated)	Talk1 (KCNK16) Talk2 (KCNK17)	Outward rectifier	Alkaline pH_o	/
THIK (Twik-related Halothane-inhibited)	Thik1 (KCNK13) Thik2 (KCNK12)	Outward rectifier	Arachidonic acid Halothane	/
TRESK (Twik-related Spinal Cord)	Tresk (KCNK18)	Outward rectifier	Volatile anesthetics Calicum, PKC	Spinal cord

Table 1 : The K2P family

The diversity of properties of K2P channels is further increased by their capacity to heterodimerize, thus creating channels with mixed properties (Blin et al., 2016; Lengyel et al., 2016.; Ma et al., 2012).

Task channels are sensitive to variations in extracellular pH (Lesage, 2003). Since neighboring neurons with intact KCC2 expression did not exhibit any modifications of their intrinsic properties (cf. manuscript, Fig.S2), I ruled out a potential role of extracellular pH variation in the observed effect. This led us to investigate the cell-autonomous mechanisms through which KCC2 could affect Task-3 expression and function.

1. Possible mechanisms for Task-3 regulation by KCC2

The last few years have witnessed increasing interest for KCC2 interactions with protein partners. A classical standpoint in these studies is to examine how KCC2 interactors influence its membrane stability and function (M. Chen et al., 2017; Ivakine et al., 2013; Mahadevan et al., 2014; Wenz et al., 2009) and thereby GABAergic signaling. However, several studies have also revealed a critical role of KCC2 structural interaction with cytoskeleton components and regulators for dendritic spine formation (Li et al., 2007) as well as efficacy (Gauvain et al., 2011) and long-term potentiation (Chevy et al., 2015) of excitatory synapses. Hence, KCC2 within protein complexes is not only regulated by its partners but can also itself influence their activity or expression. Based on these observations, I suggest Task-3 membrane expression and function may be directly controlled by its interaction with KCC2. Indeed, I showed that the two proteins interact together both in brain extracts and when overexpressed in heterologous cells (manuscript Fig 3B-C).

How could the interaction between KCC2 and Task-3 influence the expression and function of the K2P channel ? Possible mechanisms involve regulation of Task-3 function by KCC2 interaction but also decreased membrane stability or deficit in membrane targeting. Using a neuroblastoma cell line, I revealed that, in the absence of KCC2 expression, Task-3 accumulated in intracellular compartments thus suggesting a default in membrane targeting (manuscript Fig 3D-E). Yeast 2-hybrid studies have revealed that K2P channels from the Task subfamily interact with 14-3-3 proteins (Rajan et al., 2002) through their C-terminal domain. 14-3-3 proteins are a family of chaperone proteins involved in multiple physiological processes such as apoptosis, control of cell cycle and intracellular trafficking (Fu et al., 2000; Mrowiec and Schwappach, 2006). Membrane expression of Task channels directly correlate with their interaction with 14-3-3 (O'Kelly et al., 2002; Rajan et al., 2002). A later study showed that Task interaction with 14-3-3 in the C-terminal domain masks the dibasic motif KRR that constitutes a retention signal in the

endoplasmic reticulum (Zuzarte et al., 2009), thereby enabling the membrane targeting of the channel. In the absence of 14-3-3, β coatomer protein complex I (COPI) can bind to the KRR motif, resulting in retention of the protein in the endoplasmic reticulum. Interestingly, a recent proteomic study of KCC2 identified 14-3-3 as a putative interactor of the transporter (Mahadevan et al., 2017). Therefore, a seducing hypothesis would be that KCC2 interaction with Task-3 is required for 14-3-3 binding and subsequent targeting to the plasma membrane of the K2P channel either due to conformational changes or simply by bringing 14-3-3 and Task-3 closer to favor their interaction. Further studies are still needed to decipher more precisely the interactions between KCC2, Task-3 and 14-3-3 in order to better understand the potential role of KCC2 in Task-3 trafficking.

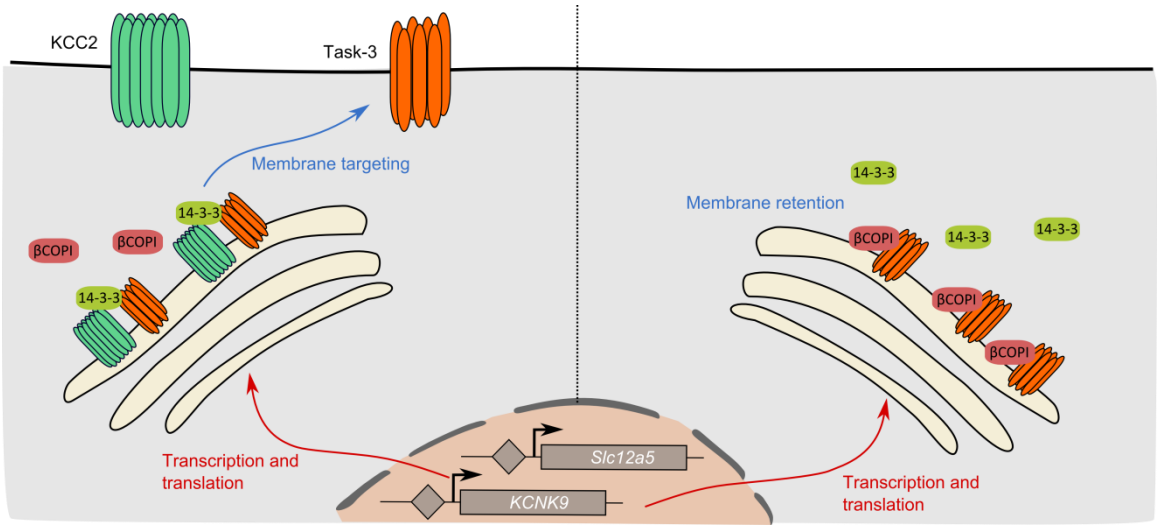

Figure 29 : Proposed mechanism of regulation of Task-3 by KCC2
In our model, KCC2 interacts with the protein 14-3-3. This interaction favors Task-3 interaction with 14-3-3 and thereby its targeting to the plasma membrane (left). In absence of KCC2, βCOPI can bind to Task-3 retention domain KRR, thus constraining the channel in intracellular compartments.

My data suggest that downregulation of Task-3 expression in KCC2 knockdown neurons involves an alteration of its membrane targeting. However, other mechanisms may also contribute to this effect, which are not mutually exclusive. They include i) stabilization through direct interaction at the plasma membrane, ii) modification of the activity of the channel or iii) regulation of gene expression. Interestingly, during development, expression of Task-3 is upregulated (Aller and Wisden, 2008) with a timing that matches the developmental upregulation of KCC2. Hence, in the rat dentate gyrus, levels of KCC2 gradually increase from the second postnatal week (Wang et al., 2002), which corresponds to the period when Task-3 starts to be expressed in dentate

granule cells (Aller and Wisden, 2008). Based on these observations, it is tempting to speculate on a causal relationship between the increase of KCC2 expression and that of Task-3. Yet, the concomitant upregulation of the two proteins may also only be coincidental. Indeed, Task-3 mRNA levels also gradually increase during development in the cerebellum (Zanzouri et al., 2006). There, however, the effect seems to involve calcium influx through L-type voltage gated calcium channels and subsequent calcineurin activation.

Identifying the mechanisms through which Task-3 expression and activity are modified may also provide relevant information considering the timing of this regulation. This is important since KCC2 membrane stability can be rapidly regulated by activity (Lee et al., 2007; Chamma et al., 2013; Heubl et al., 2017). In my study, I only investigated the effect of chronic KCC2 suppression on Task-3. It would therefore be interesting to determine whether such regulation could also occur at a fast timescale and rapidly influence cell properties in conditions where KCC2 is dynamically regulated.

2. Physiological consequences of KCC2 and Task-3 downregulation

Task-3 is widely expressed throughout the central nervous system (Karschin et al., 2001) where it plays a major role in setting membrane potential and resistance, thereby tightly controlling neuronal excitability. In line with this broad pattern of expression, suppression of KCC2 and subsequent loss of Task-3 – mediated conductance considerably increases cell excitability in dentate granule cells but also in CA1 pyramidal neuron (cf. manuscript, Fig. S3). In the cerebellum, Task-3 is highly expressed in granule cells but not in Purkinje cells. Interestingly, conditional KCC2 knockout led to depolarized membrane potential in cerebellar granule cells but not in Purkinje cells (Seja et al., 2012). Although the authors of this study did not investigate the specific mechanism of this effect, their observations perfectly fit with a regulation of Task-3 expression and function.

In addition to its role in regulating cellular excitability, Task-3 is also required to sustain high frequency firing in cerebellar granule cells (Brickley et al., 2007). Although I did not study this phenomenon in detail, I observed a similar effect in dentate granule cells. Indeed, suppression of KCC2 and subsequent regulation of Task-3 conductance led to an increased excitability at first but a decreased ability to maintain high-frequency firing upon high current injection (cf.

manuscript Fig 2C). In physiological conditions, this consideration is of little importance in dentate granule cells since they are known to exhibit sparse firing and rarely fire at high frequency *in vivo* (Jung and McNaughton, 1993). However, this could be critical in other cell types. In particular, Task-3 is expressed in hippocampal parvalbumin (PV) interneurons (Torborg et al., 2006), which also express KCC2 (Gulyás et al., 2001, unpublished data from our group). My data thus suggest that suppression of KCC2 in PV interneurons could regulate Task-3 expression, which would in turn affect their ability to discharge at high frequency. This hypothesis is further supported by the observation that developmental upregulation of K2P channels, and in particular of Task-1, in cortical fast-spiking interneurons correlates with an increase of their maximal firing rate (Okaty et al., 2009). The ability of PV interneuron to fire at high frequency is critical to maintain the excitation / inhibition balance in the brain but also for the emergence of specific brain oscillations such as ripples (see Introduction II.2.c). Hence, KCC2 suppression in PV interneurons may have drastic effects on their firing pattern and subsequently on network activity.

As mentioned in my introduction (part I.6), KCC2 is dysregulated in many neurological disorders including epilepsy (Huberfeld et al., 2007) but also neuropathic pain and spasticity following traumatic injury (Boulenguez et al., 2010), Huntington's disease (Dargaei et al., 2018) or Rett syndrome (Duarte et al., 2013). In most cases, since downregulation of KCC2 was associated with depolarized E_{GABA}, treatments aiming to restore chloride homeostasis such as NKCC1 antagonist have been widely tested and proved beneficial in a number of cases (Lemonnier and Ben-Ari 2010; Banerjee et al., 2016; Dargaei et al., 2018). However, my data predict that Task-3 function and thereby neuronal excitability may also be affected and contribute to altered neuronal activity that underlie the physiopathology of these disorders. Such defects would not be restored by a sole action on chloride homeostasis. Hence, K2P in general and Task-3 in particular offer novel interesting therapeutic targets that could be used in combination with an action on neuronal chloride transport.

The interaction between KCC2 and Task-3 is particularly promising in the context of traumatic nerve injury. Indeed, K2P have been largely studied in the context of neuropathic pain since their downregulation in somatosensory neurons lead to increased excitability and exacerbated pain sensation (Plant, 2012). Most studies focused on the function of Trek channels since their expression is predominant in the dorsal root ganglia neurons (Maingret et al., 2000). However, interestingly, downregulation of Task-3 has been observed in dorsal root ganglia neurons following peripheral nerve injury (Pollema-Mays et al., 2013), a protocol which is also known to

affect KCC2 expression (Gagnon et al., 2013). To the best of my knowledge, to date, no specific Task-3 opener is available. However, the dihydroacridine analogue (ML67-33) has been found to selectively and directly activate Trek-1, Trek-2 and TRAAK channels (Bagriantsev et al., 2013) while a specific Trek-1 opener, Gi-530159, has recently been described (Loucif et al., 2017). These pharmacological agents might be used to restore altered excitability following KCC2 and Task-3 downregulation. Although both Task-3 and Trek channels are widely expressed in the CNS, their expression patterns are not entirely redundant. Thus, Trek channels are much less expressed in the cerebellum compared with Task channels (Talley et al., 2001). This indicates that deficits due to Task-3 regulation may not be entirely restored by Trek activation. Thus, my data advocate for more research on selective Task openers as new therapeutic targets in various neuronal disorders associated with KCC2 downregulation.

II- KCC2 AND HIPPOCAMPAL RHYTHMOPATHY : MECHANISMS AND CONSEQUENCES

1. Mechanisms of hippocampal rhythmopathy following KCC2 suppression in the dentate gyrus

Hippocampal rhythmogenesis relies on an exquisite control of GABAergic and glutamatergic transmissions as well as neuronal intrinsic properties. I showed that KCC2 suppression in dentate granule resulted in altered network activity, as evidenced by increased amplitude and frequency of dentate spikes during sleep. At the cellular level, the main effect of KCC2 downregulation was an increased neuronal excitability and EPSP/spike coupling with no change in the driving force of GABAA receptor mediated transmission. Hence, I hypothesized that changes in network activity *in vivo* primarily reflected changes in neuronal excitability observed *in vitro*. In support of this hypothesis, I found that chemogenetic hyperpolarization of dentate granule cells completely rescued dentate spike properties.

The dentate gyrus represents a major entry point to the hippocampus. Due to the sparse firing properties of dentate granule cells, the region has often been considered as a gate, acting to

filter inputs from entorhinal afferents into the hippocampal circuit (Hsu, 2007, Introduction II.1.b). I therefore asked whether increased excitability of granule might have downwards effects on the rest of the hippocampal network. Indeed, suppression of KCC2 in the dentate gyrus also induced a decrease in slow gamma power in CA1 region along with a slight decrease in ripples envelope amplitude (cf. Fig 26-27). Interestingly, these two rhythms directly depend on the activity of the CA3 area. Thus, slow gamma is generated in CA3 and propagates to CA1 (Colgin et al., 2009), while excitatory drive from CA3 is required for ripple formation in CA1 (Buzsáki et al., 1992). Hence, the changes I observed in slow gamma and ripple activity could reflect a reduced activity in CA3. This would be consistent with an increased excitability of dentate granule cells since its relative output on CA3 is mostly inhibitory (Mori et al., 2007). Therefore, I expected that deficits in slow gamma and ripple activity might also be rescued upon dentate granule cell chemogenetic silencing. However, this was not the case. Instead, despite a complete rescue of dentate spike activity upon CNO application in rats injected with hM4D-expressing AAV (cf. manuscript Fig. 5H), ripple features were further degraded in both control and KCC2 knockdown animals as evidenced by their decreased envelope amplitude and rate of occurrence.

How may such divergent observations be reconciled ? CNO injection hyperpolarizes granule cells by its action on the inhibitory DREADD, thereby reducing neuronal excitability. However, in doing so, it also affects the driving force of GABAA receptor-mediated currents. In the dentate gyrus, GABAergic transmission is already depolarizing at rest (Staley and Mody, 1992) and yet inhibitory due to shunting of the membrane resistance (see manuscript Fig 1 and 4). Hyperpolarizing resting membrane potential of granule cells with hM4D activation will then further increase the depolarizing driving force of GABAergic transmission, which may then switch from shunting inhibitory to excitatory. This would then act to strengthen the output of the dentate gyrus to CA3 despite a decreased intrinsic excitability of granule cells. This may explain why slow gamma and ripple activity in CA1 were not rescued by chemogenetic silencing. In contrast, dentate spike activity reflects the direct recruitment of dentate granule cells by their entorhinal afferents. Hence, they are relatively independent of GABAergic transmission and could be rescued by hM4D activation in granule cells.

Another possible explanation could be based on altered properties of interneurons. Indeed, in my study, KCC2-targeted shRNA was expressed under the control of a ubiquitous promoter and could therefore be expressed in interneurons. To date, the functional impact of KCC2

suppression in interneurons has not been investigated. However, based on my data as well as unpublished observations from our group, both intrinsic properties of the interneurons and their ability to maintain transmembrane chloride gradients may be affected upon KCC2 knockdown. Subsequent dysregulation of their activity patterns could therefore contribute to the rhythmopathies I observed.

2. Functional consequences of these alterations

Hippocampal network activity is critical for several cognitive processes and, in particular, for memory encoding and consolidation. Dentate gyrus is thought to be critical for its ability to implement pattern separation thus allowing discrimination between different contexts (O'Reilly and McClelland, 1994, see Introduction II.1.c). In line with this idea, dentate gyrus activity has been shown critical for memory encoding in contextual fear conditioning tasks (Bernier et al., 2017; Kheirbek et al., 2013). Inhibiting dentate activity during recall phase also impaired memory performance but only when animals had to distinguish between very similar contexts (Bernier et al., 2017). The ability of the dentate gyrus to perform pattern separation is thought to rely on its sparse firing. Indeed, sparse optogenetic activation of dentate granule cells during recall phase specifically impairs contextual memory in a fear conditioning protocol (Cho et al., 2017). This set of experiments highlights the importance of a strict regulation of dentate excitability since both inhibition and additional sparse activation are sufficient to alter mnesic performances. I showed that chronic KCC2 knockdown in the dentate gyrus increased local activity by promoting the recruitment of granule cells by entorhinal afferents. Based on the literature, I predict this could induce deficits in contextual memory tasks, a hypothesis which could be tested using a contextual fear memory paradigm. However, I did not have time to set up this experiment in our laboratory during my thesis.

The aforementioned studies mainly focused on dentate gyrus function during encoding and recall phases. Nevertheless, I showed that enhanced excitability of dentate granule cells also affects sleep rhythmogenesis by increasing dentate spikes amplitude and frequency. This could also induce memory deficits since a recent study showed that electrical stimulations of the hippocampus impair associative learning when coupled to dentate spikes (Nokia et al., 2017). Two additional observations may however complicate the interpretation of potential memory

deficits following KCC2 suppression in the dentate gyrus. First, I observed a slight decrease in ripple envelope amplitude upon KCC2 knockdown. Ripples have been shown to play a predominant role in both memory encoding and consolidation (Ego-Stengel and Wilson, 2010; Girardeau et al., 2009; Jadhav et al., 2012). Hence their alteration could contribute to cognitive defects. In addition, a previous study from our lab revealed that KCC2 suppression precludes long-term potentiation at glutamatergic synapses (Chevy et al., 2015) which constitutes one of the cellular bases of memory encoding.

Many neurological and psychiatric disorders associated with reduced KCC2 expression include cognitive deficits. In several studies, restoring chloride homeostasis with NKCC1 antagonist improved performance in some cognitive tasks (Deidda et al., 2016; Dargaei et al. 2018), arguing for the importance of rescuing GABA signaling. However, as I have shown in t,his thesis, KCC2 suppression triggers a variety of cellular and synaptic alterations that likely compromise network activity and may then contribute to cognitive deficits. A better understanding of the precise mechanisms underlying these deficits may then permit to best compensate them in the pathology. To this end, studies aiming to decipher the role of KCC2 in memory through regulation of long-term potentiation of glutamatergic synapses, GABAergic transmission or hippocampal rhythmogenesis are currently being carried in our lab.

III- KCC2 IN EPILEPTOGENESIS

One of the original objectives of my PhD work was to examine the potential causal link between KCC2 downregulation and epileptogenesis. As discussed in my introduction (see Introduction I.5), in spite of years of extensive research on the subject, convincing evidence for this causality is still lacking. In particular, it has been difficult to test whether KCC2 downregulation is a cause or a mere consequence of epilepsy. I therefore chose an experimental paradigm based on chronic KCC2 extinction in adult animals. This paradigm was superior to studying mutant or KO animals as these may have profound consequences on the developing brain as well as on the maturation of glutamatergic synapses (Li et al., 2007).

In spite of a large longitudinal spread of infection (~ 1.5 - 2 mm, thus covering most of the dorsal hippocampus, manuscript Fig 5B), I showed that lentiviral-based suppression of KCC2 in dentate granule was not sufficient to trigger spontaneous seizures. Furthermore, using intrahippocampal recordings, I did not record abnormal, epileptiform activities. Finally, susceptibility to seizures in the pilocarpine model was not reduced upon KCC2 suppression (manuscript Fig S5). These observations question the importance of KCC2 downregulation in the dentate gyrus in the context of epileptogenesis.

Dentate granule cells receive considerable excitatory inputs from the entorhinal cortex with a single cell receiving inputs from up to 5000 entorhinal neurons (Patton and McNaughton, 1995). However, despite this intense excitatory drive, activity in the dentate gyrus is particularly sparse with a majority of neurons exhibiting firing rate < 0.5 Hz i*n vivo* (Jung and McNaughton, 1993). This pattern of activity relies on specific cellular properties of dentate granule cells such as their hyperpolarized membrane potential (see Introduction II.1.a) and has been suggested to be essential in the context of epilepsy (Introduction II.3.a). Indeed, the DG can prevent the relay of abnormal hypersynchronous activity from the entorhinal cortex to the hippocampus. This phenomenon has been called “dentate gating” (Heinemann et al., 1992). In contrast, maximal dentate activation triggered by electrical stimulations elicits synchronous epileptiform discharges that propagate to CA3 and CA1 (Lothman et al., 1992) indicating that hyperexcitability of the DG may favor or even initiate pathological activity in the hippocampus. In line with this hypothesis, in human organotypic slices resected from epileptic patients, spontaneous epileptiform activity can be generated in the dentate gyrus – although less often than in the subiculum - and propagate to other hippocampal regions (Eugene et al., 2014). The loss of dentate gating may be particularly relevant in the context of traumatic brain injury (TBI), a condition highly correlated with further development of temporal lobe epilepsy (Jennett et al., 1975). Indeed, brain trauma results in increased excitability of dentate granule cells and massive loss of hilar interneurons (Lowenstein et al., 1992). Additionally, KCC2 mRNA and protein levels are downregulated in the dentate gyrus following fluid percussion injury leading to depolarized reversal potential of GABAergic currents and impaired chloride extrusion capacity (Bonislawski et al., 2007). Downregulation of KCC2 is also observed in the dentate gyrus during two weeks following pilocarpine-induced seizures (Pathak et al., 2007; Kourdougli et al., 2017). In this latter study, authors identified a novel mechanism through which downregulation of KCC2 and subsequent depolarizing GABA signaling triggers mossy fibers sprouting (Kourdougli et al., 2017). This effect depended on impaired chloride homeostasis and activation of pan neurotrophin

receptor $p75^{NTR}$. Thus, blocking NKCC1 or $p75^{NTR}$ activation reduced mossy fiber sprouting and seizure frequency during the chronic phase of epilepsy. Hence, a transient decrease of KCC2 function might participate in the long-term impairment of dentate gating by favoring the establishment aberrant recurrent excitatory connections. However, in my experiments, I did not observe mossy fiber sprouting following KCC2 suppression in dentate granule cells suggesting that other mechanisms may also be at play to promote sprouting upon TBI.

How may my results be reconciled with this set of observations ? First, both in the TBI and in the pilocarpine model, KCC2 suppression is massive throughout the dentate gyrus. In contrast, since downregulation of KCC2 was only observed in about 30% of principal cells in epileptic patients (Huberfeld et al., 2007), I chose a model of lentiviral-based knockdown of KCC2 expression resulting in only a fraction of infected cells. Furthermore, in the pilocarpine model, the downregulation of KCC2 was paralleled by an increase in NKCC1 protein levels (Kourdougli et al., 2017). A similar upregulation of NKCC1 mRNA levels was described in the subiculum of epileptic patients (Palma et al., 2006). This produces an even greater shift in intraneuronal chloride concentration and may enhance the pathological consequences of dysregulated chloride homeostasis. In my study, although I did not specifically test this point, shRNA-induced KCC2 suppression of KCC2 is not expected to modify NKCC1 expression. In contrast and somewhat unexpectedly, I showed that steady-state GABAergic transmission was not affected by chronic KCC2 suppression. Indeed, depolarization of E_{GABA} was accompanied by a depolarizing shift of the membrane potential of similar magnitude. Nevertheless, in the absence of KCC2, neuronal chloride extrusion capacity is drastically reduced (Pellegrino et al., 2011; Gauvain et al., 2011) thereby impairing the ability of the neuron to cope with massive activation of GABAA receptors. Hence, although steady state GABA signaling was unaffected, KCC2 suppression may still alter GABA transmission during repetitive activation thereby affecting network activity. This point should be tested experimentally in gramicidin-perforated patch recordings such as in Fig 1. However, it is common knowledge that such recordings are extremely unstable and I was not able to include this paradigm during my gramicidin-perforated patch recordings

My data also strongly contrast with two recent studies suggesting that dysregulation of chloride homeostasis in a subset of principal neurons could be sufficient to favor the emergence of pathological events (Alfonsa et al., 2015; Buchin et al., 2016). However, several parameters differ between my study and these two publications. In the first study, the authors took

advantage of optogenetic tools to artificially load neurons with chloride ions and examined the subsequent effects on network activity. They observed this load was sufficient to increase excitability of the network and generate high-frequency oscillations reminiscent of epileptic fast-ripples. Based on further modeling studies, they suggested a simple shift in E_{GABA} in a small proportion of neurons could be sufficient to favor the emergence of these pathological oscillations. However, their observations and models are only based on the effect of raised intraneuronal chloride in absence of other concomitant changes. This is therefore quite different from the effect of KCC2 suppression which, as I showed in my data, mainly impact neuronal excitability while preserving GABA transmission at rest. In Buchin et al., the authors modeled a subicular network and investigated the effect of the suppression of KCC2 in principal neurons. They showed that suppressing KCC2 in 40% of the neurons was sufficient to trigger ictal activity. Nevertheless, as I described in my introduction (see Introduction I.5.d), this computational model presents several limitations (including a lack of perisomatic inhibition and the use of high, non-physiological extracellular potassium concentration). Furthermore, there again, the effect of KCC2 knockdown on intrinsic properties of the neuron was not taken into account.

Aside from GABAergic transmission, I observed an increased activity of dentate granule cells upon KCC2 knockdown. Consequently, my results could still predict an impaired dentate gating through enhanced recruitment of granule cells. Yet, I did not observe increased susceptibility to seizures induced by pilocarpine injection upon KCC2 suppression. It should however be noted that systemic pilocarpine injection triggers generalized seizures (Cavalheiro et al., 1991) and may mask the effects of a local increase of dentate excitability. Hence, in my model, testing seizure susceptibility may be better assessed using an induction protocol targeting more specifically the dentate gyrus, such as intra-hippocampal kainate infusion or electrical kindling of the perforant path. Hence, it would be interesting to implement these new models in our laboratory in the future to test this hypothesis.

Overall, my results highlighted a novel pathway through which loss of KCC2 increases network activity. Yet, I did not observe evidence supporting a direct causal relationship between KCC2 downregulation and the emergence of epileptiform activity. Based on data from TBI and pilocarpine models, I targeted the dorsal dentate gyrus in my study. However, data from epileptic patients suggest that temporal hippocampus may play a major role in epileptogenesis since seizure onset mainly occurs near the temporal pole of the hippocampus (which

corresponds to the ventral part in rodents) (King et al., 1997). More specifically, several lines of evidence suggest the subiculum may have a prominent role in ictogenesis in TLE. Thus, *in* vitro studies showed that the subiculum gates the propagation of epileptic activity to the hippocampus (Behr and Heinemann, 1996). In particular, in rat slices, epileptiform activity was generated in the subiculum and back-propagated to CA1 (Harris and Stewart, 2001). This could be partly favored by the sprouting and reorganization of the connections between CA1 and the subiculum in epilepsy (Cavazos et al., 2004), although CA1 is most often sclerotic in the epileptic hippocampus (Coras and Blümcke, 2015). Consistent with these observations, the earliest signs of pre-ictal activity were recorded in the ventral hippocampus and in particular in the ventral subiculum in a pilocarpine model of TLE in rodents (Toyoda et al., 2013). Subsequent studies from the same group revealed that during the pre-ictal phase, firing of principal cells gradually increased in the DG, the subiculum and to a lesser extent in CA1 but not in CA3 (Fujita et al., 2014). Additionally, in the subiculum, about 20 % of the regular-firing cells (likely principal neurons) switched to a bursting mode. This may then contribute to ictogenesis since bursting cells were shown to initiate epileptiform activity in a 0 Mg^{2+} slice model of epilepsy (Menendez de la Prida and Gal, 2004). Finally, increased firing of subicular interneurons was identified more than 4 minutes prior to the ictal activity (Toyoda et al., 2015). Altogether, these studies indicate that major network changes occur before seizure onset in the ventral subiculum and to a lesser degree in the ventral DG and CA1 but not in CA3 region. Although no precise mechanism underlying these changes has been identified yet, these observations clearly point to a critical role of the ventral subiculum in ictogenesis in TLE.

IV- GENERAL CONCLUSION

During my PhD, I aimed to describe the cellular and network alterations following KCC2 downregulation in order to better understand its impact in disorders such as epilepsy. My results shed light on a novel critical function of KCC2 in regulating neuronal excitability through its interaction with Task-3 channels. In dentate granule cells, this effect was predominant over all previously described synaptic modifications. Therefore, I propose that this regulation could underlie several of the symptoms observed in disorders associated with KCC2 downregulation. In particular, I suggest that suppression of KCC2 could result in memory deficits primarily due to enhanced neuronal excitability and altered hippocampal rhythmogenesis. Most importantly, my

work predicts that acting on chloride homeostasis (and GABAergic transmission) alone with bumetanide may not fully compensate for the lack of KCC2. In contrast, it suggests leak potassium channels as novel potential therapeutic targets to compensate for deficits induced by KCC2 downregulation. I propose that combined use of bumetanide and potassium channels openers may represent a promising therapeutic strategy in several neurological and psychiatric disorders.

ADDITIONAL PUBLICATION

ADDITIONAL PUBLICATION

KCC2 forms clusters in dendritic spines (Chamma et al., 2013; Gauvain et al., 2011; Gulyás et al., 2001). Previous work from our team showed that KCC2 interaction with spine actin cytoskeleton through the FERM-domain protein protein 4.1N was critical to maintain the synaptic pool of AMPA receptors (Gauvain et al., 2011). Hence, KCC2 acts as a diffusion barrier for transmembrane proteins within spine head and hinders their lateral diffusion. Suppressing KCC2 therefore leads to an escape of perisynaptic, GluA1-containing AMPARs and a subsequent decreased efficacy of glutamatergic synapses (Gauvain et al., 2011). Since lateral diffusion of AMPARs is critical to the expression of long-term potentiation (LTP) at most glutamatergic synapses (e.g., Makino and Malinow, 2009), we asked whether KCC2 downregulation may also affect LTP.

Our results show that:

- LTP is compromised upon KCC2 suppression by inhibition of activity-driven AMPAR exocytosis downstream NMDAR and CaMKII activation
- This effect is associated with activation of the Rac1/PAK pathway, cofilin inhibition and enhanced F-actin in dendritic spine
- LTP can be rescued by preventing cofilin inhibition upon KCC2 suppression.

In conclusion these results reveal a novel function for KCC2 at glutamatergic synapses for controlling both actin cytoskeleton dynamics and the expression of long-term potentiation. They suggest that dysregulation of KCC2, as observed in many neurological conditions, could underlie cognitive deficits due to impaired interactions with protein partners, independently of GABAergic transmission. My contribution to this work was to provide analytical tools to study the distribution of actin in dendritic spines and to perform stereotaxic injections for *ex vivo* study of LTP.

Cellular/Molecular

KCC2 Gates Activity-Driven AMPA Receptor Traffic through Cofilin Phosphorylation

Quentin Chevy,[1,2,3] Martin Heubl,[1,2,3] Marie Goutierre,[1,2,3] Stéphanie Backer,[4] Imane Moutkine,[1,2,3] Emmanuel Eugène,[1,2,3] Evelyne Bloch-Gallego,[4] Sabine Lévi,[1,2,3] and Jean Christophe Poncer[1,2,3]

[1]Institut National de la Santé et de la Recherche Médicale, Unité Mixte de Recherche-S 839, F-75005, Paris, France, [2]Sorbonne Universités, Université Pierre et Marie Curie Université Paris 06, Unité Mixte de Recherche-S 839, F-75005, Paris, France, [3]Institut du Fer a Moulin, F-75005, Paris, France, and [4]Institut Cochin, Institut National de la Santé et de la Recherche Médicale, U 1016, Centre National de la Recherche Scientifique, Unité Mixte de Recherche 8104, Université Paris Descartes, F-75014, Paris, France

Expression of the neuronal K/Cl transporter KCC2 is tightly regulated throughout development and by both normal and pathological neuronal activity. Changes in KCC2 expression have often been associated with altered chloride homeostasis and GABA signaling. However, recent evidence supports a role of KCC2 in the development and function of glutamatergic synapses through mechanisms that remain poorly understood. Here we show that suppressing KCC2 expression in rat hippocampal neurons precludes long-term potentiation of glutamatergic synapses specifically by preventing activity-driven membrane delivery of AMPA receptors. This effect is independent of KCC2 transporter function and can be accounted for by increased Rac1/PAK- and LIMK-dependent cofilin phosphorylation and actin polymerization in dendritic spines. Our results demonstrate that KCC2 plays a critical role in the regulation of spine actin cytoskeleton and gates long-term plasticity at excitatory synapses in cortical neurons.

Key words: actin; AMPA receptor; KCC2; spine; STED microscopy; synaptic plasticity

Significance Statement

Changes in the expression of neuronal chloride transporters, such as KCC2, occur during postnatal development and are induced in a variety of neurological and psychiatric conditions. Such changes are expected to primarily impact GABA signaling because GABAA receptors are predominantly permeable to chloride ions. However, the KCC2 transporter forms clusters near glutamatergic synapses and interacts with several actin-related proteins. We show that KCC2 is strictly required for LTP expression at hippocampal excitatory synapses. This effect is due to KCC2 interaction with the Rac1/PAK signaling pathway that controls actin polymerization. Suppressing this interaction promotes actin polymerization thereby hindering AMPA receptor traffic upon KCC2 suppression. Alterations of KCC2 expression therefore impact not only GABAergic signaling but also glutamatergic synaptic function and long term plasticity.

Introduction

Fast synaptic inhibition in the brain relies on activation of chloride-permeant GABAA and glycine receptor channels. Hence, chloride homeostasis is critical to maintain the efficacy and polarity of signals mediated by these receptors. In mature neurons, transmembrane Cl gradients are primarily established by opposing actions of the NKCC1 and KCC2 cotransporters, resulting in a net efflux of chloride (Blaesse et al., 2009). Upregulation of KCC2 expression during development is associated with a progressive hyperpolarizing shift in the reversal potential of IPSCs (Rivera et al., 1999). KCC2 may also be rapidly downregulated by neuronal activity through post-translational modifications (Chamma et al., 2012) as well as modifications at the

Received May 4, 2015; revised Sept. 1, 2015; accepted Sept. 26, 2015.

Author contributions: Q.C., E.B.-G., S.L., and J.C.P. designed research; Q.C., M.H., and S.B. performed research; M.G., I.M., and E.E. contributed unpublished reagents/analytic tools; Q.C., M.H., and S.B. analyzed data; Q.C. and J.C.P. wrote the paper.

This work was supported by Human Frontier Science Program Research Grant (RGP0022/2013) to J.C.P., Institut National de la Santé et de la Recherche Médicale, Ville de Paris Biomedical and Health Research Program to J.C.P., Fédération pour la Recherche sur le Cerveau to J.C.P., Fondation pour la Recherche Médicale (DEQ20140329539) to J.C.P., and PICPEN (Center for Psychiatry and Neuroscience, Paris). Q.C. was the recipient of doctoral fellowships from Université Pierre and Marie Curie and Fondation pour la Recherche Médicale. We thank Ingrid Chamma for the quantitative analysis of phalloidin staining data; Theano Irinopoulou for support with spinning disc and confocal imaging; David Geny at PICPEN for assistance with STED microscopy; Alain Prochiantz and David diGregorio for helpful discussions; and Eric J. Schwartz, Manuel Mameli, Kai Kaila, Kevin J. Staley, and Richard Miles for constructive comments on an earlier version of the manuscript.

The authors declare no competing financial interests.

Correspondence should be addressed to Dr. Jean Christophe Poncer, INSERM U839, Institut du Fer à Moulin, 17 rue du Fer à Moulin, F-75005, Paris, France. E-mail: jean-christophe.poncer@inserm.fr.

DOI:10.1523/JNEUROSCI.1735-15.2015

 0270-6474/15/3515772-15$15.00/0

transcriptional level in a variety of neurological and psychiatric disorders (Coull et al., 2003; Cohen et al., 2002; Boulenguez et al., 2010; Tyzio et al., 2014). Because most of these conditions are associated with partial loss of inhibition, high expectations are put on diuretic drugs that may act to compensate for the loss of KCC2 function and thereby restore neuronal chloride homeostasis and synaptic inhibition (Kahle et al., 2008; Gagnon et al., 2013; Löscher et al., 2013).

KCC2, however, is not specifically enriched near GABAergic synapses but instead shows diffuse somatodendritic distribution with large clusters in dendritic spines near postsynaptic densities (Gulyás et al., 2001; Chamma et al., 2013), suggestive of interactions with glutamatergic signaling. Precocious expression of recombinant KCC2 in embryonic cortical neurons leads to exuberant spinogenesis and excitatory synapse density (Fiumelli et al., 2013). Conversely, genetic ablation of KCC2 precludes spine morphogenesis and excitatory synapse formation (Li et al., 2007), whereas chronic KCC2 suppression in mature neurons reduces the confinement of several transmembrane proteins, including AMPARs within dendritic spines (Gauvain et al., 2011). Interestingly, these effects are independent of ion transport and instead involve KCC2 interactions with intracellular partners. KCC2 has been shown to be engaged in variety of protein interactions that may impact its aggregation and function in dendritic spines (Medina et al., 2014). These include synaptic proteins, such as GluK2 (Mahadevan et al., 2014) and its interacting protein Neto2 (Ivakine et al., 2013), acting to enhance KCC2 membrane stability, as well as actin-related proteins, such as 4.1N (Li et al., 2007) and βPIX (Llano et al., 2015), which may influence KCC2 anchoring to spine cytoskeleton (Chamma et al., 2013) and actin polymerization (Saneyoshi et al., 2008), respectively. Such interactions are therefore predicted to influence spine actin cytoskeleton.

Dendritic spines exhibit various forms of activity-driven plasticity leading to coordinated modulation of their structure and synaptic function (Bosch and Hayashi, 2012). Long-term potentiation (LTP) of excitatory synapses involves synaptic translocation of proteins, including AMPARs (Malinow and Malenka, 2002) and a persistent increase in spine volume (Kopec et al., 2006; Harvey and Svoboda, 2007). The two processes are mechanistically correlated (Kopec et al., 2007) and rely on rapid remodeling of actin cytoskeleton within dendritic spines. This remodeling may be both permissive for activity-driven AMPA receptor membrane insertion (Gu et al., 2010) and lateral diffusion (Rust et al., 2010) as well as required for spine head enlargement (Okamoto et al., 2004). Here, we therefore tested whether the reciprocal interaction between KCC2 and spine actin cytoskeleton may impact LTP at excitatory synapses in hippocampal neurons. We show that KCC2 is strictly required for LTP expression and that suppressing KCC2 expression or protein interactions with its carboxy-terminal domain prevents activity-driven membrane insertion of AMPARs. This effect reflects remodeling of F-actin in dendritic spines due to Rac1/PAK- and LIMK-dependent inhibition of cofilin. Our results reveal that KCC2 plays a critical role at mature cortical excitatory synapses where it not only controls synaptic efficacy but also gates the expression of long-term plasticity.

Materials and Methods

DNA and lentiviral constructs. Rat *Slc12a5*-specific and nontarget shRNA sequences (Gauvain et al., 2011) were inserted in a pGeneClip hMGFP vector (Promega) for neuronal transfection *in vitro*. For some experiments requiring massive transduction (see Figs. 1, 4*E*, 7*A*), the same sequences were introduced in pTRIP vector under U6 promoter and used to produce purified lentiviral particles (titer 7–9 $\times$ 10^9 IU/ml, UNC Vector Core facility). Knockdown efficiency was verified by both immunohistochemistry (see Fig. 1*B*) and Western blotting (-70%, $p = 0.04$). The pEGFP-N1 vector used in some experiments was from Clontech. The GluA1-superecliptic pHluorin (SEP) construct in pCI vector from the Malinow laboratory (Kopec et al., 2006) was obtained from Addgene. Rat KCC2-CTD (amino acids 637–1116) was cloned into the pEGFP-IRES vector as described previously (Gauvain et al., 2011). The LifeAct Venus construct was obtained by replacing GFP by Venus sequence from a pCMV LifeAct-GFP2 construct (Gauvain et al., 2011). mCherry-tCaMKII was obtained by replacing GFP by mCherry from GFP-tCaMKII plasmid from the Malinow laboratory. mCherry-tCaMKII was then cloned into a pCMV-Tet3G-TRE vector (Clontech) to allow for doxycycline-induced expression (TET-ON system). For rescue experiments, recombinant KCC2 4904–4924 nucleotide sequence AAC GAG GTC ATC GTG AAT AAA TCC was replaced with AAT GAA GTT ATT GTT AAC AAG TCT to preserve amino acid sequence. Rescue efficacy was verified both by KCC2 immunocytochemistry and in electrophysiological assays of chloride extrusion (data not shown).

Cell culture and transfection. Hippocampal neurons were prepared as described previously (Gauvain et al., 2011) from embryonic day 19 Sprague Dawley rat pups. After dissociation, cells were plated on polyornithine-coated glass coverslips at a density of 3.4×10^4 cells/cm^{-2} and maintained in a CO_2 incubator set at 37°C in a culture medium composed of Neurobasal supplemented with B27 (Invitrogen), 2 mM glutamine, and penicillin/streptomycin. After 2 weeks, neurons were transfected using transfectin (Bio-Rad) according to the manufacturer's instructions (with 1 μg DNA for 3 μl transfectin per well). Neurons were then used for biological assays within 7–10 d. KCC2 extinction by RNA interference was detected from 4 d after transfection (Gauvain et al., 2011). To maintain a similar timeframe, pharmacological blockade experiments were performed by applying the specific KCC2 antagonist VU0240551 (6 μM) for 3 days.

In some experiments shown in Figure 8, neurons were exposed to LIMK or GTPase inhibitors. Ser3 peptide was synthesized by Proteogenix and contained the 16 N-terminal amino-acid sequence of cofilin (MASGVAVSDGVIKVFN) fused after 3 glycine residues to the penetratin sequence (RQIKIWFQNRRMKWKK), as described previously (Gu et al., 2010). Ser3 peptide (20 μg/ml), LIMKi (10 μM in DMSO, Millipore), and Rhosin (30 μM, Millipore) were applied onto neuron cultures for 4–5 h before experiments. IPA-3 (5 μM, Millipore) was applied for 24 h. LIMKi, IPA-3, and Rhosin were also present during recordings.

Electrophysiology. Cultured neurons were recorded at 31°C under superfusion with a HEPES-buffered, artificial CSF (H-ACSF) containing (in mM) the following: 125 NaCl, 20 D-glucose, 10 HEPES, 4 $MgCl_2$, 2 KCl, 1 $CaCl_2$, pH 7.4. For miniature EPSC (mEPSC) recordings, neurons were recorded in whole-cell configuration with borosilicate glass micropipettes filled with a solution containing (in mM) the following: 110 $CsMeSO_4$, 20 CsCl, 10 HEPES, 10 EGTA, 4 MgATP, and 0.4 Na_3GTP, pH 7.4. Cells were held at −70 mV, and mEPSCs were isolated by adding TTX (1 μM) and bicuculline methochloride (20 μM) to the extracellular solution. Currents were recorded with a Multiclamp 700B amplifier (Molecular Devices), filtered at 2 kHz, and digitized at 20 kHz. Access and input resistance were regularly monitored with −5 mV voltage steps. mEPSCs were detected and analyzed offline using Detectivent software.

Chemical LTP (cLTP) was induced as described previously (Kopec et al., 2006) by switching extracellular solution for 16 min to a nominally Mg-free solution containing (in mM) the following: 125 NaCl, 20 D-glucose, 10 HEPES, 2 KCl, 5 $CaCl_2$, pH 7.4, supplemented with 50 μM forskolin, 0.1 μM rolipram, and 20 μM bicuculline. Forskolin and rolipram stock solutions were prepared in anhydrous DMSO, leading to a final DMSO concentration of 0.2%. Hence, control experiments involved a 16 min application of a solution containing an equivalent DMSO concentration.

For *ex vivo* field EPSP (fEPSP) recordings, 3-week-old male Wistar rats were anesthetized by intraperitoneal injection of ketamine/xylazine (of 75/10 mg/kg). Rats were head-fixed into a stereotaxic apparatus, and holes were drilled bilaterally in the skull above the dorsal hippocampus

(from bregma: −3.3 mm anteroposterior, ±2.3 mm mediolateral, −3.0 mm dorsoventral); 1 μl of a concentrated lentiviral solution (diluted at 1:10 from a titer of 375–440 ng/ml p24, as detected by ELISA) was injected in each site. After 2 weeks, acute hippocampal slices were prepared. Rats were anesthetized and perfused with ice-cold cutting solution containing the following (in mM): 110 choline chloride, 25 $NaHCO_3$, 1.25 NaH_2PO_4, 2.5 KCl, 0.5 $CaCl_2$, 7 $MgCl_2$, 25 glucose, 11.6 ascorbic acid, and 3.1 pyruvic acid. The brain was then rapidly removed, and 450-μm-thick parasagital slices were prepared with a vibratome (Microm, Thermo Fisher). Slices were then transferred and allowed to recover for 1 h in an interface chamber filled with bicarbonate-buffered ACSF (B-ACSF) preheated at 37°C and oxygenated with 5% CO_2 in O_2, containing the following (in mM): 124 NaCl, 1 NaH_2PO_4, 26.2 $NaHCO_3$, 2.5 KCl, 11 glucose, 1.6 $CaCl_2$, 1.2 $MgCl_2$. For recordings, slices were transferred in a submerged recording chamber and superperfused with B-ACSF after a cut was made between the CA3 and CA1 areas. A recording borosilicate glass pipette (2–4 MΩ) filled with B-ACSF was inserted in the molecular layer of a densely infected dentate gyrus area, and a tungsten bipolar electrode (0.5 MΩ) was used to stimulate the perforant pathway. fEPSPs were recorded in the presence of the GABAA receptor antagonist bicuculline methochloride (20 μM), using a Multiclamp 700B amplifier (Molecular Devices) low-pass filtered at 5 kHz, and digitized at 20 kHz. fEPSP slopes were analyzed offline using Clampfit software (Molecular Devices). Briefly, baseline potential was set to zero, and recordings were low-pass filtered at 1 kHz using a Bessel filter. The initial slope of the fEPSP was then automatically measured using a 1 ms time-window manually positioned at the onset of the fEPSP. Data were acquired and analyzed blind to the experimental condition.

Immunocytochemistry and fluorescence image acquisition. Cultures were fixed in 4% PFA and permeabilized with 0.2% Triton X-100 in PBS. KCC2 immunostaining was performed using rat KCC2 antibody (1:400, Sigma-Aldrich) and Cy3-coupled goat anti-rabbit (1:400); 4.1N (1:500, BD Biosciences) immunostainings were performed after methanol fixation and permeabilization (10 min at −20°C) and revealed with Cy3-coupled donkey anti-mouse antibodies (1:400). GFP immunostainings were performed using GFP (1:1000, Millipore Bioscience Research Reagents) and Alexa-488-coupled goat anti-chicken secondary antibodies (1:400). Rac1 GEF and GAP immunostaining was performed after 5 min fixation in 4% PFA by overnight incubation at 4°C with rabbit βPIX (1:100, Millipore) and monoclonal G protein-coupled receptor kinase-interacting protein 1 (GIT1, 1:100, clone N39B-8, Anticorpsenligne) antibodies, as in Smith et al. (2014). All secondary antibodies were from Jackson ImmunoResearch Laboratories. Alexa-456-coupled phalloidin (1:250, Invitrogen) was sometimes added, in the absence of serum, to stain F-actin.

Neurons were then imaged on a Leica DM6000 upright microscope using 40× (1.25 NA, for KCC2 immunofluorescence) or 100× (1.40 NA, for all other experiments) objectives. Images were acquired with a 12-bit cooled CCD camera (Micromax or Coolsnap fx, Roper Scientific) operated with MetaMorph (Molecular Devices). For quantification, cultures were stained simultaneously and images were acquired using the same exposure time. Mean or integrated fluorescence intensities were then quantified using ImageJ, blind to the experimental conditions. Normalization was performed for each culture by dividing mean fluorescence intensity from each cell by the average of the mean fluorescence intensity of all cells of the control group.

Immunohistochemistry and fluorescence image acquisition. P40 rats were anesthetized by intraperitoneal injection of ketamine/xylazine and perfused transcardially with 4% PFA in PBS. Brains were then removed, postfixed overnight, and stored at −20°C in 30% ethylene glycol and 30% glycerol in PBS. Parasagital sections (40 μm thick) were obtained using a cryotome. Brain slices were preincubated 1 h with 0.5% Triton and 10% goat serum in PBS and incubated overnight at 4°C with the primary antibodies: GFP (chicken, 1:1000, Millipore Bioscience Research Reagents), KCC2 (rabbit, 1:400, Millipore). Slices were then incubated 1 h with secondary antibodies (goat CY3-coupled and donkey FITC-coupled directed against rabbit and chicken antibodies, respectively) and mounted with Mowiol/Dabco (25 mg/ml). Stacks of 10–40 sections (0.2 μm apart) were acquired using an upright confocal microscope (Leica TCS SP5, 40×/1.25 NA objective).

GluA-SEP fluorescence and spine tracking. Neurons expressing GluA1/2-SEP and mCherry were maintained at 37°C in a thermostatted chamber and superfused with H-ACSF preheated at 37°C. Time-lapse confocal images of neurons were acquired using an inverted spinning-disc microscope (Leica DMI4000, Yokogawa CS20 spinning Nipkow disk, 100×/1.4 NA objective). At every time point, neurons were successively illuminated by 491 nm/561 nm light from an Ar/Kr laser. Emitted light was collected using corresponding emission filters (525-39 and 607-36 nm) and a cooled EM-CCD camera (512 × 512, 16 μm pixel size). Importantly, laser intensity, time of illumination, and acquisition parameters of the camera remained identical to allow comparison between experiments and bleach correction. An X, Y, Z motorized platform (Märzhäuser) was used to perform acquisition from multiple neurons and *z*-stacks (6 μm stack, 0.2 μm steps).

Confocal stacks were analyzed with Neuronstudio (Dumitriu et al., 2011), blind to experimental conditions, to quantify changes in spine head volume overtime using the mCherry channel. Only spines that could be accurately followed over the entire experiments were measured. Spine volumes from each cell were then averaged to test statistical significance. SEP fluorescence was measured on registered maximal projection in *z* of confocal stacks. ROIs were automatically drawn around the entire dendrites using thresholded mCherry signal, and mean SEP fluorescence intensity was calculated. Fluorescence intensity values were then background-subtracted and bleach-corrected. Normalization of SEP intensity was performed for each cell by dividing the mean fluorescence intensity by the average of fluorescence intensities of the three time points before cLTP induction.

In experiments using NH_4 Cl application to collapse transmembrane pH gradients (Ashby et al., 2006) (see Fig. 3), rapid alkalization of intracellular compartments due to passive NH_3 diffusion through membranes was followed by a delayed, rebound acidification, likely reflecting KCC2-mediated ammonium transport (Tietz et al., 1999). Accordingly, this rebound acidification was not observed in neurons with suppressed KCC2 expression, whereas the initial alkalization was unaffected (data not shown). We therefore always measured SEP fluorescence before the onset of the rebound acidification (<7 min).

In experiments shown in Figure 4, $\alpha CaMKII_{1-290}$ expression was induced by 24 h application of doxycycline (2 μg/ml). Neurons were then maintained in H-ACSF in a thermostatted chamber for acquisition using an upright confocal microscope (Leica TCS SP5, 40×/0.8 NA, water-immersion objective). GluA1-SEP and mCherry were successively excited by 488 nm (Ar laser) and 561 nm (HeNe laser), and emitted fluorescence was filtered by 500–600 nm and 570–700 nm (Leica AOBS). Pinhole was set as fully open (600 μm, 10 μm thickness) to collect fluorescence originating from the entire dendritic section. Laser power and scanning parameters were maintained identical to allow quantitative measurements and comparison of SEP fluorescence between conditions. All mCherry-positive neurons were imaged, and GluA1-SEP-negative neurons were discarded during the analysis process.

STED microscopy. Neurons expressing LifeAct-Venus and mCherry were fixed and mounted in mowiol. The STED microscope consisted of an inverted Leica TCS SP5 STED CW microscope with a 100×/1.4 NA objective, 488 nm Ar laser, 594 HeNe laser, and 561 nm 10 mW DPSS laser for depletion, nonresonant galvanometer mirror (used at 400 Hz, 1024 × 1024, 28.7 nm pixel size), Leica AOBS for emission filters, and GaAsP hybrid detectors (HyD). Focusing onto dendritic spines was performed using the mCherry signal, and a single confocal slice was acquired for each dendritic section. Diffraction limited- and STED-resolution images of LifeAct-Venus were successively acquired. STED images were then deconvolved using special Leica CW-STED plugin of Huygens (SVI) and recommended parameters from Huygens. A custom plugin on ImageJ was used to outline individual spines and measure the FWHM of LifeAct-labeled spine necks based on a Gaussian fit (accuracy of the fit was evaluated both by eye and by r^2 measurements, blind to experimental conditions). Several spine head parameters were also computed: mean and variance of LifeAct-Venus fluorescence intensity and geometric center of the spine. Spine heads were then realigned using a line originating

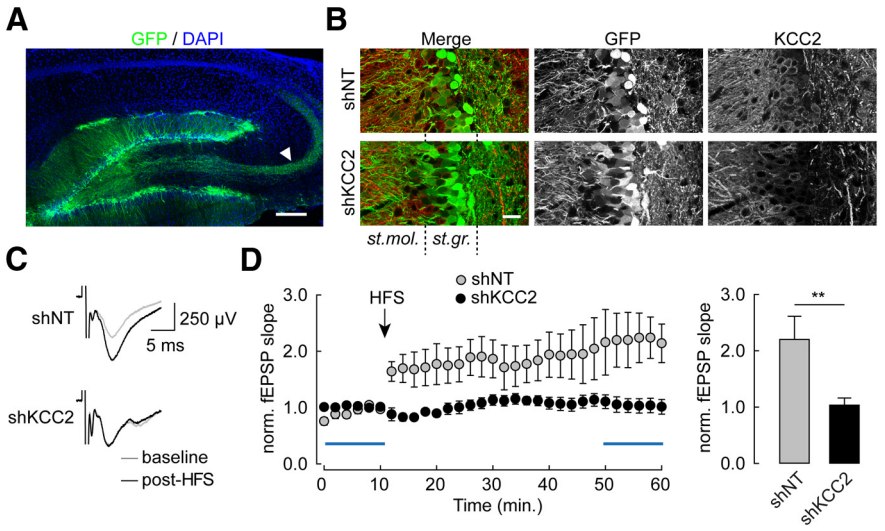

Figure 1. Chronic knockdown of KCC2 precludes LTP at perforant path inputs onto dentate gyrus granule cells. ***A***, Maximal intensity projection of confocal micrographs showing EGFP (green) and DAPI (blue) staining in parasagittal hippocampal slices 2 weeks after stereotaxic injection of a lentivirus-expressing nontarget (shNT) shRNA sequence and EGFP. Arrowhead indicates mossy fibers from infected granule cells. Scale bar, 200 μm. ***B***, Maximal intensity projection of confocal micrographs of dentate gyrus areas infected with lentiviruses expressing either nontarget (shNT) or KCC2-directed (shKCC2) shRNA, showing massive silencing of KCC2 expression in the latter (see in particular KCC2 immunostaining in *st. granulosum* [*st.gr.*]). Scale bar, 25 μm. ***C***, Superimposed average of 60 consecutive fEPSPs recorded within *st. moleculare* (*st. mol.*) upon extracellular stimulation of perforant path inputs, before (gray) and 40 min after (black) high-frequency stimulation (HFS, 4 × 1 s at 100 Hz). ***D***, Left, Time course of changes in fEPSP slope upon HFS protocol in slices from animals infected with lentiviruses expressing shNT ($n = 8$) or shKCC2 ($n = 10$). Blue bars represent the time windows used for averages. Right, Summary data of fEPSP slope 40 min after HFS, normalized to the mean of 10 min baseline. $^{**}p < 0.01$.

from the attachment point of the spine neck to the head (manually determined) and passing through the geometric center.

For spatial autocorrelation analysis of LifeAct-Venus signal (see Fig. 5), data from isolated spine heads were first normalized. The degree of clustering in each dataset was assessed using Moran's index analysis (Moran, 1948). This index ranges values from −1 (complete dispersion) to 1 (complete clustering), with 0 representing random distribution. For each pixel i, local Moran's index (I_i) was computed as follows:

$$I_i = z_i \cdot \sum_j W_{i,j} \cdot z_j$$

where z_i is the value of the pixel i and W represents the matrix of neighboring weights. Equal weights were attributed to all pixels within a 2-pixel distance from pixel i, all other weights being set to 0. To compute a statistical significance threshold for I, a bootstrap analysis was performed for each spine head. Data were resampled randomly 1000 times, and local Moran's indexes were computed for each pixel in the random distributions. For each pixel, Moran's index was compared with the 1000 values derived from bootstrap analysis to compute a local p value. Statistical significance of positive spatial autocorrelation was considered for pixels with p values <0.05. The proportion of high-intensity clustered pixels per spine was then computed as the proportion of pixels with significant autocorrelation index and intensity above the mean, and was used for statistical comparison between experimental groups.

Biochemical assays. Hippocampal cultures were infected at 15–17 DIV using lentiviral vectors expressing shRNAs and eGFP using 500 ng/ml of purified virus solution as above. One week later, cultures were processed for cLTP (see below) or exposed to vehicle only (DMSO 0.2%) for 2–16 min. Immediately after cLTP induction, cultures were washed twice in ice-cold PBS and lysed in lysis buffer (25 mM Tris-HCl, pH 7.4, 250 mM NaCl, 50 mM NaF, 5 mM PPi, 5 mM EDTA, 5 mM EGTA, 1 mM sodium orthovanadate, 1% Triton-X, and protease inhibitor mixture; Roche). After centrifugation at 14.000 × g for 15 min., supernatants were mixed with Laemmli sample buffer and boiled at 95°C for 5 min. Samples were subjected to standard SDS-PAGE and transferred to nitrocellulose membranes. Blots were probed with primary antibodies against cofilin (Abcam), cofilin phospho-Ser3 (Abcam), GluA1 (Millipore), GluA1 phospho-Ser845 (Millipore), KCC2 (Millipore), Tuj1 (R&D Systems), and detected with fluorescent secondary antibodies (DyLight 800) using Odyssey infrared imaging system (LI-COR Bioscience). For quantification, all data were normalized to internal Tuj1 control signals.

For coimmunoprecipitation, neurons were homogenized in modified RIPA buffer (50 mM Tris-HCl, pH 7.4, 150 mM NaCl, 1 mM EDTA, 1% Nonidet P-40, 0.1% SDS, 0.5% DOC, and protease inhibitors; Roche). Lysed cells were kept on ice for 20 min and then centrifuged at 14,000 × g for 10 min. Lysates were then incubated with KCC2 (Millipore) or βPIX IgG (Millipore, 2 μg) (Smith et al., 2014) overnight at 4°C. The pulldown was performed using Protein G Magnetic beads (Invitrogen) for 2 h at 4°C. The beads were washed 3 times in RIPA buffer and one time in RIPA buffer without detergents. Bound proteins were eluted in SDS sample and separated by SDS-PAGE.

Rac1 and RhoA activity was measured using effector pulldown assays. Briefly, neurons infected with lentiviruses expressing shRNA sequences were washed with PBS, lysed with ice-cold lysis buffer (25 mM Tris pH 7.5, 1% NP40, 100 mM NaCl, 10 mM $MgCl_2$, 5% glycerol, 5 mM NaF, 1 mM PMSF, 1 μl/ml protease inhibitor mixture; Sigma) and clarified by centrifugation at 1600 × g for 5 min at 4°C; 300 μg of lysate proteins was incubated with 10 or 50 μg of PAK-PBD or Rhotekin-RBD beads (Cytoskeleton), respectively, for 1 h at 4°C. Bead pellets were washed twice with 25 mM Tris, pH 7.5, 0.5% NP40, 40 mM NaCl, 30 mM $MgCl_2$, 1 mM DTT, 1 mM PMSF, 1 μl/ml protease inhibitor mixture (Sigma) before addition of 5× Laemmli buffer. Fractions were analyzed by Western blotting. Proteins were separated on a 12% SDS polyacrylamide gel and transferred onto a nitrocellulose or PVDF membrane (GE Healthcare). Blots were probed with mouse monoclonal anti-Rac1 (1:1000, BD Transduction Laboratory) or anti-RhoA (1:200, Santa Cruz Biotechnology), as described previously (Causeret et al., 2004; Backer et al., 2007). Band densities were quantified by Fusion software (Vilber Lourmat). The relative densities of pulled down activated Rac1 and RhoA were normalized to the maximal Rac1 or RhoA in the same samples incubated with 200 μM GTP-γS for 15 min at room temperature, according to the manufacturer's instructions.

Biochemical assays were repeated at least 3–4 times on independent cultures, and data were compared using Student's t test, after testing normality and equal variance of the data with SigmaPlot 12.5 (SPSS). In all other experiments, data were compared using nonparametric paired (Wilcoxon) or unpaired (Mann–Whitney) tests. Differences were considered significant for p values <0.05.

Results

Suppressing KCC2 expression, but not function, precludes LTP in hippocampal neurons

We first investigated the impact of KCC2 expression on LTP in hippocampal slices using *in vivo* RNA interference. Juvenile rats (P21) were stereotaxically injected in the dorsal dentate gyrus with lentiviruses expressing previously validated either nontarget or KCC2-directed small hairpin RNA sequences (Gauvain et al., 2011). Suppression of KCC2 expression in transduced neurons was confirmed by immunohistofluorescence imaging 2 weeks after infection (Fig. 1*A*,*B*). An fEPSP was evoked in the molecular layer of densely infected areas of the dentate gyrus by extracellular stimulation of perforant path inputs in the pres-

ence of the GABAA receptor antagonist bicuculline (20 μM). High-frequency stimulation (4 × 1 s at 100 Hz) induced a robust and long-lasting (>60 min) increase in the initial slope of the fEPSP with no detectable post-tetanic potentiation, in both uninfected slices (data not shown) as well as slices infected with nontarget shRNA lentiviruses (220.4 ± 40.9% of control, $n = 8$ slices, $p < 0.01$; Fig. 1*C*). In slices infected with KCC2-directed shRNA lentiviruses, however, this form of LTP was suppressed (103.5 ± 12.8%, $n = 10$ slices, $p = 1.0$; Fig. 1*D*).

To explore the molecular mechanisms involved in LTP hindrance upon KCC2 suppression, we next used a classical, cLTP paradigm in primary hippocampal neurons. This paradigm consisted of a 16 min application of rolipram/forskolin/bicuculline in the absence of external Mg (Otmakhov et al., 2004; Kopec et al., 2006) to induce a persistent (>80 min) potentiation in the efficacy of excitatory synapses (Fig. 2*A*,*B*). This potentiation was detected as a 30% increase in mEPSC amplitude compared with neurons exposed to vehicle only (26.8 ± 1.6 vs 20.6 ± 1.6 pA, $p = 0.01$) with no significant change in their mean frequency (34.7 ± 5.5 vs 29.6 ± 5.6 Hz, $n = 19$ and $n = 16$ cells, respectively, $p = 0.48$), suggesting that its locus of expression was primarily postsynaptic (Otmakhov et al., 2004; Kopec et al., 2006).

Suppressing KCC2 expression for 7–10 d by RNA interference completely abolished cLTP in mature hippocampal neurons (Fig. 2*A*–*C*). Thus, mEPSC amplitude was not significantly different after a cLTP paradigm compared with control (19.2 ± 0.6 vs 18.4 ± 0.5 pA, $n = 13$ cells each, $p = 0.34$). In contrast, expression of a nontarget shRNA sequence did not affect cLTP expression (24.1 ± 1.0 vs 20.2 ± 0.8 pA, $n = 12$ and $n = 13$ cells, respectively, $p = 0.006$). This effect of KCC2 suppression was independent of the loss of ion transport function because chronic application of the specific antagonist VU0240551 (Delpire et al., 2009; Gauvain et al., 2011) (6 μM) had no effect on cLTP expression (30.0 ± 2.6 vs 23.0 ± 1.7 pA, $n = 12$ cells each, $p < 0.05$; Fig. 2*C*). In contrast, specifically preventing KCC2 interactions with intracellular partners, using overexpression of a dominant-negative peptide (KCC2-CTD) (Li et al., 2007; Gauvain et al., 2011; Puskarjov et al., 2014), completely abolished cLTP (20.2 ± 1.0 vs 21.3 ± 0.9 pA, $n = 11$ and $n = 18$ cells, respectively, $p = 0.44$).

LTP at hippocampal synapses is associated with a concomitant and persistent increase in spine volume (e.g., Kopec et al., 2006, 2007; Harvey and Svoboda, 2007). We monitored spine volume in cLTP experiments using time-lapse, spinning-disc confocal imaging of mCherry-expressing neurons (Fig. 2*D*–*F*). In neurons expressing mCherry only, cLTP was associated with a significant increase in spine volume that persisted >30 min after induction (to 27.8 ± 3.0% of control at 30 min after induction, $n = 143$ spines from 7 cells, $p < 0.05$; Fig. 2*F*). Similarly, neurons expressing nontarget shRNA showed a 33.4 ± 8.9% increase in spine volume 30 min after cLTP induction. In contrast, no significant change in spine volume was detected in neurons expressing KCC2-directed shRNA (−9.5 ± 4.7% of control, $n = 9$ cells, $p = 0.1$; Fig. 2*D*–*F*), similar to shNT-expressing neurons exposed to vehicle only (DMSO 0.2%, −12.6 ± 3.7% of control, $n = 6$ cells, $p = 0.06$; Fig. 2*E*). Again, this effect did not involve KCC2 function because a 72 h exposure to the specific antagonist VU0240551 did not prevent a cLTP-induced increase in spine volume (to 19.7 ± 5.1% of control, $n = 576$ spines from 20 cells, $p < 0.005$ Fig. 2*F*) to a similar extent as in neurons exposed to vehicle only ($n = 20$ and $n = 15$ cells, respectively, $p = 0.6$). Our results show that KCC2 is strictly required for both synaptic and structural LTP at hippocampal excitatory synapses, through a mechanism likely requiring intracellular protein interactions but independent of ion transport.

KCC2 is required for activity-driven GluA1 exocytosis

LTP in hippocampal pyramidal neurons relies in part on activity-driven membrane insertion of AMPARs (Malinow and Malenka, 2002; Poncer, 2003; Huganir and Nicoll, 2013). We therefore asked whether activity-driven AMPAR exocytosis might be compromised in the absence of KCC2. We used SEP-tagged GluA1 to specifically monitor the membrane-inserted pool of GluA1-containing AMPARs (Ashby et al., 2006; Kopec et al., 2006; Lin et al., 2009; Makino and Malinow, 2011) (Fig. 3*A*). Application of a pH 5.5 external solution led to complete quenching of SEP-GluA1 (to 12.7 ± 3.1% of control, $n = 11$ cells, $p < 0.001$), whereas a collapse of transmembrane proton gradients by ammonium increased SEP-GluA1 fluorescence (to 125.0 ± 13.3% of control, $n = 26$ cells, $p < 0.001$), likely revealing intracellular receptor pools (Fig. 3*A*). SEP-GluA1 fluorescence was rapidly and persistently increased upon cLTP induction in hippocampal neurons, indicating membrane insertion of new SEP-GluA1-containing AMPARs (23.0 ± 5.1% of control after 35 min, $n = 19$ cells, $p < 0.001$; Fig. 3*B*,*C*). This effect was not observed upon application of vehicle only (DMSO, −2.1 ± 3.7% of control, $n = 5$ cells, $p = 0.3$) and was specific to SEP-GluA1 but not SEP-GluA2-containing receptors (2.3 ± 3.2% of control, $n = 18$ cells, $p = 0.33$).

Using this assay, we then examined how SEP-GluA1 trafficking may be affected by altering KCC2 expression or function. Chronic suppression of KCC2 expression by RNA interference prevented cLTP-induced membrane insertion of SEP-GluA1 containing receptors (3.2 ± 1.7% of control, $n = 21$ cells, $p = 0.44$; Fig. 3*B*,*C*). This effect was specific to KCC2 suppression as it could be rescued by overexpressing an shRNA-proof recombinant KCC2 (17.4 ± 4.5% of control, $n = 20$ cells, $p < 0.001$; Fig. 3*C*; see Materials and Methods). However, it was not mimicked by chronically blocking KCC2 function using the specific antagonist VU0240551 (Fig. 3*C*), again suggesting that KCC2 expression, but not function, is required for cLTP-induced AMPAR membrane traffic. Importantly, SEP-GluA1 steady-state fluorescence was reduced in neurons expressing KCC2-specific compared with nontarget shRNA (−24.8 ± 9.5%, $n = 28$ and $n = 23$ cells, respectively, $p < 0.01$). However, its relative increase upon application of NH_4Cl was similar in both conditions (20.6 ± 2.2%, $n = 28$ cells, $p < 0.001$ and 22.1 ± 4.0%, $n = 23$ cells, $p < 0.001$, respectively; Fig. 3*D*). These results suggest that altered GluA1 membrane insertion in the absence of KCC2 may not reflect a loss of intracellular GluA1, but rather a specific disruption of its activity-driven exocytosis.

During LTP in hippocampal neurons, αCaMKII activation induces membrane insertion of GluA1-containing AMPARs (Hayashi et al., 2000; Esteban et al., 2003), which requires PKA phosphorylation of GluA1 Ser845 (Esteban et al., 2003). A defect in either αCaMKII activation or GluA1 phosphorylation on Ser845 in neurons lacking KCC2 may then preclude activity-dependent AMPAR traffic. To bypass αCaMKII activation, we overexpressed a constitutively active αCaMKII to directly promote GluA1 exocytosis. The catalytic domain of αCaMKII ($CaMKII_{1–290}$) (Hayashi et al., 2000; Poncer et al., 2002; Esteban et al., 2003) fused to mCherry was expressed under a doxycycline-inducible promoter to allow for a precise control over the timing of its expression (Fig. 4*A*). We first verified that mCherry-$CaMKII_{1–290}$ transgene expression was strictly restricted to neurons

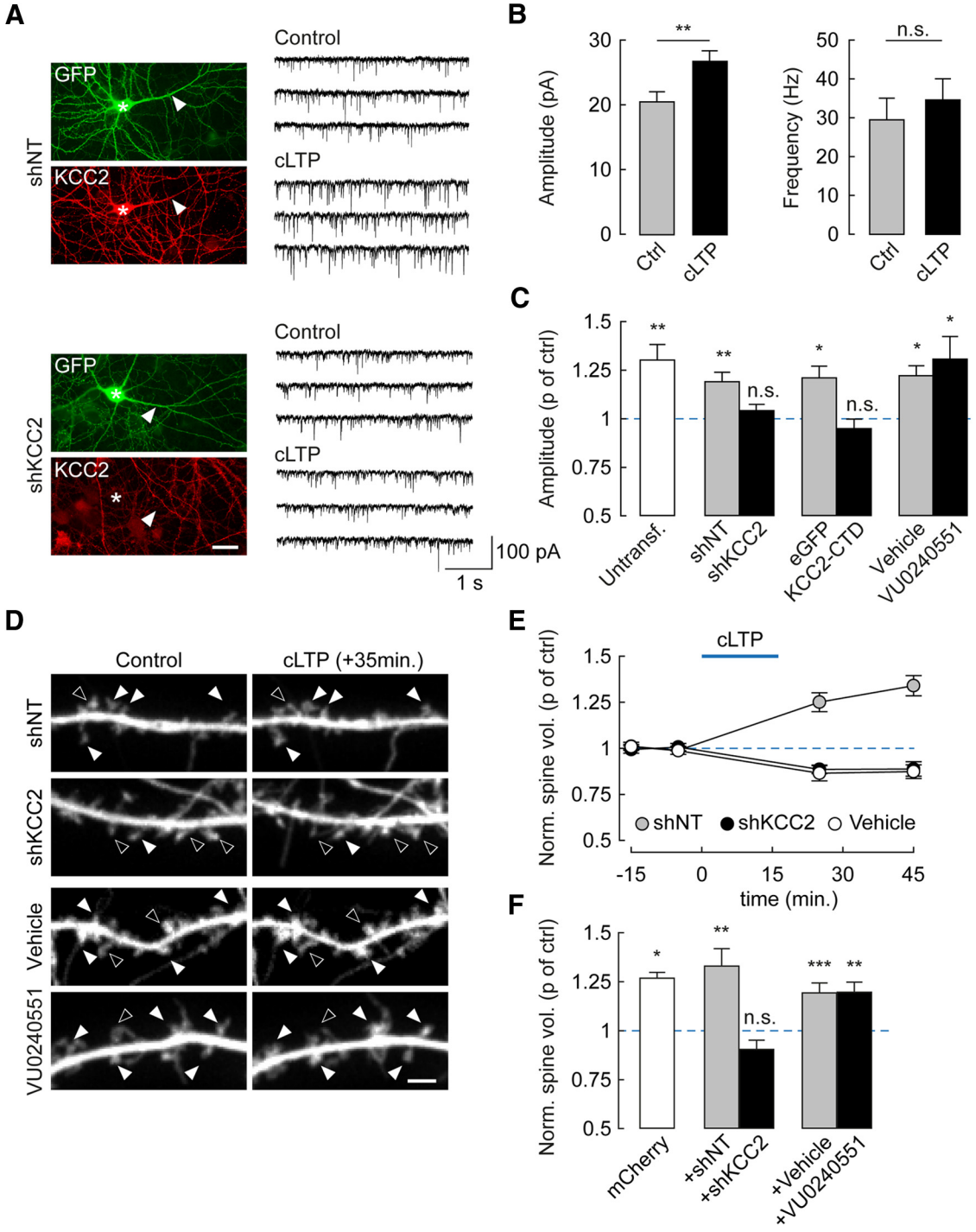

Figure 2. KCC2 suppression precludes cLTP expression through an ion transport-independent mechanism. ***A***, Left, Wide-field fluorescence micrographs showing GFP fluorescence and KCC2 immunolabeling in hippocampal neurons transfected with nontarget (shNT, top) or KCC2-specific (shKCC2, bottom) shRNA. Stars and arrows represent the soma and primary dendrite of transfected cells, respectively. Scale bar, 20 μm. Right, 12 s recordings of mEPSCs from neurons either after cLTP protocol (see Materials and Methods, cLTP) or vehicle application only (DMSO 0.6 μl/ml, Control). ***B***, Summary data from 16 (Ctrl) and 19 (cLTP) untransfected neurons showing that cLTP specifically increases mEPSC amplitude ($p < 0.01$) but not frequency ($p = 0.5$). ***C***, Summary data showing change in mEPSC amplitude (proportion of control) upon cLTP in untransfected neurons ($p < 0.01$), or neurons expressing either nontarget ($p < 0.01$) or KCC2-specific shRNA ($p = 0.2$), eGFP alone ($p < 0.05$), or eGFP with KCC2 carboxy-terminal domain (KCC2-CTD, $p = 0.4$), and neurons exposed to the KCC2 antagonist VU0240551 (6 μM, $p < 0.05$) or vehicle only (DMSO, $p < 0.05$). $n = 11$–18 in each condition. ***D***, Spinning disc confocal fluorescence micrographs of dendritic sections of neurons expressing mCherry and either shNT or shKCC2, or exposed for 72 h to VU0240551 or vehicle only. Images represent maximal projections of confocal stacks acquired 15 min before and 35 min after cLTP induction. Filled arrowheads indicate spines that increased in volume during cLTP. Open arrowheads indicate spines that decreased in volume or remained unchanged. Scale bar, 2 μm. ***E***, Time course of changes in spine volume upon cLTP in neurons expressing shNT ($n = 11$), shKCC2 ($n = 9$), and neurons expressing mCherry only and exposed for 16 min to vehicle only (vehicle, $n = 6$). ***F***, Summary graph of average spine volume (normalized to control before cLTP induction) measured 30 min after cLTP induction in neurons expressing mCherry alone ($n = 7$), or together with shNT ($n = 11$), shKCC2 ($n = 9$), or after 72 h exposure to VU0240551 ($n = 14$) or vehicle only ($n = 20$). *$p < 0.05$. **$p < 0.01$. ***$p < 0.005$. n.s., Nonsignificant difference.

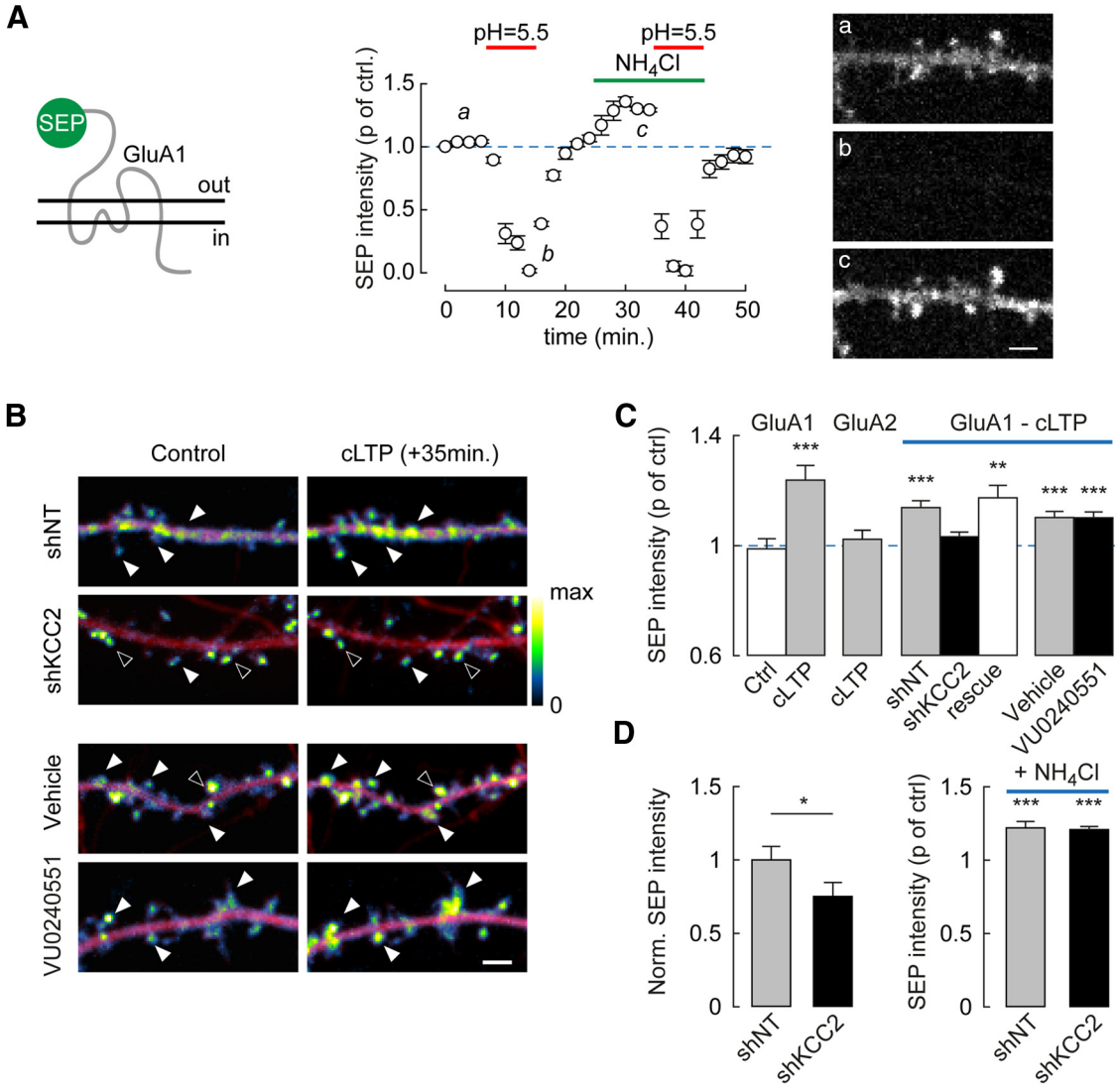

Figure 3. Suppression of activity-driven, membrane insertion of AMPARs in neurons lacking KCC2. ***A***, Neurons were transfected with GluA1-SEP. Left, Summary graph of mean SEP fluorescence (normalized to control) at pH 5.5 ($n = 11$) and upon NH_4Cl application ($n = 26$ cells). ***$p < 0.005$. SEP fluorescence was detected in neurons imaged at pH 7.4 (***Aa***) but was near-completely quenched at pH 5.5 (***Ab***). Upon collapse of pH gradients using 50 mM NH_4Cl at pH 7.4 (***Ac***), additional fluorescence was detected reflecting an intracellular pool of SEP-GluA1. Right, Spinning disc confocal fluorescence micrographs of SEP-GluA1-expressing hippocampal neurons at time points *a–c*. Scale bar, 2 μm. ***B***, Overlay of mCherry (red) and SEP (pseudocolors) fluorescence micrographs of dendritic sections of neurons before (Control) and 35 min after cLTP induction. Filled arrowheads indicate cLTP-induced SEP fluorescence spots. Open arrowheads indicate spines with unchanged SEP fluorescence. KCC2 suppression by RNA interference, but not blockade by the antagonist VU0240551 (6 μM), abolished cLTP-induced increase in SEP fluorescence. Scale bar, 2 μm. ***C***, SEP fluorescence 35 min after cLTP induction normalized to control in neurons expressing SEP-GluA1 or SEP-GluA2 and either nontarget (shNT) or KCC2-directed (shKCC2) shRNA, KCC2 shRNA together with shRNA-proof recombinant KCC2 (rescue) or neurons exposed to KCC2 antagonist VU0240551 (6 μM) or vehicle only. **$p < 0.01$. ***$p < 0.005$. $n = 18–29$ neurons in each condition. ***D***, Left, SEP fluorescence before cLTP induction in neurons expressing SEP-GluA1 and either nontarget ($n = 47$) or KCC2-directed ($n = 56$) shRNA, normalized to the mean SEP fluorescence in shNT-expressing neurons. *$p < 0.05$. Right, Change in SEP fluorescence (p of control) upon 5 min perfusion of NH_4Cl solution, pH 7.4, to reveal intracellular SEP-GluA1 pool (shNT, $n = 23$; shKCC2, $n = 28$). ***$p < 0.005$.

exposed to doxycycline, as shown by the lack of mCherry expression in neurons transfected with this construct for 8–10 d (Fig. 4*B*).

Doxycycline-induced overexpression of $CaMKII_{1–290}$ for 24 h led to a significant increase in SEP-GluA1 fluorescence in neurons expressing nontarget shRNA (28.3 ± 8.8% of control, $n = 105$ and $n = 121$ cells, respectively, $p = 0.006$; Fig. 4*C*,*D*). However, this effect was abolished in neurons in which KCC2 expression was suppressed (9.3 ± 12.1% of control, $n = 84$ and $n = 90$ cells, respectively, $p = 0.8$; Fig. 4*C*,*D*). In contrast, in hippocampal neurons transduced with shRNA-expressing lentiviruses, we observed no difference in GluA1 Ser845 phosphorylation in neurons expressing KCC2-specific compared with nontarget shRNA, either at rest (1.7 ± 4.5%, $n = 3$ experiments, $p = 0.9$) or upon cLTP (758 ± 131% vs 687 ± 246% of control, respectively, $p = 1.0$; Fig. 4*E*,*F*). These results demonstrate that KCC2 is required for activity-dependent GluA1 membrane delivery in hippocampal neurons and acts via mechanisms downstream of αCaMKII activation and pKA-dependent GluA1 phosphorylation on Ser845.

Altered spine actin polymerization upon KCC2 suppression

How may KCC2 gate activity-driven AMPAR membrane insertion? KCC2 has been shown to interact with spine cytoskeleton through the FERM-domain protein 4.1N (Li et al., 2007) and GluA1 binding to 4.1N is required for its activity-dependent membrane insertion (Lin et al., 2009). We therefore tested

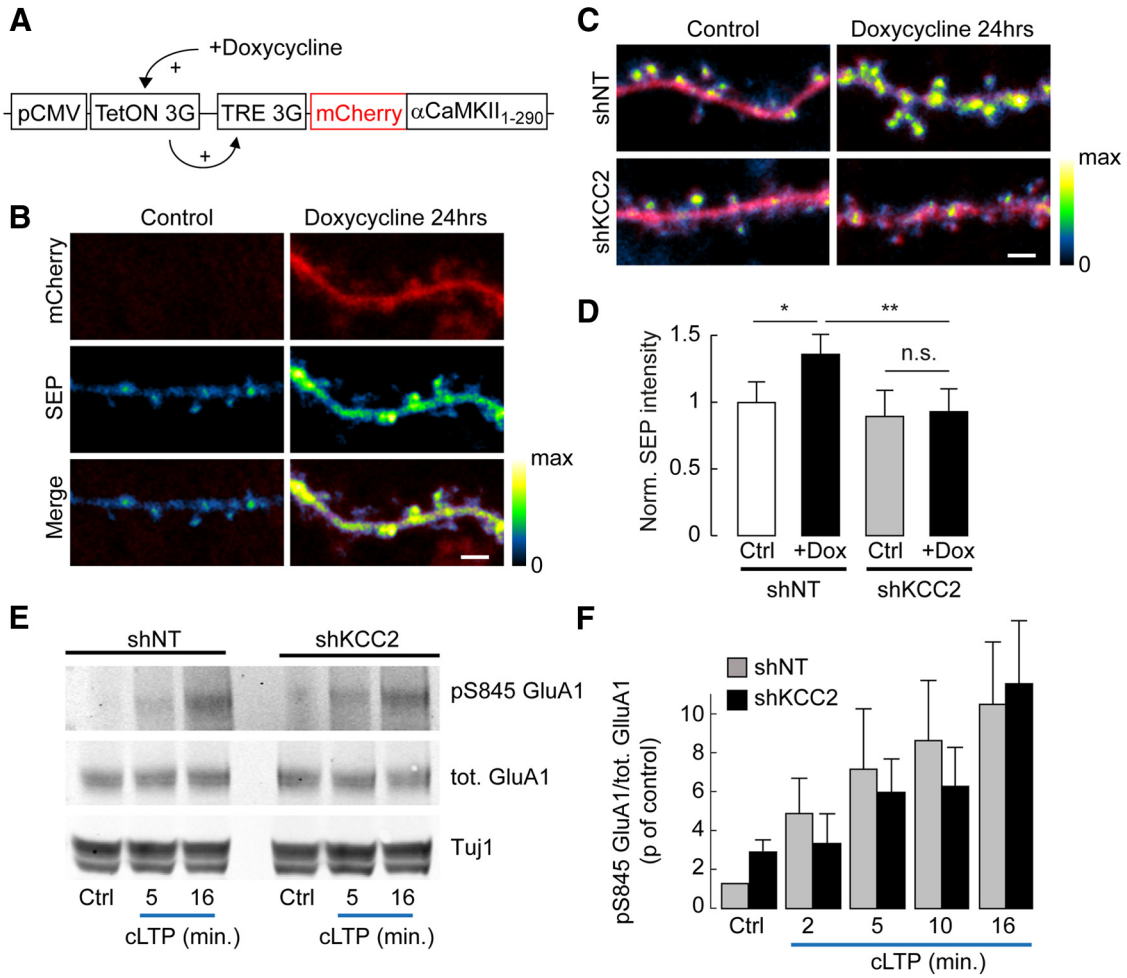

Figure 4. Defect in activity-dependent GluA1 membrane delivery downstream αCaMKII activation and GluA1 S845 phosphorylation. ***A***, Schematic representation of construct used for doxycycline-inducible, truncated (constitutively active) αCaMKII expression in hippocampal neurons. ***B***, Confocal fluorescence micrographs of mCherry (red) and SEP-GluA1 (pseudocolors) in dendritic sections of neurons expressing mCherry, SEP-GluA1, and inducible truncated αCaMKII, in the absence (Control) or after 24 h exposure to 2 μg/ml doxycycline. No mCherry expression was detected in the absence of doxycycline. Scale bar, 2 μm. ***C***, Overlay of confocal fluorescence micrographs of mCherry and SEP-GluA1 in neurons expressing mCherry, SEP-GluA1, and inducible truncated αCaMKII and either nontarget (shNT) or KCC2-directed (shKCC2) shRNA, in the absence or 24 h presence of doxycycline. Scale bar, 2 μm. ***D***, Quantification of SEP fluorescence in neurons not exposed to doxycycline (Ctrl) or exposed to doxycycline for 24 h (+Dox), normalized to the mean SEP fluorescence in the absence of doxycycline (shNT: Ctrl, $n = 105$; +Dox, $n = 121$ shKCC2: Ctrl, $n = 84$; +Dox, $n = 90$). $^*p < 0.05$. $^{**}p < 0.01$. n.s., Nonsignificant. ***E***, Representative immunoblots of total or Ser845-phosphorylated GluA1 and Tuj1 from hippocampal cultures infected with lentiviruses expressing either nontarget (shNT) or KCC2-directed (shKCC2) shRNA, before (Ctrl) or at different times of cLTP induction. ***F***, Quantification from 3 or 4 independent experiments of pS845/total GluA1 ratios from immunoblots as in ***D***, normalized to that in shNT-expressing neurons before cLTP induction. No significant difference in GluA1 S845 phosphorylation was observed between shNT- and shKCC2-expressing neurons, either in control or upon cLTP induction.

whether the loss of KCC2 may affect 4.1N expression in hippocampal neurons. However, suppressing KCC2 or overexpressing KCC2-CTD had no apparent effect on 4.1N expression as detected by immunofluorescence, as measured either in the dendritic spines and shafts together (97.2 ± 3.4% and 104.3 ± 5.3% of control intensity, $p = 0.7$ and $p = 0.6$, respectively) or specifically in dendritic spines (97.7 ± 4.0% and 110.7 ± 5.2% of control, $n = 37$ (41 control) and $n = 43$ (54 control) cells, $p = 0.6$ and $p = 0.1$, respectively; Figure 5*A*,*B*). Therefore, altered 4.1N expression and/or clustering seem unlikely to be responsible for the defect in GluA1 membrane traffic upon KCC2 suppression.

Both activity-driven AMPAR trafficking and spine enlargement rely on remodeling of actin cytoskeleton. Whereas transient actin depolymerization by cofilin may be permissive for AMPAR membrane insertion (Gu et al., 2010), delayed increase in F-actin spine content may be required for spine enlargement (Okamoto et al., 2004). We previously reported increased lateral diffusion of several transmembrane actin-binding proteins in dendritic spines upon KCC2 suppression (Gauvain et al., 2011), suggestive of submembrane cytoskeleton alterations. This hypothesis was tested by using phalloidin staining of F-actin in dendritic spines, revealing a 40% increase of fluorescence in neurons with suppressed KCC2 expression (1.42 ± 0.12 of control, $n = 29$ and $n = 36$ cells, respectively, $p < 0.005$; Fig. 5*C*,*D*). This effect was even more pronounced in neurons expressing KCC2-CTD (1.84 ± 0.22 of control, $n = 18$ and $n = 15$ cells, respectively, $p < 0.001$) and was likely independent of changes in spine volume because no significant correlation was detected between phalloidin staining and spine size (Fig. 5*E*). To examine the subspine spatial distribution of actin, we next used STED microscopy of the synthetic, actin-binding peptide LifeAct-Venus (Riedl et al., 2008; Urban et al., 2011). Using this approach, we could resolve individual actin bundles within spine necks and heads (Fig. 6*A*). The FWHM of LifeAct-labeled spine necks in neurons transfected with nontarget shRNA was 93.7 ± 1.9 nm, ($n = 128$ spines from 19 neurons, Fig. 6*B*), consistent with previous data in hippocam-

pal pyramidal neurons (Urban et al., 2011). In neurons with suppressed KCC2 expression, however, the FWHM of LifeAct-labeled spine necks was significantly increased by 20.3% (112.8 ± 5.6 nm, $n = 60$ spines from 18 neurons, $p = 0.001$; Fig. 6C), suggestive of an increased recruitment of actin bundles in spine necks. We next asked whether suppression of KCC2 might lead to a redistribution of F-actin within spines or a global increase in F-actin content. LifeAct-Venus fluorescence was heterogeneously distributed within individual spines with some spines showing intense, calyx-shaped bundles and others more widely distributed signal (Fig. 6D,E). Overall, however, we could not detect a significant difference in the coefficient of variation of LifeAct-Venus fluorescence between neurons expressing nontarget or KCC2-directed shRNA (0.57 ± 0.02 vs 0.60 ± 0.02, $n = 149$ and 85 spines, from 19 and 20 neurons, respectively, $p = 0.13$; Fig. 6E–G). To compare the spatial distribution of F-actin within spines, we performed spatial autocorrelation analysis of LifeAct-Venus signal using Moran's index (Moran, 1948) (see Materials and Methods; Fig. 6F). Again, we found no significant difference in the proportion of high-intensity clustered pixels (Moran's index p value <0.05) between neurons expressing nontarget or KCC2-directed shRNA (23.0 ± 0.3% vs 23.1 ± 0.4%, same dataset as above, $p = 1.0$; Fig. 6F–H). Together, our results show that suppression of KCC2 results in a net increase in F-actin accumulation within dendritic spines with no substantial subspine redistribution.

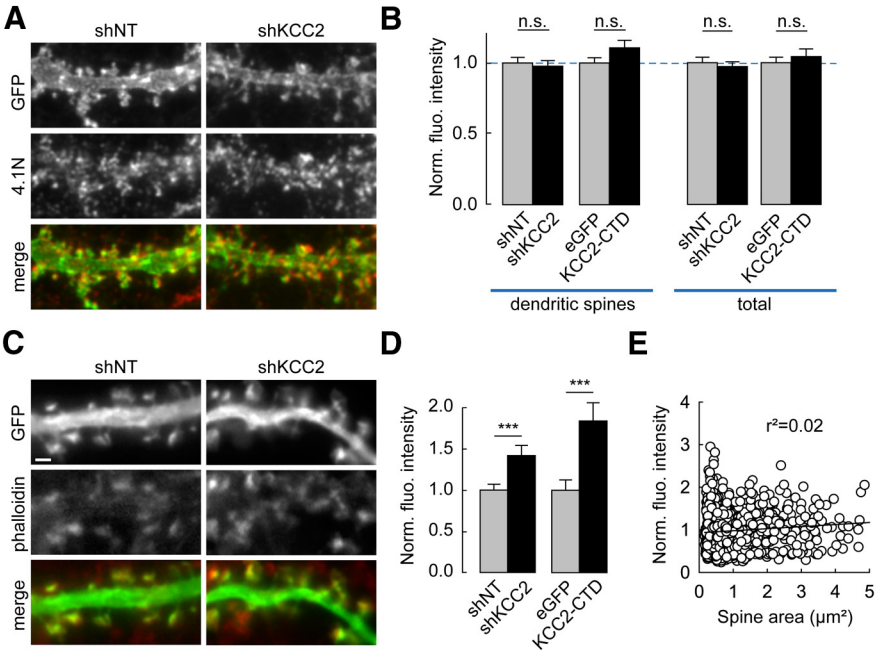

Figure 5. Enhanced F-actin content in dendritic spines upon KCC2 suppression. ***A***, ***C***, Wide-field fluorescent micrographs of representative dendritic sections of neurons expressing plasma-membrane (***A***) or cytosolic (***C***) EGFP and either nontarget (shNT) or KCC2-directed shRNA (shKCC2). Neurons were immunostained for GFP (green) and 4.1N (red, in ***A***) or stained with Alexa-546-phalloidin (red, in ***C***). Scale bar, 1 μm. ***B***, Quantification of immunostainings as in ***A*** showing 4.1N mean immunofluorescence intensity per pixel either from dendritic spines only (left) or from entire dendritic sections (right), normalized to internal controls (gray bars) for each experimental condition (black bars). $n = 41$ (shNT), $n = 37$ (shKCC2), $n = 54$ (GFP), and $n = 43$ (KCC2-CTD) cells, respectively. n.s., Nonsignificant difference. ***D***, Normalized fluorescence intensity of phalloidin staining in dendritic spines from neurons expressing shNT (1022 spines from 36 cells), shKCC2 (861 spines, from 29 cells), EGFP (538 spines from 15 cells), or KCC2-CTD (591 spines from 18 cells) from two independent experiments. ***$p < 0.005$. ***E***, Normalized fluorescence intensity of phalloidin staining in dendritic spines from shNT-expressing neurons plotted against spine area. No significant correlation was observed between these variables (linear regression $r^2 = 0.02$; $p > 0.05$, Spearman rank order correlation test).

Rac1- and LIMK-mediated reduction of cofilin activity accounts for the lack of activity-driven GluA1 traffic and LTP upon KCC2 suppression

We asked whether increased actin polymerization upon KCC2 suppression might be responsible for the defect in LTP expression in hippocampal neurons. Transient actin depolymerization has been shown to be required for activity-driven AMPAR membrane traffic and spine enlargement (Ouyang et al., 2005; Gu et al., 2010). This reflects a transient activation (i.e., dephosphorylation) of the actin-severing enzyme cofilin upon LTP induction. We therefore compared cofilin phosphorylation in hippocampal neurons transduced with lentiviruses expressing nontarget or KCC2-specific shRNA and observed a nearly twofold increase in phospho-cofilin/total cofilin ratio upon KCC2 suppression under basal conditions (85.8 ± 14.3%, $n = 3$ independent experiments, $p < 0.02$; Fig. 7A,B). However, the lack of KCC2 did not prevent cLTP-induced decrease in cofilin phosphorylation (−79.7 ± 9.4% of control after 16 min of cLTP induction, $p < 0.001$), to a similar extent as in neurons expressing nontarget shRNA ($p = 0.4$).

Two major signaling pathways involving the Rho GTPases RhoA and Rac1 converge on LIM kinase to control cofilin phosphorylation and actin dynamics (Cingolani and Goda, 2008) (Fig. 8D). We tested whether enhanced cofilin phosphorylation may result from activation of either GTPase. Pulldown experiments revealed a specific increase in active (GTP-bound) Rac1 in neurons with suppressed KCC2 expression. Thus, we observed a near fivefold increase in activated/total Rac1 ratio in neurons transduced with KCC2-directed compared with with nontarget shRNA (471 ± 131% of shNT ratio, $n = 4$ independent experiments, $p < 0.01$; Figure 7C,D) with no significant change in RhoA activity (92 ± 19% of shNT ratio, $n = 3$ independent experiments, $p = 0.5$).

KCC2 was recently reported to interact with the Rac1-specific guanine nucleotide exchange factor βPIX, both in adult mouse brain extracts and in heterologous cells, and to inhibit βPIX-induced Rac1 activation (Llano et al., 2015). βPIX is also known to interact with GIT1, and their recruitment to specific subcellular compartments together with downstream effectors may serve to locally regulate actin dynamics (Zhang et al., 2003). We confirmed KCC2 interaction with βPIX in primary hippocampal neurons using coimmunoprecipitation assays using antibodies against either protein (Fig. 7E). Suppressing KCC2 expression resulted in changes in both βPIX and GIT1 clustering, as detected in immunostaining experiments (Fig. 7F,G). Thus, the integrated intensity of βPIX and GIT1 clusters was increased by 55.0 ± 9.4% and 30.6 ± 7.2%, respectively, in the dendrites of neurons expressing KCC2-specific compared with with nontarget shRNA ($p < 0.001$ for both). Suppression of KCC2 also resulted in a 27.3 ± 5.0% increase in the density of βPIX clusters ($p < 0.001$, $n = 110$ and $n = 104$ cells, respectively). Together, our results suggest that KCC2 suppression may enhance actin polymerization through Rac1- and LIMK-

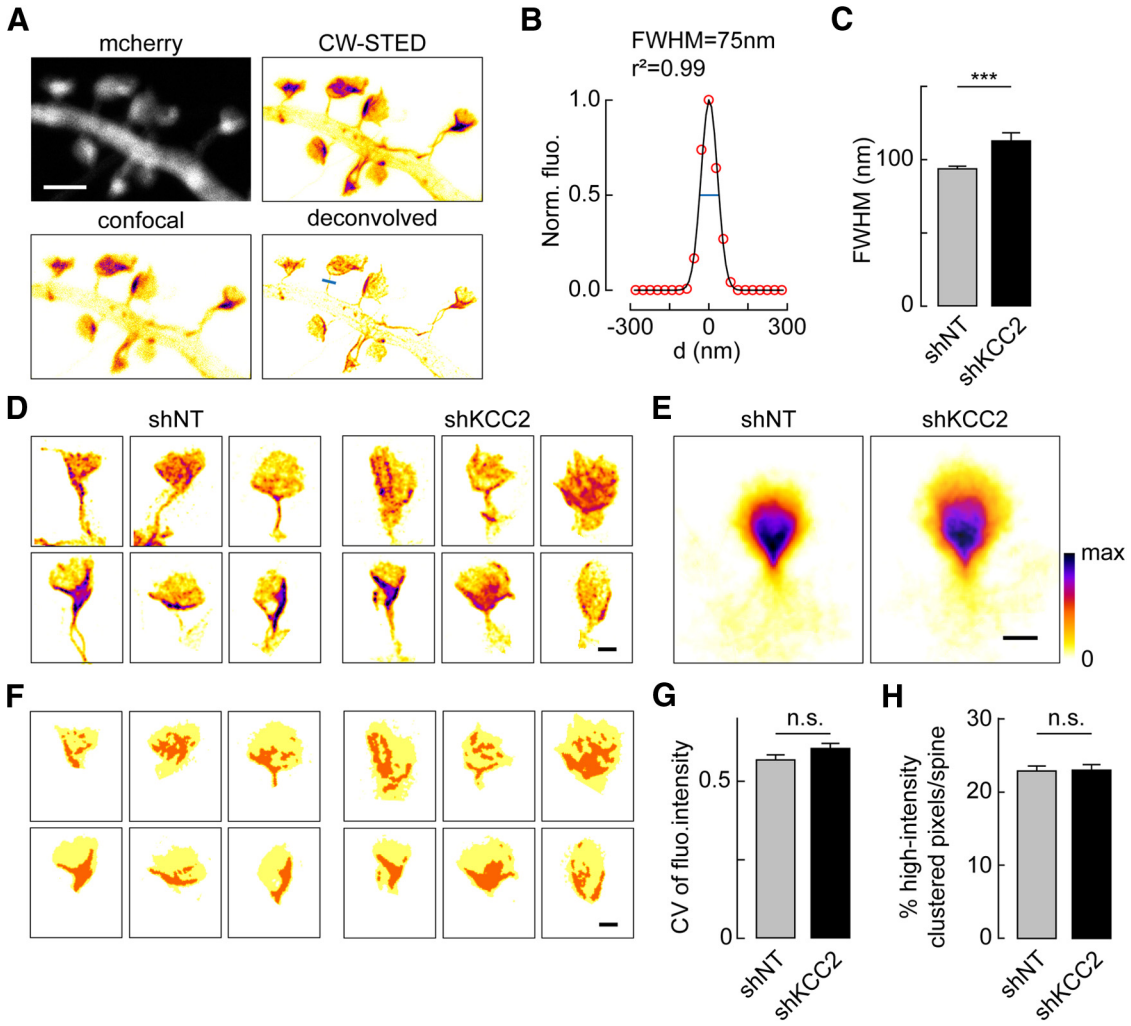

Figure 6. Subspine distribution of F-actin is unchanged upon KCC2 suppression. ***A***, Representative fluorescence micrographs of a dendritic section of a neuron expressing mCherry and LifeAct-Venus (pseudocolors), imaged in confocal (left) and CW-STED microscopy with or without deconvolution (right). ***B***, Gaussian fit of the pixel intensity profile across spine neck following the blue line shown in ***A***. ***C***, Summary graph showing FWHM of Gaussian fit of LifeAct-Venus signals across spine necks of neurons expressing nontarget or KCC2-directed shRNA ($n = 128$ and $n = 60$ spines from 19 and 18 neurons, respectively). ***$p < 0.001$. ***D***, Representative, pseudocolored fluorescence STED micrographs of 6 individual spines from 12 different neurons expressing either nontarget or KCC2-directed shRNA. Scale bar, 500 nm. ***E***, Pseudocolored averages of 149 and 85 individual spine images from 19 and 20 neurons, respectively, as in ***D***, aligned as described in Materials and Methods to show the mean distribution of LifeAct-Venus fluorescence within spine heads. Scale bar, 500 nm. ***F***, Schematic representation of spine heads (yellow) isolated from the micrographs shown in ***D*** with high-intensity clustered pixels (orange), as derived from spatial autocorrelation analysis using Moran's index (for details, see Materials and Methods). ***G***, ***H***, Summary graphs of the mean coefficient of variation (CV) of LifeAct-Venus fluorescence (***G***) and the mean percentage of high-intensity clustered pixels (***H***) in spine heads of neurons expressing nontarget or KCC2-directed shRNA (same dataset as in ***E***). n.s., Nonsignificant difference.

mediated inhibition of cofilin, likely due to subcellular recruitment of βPIX-GIT1 complexes.

Enhanced cofilin phosphorylation at the time of cLTP induction may then occlude activity-driven AMPAR membrane insertion (Gu et al., 2010). Inhibiting steady-state cofilin phosphorylation in neurons lacking KCC2 might then be sufficient to rescue LTP expression. We tested this hypothesis by monitoring cLTP-induced SEP-GluA1 exocytosis in neurons pretreated with either LIMK or Rac1-PAK inhibitors. A peptide containing the first 16-amino acid sequence of cofilin (Ser3) fused to penetratin for cell internalization was first used to inhibit endogenous LIMK activity (Gu et al., 2010). A 4 h application of Ser3 peptide had no effect on cLTP-induced SEP-GluA1 membrane insertion in neurons transfected with nontarget shRNA (11.2 ± 1.8% vs 9.6 ± 1.9% of control, $n = 13$ and $n = 17$ cells, respectively, $p = 0.6$; Fig. 8*A*,*B*) but rescued it in neurons with suppressed KCC2 expression (8.6 ± 1.4% vs −1.6 ± 2.0% of control, $n = 24$ and $n = 21$ cells, respectively, $p < 0.001$). A similar rescue was obtained in experiments using the LIMK inhibitor LIMKi (Ross-Macdonald et al., 2008) (15.7 ± 2.9% of control, $n = 20$ cells, $p < 0.001$) or the PAK inhibitor IPA-3 (13.3 ± 3.3% of control, $n = 29$ and $n = 22$ cells, respectively, $p < 0.001$). In contrast, prior incubation with the RhoA-specific inhibitor Rhosin failed to rescue cLTP-induced SEP-GluA1 membrane insertion in neurons transfected with KCC2-specific shRNA (−0.2 ± 1.5% of control, $n = 14$ and $n = 13$ cells, respectively, $p = 0.98$; Fig. 8*A*,*B*).

Finally, because activity-induced GluA1 traffic gates spine enlargement during LTP (Kopec et al., 2007), we asked whether rescuing activity-driven AMPAR insertion by inhibiting LIMK or PAK upon KCC2 suppression may be sufficient to also restore structural LTP. In neurons treated with either Ser3 peptide or LIMKi, cLTP led to a similar increase in spine volume in neurons expressing KCC2-specific (17.3 ± 5.5% of control, $n = 355$ spines from 21 cells) and nontarget shRNA (19.2 ± 4.7% of control, $n = 208$ spines from 9 cells, $p = 0.8$; Fig. 8*C*). Similar results were obtained upon pretreatment with the PAK

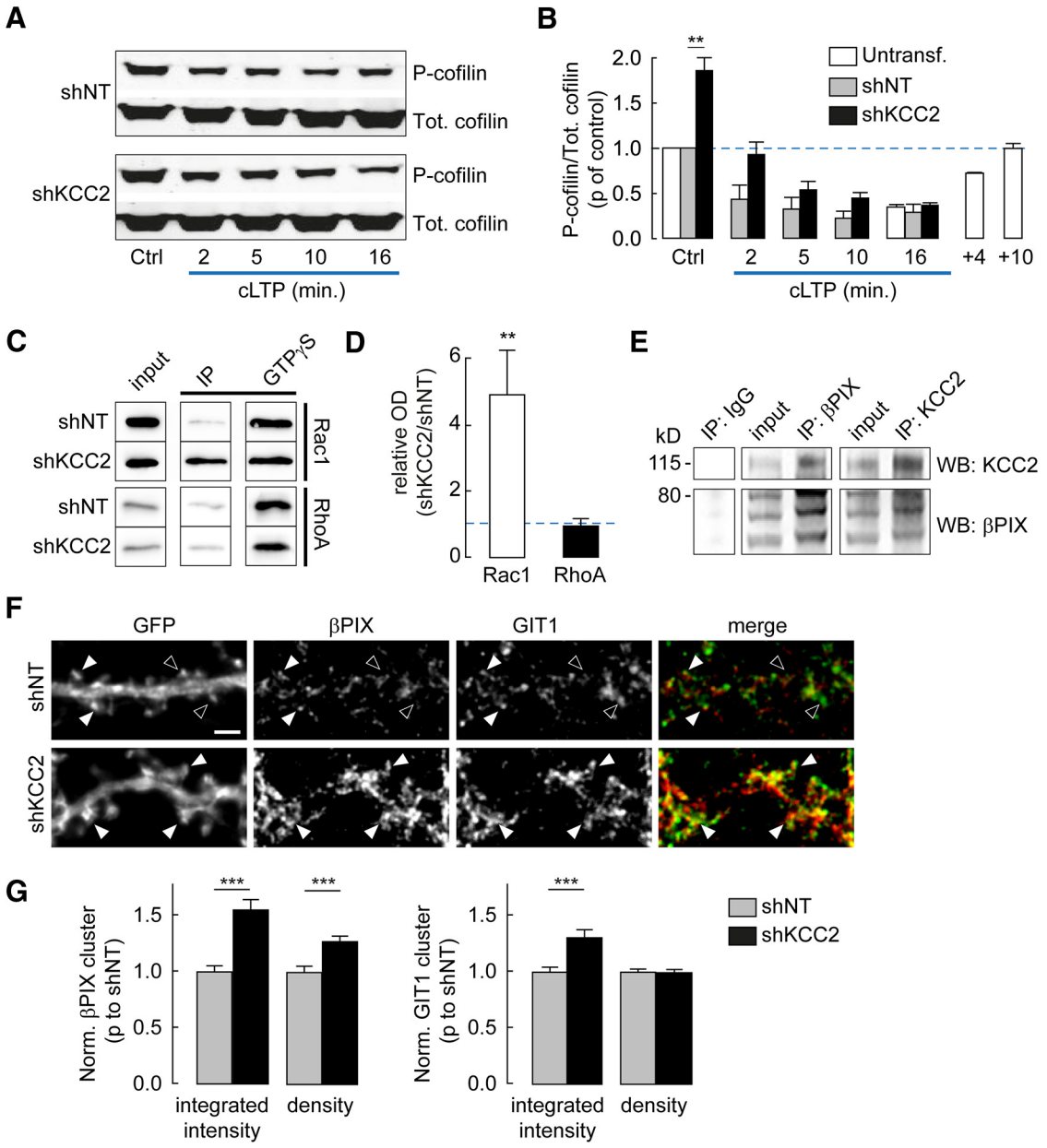

Figure 7. Phosphorylation of cofilin and recruitment of Rac1 signaling in neurons lacking KCC2. ***A***, Representative immunoblots of total (Tot.) or Ser3-phosphorylated (P-) cofilin from hippocampal cultures transduced with lentiviruses expressing either nontarget (shNT) or KCC2-directed (shKCC2) shRNA, before (Ctrl) or at different times of cLTP induction. ***B***, Quantification from three independent experiments of pSer3/total cofilin ratios from immunoblots as in ***A***, normalized to that in shNT-expressing neurons before cLTP induction. Note the twofold increase in pSer3/total cofilin ratio in shKCC2-expressing neurons before cLTP induction. $^{**}p < 0.01$. White bars represent data from uninfected neurons, showing a transient, ≈75% decrease in pSer3/total cofilin ratio during cLTP induction with complete recovery within 10 min. ***C***, Western blots from cultures transduced with lentiviruses expressing shNT or shKCC2, probed with Rac1 (left) or RhoA (right) antisera after pull-down assays using GST-PAK (Rac1) or GST-Rhotekin (RhoA) in the absence (IP) or presence (GTPγS) of 200 μM GTPγS. ***D***, Quantification from 4 (Rac1) and 3 (RhoA) experiments as in ***C***, expressed as the ratio of activated Rho GTPase signal normalized to maximal activity in GTPγS, in protein extracts from neurons expressing shKCC2 over neurons expressing shNT. $^{**}p < 0.01$. ***E***, Coimmunoprecipitation (IP) experiment from uninfected neuron cultures at 21 DIV. Western blots (WB) show enrichment and detection of βPIX after KCC2 pull-down (middle) and reciprocally (left). ***F***, Wide-field fluorescent micrographs of representative dendritic sections of neurons expressing EGFP and either nontarget (shNT) or KCC2-directed shRNA (shKCC2). Neurons were immunostained for GFP, βPIX (red), and GIT1 (green). Filled arrowheads indicate dendritic spines immunopositive for both βPIX and GIT1. Open arrowheads indicate spines with no colocalization. Scale bar, 2 μm. ***G***, Quantification of βPIX (left) and GIT1 (right) cluster integrated intensity and density, normalized to that in shNT-expressing neurons. Data are from two independent experiments as in ***F***, and 104 (shNT) and 110 (shKCC2) cells, respectively. $^{***}p < 0.001$.

inhibitor IPA-3 (13.3 ± 2.3 vs 14.7 ± 2.9% of control spine volume; $n = 29$ and $n = 23$ cells, respectively, $p = 0.9$; Fig. 8*C*). Together, these data demonstrate that the loss of KCC2 expression affects actin polymerization through enhanced cofilin phosphorylation and thereby precludes both synaptic and structural LTP expression.

Discussion

Our results reveal an unexpected role of KCC2 in the regulation of glutamatergic signaling in hippocampal neurons. We show that KCC2 membrane expression, but not function, is required for activity-driven AMPAR membrane insertion and thereby gates the expression of LTP at glutamatergic synapses. This effect

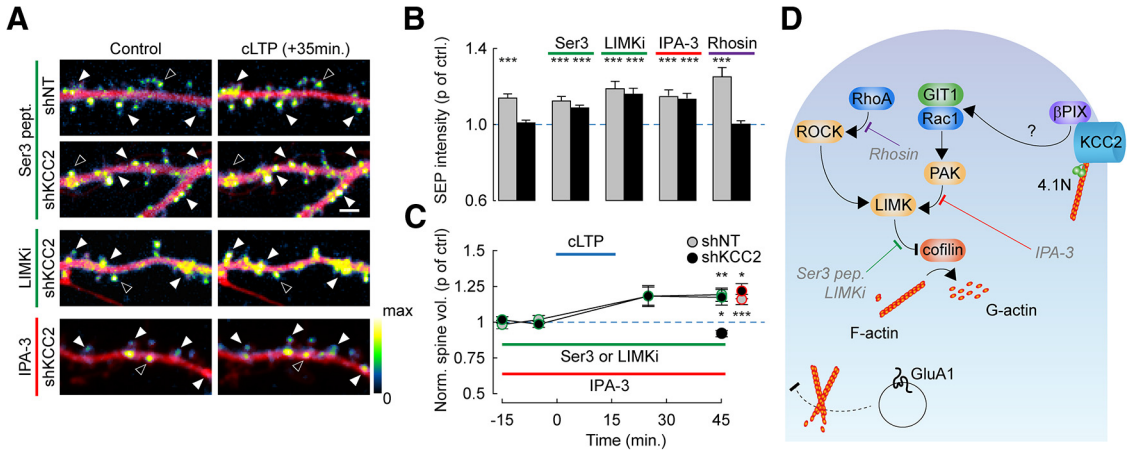

Figure 8. KCC2 controls actin depolymerization through a Rac1-PAK-LIMK pathway. ***A***, Overlay of mCherry (red) and SEP (pseudocolors) spinning-disc fluorescence micrographs of dendritic sections of shNT or shKCC2-expressing neurons before (Control) and 35 min after cLTP induction. Neuron cultures were exposed either for 4 h to cofilin N-ter hexadeca-peptide fused to penetratin (Ser3 pept., 20 μg/ml) or the LIMK inhibitor LIMKi (10 μM), or for 24 h to the PAK inhibitor IPA-3 (5 μM). Filled arrowheads indicate cLTP-induced SEP fluorescence spots. Open arrowheads indicate spines with unchanged or reduced SEP fluorescence. Scale bar, 2 μm. ***B***, Summary graph of SEP fluorescence as in ***A*** measured 35 min after cLTP induction and normalized to control, in neurons expressing SEP-GluA1 and either shNT or shKCC2 exposed to Ser3 peptide, LIMKi, IPA-3, or the RhoA inhibitor Rhosin (30 μM). $^{***}p < 0.005$. $n = 7$–29 neurons from the same cultures in each condition. ***C***, Summary graph of average spine volume (normalized to control before cLTP induction) measured 30 min after cLTP induction, from the same experiments as above, either in control neurons (shKCC2; black symbols) or after 4 h exposure to LIMK inhibitors (Ser 3 peptide or LIMKi; green symbols) or 24 h exposure to IPA-3 (red symbols). $^{*}p < 0.05$. $^{**}p < 0.01$. $^{***}p < 0.005$. ***D***, Scheme representing how cofilin plays a central role in regulating actin dynamics as it catalyzes depolymerization of F-actin into G-actin. Cofilin activity is inhibited by phosphorylation of its Ser3 residue by LIMK. Several signaling cascades converge to activate LIMK in neurons. These include the RhoA/ROCK as well as the Rac1/PAK pathways. βPIX, a guanine nucleotide exchange factor (GEF) involved in Rac1 activation, has been shown to interact with KCC2 (Fig. 7 *D*, *E*) (Llano et al., 2015). We propose that this interaction may hinder recruitment of βPIX and its scaffolding molecule GIT1 and, consequently, activation of Rac1/PAK at rest. Disrupting this interaction may then favor Rac1/PAK activation, increase LIMK activity, and thereby inactivate cofilin through Ser3 phosphorylation, resulting in enhanced actin polymerization. This in turn prevents LTP-induced membrane traffic of GluA1-containing AMPA receptors and increase in spine volume. The LIMK inhibitor LIMKi as well as the dominant-negative peptide Ser 3 pept. (gray) both favor actin depolymerization by antagonizing LIMK-mediated cofilin phosphorylation. The PAK inhibitor IPA-3 acts upstream to inhibit Rac1-mediated activation of LIMK. Rhosin specifically inhibits RhoA. In this scheme: orange represents kinases; blue represents Rho GTPases; purple represents GEF. Adapted from Cingolani and Goda (2008).

involves enhanced Rac-1- and LIMK-mediated cofilin phosphorylation resulting in increased F-actin mobilization in dendritic spines. Thus, preventing Rac1/PAK activation or cofilin phosphorylation upon KCC2 suppression rescues activity-driven AMPAR membrane insertion as well as structural LTP. KCC2-mediated control of actin polymerization may then represent a new modality of metaplasticity at hippocampal glutamatergic synapses.

LTP of excitatory synapses involves a cascade of biochemical events (Poncer, 2003), each of which could in principle be perturbed by KCC2 suppression. Our results, however, suggest that synaptic and structural LTP was primarily compromised due to altered actin dynamics. Direct activation of CaMKII failed to induce AMPAR membrane insertion, suggesting that LTP was likely not compromised due to a defect in induction mechanisms. In addition, cLTP-induced GluA1 Ser845 phosphorylation was unaffected in neurons lacking KCC2, suggesting that only the ultimate steps of activity-driven AMPAR traffic were affected. The reduced density of extrasynaptic, GluA1-containing AMPARs upon KCC2 suppression (Fig. 3*D*) may in principle contribute to hinder LTP expression by limiting their activity-dependent recruitment at synapses. However, our data are based on total GluA1-SEP fluorescence in dendritic sections and therefore suggest instead a defect in activity-dependent membrane insertion in neurons lacking KCC2. Phalloidin staining showed that suppressing KCC2 expression or overexpressing its C-terminal domain increases F-actin content in spines (Fig. 5). This may reflect increased aggregation of F-actin bundles within spines or increased actin polymerization. KCC2 interaction with the spectrin/actin-binding protein 4.1N (Li et al., 2007) suggests that KCC2 may be part of a complex anchoring submembrane actin cytoskeleton to plasma membrane. A similar role has been ascribed to other ion-transport proteins in various cell types (Baines et al., 2014). Accordingly, we previously observed that suppressing KCC2 increased membrane diffusion of GluA1-containing AMPARs and NCAM180 (Gauvain et al., 2011), both of which interact with actin. Conversely, suppressing 4.1N expression increased membrane diffusion of KCC2 (Chamma et al., 2013). However, we could not detect changes in 4.1N expression in spines upon KCC2 suppression, suggesting that KCC2 is not strictly required for 4.1N aggregation in spines. In addition, phalloidin staining of endogenous F-actin and STED imaging of Life-Act, respectively, reveal an increased F-actin content in dendritic spines with no significant difference in its intraspine distribution (Fig. 6). Although more subtle changes in F-actin interactions with plasma membrane may occur upon KCC2 suppression, our observations are consistent with increased actin polymerization rather than a major reorganization of actin cytoskeleton within dendritic spines.

Consistent with this conclusion, we observed a reduction in active cofilin in neurons lacking KCC2 (Fig. 7). Cofilin plays a major role in actin signaling (Cingolani and Goda, 2008; Bosch and Hayashi, 2012). Its active, dephosphorylated form promotes actin depolymerization. Our results show a near-complete recovery of AMPAR traffic and structural LTP by LIMK inhibitors. This strongly suggests that LIMK is hyperactivated in the absence of KCC2, resulting in enhanced actin polymerization. Importantly, we observed a twofold increase in cofilin phosphorylation upon suppression of KCC2 expression at rest. However, phosphorylation was still reduced during cLTP (Fig. 7*A*,*B*), suggesting that steady-state, but not activity-driven, regulation of cofilin was specifically affected by KCC2 suppression. How may KCC2 influence LIMK activity? Among the numerous molecular interactions KCC2 may be engaged in, a recent report shows that

KCC2 directly interacts with the Rac1 GEF βPIX, thereby inhibiting β-PIX-induced Rac1 activation (Llano et al., 2015). In addition, KCC2 interaction with β-PIX prevented Rac1 activation in heterologous cells. Our data support direct interaction between KCC2 and βPIX and further demonstrate (1) subcellular redistribution of both βPIX and its partner GIT1 in dendrites and (2) enhanced Rac1, but not RhoA, activity upon KCC2 suppression. Subcellular recruitment of βPIX and GIT1 with their downstream effectors mediates local Rac1 activation in neurons (Zhang et al., 2003). Because F-actin content in dendritic spines is similarly increased in neurons lacking KCC2 or overexpressing its C-terminal domain, it seems unlikely that KCC2 may solely compete with βPIX binding to other proteins. Instead, because membrane-inserted KCC2 usually surrounds but is excluded from the PSD (Gulyás et al., 2001; Chamma et al., 2013), it may act to trap βPIX at distance from PSD partners (Park et al., 2003), such as GIT1 and downstream effectors (Zhang et al., 2003), thereby spatially restricting βPIX-driven Rac1/PAK activation. Together, our results therefore strongly support that loss of KCC2 interaction with βPIX results in Rac1 activation, leading to LIMK activation and inhibition of cofilin. Finally, pharmacological blockade of the Rac1-PAK pathway, but not RhoA, fully restored activity-driven GluA1 membrane traffic and increased spine volume during cLTP. These observations demonstrate that LTP hindrance upon KCC2 suppression primarily relies on the loss of KCC2-βPIX interaction and subsequent hyperactivation of the Rac1/PAK/LIMK pathway.

How may reduced cofilin activity prevent activity-driven AMPAR exocytosis and spine enlargement? Although LTP is associated with F-actin accumulation in dendritic spines (Bosch and Hayashi, 2012), a transient increase in both cofilin activity and density of actin barbed ends has been reported during cLTP induction (Gu et al., 2010). Preventing cofilin activation by dephosphorylation or stabilizing F-actin pharmacologically compromised AMPAR membrane insertion during cLTP. Therefore, transient, cofilin-mediated, actin depolymerization represents a permissive step for activity-driven AMPAR membrane insertion. The underlying mechanisms remain unclear but may involve hindering of vesicle fusion to plasma membrane by cortical actin, as described in non-neuronal cells (Gasman et al., 1999), or cytoskeleton entrapping of secretory vesicles preventing their traffic toward the membrane. Suppressing KCC2 expression also abolished cLTP-induced spine enlargement. This effect is unlikely to be due to the increase in spine volume induced by the loss of KCC2 function (Gauvain et al., 2011) because the KCC2 antagonist VU0241550 produced the same increase in volume as KCC2 suppression but did not prevent cLTP-induced spine enlargement (Fig. 2*F*). In neurons lacking KCC2, inhibiting PAK or LIMK rescued both activity-driven AMPAR insertion and spine enlargement (Fig. 8). This suggests the two processes may either be linked together or both independently linked to actin dynamics. Although not sufficient on its own, synaptic translocation of GluA1-containing AMPARs is permissive to cLTP-induced spine enlargement (Kopec et al., 2007). However, GluA1 synaptic translocation in the absence of actin polymerization fails to induce spine enlargement. These observations suggest spine enlargement during LTP requires both activity-driven GluA1 translocation and actin polymerization. Therefore, Rac1/PAK- and LIMK-mediated cofilin inactivation in neurons lacking KCC2 is likely to prevent spine enlargement during cLTP primarily by hindering GluA1 traffic.

KCC2 membrane expression and stability are tightly regulated by neuronal activity (Chamma et al., 2012; Kahle et al., 2013). In particular, Ca^{2+} influx through postsynaptic NMDARs rapidly reduces KCC2 function at least in part through calcium-dependent Ser940 dephosphorylation (Lee et al., 2011; Chamma et al., 2013) and calpain-mediated cleavage (Puskarjov et al., 2012; Chamma et al., 2013), leading to reduced membrane stability of the transporter. Phosphorylation of Tyr903 and Tyr1087 by Src-family tyrosine kinases on the other hand was suggested to enhance (Wake et al., 2007; Watanabe et al., 2009) or reduce (Lee et al., 2010) KCC2 membrane stability. Activation of muscarinic acetylcholine receptors enhances KCC2 tyrosine phosphorylation while promoting its endocytosis and degradation (Lee et al., 2010). Thus, both Ca^{2+} influx and tyrosine kinase activation may rapidly affect the membrane pool of KCC2. Our results predict that this may in turn influence the ability of excitatory synapses to undergo LTP. This raises the possibility that activity-dependent regulation of KCC2 membrane stability may not only tune GABA signaling to ongoing neuronal activity (Woodin et al., 2003; Fiumelli et al., 2005) but also act as a metaplastic switch at glutamatergic synapses. In this context, it is interesting to note that NMDA receptor activation before induction was shown to suppress LTP at hippocampal synapses (Huang et al., 1992). Although the underlying mechanisms were not fully identified, they may involve recruitment of protein phosphatase 1 (Kato et al., 1999), which mediates KCC2 membrane destabilization (Lee et al., 2011), consistent with a contribution of activity-dependent KCC2 internalization in gating LTP expression at excitatory synapses. More experiments are clearly needed to fully explore how activity-driven downregulation of KCC2 membrane stability may affect plasticity rules at glutamatergic synapses.

In addition to activity-induced changes at the post-translational level, KCC2 expression is also down-regulated in a variety of pathological conditions ranging from epilepsy (Rivera et al., 2004; Jin et al., 2005; Miles et al., 2012; Pallud et al., 2014), stroke (Jaenisch et al., 2010), to schizophrenia (Hyde et al., 2011) and autism (Tyzio et al., 2014). These conditions are associated with increased neuronal activity, which is often assumed to reflect reduced GABAergic signaling due to altered chloride extrusion. Therefore, agents acting to compensate for the loss of KCC2 function represent promising therapeutic options. For instance, antagonists of the NKCC1 chloride importer, such as bumetanide, effectively suppress interictal discharges in human epileptic cortex *in vitro* (Pallud et al., 2014). These strategies, however, are predicted not to compensate altered glutamatergic signaling induced by KCC2 suppression. Although the net impact of a reduced excitatory synaptic function (Gauvain et al., 2011) and long-term plasticity (this study) on network activity is somewhat difficult to predict, rhythmogenesis and mnesic performances are likely to be affected. In this respect, therapeutic strategies acting to restore KCC2 expression or membrane stability (Bos et al., 2013; Gagnon et al., 2013) rather than just chloride homeostasis may be more effective in fully compensating the effects of its suppression in neurological and psychiatric disorders.

References

Ashby MC, Maier SR, Nishimune A, Henley JM (2006) Lateral diffusion drives constitutive exchange of AMPA receptors at dendritic spines and is regulated by spine morphology. J Neurosci 26:7046–7055. CrossRef Medline

Backer S, Hidalgo-Sánchez M, Offner N, Portales-Casamar E, Debant A, Fort P, Gauthier-Rouvière C, Bloch-Gallego E (2007) Trio controls the mature organization of neuronal clusters in the hindbrain. J Neurosci 27:10323–10332. CrossRef Medline

Baines AJ, Lu HC, Bennett PM (2014) The Protein 4.1 family: hub proteins

in animals for organizing membrane proteins. Biochim Biophys Acta 1838:605–619. CrossRef Medline

Blaesse P, Airaksinen MS, Rivera C, Kaila K (2009) Cation-chloride cotransporters and neuronal function. Neuron 61:820–838. CrossRef Medline

Bos R, Sadlaoud K, Boulenguez P, Buttigieg D, Liabeuf S, Brocard C, Haase G, Bras H, Vinay L (2013) Activation of 5-HT2A receptors upregulates the function of the neuronal K-Cl cotransporter KCC2. Proc Natl Acad Sci U S A 110:348–353. CrossRef Medline

Bosch M, Hayashi Y (2012) Structural plasticity of dendritic spines. Curr Opin Neurobiol 22:383–388. CrossRef Medline

Boulenguez P, Liabeuf S, Bos R, Bras H, Jean-Xavier C, Brocard C, Stil A, Darbon P, Cattaert D, Delpire E, Marsala M, Vinay L (2010) Down-regulation of the potassium-chloride cotransporter KCC2 contributes to spasticity after spinal cord injury. Nat Med 16:302–307. CrossRef Medline

Causeret F, Hidalgo-Sanchez M, Fort P, Backer S, Popoff MR, Gauthier-Rouvière C, Bloch-Gallego E (2004) Distinct roles of Rac1/Cdc42 and Rho/Rock for axon outgrowth and nucleokinesis of precerebellar neurons toward netrin 1. Development 131:2841–2852. CrossRef Medline

Chamma I, Chevy Q, Poncer JC, Lévi S (2012) Role of the neuronal K-Cl co-transporter KCC2 in inhibitory and excitatory neurotransmission. Front Cell Neurosci 6:5. CrossRef Medline

Chamma I, Heubl M, Chevy Q, Renner M, Moutkine I, Eugène E, Poncer JC, Lévi S (2013) Activity-dependent regulation of the K/Cl transporter KCC2 membrane diffusion, clustering, and function in hippocampal neurons. J Neurosci 33:15488–15503. CrossRef Medline

Cingolani LA, Goda Y (2008) Actin in action: the interplay between the actin cytoskeleton and synaptic efficacy. Nat Rev Neurosci 9:344–356. CrossRef Medline

Cohen I, Navarro V, Clemenceau S, Baulac M, Miles R (2002) On the origin of interictal activity in human temporal lobe epilepsy in vitro. Science 298:1418–1421. CrossRef Medline

Coull JA, Boudreau D, Bachand K, Prescott SA, Nault F, Sík A, De Koninck P, De Koninck Y (2003) Trans-synaptic shift in anion gradient in spinal lamina I neurons as a mechanism of neuropathic pain. Nature 424:938–942. CrossRef Medline

Delpire E, Days E, Lewis LM, Mi D, Kim K, Lindsley CW, Weaver CD (2009) Small-molecule screen identifies inhibitors of the neuronal K-Cl cotransporter KCC2. Proc Natl Acad Sci U S A 106:5383–5388. CrossRef Medline

Dumitriu D, Rodriguez A, Morrison JH (2011) High-throughput, detailed, cell-specific neuroanatomy of dendritic spines using microinjection and confocal microscopy. Nat Protoc 6:1391–1411. CrossRef Medline

Esteban JA, Shi SH, Wilson C, Nuriya M, Huganir RL, Malinow R (2003) PKA phosphorylation of AMPA receptor subunits controls synaptic trafficking underlying plasticity. Nat Neurosci 6:136–143. CrossRef Medline

Fiumelli H, Cancedda L, Poo MM (2005) Modulation of GABAergic transmission by activity via postsynaptic Ca^{2+}-dependent regulation of KCC2 function. Neuron 48:773–786. CrossRef Medline

Fiumelli H, Briner A, Puskarjov M, Blaesse P, Belem BJ, Dayer AG, Kaila K, Martin JL, Vutskits L (2013) An ion transport-independent role for the cation-chloride cotransporter KCC2 in dendritic spinogenesis in vivo. Cereb Cortex 23:378–388. CrossRef Medline

Gagnon M, Bergeron MJ, Lavertu G, Castonguay A, Tripathy S, Bonin RP, Perez-Sanchez J, Boudreau D, Wang B, Dumas L, Valade I, Bachand K, Jacob-Wagner M, Tardif C, Kianicka I, Isenring P, Attardo G, Coull JA, De Koninck Y (2013) Chloride extrusion enhancers as novel therapeutics for neurological diseases. Nat Med 19:1524–1528. CrossRef Medline

Gasman S, Chasserot-Golaz S, Popoff MR, Aunis D, Bader MF (1999) Involvement of Rho GTPases in calcium-regulated exocytosis from adrenal chromaffin cells. J Cell Sci 112:4763–4771. Medline

Gauvain G, Chamma I, Chevy Q, Cabezas C, Irinopoulou T, Bodrug N, Carnaud M, Lévi S, Poncer JC (2011) The neuronal K-Cl cotransporter KCC2 influences postsynaptic AMPA receptor content and lateral diffusion in dendritic spines. Proc Natl Acad Sci U S A 108:15474–15479. CrossRef Medline

Gu J, Lee CW, Fan Y, Komlos D, Tang X, Sun C, Yu K, Hartzell HC, Chen G, Bamburg JR, Zheng JQ (2010) ADF/cofilin-mediated actin dynamics regulate AMPA receptor trafficking during synaptic plasticity. Nat Neurosci 13:1208–1215. CrossRef Medline

Gulyás AI, Sík A, Payne JA, Kaila K, Freund TF (2001) The KCl cotransporter, KCC2, is highly expressed in the vicinity of excitatory synapses in the rat hippocampus. Eur J Neurosci 13:2205–2217. CrossRef Medline

Harrington WW, Britt C, Wilson J, Milliken N, Binz J, Lobe D, Oliver W, Lewis M, Ignar D (2007) The effect of PPARalpha, PPARdelta, PPARgamma, and PPARpan agonists on body weight, body mass, and serum lipid profiles in diet-induced obese AKR/J Mice. PPAR Res 2007:97125. CrossRef Medline

Harvey CD, Svoboda K (2007) Locally dynamic synaptic learning rules in pyramidal neuron dendrites. Nature 450:1195–1200. CrossRef Medline

Hayashi Y, Shi SH, Esteban JA, Piccini A, Poncer JC, Malinow R (2000) Driving AMPA receptors into synapses by LTP and CaMKII: requirement for GluR1 and PDZ domain interaction. Science 287:2262–2267. CrossRef Medline

Huang YY, Colino A, Selig DK, Malenka RC (1992) The influence of prior synaptic activity on the induction of long-term potentiation. Science 255:730–733. CrossRef Medline

Huganir RL, Nicoll RA (2013) AMPARs and synaptic plasticity: the last 25 years. Neuron 80:704–717. CrossRef Medline

Hyde TM, Lipska BK, Ali T, Mathew SV, Law AJ, Metitiri OE, Straub RE, Ye T, Colantuoni C, Herman MM, Bigelow LB, Weinberger DR, Kleinman JE (2011) Expression of GABA signaling molecules KCC2, NKCC1, and GAD1 in cortical development and schizophrenia. J Neurosci 31:11088–11095. CrossRef Medline

Ivakine EA, Acton BA, Mahadevan V, Ormond J, Tang M, Pressey JC, Huang MY, Ng D, Delpire E, Salter MW, Woodin MA, McInnes RR (2013) Neto2 is a KCC2 interacting protein required for neuronal Cl- regulation in hippocampal neurons. Proc Natl Acad Sci U S A 110:3561–3566. CrossRef Medline

Jaenisch N, Witte OW, Frahm C (2010) Downregulation of potassium chloride cotransporter KCC2 after transient focal cerebral ischemia. Stroke 41:e151–e159. CrossRef Medline

Jin X, Huguenard JR, Prince DA (2005) Impaired Cl^- extrusion in layer V pyramidal neurons of chronically injured epileptogenic neocortex. J Neurophysiol 93:2117–2126. CrossRef Medline

Kahle KT, Staley KJ, Nahed BV, Gamba G, Hebert SC, Lifton RP, Mount DB (2008) Roles of the cation-chloride cotransporters in neurological disease. Nat Clin Pract Neurol 4:490–503. CrossRef Medline

Kahle KT, Deeb TZ, Puskarjov M, Silayeva L, Liang B, Kaila K, Moss SJ (2013) Modulation of neuronal activity by phosphorylation of the K-Cl cotransporter KCC2. Trends Neurosci 36:726–737. CrossRef Medline

Kato K, Li ST, Zorumski CF (1999) Modulation of long-term potentiation induction in the hippocampus by N-methyl-D-aspartate-mediated presynaptic inhibition. Neuroscience 92:1261–1272. CrossRef Medline

Kopec CD, Li B, Wei W, Boehm J, Malinow R (2006) Glutamate receptor exocytosis and spine enlargement during chemically induced long-term potentiation. J Neurosci 26:2000–2009. CrossRef Medline

Kopec CD, Real E, Kessels HW, Malinow R (2007) GluR1 links structural and functional plasticity at excitatory synapses. J Neurosci 27:13706–13718. CrossRef Medline

Lee HH, Jurd R, Moss SJ (2010) Tyrosine phosphorylation regulates the membrane trafficking of the potassium chloride co-transporter KCC2. Mol Cell Neurosci 45:173–179. CrossRef Medline

Lee HH, Deeb TZ, Walker JA, Davies PA, Moss SJ (2011) NMDA receptor activity downregulates KCC2 resulting in depolarizing GABA(A) receptor-mediated currents. Nat Neurosci 14:736–743. CrossRef Medline

Li H, Khirug S, Cai C, Ludwig A, Blaesse P, Kolikova J, Afzalov R, Coleman SK, Lauri S, Airaksinen MS, Keinänen K, Khiroug L, Saarma M, Kaila K, Rivera C (2007) KCC2 interacts with the dendritic cytoskeleton to promote spine development. Neuron 56:1019–1033. CrossRef Medline

Lin DT, Makino Y, Sharma K, Hayashi T, Neve R, Takamiya K, Huganir RL (2009) Regulation of AMPA receptor extrasynaptic insertion by 4.1N, phosphorylation and palmitoylation. Nat Neurosci 12:879–887. CrossRef Medline

Llano O, Smirnov S, Soni S, Golubtsov A, Guillemin I, Hotulainen P, Medina I, Nothwang HG, Rivera C, Ludwig A (2015) KCC2 regulates actin dynamics in dendritic spines via interaction with beta-PIX. J Cell Biol 209:671–686. CrossRef Medline

Löscher W, Puskarjov M, Kaila K (2013) Cation-chloride cotransporters NKCC1 and KCC2 as potential targets for novel antiepileptic and antiepileptogenic treatments. Neuropharmacology 69:62–74. CrossRef Medline

Mahadevan V, Pressey JC, Acton BA, Uvarov P, Huang MY, Chevrier J, Puchalski A, Li CM, Ivakine EA, Airaksinen MS, Delpire E, McInnes RR, Woodin MA (2014) Kainate receptors coexist in a functional complex with KCC2 and regulate chloride homeostasis in hippocampal neurons. Cell Rep 7:1762–1770. CrossRef Medline

Makino H, Malinow R (2011) Compartmentalized versus global synaptic plasticity on dendrites controlled by experience. Neuron 72:1001–1011. CrossRef Medline

Malinow R, Malenka RC (2002) AMPA receptor trafficking and synaptic plasticity. Annu Rev Neurosci 25:103–126. CrossRef Medline

Medina I, Friedel P, Rivera C, Kahle KT, Kourdougli N, Uvarov P, Pellegrino C (2014) Current view on the functional regulation of the neuronal K(+)-Cl(−) cotransporter KCC2. Front Cell Neurosci 8:27. CrossRef Medline

Miles R, Blaesse P, Huberfeld G, Wittner L, Kaila K (2012) Chloride homeostasis and GABA signaling in temporal lobe epilepsy. In: Jasper's basic mechanisms of the epilepsies (Noebels JL, Avoli M, Rogawski MA, Olsen RW, Delgado-Escueta AV, eds). Bethesda, MD: National Center for Biotechnology Information.

Moran PA (1948) The interpretation of statistical maps. J R Stat Soc Series B 10:243–251.

Okamoto K, Nagai T, Miyawaki A, Hayashi Y (2004) Rapid and persistent modulation of actin dynamics regulates postsynaptic reorganization underlying bidirectional plasticity. Nat Neurosci 7:1104–1112. CrossRef Medline

Otmakhov N, Tao-Cheng JH, Carpenter S, Asrican B, Dosemeci A, Reese TS, Lisman J (2004) Persistent accumulation of calcium/calmodulin-dependent protein kinase II in dendritic spines after induction of NMDA receptor-dependent chemical long-term potentiation. J Neurosci 24: 9324–9331. CrossRef Medline

Ouyang Y, Wong M, Capani F, Rensing N, Lee CS, Liu Q, Neusch C, Martone ME, Wu JY, Yamada K, Ellisman MH, Choi DW (2005) Transient decrease in F-actin may be necessary for translocation of proteins into dendritic spines. Eur J Neurosci 22:2995–3005. CrossRef Medline

Pallud J, Le Van Quyen M, Bielle F, Pellegrino C, Varlet P, Labussiere M, Cresto N, Dieme MJ, Baulac M, Duyckaerts C, Kourdougli N, Chazal G, Devaux B, Rivera C, Miles R, Capelle L, Huberfeld G (2014) Cortical GABAergic excitation contributes to epileptic activities around human glioma. Sci Transl Med 6:244ra289. CrossRef Medline

Park E, Na M, Choi J, Kim S, Lee JR, Yoon J, Park D, Sheng M, Kim E (2003) The Shank family of postsynaptic density proteins interacts with and promotes synaptic accumulation of the beta PIX guanine nucleotide exchange factor for Rac1 and Cdc42. J Biol Chem 278:19220–19229. CrossRef Medline

Poncer JC (2003) Hippocampal long term potentiation: silent synapses and beyond. J Physiol 97:415–422. CrossRef Medline

Poncer JC, Esteban JA, Malinow R (2002) Multiple mechanisms for the potentiation of AMPA receptor-mediated transmission by alpha-Ca^{2+}/calmodulin-dependent protein kinase II. J Neurosci 22:4406–4411. Medline

Puskarjov M, Ahmad F, Kaila K, Blaesse P (2012) Activity-dependent cleavage of the K-Cl cotransporter KCC2 mediated by calcium-activated protease calpain. J Neurosci 32:11356–11364. CrossRef Medline

Puskarjov M, Seja P, Heron SE, Williams TC, Ahmad F, Iona X, Oliver KL, Grinton BE, Vutskits L, Scheffer IE, Petrou S, Blaesse P, Dibbens LM, Berkovic SF, Kaila K (2014) A variant of KCC2 from patients with febrile seizures impairs neuronal Cl^- extrusion and dendritic spine formation. EMBO Rep 15:723–729. CrossRef Medline

Rho GJ, Kim DS, Son WJ, Cho SR, Kim JG, Choe SY (2007) Influence of in vitro oxygen concentrations on preimplantation embryo development, gene expression and production of Hanwoo calves following embryo transfer. Mol Reprod Dev 74:486–496. CrossRef Medline

Riedl J, Crevenna AH, Kessenbrock K, Yu JH, Neukirchen D, Bista M, Bradke F, Jenne D, Holak TA, Werb Z, Sixt M, Wedlich-Soldner R (2008) Life-Act: a versatile marker to visualize F-actin. Nat Methods 5:605–607. CrossRef Medline

Rivera C, Voipio J, Payne JA, Ruusuvuori E, Lahtinen H, Lamsa K, Pirvola U, Saarma M, Kaila K (1999) The K^+/Cl^- co-transporter KCC2 renders GABA hyperpolarizing during neuronal maturation. Nature 397:251–255. CrossRef Medline

Rivera C, Voipio J, Thomas-Crusells J, Li H, Emri Z, Sipilä S, Payne JA, Minichiello L, Saarma M, Kaila K (2004) Mechanism of activity-dependent downregulation of the neuron-specific K-Cl cotransporter KCC2. J Neurosci 24:4683–4691. CrossRef Medline

Ross-Macdonald P, de Silva H, Guo Q, Xiao H, Hung CY, Penhallow B, Markwalder J, He L, Attar RM, Lin TA, Seitz S, Tilford C, Wardwell-Swanson J, Jackson D (2008) Identification of a nonkinase target mediating cytotoxicity of novel kinase inhibitors. Mol Cancer Ther 7:3490–3498. CrossRef Medline

Rust MB, Gurniak CB, Renner M, Vara H, Morando L, Görlich A, Sassoè-Pognetto M,, Banchaabouchi MA, Giustetto M, Triller A, Choquet D, Witke W (2010) Learning, AMPA receptor mobility and synaptic plasticity depend on n-cofilin-mediated actin dynamics. EMBO J 29:1889–1902. CrossRef Medline

Saneyoshi T, Wayman G, Fortin D, Davare M, Hoshi N, Nozaki N, Natsume T, Soderling TR (2008) Activity-dependent synaptogenesis: regulation by a CaM-kinase kinase/CaM-kinase I/betaPIX signaling complex. Neuron 57:94–107. CrossRef Medline

Smith KR, Davenport EC, Wei J, Li X, Pathania M, Vaccaro V, Yan Z, Kittler JT (2014) GIT1 and betaPIX are essential for GABA(A) receptor synaptic stability and inhibitory neurotransmission. Cell Rep 9:298–310. CrossRef Medline

Tietz EI, Kapur J, Macdonald RL (1999) Functional GABAA receptor heterogeneity of acutely dissociated hippocampal CA1 pyramidal cells. J Neurophysiol 81:1575–1586. Medline

Tyzio R, Nardou R, Ferrari DC, Tsintsadze T, Shahrokhi A, Eftekhari S, Khalilov I, Tsintsadze V, Brouchoud C, Chazal G, Lemonnier E, Lozovaya N, Burnashev N, Ben-Ari Y (2014) Oxytocin-mediated GABA inhibition during delivery attenuates autism pathogenesis in rodent offspring. Science 343:675–679. CrossRef Medline

Urban NT, Willig KI, Hell SW, Nägerl UV (2011) STED nanoscopy of actin dynamics in synapses deep inside living brain slices. Biophys J 101:1277–1284. CrossRef Medline

Wake H, Watanabe M, Moorhouse AJ, Kanematsu T, Horibe S, Matsukawa N, Asai K, Ojika K, Hirata M, Nabekura J (2007) Early changes in KCC2 phosphorylation in response to neuronal stress result in functional down-regulation. J Neurosci 27:1642–1650. CrossRef Medline

Watanabe M, Wake H, Moorhouse AJ, Nabekura J (2009) Clustering of neuronal K^+-Cl^- cotransporters in lipid rafts by tyrosine phosphorylation. J Biol Chem 284:27980–27988. CrossRef Medline

Woodin MA, Ganguly K, Poo MM (2003) Coincident pre- and postsynaptic activity modifies GABAergic synapses by postsynaptic changes in Cl^- transporter activity. Neuron 39:807–820. CrossRef Medline

Zhang H, Webb DJ, Asmussen H, Horwitz AF (2003) Synapse formation is regulated by the signaling adaptor GIT1. J Cell Biol 161:131–142. CrossRef Medline

REFERENCES

REFERENCES

Acsády, L., Görcs, T.J., Freund, T.F., 1996. Different populations of vasoactive intestinal polypeptide-immunoreactive interneurons are specialized to control pyramidal cells or interneurons in the hippocampus. Neuroscience 73, 317–334.

Acsády, L., Kamondi, A., Sík, A., Freund, T., Buzsáki, G., 1998. GABAergic cells are the major postsynaptic targets of mossy fibers in the rat hippocampus. J. Neurosci. 18, 3386–403.

Acton, B.A., Mahadevan, V., Mercado, A., Uvarov, P., Ding, Y., Pressey, J., Airaksinen, M.S., Mount, D.B., Woodin, M.A., 2012. Hyperpolarizing GABAergic transmission requires the KCC2 C-terminal ISO domain. J. Neurosci. 32, 8746–51.

Agez, M., Schultz, P., Medina, I., Baker, D.J., Burnham, M.P., Cardarelli, R.A., Conway, L.C., Garnier, K., Geschwindner, S., Gunnarsson, A., McCall, E.J., Frechard, A., Audebert, S., Deeb, T.Z., Moss, S.J., Brandon, N.J., Wang, Q., Dekker, N., Jawhari, A., 2017. Molecular architecture of potassium chloride co-transporter KCC2. Sci. Rep. 7, 16452.

Aguado, F., Carmona, M.A., Pozas, E., Aguiló, A., Martínez-Guijarro, F.J., Alcantara, S., Borrell, V., Yuste, R., Ibañez, C.F., Soriano, E., 2003. BDNF regulates spontaneous correlated activity at early developmental stages by increasing synaptogenesis and expression of the K+/Cl- co-transporter KCC2. Development 130, 1267–80.

Aivar, P., Valero, M., Bellistri, E., Menendez de la Prida, L., 2014. Extracellular calcium controls the expression of two different forms of ripple-like hippocampal oscillations. J. Neurosci. 34, 2989–3004.

Akerman, C.J., Cline, H.T., 2006. Depolarizing GABAergic conductances regulate the balance of excitation to inhibition in the developing retinotectal circuit in vivo. J. Neurosci. 26, 5117–30.

Alfonsa, H., Merricks, E.M., Codadu, N.K., Cunningham, M.O., Deisseroth, K., Racca, C., Trevelyan, A.J., 2015. The contribution of raised intraneuronal chloride to epileptic network activity. J. Neurosci. 35, 7715–26.

Aller, M.I., Wisden, W., 2008. Changes in expression of some two-pore domain potassium channel genes (KCNK) in selected brain regions of developing mice. Neuroscience 151, 1154–1172.

Altman, J., Das, G.D., 1965. Post-natal origin of microneurones in the rat brain. Nature 207, 953–6.

Alvarez, V., Lee, J.W., Westover, M.B., Drislane, F.W., Novy, J., Faouzi, M., Marchi, N.A., Dworetzky, B.A., Rossetti, A.O., 2016. Therapeutic coma for status epilepticus: Differing practices in a prospective multicenter study. Neurology 87, 1650–1659.

Amaral, D.G., Witter, M.P., 1989. The three-dimensional organization of the hippocampal formation: A review of anatomical data. Neuroscience 31, 571–591.

Ambrogini, P., Lattanzi, D., Ciuffoli, S., Agostini, D., Bertini, L., Stocchi, V., Santi, S., Cuppini, R., 2004. Morpho-functional characterization of neuronal cells at different stages of maturation in granule cell layer of adult rat dentate gyrus. Brain Res. 1017, 21–31.

Amilhon, B., Huh, C.Y.L., Manseau, F., Ducharme, G., Nichol, H., Adamantidis, A., Williams, S., 2015. Parvalbumin Interneurons of Hippocampus Tune Population Activity at Theta Frequency. Neuron 86, 1277–1289.

Amin, H., Marinaro, F., De Pietri Tonelli, D., Berdondini, L., 2017. Developmental excitatory-to-inhibitory GABA-polarity switch is disrupted in 22q11.2 deletion syndrome: a potential target for clinical therapeutics. Sci. Rep. 7, 15752.

Amiry-Moghaddam, M., Ottersen, O.P., 2003. The molecular basis of water transport in the brain. Nat. Rev. Neurosci. 4, 991–1001.

Andersen, P., Bliss, T. V, Skrede, K.K., 1971. Lamellar organization of hippocampal pathways. Exp. brain Res. 13, 222–38.

Andersen, P., Holmqvist, B., Voorhoeve, P.E., 1966. Entorhinal Activation of Dentate Granule Cells. Acta Physiol. Scand. 66, 448–460.

Aronov, D., Nevers, R., Tank, D.W., 2017. Mapping of a non-spatial dimension by the hippocampal-entorhinal circuit. Nature 543, 719–722.

Artinian, J., Peret, A., Marti, G., Epsztein, J., Crépel, V., 2011. Synaptic kainate receptors in interplay with INaP shift the sparse firing of dentate granule cells to a sustained rhythmic mode in temporal lobe epilepsy. J. Neurosci. 31, 10811–8.

Avoli, M., Biagini, G., de Curtis, M., 2006. Do interictal spikes sustain seizures and epileptogenesis? Epilepsy Curr. 6, 203–7.

Bagriantsev, S.N., Ang, K.-H., Gallardo-Godoy, A., Clark, K.A., Arkin, M.R., Renslo, A.R., Minor, D.L., Jr., 2013. A high-throughput functional screen identifies small molecule regulators of temperature- and mechano-sensitive K2P channels. ACS Chem. Biol. 8, 1841–51.

Báldi, R., Varga, C., Tamás, G., 2010. Differential distribution of KCC2 along the axo-somato-dendritic axis of hippocampal principal cells. Eur. J. Neurosci. 32, 1319–1325.

Banerjee, A., Rikhye, R. V, Breton-Provencher, V., Tang, X., Li, C., Li, K., Runyan, C.A., Fu, Z., Jaenisch, R., Sur, M., 2016. Jointly reduced inhibition and excitation underlies circuit-wide changes in cortical processing in Rett syndrome. Proc. Natl. Acad. Sci. U. S. A. 113, E7287–E7296.

Banke, T.G., Gegelashvili, G., 2008. Tonic activation of group I mGluRs modulates inhibitory synaptic strength by regulating KCC2 activity. J. Physiol. 586, 4925–34.

Barbarosie, M., Avoli, M., 1997. CA3-driven hippocampal-entorhinal loop controls rather than sustains in vitro limbic seizures. J. Neurosci. 17, 9308–14.

Barmashenko, G., Hefft, S., Aertsen, A., Kirschstein, T., Köhling, R., 2011. Positive shifts of the GABAA receptor reversal potential due to altered chloride homeostasis is widespread after status epilepticus. Epilepsia 52, 1570–1578.

Barthó, P., Payne, J.A., Freund, T.F., Acsády, L., 2004. Differential distribution of the KCl cotransporter KCC2 in thalamic relay and reticular nuclei. Eur. J. Neurosci. 20, 965–75.

Behr, J., Heinemann, U., 1996. Effects of serotonin on different patterns of low Mg2+-induced epileptiform activity in the subiculum of rats studied in vitro. Brain Res. 737, 331–334.

Belluscio, M.A., Mizuseki, K., Schmidt, R., Kempter, R., Buzsáki, G., 2012. Cross-frequency phase-phase coupling between θ and γ oscillations in the hippocampus. J. Neurosci. 32, 423–35.

Ben-Ari, Y., Cherubini, E., Corradetti, R., Gaiarsa, J.L., 1989. Giant synaptic potentials in immature rat CA3 hippocampal neurones. J. Physiol. 416, 303–25.

Bernier, B.E., Lacagnina, A.F., Ayoub, A., Shue, F., Zemelman, B. V, Krasne, F.B., Drew, M.R., 2017. Dentate Gyrus Contributes to Retrieval as well as Encoding: Evidence from Context Fear Conditioning, Recall, and Extinction. J. Neurosci. 37, 6359–6371.

Berninger, B., Marty, S., Zafra, F., da Penha Berzaghi, M., Thoenen, H., Lindholm, D., Borrell, V., Yuste, R., Ibañez, C.F., Soriano, E., 1995. GABAergic stimulation switches from enhancing to repressing BDNF expression in rat hippocampal neurons during maturation in vitro. Development 121, 2327–35.

Bieri, K.W., Bobbitt, K.N., Colgin, L.L., 2014. Slow and fast γ rhythms coordinate different spatial coding modes in hippocampal place cells. Neuron 82, 670–81.

Blaesse, P., Guillemin, I., Schindler, J., Schweizer, M., Delpire, E., Khiroug, L., Friauf, E., Nothwang, H.G., 2006. Oligomerization of KCC2 correlates with development of inhibitory neurotransmission. J. Neurosci. 26, 10407–19.

Blin, S., Ben Soussia, I., Kim, E.-J., Brau, F., Kang, D., Lesage, F., Bichet, D., 2016. Mixing and matching TREK/TRAAK subunits generate heterodimeric K2P channels with unique properties. Proc. Natl. Acad. Sci. U. S. A. 113, 4200–5.

Bliss, T. V, Lomo, T., 1973. Long-lasting potentiation of synaptic transmission in the dentate area of the anaesthetized

rabbit following stimulation of the perforant path. J. Physiol. 232, 331–56.

Blumcke, I., Cross, J.H., Spreafico, R., 2013. The international consensus classification for hippocampal sclerosis: an important step towards accurate prognosis. Lancet Neurol. 12, 844–846.

Blümcke, I., Suter, B., Behle, K., Kuhn, R., Schramm, J., Elger, C.E., Wiestler, O.D., 2000. Loss of hilar mossy cells in Ammon's horn sclerosis. Epilepsia 41 Suppl 6, S174-80.

Boettger, T., Hübner, C.A., Maier, H., Rust, M.B., Beck, F.X., Jentsch, T.J., 2002. Deafness and renal tubular acidosis in mice lacking the K-Cl co-transporter Kcc4. Nature 416, 874–878.

Bonislawski, D.P., Schwarzbach, E.P., Cohen, A.S., 2007. Brain injury impairs dentate gyrus inhibitory efficacy. Neurobiol. Dis. 25, 163–9.

Bortone, D., Polleux, F., 2009. KCC2 expression promotes the termination of cortical interneuron migration in a voltage-sensitive calcium-dependent manner. Neuron 62, 53–71.

Bos, R., Sadlaoud, K., Boulenguez, P., Buttigieg, D., Liabeuf, S., Brocard, C., Haase, G., Bras, H., Vinay, L., 2013. Activation of 5-HT2A receptors upregulates the function of the neuronal K-Cl cotransporter KCC2. Proc. Natl. Acad. Sci. U. S. A. 110, 348–53.

Bösl, M.R., Stein, V., Hübner, C., Zdebik, A.A., Jordt, S.E., Mukhopadhyay, A.K., Davidoff, M.S., Holstein, A.F., Jentsch, T.J., 2001. Male germ cells and photoreceptors, both dependent on close cell-cell interactions, degenerate upon ClC-2 Cl(-) channel disruption. EMBO J. 20, 1289–99.

Boulenguez, P., Liabeuf, S., Bos, R., Bras, H., Jean-Xavier, C., Brocard, C., Stil, A., Darbon, P., Cattaert, D., Delpire, E., Marsala, M., Vinay, L., 2010. Down-regulation of the potassium-chloride cotransporter KCC2 contributes to spasticity after spinal cord injury. Nat. Med. 16, 302–307.

Bragin, A., Benassi, S.K., Kheiri, F., Engel, J., Jr., 2011. Further evidence that pathologic high-frequency oscillations are bursts of population spikes derived from recordings of identified cells in dentate gyrus. Epilepsia 52, 45–52.

Bragin, A., Engel, J., Wilson, C.L., Fried, I., Buzs  i, G., 1999. High-frequency oscillations in human brain. Hippocampus 9, 137–142.

Bragin, A., Jandó, G., Nádasdy, Z., Hetke, J., Wise, K., Buzsáki, G., Szabó, G., Freund, T.F., Hájos, N., 1995a. Gamma (40-100 Hz) oscillation in the hippocampus of the behaving rat. J. Neurosci. 15, 47–60.

Bragin, A., Jandó, G., Nádasdy, Z., van Landeghem, M., Buzsáki, G., 1995b. Dentate EEG spikes and associated interneuronal population bursts in the hippocampal hilar region of the rat. J. Neurophysiol. 73, 1691–705.

Bragin, A., Wilson, C.L., Staba, R.J., Reddick, M., Fried, I., Engel, J., 2002. Interictal high-frequency oscillations (80-500Hz) in the human epileptic brain: Entorhinal cortex. Ann. Neurol. 52, 407–415.

Bragin, D.E., Sanderson, J.L., Peterson, S., Connor, J.A., Müller, W.S., 2009. Development of epileptiform excitability in the deep entorhinal cortex after status epilepticus. Eur. J. Neurosci. 30, 611–24.

Braham, R., 1998. Incorporation of Long-Range Feedback in Neural Networks Under Stability Conditions. Neural Networks 11, 141–144.

Brandt, C., Nozadze, M., Heuchert, N., Rattka, M., Löscher, W., 2010. Disease-modifying effects of phenobarbital and the NKCC1 inhibitor bumetanide in the pilocarpine model of temporal lobe epilepsy. J. Neurosci. 30, 8602–12.

Branston, N.M., Strong, A.J., Symon, L., 1982. Kinetics of resolution of transient increases in extracellular potassium activity: relationships to regional blood flow in primate cerebral cortex. Neurol. Res. 4, 1–19.

Brickley, S.G., Aller, M.I., Sandu, C., Veale, E.L., Alder, F.G., Sambi, H., Mathie, A., Wisden, W., 2007. TASK-3 two-pore domain potassium channels enable sustained high-frequency firing in cerebellar granule neurons. J. Neurosci. 27, 9329–40.

Buchin, A., Chizhov, A., Huberfeld, G., Miles, R., Gutkin, B.S., 2016. Reduced Efficacy of the KCC2 Cotransporter Promotes Epileptic Oscillations in a Subiculum Network Model. J. Neurosci. 36, 11619–11633.

Buckmaster, P.S., Wenzel, H.J., Kunkel, D.D., Schwartzkroin, P.A., 1996. Axon arbors and synaptic connections of hippocampal mossy cells in the rat in vivo. J. Comp. Neurol. 366, 271–92.

Bui, A.D., Nguyen, T.M., Limouse, C., Kim, H.K., Szabo, G.G., Felong, S., Maroso, M., Soltesz, I., 2018. Dentate gyrus mossy cells control spontaneous convulsive seizures and spatial memory. Science 359, 787–790.

Buzsáki, G., 2002. Theta Oscillations in the Hippocampus. Neuron 33, 325–340.

Buzsáki, G., 1986. Hippocampal sharp waves: Their origin and significance. Brain Res. 398, 242–252.

Buzsáki, G., Anastassiou, C.A., Koch, C., 2012. The origin of extracellular fields and currents--EEG, ECoG, LFP and spikes. Nat. Rev. Neurosci. 13, 407–20.

Buzsáki, G., Horváth, Z., Urioste, R., Hetke, J., Wise, K., 1992. High-frequency network oscillation in the hippocampus. Science 256, 1025–7.

Cajal, S.R. y, 1909. Histologie du système nerveux de l'homme & des vertébrés. Maloine, Paris.

Canteras, N.S., Swanson, L.W., 1992. Projections of the ventral subiculum to the amygdala, septum, and hypothalamus: A PHAL anterograde tract-tracing study in the rat. J. Comp. Neurol. 324, 180–194.

Caron, L., Rousseau, F., Gagnon, E., Isenring, P., 2000. Cloning and functional characterization of a cation-Cl-cotransporter-interacting protein. J. Biol. Chem. 275, 32027–36.

Casula, S., Shmukler, B.E., Wilhelm, S., Stuart-Tilley, A.K., Su, W., Chernova, M.N., Brugnara, C., Alper, S.L., 2001. A dominant negative mutant of the KCC1 K-Cl cotransporter: both N- and C-terminal cytoplasmic domains are required for K-Cl cotransport activity. J. Biol. Chem. 276, 41870–8.

Cavalheiro, E.A., Leite, J.P., Bortolotto, Z.A., Turski, W.A., Ikonomidou, C., Turski, L., 1991. Long-Term Effects of Pilocarpine in Rats: Structural Damage of the Brain Triggers Kindling and Spontaneous I Recurrent Seizures. Epilepsia 32, 778–782.

Cavazos, J.E., Jones, S.M., Cross, D.J., 2004. Sprouting and synaptic reorganization in the subiculum and CA1 region of the hippocampus in acute and chronic models of partial-onset epilepsy. Neuroscience 126, 677–88.

Cellot, G., Cherubini, E., 2014. Reduced inhibitory gate in the barrel cortex of Neuroligin3R451C knock-in mice, an animal model of autism spectrum disorders. Physiol. Rep. 2.

Chamma, I., Chevy, Q., Poncer, J.C., Lévi, S., 2012. Role of the neuronal K-Cl co-transporter KCC2 in inhibitory and excitatory neurotransmission. Front. Cell. Neurosci. 6, 5.

Chamma, I., Heubl, M., Chevy, Q., Renner, M., Moutkine, I., Eugène, E., Poncer, J.C., Lévi, S., 2013. Activity-dependent regulation of the K/Cl transporter KCC2 membrane diffusion, clustering, and function in hippocampal neurons. J. Neurosci. 33, 15488–503.

Chandra, D., Jia, F., Liang, J., Peng, Z., Suryanarayanan, A., Werner, D.F., Spigelman, I., Houser, C.R., Olsen, R.W., Harrison, N.L., Homanics, G.E., 2006. GABAA receptor alpha 4 subunits mediate extrasynaptic inhibition in thalamus and dentate gyrus and the action of gaboxadol. Proc. Natl. Acad. Sci. U. S. A. 103, 15230–5.

Chauvière, L., Rafrafi, N., Thinus-Blanc, C., Bartolomei, F., Esclapez, M., Bernard, C., 2009. Early deficits in spatial memory and theta rhythm in experimental temporal lobe epilepsy. J. Neurosci. 29, 5402–10.

Chen, L., Wan, L., Wu, Z., Ren, W., Huang, Y., Qian, B., Wang, Y., 2017. KCC2 downregulation facilitates epileptic seizures. Sci. Rep. 7, 156.

Chen, M., Wang, J., Jiang, J., Zheng, X., Justice, N.J., Wang, K., Ran, X., Li, Y., Huo, Q., Zhang, J., Li, H., Lu, N., Wang, Y., Zheng, H., Long, C., Yang, L., 2017. APP modulates KCC2 expression and function in hippocampal GABAergic inhibition. Elife 6.

Cherubini, E., Gaiarsa, J.L., Ben-Ari, Y., 1991. GABA: an excitatory transmitter in early postnatal life. Trends Neurosci. 14, 515–519.

Chevaleyre, V., Siegelbaum, S.A., 2010. Strong CA2 pyramidal neuron synapses define a powerful disynaptic cortico-hippocampal loop. Neuron 66, 560–72.

Chevy, Q., Heubl, M., Goutierre, M., Backer, S., Moutkine, I., Eugène, E., Bloch-Gallego, E., Lévi, S., Poncer, J.C., 2015. KCC2 Gates Activity-Driven AMPA Receptor Traffic through Cofilin Phosphorylation. J. Neurosci. 35, 15772–86.

Cho, H.-Y., Kim, M., Han, J.-H., 2017. Specific disruption of contextual memory recall by sparse additional activity in the dentate gyrus. Neurobiol. Learn. Mem. 145, 190–198.

Chorin, E., Vinograd, O., Fleidervish, I., Gilad, D., Herrmann, S., Sekler, I., Aizenman, E., Hershfinkel, M., 2011. Upregulation of KCC2 activity by zinc-mediated neurotransmission via the mZnR/GPR39 receptor. J. Neurosci. 31, 12916–26.

Chudotvorova, I., Ivanov, A., Rama, S., Hübner, C.A., Pellegrino, C., Ben-Ari, Y., Medina, I., 2005. Early expression of KCC2 in rat hippocampal cultures augments expression of functional GABA synapses. J. Physiol. 566, 671–9.

Claiborne, B.J., Amaral, D.G., Cowan, W.M., 1986. A light and electron microscopic analysis of the mossy fibers of the rat dentate gyrus. J. Comp. Neurol. 246, 435–458.

Cohen, I., Navarro, V., Clemenceau, S., Baulac, M., Miles, R., 2002. On the origin of interictal activity in human temporal lobe epilepsy in vitro. Science 298, 1418–21.

Colgin, L.L., Denninger, T., Fyhn, M., Hafting, T., Bonnevie, T., Jensen, O., Moser, M.-B., Moser, E.I., 2009. Frequency of gamma oscillations routes flow of information in the hippocampus. Nature 462, 353–357.

Coras, R., Blümcke, I., 2015. Clinico-pathological subtypes of hippocampal sclerosis in temporal lobe epilepsy and their differential impact on memory impairment. Neuroscience 309, 153–161.

Cossart, R., Dinocourt, C., Hirsch, J.C., Merchan-Perez, A., De Felipe, J., Ben-Ari, Y., Esclapez, M., Bernard, C., 2001. Dendritic but not somatic GABAergic inhibition is decreased in experimental epilepsy. Nat. Neurosci. 4, 52–62.

Coull, J.A.M., Boudreau, D., Bachand, K., Prescott, S.A., Nault, F., Sík, A., Koninck, P. De, Koninck, Y. De, 2003. Trans-synaptic shift in anion gradient in spinal lamina I neurons as a mechanism of neuropathic pain. Nature 424, 938–942.

Csicsvari, J., Hirase, H., Mamiya, A., Buzsáki, G., 2000. Ensemble Patterns of Hippocampal CA3-CA1 Neurons during Sharp Wave–Associated Population Events. Neuron 28, 585–594.

Csicsvari, J., Jamieson, B., Wise, K.D., Buzsáki, G., 2003. Mechanisms of Gamma Oscillations in the Hippocampus of the Behaving Rat. Neuron 37, 311–322.

Daigle, N.D., Carpentier, G.A., Frenette-Cotton, R., Simard, M.G., Lefoll, M.-H., Noël, M., Caron, L., Noël, J., Isenring, P., 2009. Molecular characterization of a human cation-Cl^- cotransporter (SLC12A8A, CCC9A) that promotes polyamine and amino acid transport. J. Cell. Physiol. 220, 680–689.

Danielson, N.B., Zaremba, J.D., Kaifosh, P., Bowler, J., Ladow, M., Losonczy, A., 2016. Sublayer-Specific Coding Dynamics during Spatial Navigation and Learning in Hippocampal Area CA1. Neuron 91, 652–65.

Dargaei, Z., Bang, J.Y., Mahadevan, V., Khademullah, C.S., Bedard, S., Parfitt, G.M., Kim, J.C., Woodin, M.A., 2018. Restoring GABAergic inhibition rescues memory deficits in a Huntington's disease mouse model. Proc. Natl. Acad. Sci. U. S. A. 115, E1618–E1626.

de Lanerolle, N.C., Kim, J.H., Robbins, R.J., Spencer, D.D., 1989. Hippocampal interneuron loss and plasticity in human temporal lobe epilepsy. Brain Res. 495, 387–395.

de Los Heros, P., Alessi, D.R., Gourlay, R., Campbell, D.G., Deak, M., Macartney, T.J., Kahle, K.T., Zhang, J., 2014. The WNK-regulated SPAK/OSR1 kinases directly phosphorylate and inhibit the K+-Cl- co-transporters. Biochem. J. 458, 559–73.

Deidda, G., Parrini, M., Naskar, S., Bozarth, I.F., Contestabile, A., Cancedda, L., 2015. Reversing excitatory GABAAR signaling restores synaptic plasticity and memory in a mouse model of Down syndrome. Nat. Med. 21, 318–326.

Delpire, E., Baranczak, A., Waterson, A.G., Kim, K., Kett, N., Morrison, R.D., Daniels, J.S., Weaver, C.D., Lindsley, C.W., 2012. Further optimization of the K-Cl cotransporter KCC2 antagonist ML077: development of a highly selective and more potent in vitro probe. Bioorg. Med. Chem. Lett. 22, 4532–5.

Deng, P., Pang, Z., Zhang, Y., Xu, Z.C., 2004. Developmental changes of transient potassium currents in large aspiny neurons in the neostriatum. Dev. Brain Res. 153, 97–107.

Di Lieto, A., Rantamäki, T., Vesa, L., Yanpallewar, S., Antila, H., Lindholm, J., Rios, M., Tessarollo, L., Castrén, E., 2012.

The responsiveness of TrkB to BDNF and antidepressant drugs is differentially regulated during mouse development. PLoS One 7, e32869.

Diba, K., Buzsáki, G., 2007. Forward and reverse hippocampal place-cell sequences during ripples. Nat. Neurosci. 10, 1241–2.

Dichter, M.A., Ayala, G.F., 1987. Cellular mechanisms of epilepsy: a status report. Science 237, 157–64.

Doyon, N., Prescott, S.A., Castonguay, A., Godin, A.G., Kröger, H., De Koninck, Y., 2011. Efficacy of Synaptic Inhibition Depends on Multiple, Dynamically Interacting Mechanisms Implicated in Chloride Homeostasis. PLoS Comput. Biol. 7, e1002149.

Doyon, N., Prescott, S.A., De Koninck, Y., 2016. Mild KCC2 Hypofunction Causes Inconspicuous Chloride Dysregulation that Degrades Neural Coding. Front. Cell. Neurosci. 9, 516.

Du, F., Eid, T., Lothman, E.W., Köhler, C., Schwarcz, R., Bernard, C., 1995. Preferential neuronal loss in layer III of the medial entorhinal cortex in rat models of temporal lobe epilepsy. J. Neurosci. 15, 6301–13.

Duarte, S.T., Armstrong, J., Roche, A., Ortez, C., Pérez, A., O'Callaghan, M. del M., Pereira, A., Sanmartí, F., Ormazábal, A., Artuch, R., Pineda, M., García-Cazorla, A., 2013. Abnormal expression of cerebrospinal fluid cation chloride cotransporters in patients with Rett syndrome. PLoS One 8, e68851.

Dugladze, T., Vida, I., Tort, A.B., Gross, A., Otahal, J., Heinemann, U., Kopell, N.J., Gloveli, T., 2007. Impaired hippocampal rhythmogenesis in a mouse model of mesial temporal lobe epilepsy. Proc. Natl. Acad. Sci. U. S. A. 104, 17530–5.

Duncan, K., Ketz, N., Inati, S.J., Davachi, L., 2012. Evidence for area CA1 as a match/mismatch detector: a high-resolution fMRI study of the human hippocampus. Hippocampus 22, 389–98.

Dunham, P.B., Ellory, J.C., 1981. Passive potassium transport in low potassium sheep red cells: dependence upon cell volume and chloride. J. Physiol. 318, 511–30.

Dzhala, V., Valeeva, G., Glykys, J., Khazipov, R., Staley, K., 2012. Traumatic alterations in GABA signaling disrupt hippocampal network activity in the developing brain. J. Neurosci. 32, 4017–31.

Dzhala, V.I., Talos, D.M., Sdrulla, D.A., Brumback, A.C., Mathews, G.C., Benke, T.A., Delpire, E., Jensen, F.E., Staley, K.J., 2005. NKCC1 transporter facilitates seizures in the developing brain. Nat. Med. 11, 1205–1213.

Ego-Stengel, V., Wilson, M.A., 2010. Disruption of ripple-associated hippocampal activity during rest impairs spatial learning in the rat. Hippocampus 20, 1–10.

Eichenbaum, H., Kuperstein, M., Fagan, A., Nagode, J., 1987. Cue-sampling and goal-approach correlates of hippocampal unit activity in rats performing an odor-discrimination task. J. Neurosci. 7, 716–32.

Ellender, T.J., Nissen, W., Colgin, L.L., Mann, E.O., Paulsen, O., 2010. Priming of hippocampal population bursts by individual perisomatic-targeting interneurons. J. Neurosci. 30, 5979–91.

Ellender, T.J., Raimondo, J. V, Irkle, A., Lamsa, K.P., Akerman, C.J., 2014. Excitatory effects of parvalbumin-expressing interneurons maintain hippocampal epileptiform activity via synchronous afterdischarges. J. Neurosci. 34, 15208–22.

Engel, J., Jr, 2014. Approaches to refractory epilepsy. Ann. Indian Acad. Neurol. 17, S12-7.

Eriksson, P.S., Perfilieva, E., Björk-Eriksson, T., Alborn, A.-M., Nordborg, C., Peterson, D.A., Gage, F.H., 1998. Neurogenesis in the adult human hippocampus. Nat. Med. 4, 1313–1317.

Eugène, E., Cluzeaud, F., Cifuentes-Diaz, C., Fricker, D., Le Duigou, C., Clemenceau, S., Baulac, M., Poncer, J.-C., Miles, R., 2014. An organotypic brain slice preparation from adult patients with temporal lobe epilepsy. J. Neurosci. Methods 235, 234–44.

Fernández-Ruiz, A., Muñoz, S., Sancho, M., Makarova, J., Makarov, V.A., Herreras, O., 2013. Cytoarchitectonic and dynamic origins of giant positive local field potentials in the dentate gyrus. J. Neurosci. 33, 15518–32.

Fisahn, A., 2005. Kainate receptors and rhythmic activity in neuronal networks: hippocampal gamma oscillations as a tool. J. Physiol. 562, 65–72.

Fiumelli, H., Briner, A., Puskarjov, M., Blaesse, P., Belem, B.J., Dayer, A.G., Kaila, K., Martin, J.-L., Vutskits, L., 2013. An Ion Transport-Independent Role for the Cation-Chloride Cotransporter KCC2 in Dendritic Spinogenesis In Vivo. Cereb. Cortex 23, 378–388.

Fiumelli, H., Cancedda, L., Poo, M., 2005. Modulation of GABAergic transmission by activity via postsynaptic Ca2+-dependent regulation of KCC2 function. Neuron 48, 773–86.

Fiumelli, H., Woodin, M.A., 2007. Role of activity-dependent regulation of neuronal chloride homeostasis in development. Curr. Opin. Neurobiol. 17, 81–86.

Flynn, S.P., Barriere, S., Barrier, S., Scott, R.C., Lenck-Santini, P.-P., Holmes, G.L., 2015. Status Epilepticus Induced Spontaneous Dentate Gyrus Spikes: In Vivo Current Source Density Analysis. PLoS One 10, e0132630.

Foffani, G., Uzcategui, Y.G., Gal, B., Menendez de la Prida, L., 2007. Reduced Spike-Timing Reliability Correlates with the Emergence of Fast Ripples in the Rat Epileptic Hippocampus. Neuron 55, 930–941.

Förster, E., Zhao, S., Frotscher, M., 2006. Laminating the hippocampus. Nat. Rev. Neurosci. 7, 259–268.

Foster, D.J., Wilson, M.A., 2006. Reverse replay of behavioural sequences in hippocampal place cells during the awake state. Nature 440, 680–683.

Freiman, T.M., Eismann-Schweimler, J., Frotscher, M., 2011. Granule cell dispersion in temporal lobe epilepsy is associated with changes in dendritic orientation and spine distribution. Exp. Neurol. 229, 332–338.

Freund, T.F., Antal, M., 1988. GABA-containing neurons in the septum control inhibitory interneurons in the hippocampus. Nature 336, 170–173.

Freund, T.F., Buzsáki, G., 1996. Interneurons of the hippocampus. Hippocampus 6, 347–470.

Fried, I., MacDonald, K.A., Wilson, C.L., 1997. Single Neuron Activity in Human Hippocampus and Amygdala during Recognition of Faces and Objects. Neuron 18, 753–765.

Friedel, P., Ludwig, A., Pellegrino, C., Agez, M., Jawhari, A., Rivera, C., Medina, I., 2017. A Novel View on the Role of Intracellular Tails in Surface Delivery of the Potassium-Chloride Cotransporter KCC2. eNeuro 4.

Froriep, U.P., Kumar, A., Cosandier-Rimélé, D., Häussler, U., Kilias, A., Haas, C.A., Egert, U., 2012. Altered theta coupling between medial entorhinal cortex and dentate gyrus in temporal lobe epilepsy. Epilepsia 53, 1937–1947.

Fu, H., Subramanian, R.R., Masters, S.C., 2000. 14-3-3 Proteins: Structure, Function, and Regulation. Annu. Rev. Pharmacol. Toxicol. 40, 617–647.

Fujita, S., Toyoda, I., Thamattoor, A.K., Buckmaster, P.S., 2014. Preictal Activity of Subicular, CA1, and Dentate Gyrus Principal Neurons in the Dorsal Hippocampus before Spontaneous Seizures in a Rat Model of Temporal Lobe Epilepsy. J. Neurosci. 34, 16671–16687.

Gabriel, S., Njunting, M., Pomper, J.K., Merschhemke, M., Sanabria, E.R.G., Eilers, A., Kivi, A., Zeller, M., Meencke, H.-J., Cavalheiro, E.A., Heinemann, U., Lehmann, T.-N., 2004. Stimulus and potassium-induced epileptiform activity in the human dentate gyrus from patients with and without hippocampal sclerosis. J. Neurosci. 24, 10416–30.

Gagnon, K.B., Delpire, E., 2013. Physiology of SLC12 transporters: lessons from inherited human genetic mutations and genetically engineered mouse knockouts. Am. J. Physiol. Cell Physiol. 304, C693-714.

Gagnon, K.B.E., England, R., Delpire, E., 2006. Volume sensitivity of cation-Cl^- cotransporters is modulated by the interaction of two kinases: Ste20-related proline-alanine-rich kinase and WNK4. Am. J. Physiol. Physiol. 290, C134–C142.

Gagnon, M., Bergeron, M.J., Lavertu, G., Castonguay, A., Tripathy, S., Bonin, R.P., Perez-Sanchez, J., Boudreau, D., Wang, B., Dumas, L., Valade, I., Bachand, K., Jacob-Wagner, M., Tardif, C., Kianicka, I., Isenring, P., Attardo, G., Coull, J.A.M., De Koninck, Y., 2013. Chloride extrusion enhancers as novel therapeutics for neurological diseases. Nat. Med. 19, 1524–8.

Galeffi, F., Sah, R., Pond, B.B., George, A., Schwartz-Bloom, R.D., 2004. Changes in intracellular chloride after oxygen-glucose deprivation of the adult hippocampal slice: effect of diazepam. J. Neurosci. 24, 4478–88.

Gamba, G., 2005. Molecular Physiology and Pathophysiology of Electroneutral Cation-Chloride Cotransporters. Physiol. Rev. 85, 423–493.

Gamba, G., Saltzberg, S.N., Lombardi, M., Miyanoshita, A., Lytton, J., Hediger, M.A., Brenner, B.M., Hebert, S.C., 1993. Primary structure and functional expression of a cDNA encoding the thiazide-sensitive, electroneutral sodium-chloride cotransporter. Proc. Natl. Acad. Sci. U. S. A. 90, 2749–53.

Gauvain, G., Chamma, I., Chevy, Q., Cabezas, C., Irinopoulou, T., Bodrug, N., Carnaud, M., Levi, S., Poncer, J.C., 2011. The neuronal K-Cl cotransporter KCC2 influences postsynaptic AMPA receptor content and lateral diffusion in dendritic spines. Proc. Natl. Acad. Sci. 108, 15474–15479.

Gelinas, J.N., Khodagholy, D., Thesen, T., Devinsky, O., Buzsáki, G., 2016. Interictal epileptiform discharges induce hippocampal–cortical coupling in temporal lobe epilepsy. Nat. Med. 22, 641–648.

Gerelsaikhan, T., Turner, R.J., 2000. Transmembrane topology of the secretory Na+-K+-2Cl- cotransporter NKCC1 studied by in vitro translation. J. Biol. Chem. 275, 40471–7.

Gillen, C.M., Brill, S., Payne, J.A., Forbush, B., 1996. Molecular cloning and functional expression of the K-Cl cotransporter from rabbit, rat, and human. A new member of the cation-chloride cotransporter family. J. Biol. Chem. 271, 16237–44.

Girardeau, G., Benchenane, K., Wiener, S.I., Buzsáki, G., Zugaro, M.B., 2009. Selective suppression of hippocampal ripples impairs spatial memory. Nat. Neurosci. 12, 1222–1223.

Glykys, J., Dzhala, V., Egawa, K., Balena, T., Saponjian, Y., Kuchibhotla, K. V, Bacskai, B.J., Kahle, K.T., Zeuthen, T., Staley, K.J., 2014. Local impermeant anions establish the neuronal chloride concentration. Science 343, 670–5.

Goldstein, S.A.N., Bockenhauer, D., O'Kelly, I., Zilberberg, N., 2001. Potassium leak channels and the KCNK family of two-p-domain subunits. Nat. Rev. Neurosci. 2, 175–184.

Goutagny, R., Jackson, J., Williams, S., 2009. Self-generated theta oscillations in the hippocampus. Nat. Neurosci. 12, 1491–1493.

Grandgeorge, M., Lemonnier, E., Degrez, C., Jallot, N., 2014. The effect of bumetanide treatment on the sensory behaviours of a young girl with Asperger syndrome. BMJ Case Rep. 2014.

Gulyás, A.I., Sík, A., Payne, J.A., Kaila, K., Freund, T.F., 2001. The KCl cotransporter, KCC2, is highly expressed in the vicinity of excitatory synapses in the rat hippocampus. Eur. J. Neurosci. 13, 2205–2217.

Gulyás, A.I., Szabó, G.G., Ulbert, I., Holderith, N., Monyer, H., Erdélyi, F., Szabó, G., Freund, T.F., Hájos, N., 2010. Parvalbumin-containing fast-spiking basket cells generate the field potential oscillations induced by cholinergic receptor activation in the hippocampus. J. Neurosci. 30, 15134–45.

Guzman, S.J., Schlögl, A., Frotscher, M., Jonas, P., 2016. Synaptic mechanisms of pattern completion in the hippocampal CA3 network. Science 353, 1117–23.

Haas, C.A., Dudeck, O., Kirsch, M., Huszka, C., Kann, G., Pollak, S., Zentner, J., Frotscher, M., 2002. Role for reelin in the development of granule cell dispersion in temporal lobe epilepsy. J. Neurosci. 22, 5797–802.

Haglund, L., Swanson, L.W., Köhler, C., 1984. The projection of the supramammillary nucleus to the hippocampal formation: An immunohistochemical and anterograde transport study with the lectin PHA-L in the rat. J. Comp. Neurol. 229, 171–185.

Hájos, N., Ellender, T.J., Zemankovics, R., Mann, E.O., Exley, R., Cragg, S.J., Freund, T.F., Paulsen, O., 2009. Maintaining network activity in submerged hippocampal slices: importance of oxygen supply. Eur. J. Neurosci. 29, 319–27.

Hamidi, S., Avoli, M., 2015. KCC2 function modulates in vitro ictogenesis. Neurobiol. Dis. 79, 51–8.

Hamidi, S., D'Antuono, M., Avoli, M., 2015. On the contribution of KCC2 and carbonic anhydrase to two types of in vitro interictal discharge. Pflügers Arch. - Eur. J. Physiol. 467, 2325–2335.

Harris, E., Stewart, M., 2001. Propagation of synchronous epileptiform events from subiculum backward into area CA1 of rat brain slices. Brain Res. 895, 41–49.

Harris, K.D., Henze, D.A., Csicsvari, J., Hirase, H., Buzsáki, G., 2000. Accuracy of Tetrode Spike Separation as

Determined by Simultaneous Intracellular and Extracellular Measurements. J. Neurophysiol. 84, 401–414.

Hartmann, A.-M., Nothwang, H.G., 2014. Molecular and evolutionary insights into the structural organization of cation chloride cotransporters. Front. Cell. Neurosci. 8, 470.

Hartmann, A.-M., Tesch, D., Nothwang, H.G., Bininda-Emonds, O.R.P., 2014. Evolution of the Cation Chloride Cotransporter Family: Ancient Origins, Gene Losses, and Subfunctionalization through Duplication. Mol. Biol. Evol. 31, 434–447.

Headley, D.B., Kanta, V., Paré, D., 2017. Intra- and interregional cortical interactions related to sharp-wave ripples and dentate spikes. J. Neurophysiol. 117, 556–565.

Heinemann, U., Beck, H., Dreier, J.P., Ficker, E., Stabel, J., Zhang, C.L., 1992. The dentate gyrus as a regulated gate for the propagation of epileptiform activity. Epilepsy Res. Suppl. 7, 273–80.

Henze, D.A., Wittner, L., Buzsáki, G., 2002. Single granule cells reliably discharge targets in the hippocampal CA3 network in vivo. Nat. Neurosci. 5, 790–795.

Hernández-Rabaza, V., Hontecillas-Prieto, L., Velázquez-Sánchez, C., Ferragud, A., Pérez-Villaba, A., Arcusa, A., Barcia, J.A., Trejo, J.L., Canales, J.J., 2008. The hippocampal dentate gyrus is essential for generating contextual memories of fear and drug-induced reward. Neurobiol. Learn. Mem. 90, 553–559.

Heubl, M., Zhang, J., Pressey, J.C., Al Awabdh, S., Renner, M., Gomez-Castro, F., Moutkine, I., Eugène, E., Russeau, M., Kahle, K.T., Poncer, J.C., Lévi, S., 2017. GABAA receptor dependent synaptic inhibition rapidly tunes KCC2 activity via the Cl−-sensitive WNK1 kinase. Nat. Commun. 8, 1776.

Hiki, K., D'Andrea, R.J., Furze, J., Crawford, J., Woollatt, E., Sutherland, G.R., Vadas, M.A., Gamble, J.R., 1999. Cloning, characterization, and chromosomal location of a novel human K+-Cl- cotransporter. J. Biol. Chem. 274, 10661–7.

Hodgkin, A.L., Huxley, A.F., 1947. Potassium leakage from an active nerve fibre. J. Physiol. 106, 341–67.

Hoffmann, E.K., Dunham, P.B., 1995. Membrane mechanisms and intracellular signalling in cell volume regulation. Int. Rev. Cytol. 161, 173–262.

Holmgren, C.D., Mukhtarov, M., Malkov, A.E., Popova, I.Y., Bregestovski, P., Zilberter, Y., 2010. Energy substrate availability as a determinant of neuronal resting potential, GABA signaling and spontaneous network activity in the neonatal cortex *in vitro*. J. Neurochem. 112, 900–912.

Hoover, R.S., Poch, E., Monroy, A., Vázquez, N., Nishio, T., Gamba, G., Hebert, S.C., 2003. N-Glycosylation at two sites critically alters thiazide binding and activity of the rat thiazide-sensitive Na(+):Cl(-) cotransporter. J. Am. Soc. Nephrol. 14, 271–82.

Horn, Z., Ringstedt, T., Blaesse, P., Kaila, K., Herlenius, E., 2010. Premature expression of KCC2 in embryonic mice perturbs neural development by an ion transport-independent mechanism. Eur. J. Neurosci. 31, 2142–2155.

Houser, C.R., 1990. Granule cell dispersion in the dentate gyrus of humans with temporal lobe epilepsy. Brain Res. 535, 195–204.

Howell, B.W., Hawkes, R., Soriano, P., Cooper, J.A., 1997. Neuronal position in the developing brain is regulated by mouse disabled-1. Nature 389, 733–737.

Hsu, D., 2007. The dentate gyrus as a filter or gate: a look back and a look ahead. Prog. Brain Res. 163, 601–613.

Huberfeld, G., Menendez de la Prida, L., Pallud, J., Cohen, I., Le Van Quyen, M., Adam, C., Clemenceau, S., Baulac, M., Miles, R., 2011. Glutamatergic pre-ictal discharges emerge at the transition to seizure in human epilepsy. Nat. Neurosci. 14, 627–634.

Huberfeld, G., Wittner, L., Clemenceau, S., Baulac, M., Kaila, K., Miles, R., Rivera, C., 2007. Perturbed chloride homeostasis and GABAergic signaling in human temporal lobe epilepsy. J. Neurosci. 27, 9866–73.

Hübner, C.A., Stein, V., Hermans-Borgmeyer, I., Meyer, T., Ballanyi, K., Jentsch, T.J., 2001. Disruption of KCC2 Reveals an Essential Role of K-Cl Cotransport Already in Early Synaptic Inhibition. Neuron 30, 515–524.

Huerta, P.T., Lisman, J.E., 1993. Heightened synaptic plasticity of hippocampal CA1 neurons during a Cholinergically

induced rhythmic state. Nature 364, 723–725.

Hughes, K.R., 1965. Dorsal and ventral hippocampus lesions and maze learning: influence of preoperative environment. Can. J. Psychol. 19, 325–32.

Hyde, T.M., Lipska, B.K., Ali, T., Mathew, S. V, Law, A.J., Metitiri, O.E., Straub, R.E., Ye, T., Colantuoni, C., Herman, M.M., Bigelow, L.B., Weinberger, D.R., Kleinman, J.E., 2011. Expression of GABA signaling molecules KCC2, NKCC1, and GAD1 in cortical development and schizophrenia. J. Neurosci. 31, 11088–95.

Ibarz, J.M., Foffani, G., Cid, E., Inostroza, M., Menendez de la Prida, L., 2010. Emergent dynamics of fast ripples in the epileptic hippocampus. J. Neurosci. 30, 16249–61.

Ikeda, K., Onimaru, H., Yamada, J., Inoue, K., Ueno, S., Onaka, T., Toyoda, H., Arata, A., Ishikawa, T., Taketo, M.M., Fukuda, A., Kawakami, K., 2004. Malfunction of respiratory-related neuronal activity in Na+, K+-ATPase alpha2 subunit-deficient mice is attributable to abnormal Cl- homeostasis in brainstem neurons. J. Neurosci. 24, 10693–701.

Inglefield, J.R., Schwartz-Bloom, R.D., 1997. Confocal imaging of intracellular chloride in living brain slices: measurement of GABAA receptor activity. J. Neurosci. Methods 75, 127–135.

Inostroza, M., Brotons-Mas, J.R., Laurent, F., Cid, E., de la Prida, L.M., 2013. Specific impairment of "what-where-when" episodic-like memory in experimental models of temporal lobe epilepsy. J. Neurosci. 33, 17749–62.

Inoue, K., Ueno, S., Fukuda, A., 2004. Interaction of neuron-specific K^+-Cl^- cotransporter, KCC2, with brain-type creatine kinase. FEBS Lett. 564, 131–135.

Inoue, K., Yamada, J., Ueno, S., Fukuda, A., 2006. Brain-type creatine kinase activates neuron-specific K^+-Cl^- co-transporter KCC2. J. Neurochem. 96, 598–608.

Ishizuka, N., Weber, J., Amaral, D.G., 1990. Organization of intrahippocampal projections originating from CA3 pyramidal cells in the rat. J. Comp. Neurol. 295, 580–623.

Ivakine, E.A., Acton, B.A., Mahadevan, V., Ormond, J., Tang, M., Pressey, J.C., Huang, M.Y., Ng, D., Delpire, E., Salter, M.W., Woodin, M.A., McInnes, R.R., 2013. Neto2 is a KCC2 interacting protein required for neuronal Cl- regulation in hippocampal neurons. Proc. Natl. Acad. Sci. U. S. A. 110, 3561–6.

Jacobs, J., Levan, P., Châtillon, C.-E., Olivier, A., Dubeau, F., Gotman, J., 2009. High frequency oscillations in intracranial EEGs mark epileptogenicity rather than lesion type. Brain 132, 1022–37.

Jadhav, S.P., Kemere, C., German, P.W., Frank, L.M., 2012. Awake hippocampal sharp-wave ripples support spatial memory. Science 336, 1454–8.

Jedlicka, P., Deller, T., Gutkin, B.S., Backus, K.H., 2010. Activity-dependent intracellular chloride accumulation and diffusion controls GABAA receptor-mediated synaptic transmission. Hippocampus 21, n/a-n/a.

Jefferys, J.G.R., Menendez de la Prida, L., Wendling, F., Bragin, A., Avoli, M., Timofeev, I., Lopes da Silva, F.H., 2012. Mechanisms of physiological and epileptic HFO generation. Prog. Neurobiol. 98, 250–64.

Jennett, B., 1975. Who cares for head injuries? Br. Med. J. 3, 267–70.

Jessberger, S., Clark, R.E., Broadbent, N.J., Clemenson, G.D., Consiglio, A., Lie, D.C., Squire, L.R., Gage, F.H., 2009. Dentate gyrus-specific knockdown of adult neurogenesis impairs spatial and object recognition memory in adult rats. Learn. Mem. 16, 147–54.

Johnson, M.A., Weick, J.P., Pearce, R.A., Zhang, S.-C., 2007. Functional neural development from human embryonic stem cells: accelerated synaptic activity via astrocyte coculture. J. Neurosci. 27, 3069–77.

Jones, B.E., Moore, R.Y., 1977. Ascending projections of the locus coeruleus in the rat. II. Autoradiographic study. Brain Res. 127, 23–53.

Jourdain, P., Pavillon, N., Moratal, C., Boss, D., Rappaz, B., Depeursinge, C., Marquet, P., Magistretti, P.J., 2011. Determination of transmembrane water fluxes in neurons elicited by glutamate ionotropic receptors and by the cotransporters KCC2 and NKCC1: a digital holographic microscopy study. J. Neurosci. 31, 11846–54.

Jung, K.-Y., Kang, J.-K., Kim, J.H., Im, C.-H., Kim, K.H., Jung, H.-K., 2009. Spatiotemporospectral characteristics of scalp ictal EEG in mesial temporal lobe epilepsy with hippocampal sclerosis. Brain Res. 1287, 206–219.

Jung, M.W., McNaughton, B.L., 1993. Spatial selectivity of unit activity in the hippocampal granular layer. Hippocampus 3, 165–182.

Kahle, K.T., Khanna, A.R., Alper, S.L., Adragna, N.C., Lauf, P.K., Sun, D., Delpire, E., 2015. K-Cl cotransporters, cell volume homeostasis, and neurological disease. Trends Mol. Med. 21, 513–23.

Kahle, K.T., Merner, N.D., Friedel, P., Silayeva, L., Liang, B., Khanna, A., Shang, Y., Lachance-Touchette, P., Bourassa, C., Levert, A., Dion, P.A., Walcott, B., Spiegelman, D., Dionne-Laporte, A., Hodgkinson, A., Awadalla, P., Nikbakht, H., Majewski, J., Cossette, P., Deeb, T.Z., Moss, S.J., Medina, I., Rouleau, G.A., 2014. Genetically encoded impairment of neuronal KCC2 cotransporter function in human idiopathic generalized epilepsy. EMBO Rep. 15, 766–74.

Kahle, K.T., Rinehart, J., Lifton, R.P., 2010. Phosphoregulation of the Na-K-2Cl and K-Cl cotransporters by the WNK kinases. Biochim. Biophys. Acta 1802, 1150–8.

Kaila, K., 1994. Ionic basis of GABAA receptor channel function in the nervous system. Prog. Neurobiol. 42, 489–537.

Kaila, K., Lamsa, K., Smirnov, S., Taira, T., Voipio, J., 1997. Long-lasting GABA-mediated depolarization evoked by high-frequency stimulation in pyramidal neurons of rat hippocampal slice is attributable to a network-driven, bicarbonate-dependent K+ transient. J. Neurosci. 17, 7662–72.

Kaila, K., Price, T.J., Payne, J.A., Puskarjov, M., Voipio, J., 2014. Cation-chloride cotransporters in neuronal development, plasticity and disease. Nat. Rev. Neurosci. 15, 637–54.

Kaila, K., Voipio, J., 1987. Postsynaptic fall in intracellular pH induced by GABA-activated bicarbonate conductance. Nature 330, 163–165.

Kalkman, H.O., 2011. Alterations in the expression of neuronal chloride transporters may contribute to schizophrenia. Prog. Neuro-Psychopharmacology Biol. Psychiatry 35, 410–414.

Kamondi, A., Acsády, L., Wang, X.J., Buzsáki, G., 1998. Theta oscillations in somata and dendrites of hippocampal pyramidal cells in vivo: activity-dependent phase-precession of action potentials. Hippocampus 8, 244–61.

Karlócai, M.R., Kohus, Z., Káli, S., Ulbert, I., Szabó, G., Máté, Z., Freund, T.F., Gulyás, A.I., 2014. Physiological sharp wave-ripples and interictal events in vitro: what's the difference? Brain 137, 463–485.

Karlócai, M.R., Wittner, L., Tóth, K., Maglóczky, Z., Katarova, Z., Rásonyi, G., Erőss, L., Czirják, S., Halász, P., Szabó, G., Payne, J.A., Kaila, K., Freund, T.F., 2016. Enhanced expression of potassium-chloride cotransporter KCC2 in human temporal lobe epilepsy. Brain Struct. Funct. 221, 3601–3615.

Karschin, C., Wischmeyer, E., Preisig-Müller, R., Rajan, S., Derst, C., Grzeschik, K.-H., Daut, J., Karschin, A., 2001. Expression Pattern in Brain of TASK-1, TASK-3, and a Tandem Pore Domain K+ Channel Subunit, TASK-5, Associated with the Central Auditory Nervous System. Mol. Cell. Neurosci. 18, 632–648.

Kelley, M.R., Deeb, T.Z., Brandon, N.J., Dunlop, J., Davies, P.A., Moss, S.J., 2016. Compromising KCC2 transporter activity enhances the development of continuous seizure activity. Neuropharmacology 108, 103–110.

Kelly, T., Beck, H., 2017. Functional properties of granule cells with hilar basal dendrites in the epileptic dentate gyrus. Epilepsia 58, 160–171.

Kelsch, W., Hormuzdi, S., Straube, E., Lewen, A., Monyer, H., Misgeld, U., 2001. Insulin-like growth factor 1 and a cytosolic tyrosine kinase activate chloride outward transport during maturation of hippocampal neurons. J. Neurosci. 21, 8339–47.

Ketchum, K.A., Joiner, W.J., Sellers, A.J., Kaczmarek, L.K., Goldstein, S.A.N., 1995. A new family of outwardly rectifying potassium channel proteins with two pore domains in tandem. Nature 376, 690–695.

Khalilov, I., Dzhala, V., Ben-Ari, Y., Khazipov, R., 1999. Dual role of GABA in the neonatal rat hippocampus. Dev. Neurosci. 21, 310–9.

Khazipov, R., Khalilov, I., Tyzio, R., Morozova, E., Ben-Ari, Y., Holmes, G.L., 2004. Developmental changes in GABAergic actions and seizure susceptibility in the rat hippocampus. Eur. J. Neurosci. 19, 590–600.

Kheirbek, M.A., Drew, L.J., Burghardt, N.S., Costantini, D.O., Tannenholz, L., Ahmari, S.E., Zeng, H., Fenton, A.A., Hen, R., 2013. Differential control of learning and anxiety along the dorsoventral axis of the dentate gyrus. Neuron 77, 955–68.

Khirug, S., Huttu, K., Ludwig, A., Smirnov, S., Voipio, J., Rivera, C., Kaila, K., Khiroug, L., 2005. Distinct properties of functional KCC2 expression in immature mouse hippocampal neurons in culture and in acute slices. Eur. J. Neurosci. 21, 899–904.

Khoshkhoo, S., Vogt, D., Sohal, V.S., 2017. Dynamic, Cell-Type-Specific Roles for GABAergic Interneurons in a Mouse Model of Optogenetically Inducible Seizures. Neuron 93, 291–298.

King, D., Bronen, R.A., Spencer, D.D., Spencer, S.S., 1997. Topographic distribution of seizure onset and hippocampal atrophy: relationship between MRI and depth EEG. Electroencephalogr. Clin. Neurophysiol. 103, 692–7.

Kirmse, K., Kummer, M., Kovalchuk, Y., Witte, O.W., Garaschuk, O., Holthoff, K., 2015. GABA depolarizes immature neurons and inhibits network activity in the neonatal neocortex in vivo. Nat. Commun. 6, 7750.

Kitamura, A., Ishibashi, H., Watanabe, M., Takatsuru, Y., Brodwick, M., Nabekura, J., 2008. Sustained depolarizing shift of the GABA reversal potential by glutamate receptor activation in hippocampal neurons. Neurosci. Res. 62, 270–277.

Kitanishi, T., Ujita, S., Fallahnezhad, M., Kitanishi, N., Ikegaya, Y., Tashiro, A., 2015. Novelty-Induced Phase-Locked Firing to Slow Gamma Oscillations in the Hippocampus: Requirement of Synaptic Plasticity. Neuron 86, 1265–1276.

Kjelstrup, K.G., Tuvnes, F.A., Steffenach, H.-A., Murison, R., Moser, E.I., Moser, M.-B., 2002. Reduced fear expression after lesions of the ventral hippocampus. Proc. Natl. Acad. Sci. U. S. A. 99, 10825–30.

Klausberger, T., Somogyi, P., 2008. Neuronal diversity and temporal dynamics: the unity of hippocampal circuit operations. Science 321, 53–7.

Klein, P.M., Lu, A.C., Harper, M.E., McKown, H.M., Morgan, J.D., Beenhakker, M.P., 2018. Tenuous Inhibitory GABAergic Signaling in the Reticular Thalamus. J. Neurosci. 38, 1232–1248.

Knierim, J.J., Zhang, K., 2012. Attractor dynamics of spatially correlated neural activity in the limbic system. Annu. Rev. Neurosci. 35, 267–85.

Kohara, K., Pignatelli, M., Rivest, A.J., Jung, H.-Y., Kitamura, T., Suh, J., Frank, D., Kajikawa, K., Mise, N., Obata, Y., Wickersham, I.R., Tonegawa, S., 2014. Cell type-specific genetic and optogenetic tools reveal hippocampal CA2 circuits. Nat. Neurosci. 17, 269–79.

Köhler, C., 1986. Cytochemical architecture of the entorhinal area. Adv. Exp. Med. Biol. 203, 83–98.

Kourdougli, N., Pellegrino, C., Renko, J.-M., Khirug, S., Chazal, G., Kukko-Lukjanov, T.-K., Lauri, S.E., Gaiarsa, J.-L., Zhou, L., Peret, A., Castrén, E., Tuominen, R.K., Crépel, V., Rivera, C., 2017. Depolarizing γ-aminobutyric acid contributes to glutamatergic network rewiring in epilepsy. Ann. Neurol. 81, 251–265.

Kramis, R., Vanderwolf, C.H., Bland, B.H., 1975. Two types of hippocampal rhythmical slow activity in both the rabbit and the rat: Relations to behavior and effects of atropine, diethyl ether, urethane, and pentobarbital. Exp. Neurol. 49, 58–85.

Kron, M.M., Zhang, H., Parent, J.M., 2010. The developmental stage of dentate granule cells dictates their contribution to seizure-induced plasticity. J. Neurosci. 30, 2051–9.

Krook-Magnuson, E., Armstrong, C., Bui, A., Lew, S., Oijala, M., Soltesz, I., 2015. In vivo evaluation of the dentate gate theory in epilepsy. J. Physiol. 593, 2379–88.

Krueppel, R., Remy, S., Beck, H., 2011. Dendritic Integration in Hippocampal Dentate Granule Cells. Neuron 71, 512–528.

Kudrimoti, H.S., Barnes, C.A., McNaughton, B.L., 1999. Reactivation of hippocampal cell assemblies: effects of behavioral state, experience, and EEG dynamics. J. Neurosci. 19, 4090–101.

Kuner, T., Augustine, G.J., 2000. A Genetically Encoded Ratiometric Indicator for Chloride: Capturing Chloride Transients in Cultured Hippocampal Neurons. Neuron 27, 447–459.

Kursan, S., McMillen, T.S., Beesetty, P., Dias-Junior, E., Almutairi, M.M., Sajib, A.A., Kozak, J.A., Aguilar-Bryan, L., Di Fulvio, M., 2017. The neuronal K+Cl- co-transporter 2 (Slc12a5) modulates insulin secretion. Sci. Rep. 7, 1732.

Laffray, S., Tan, K., Dulluc, J., Bouali-Benazzouz, R., Calver, A.R., Nagy, F., Landry, M., 2007. Dissociation and trafficking of rat GABAB receptor heterodimer upon chronic capsaicin stimulation. Eur. J. Neurosci. 25, 1402–1416.

Larson, J., Wong, D., Lynch, G., 1986. Patterned stimulation at the theta frequency is optimal for the induction of hippocampal long-term potentiation. Brain Res. 368, 347–350.

Lasztóczi, B., Klausberger, T., 2014. Layer-Specific GABAergic Control of Distinct Gamma Oscillations in the CA1 Hippocampus. Neuron 81, 1126–1139.

Lauf, P.K., Theg, B.E., 1980. A chloride dependent K+ flux induced by N-ethylmaleimide in genetically low K+ sheep and goat erythrocytes. Biochem. Biophys. Res. Commun. 92, 1422–1428.

Laurent, F., Brotons-Mas, J.R., Cid, E., Lopez-Pigozzi, D., Valero, M., Gal, B., de la Prida, L.M., 2015. Proximodistal structure of theta coordination in the dorsal hippocampus of epileptic rats. J. Neurosci. 35, 4760–75.

Lee, A.K., Wilson, M.A., 2002. Memory of Sequential Experience in the Hippocampus during Slow Wave Sleep. Neuron 36, 1183–1194.

Lee, D.J., Izadi, A., Melnik, M., Seidl, S., Echeverri, A., Shahlaie, K., Gurkoff, G.G., 2017. Stimulation of the medial septum improves performance in spatial learning following pilocarpine-induced status epilepticus. Epilepsy Res. 130, 53–63.

Lee, H.H.C., Deeb, T.Z., Walker, J.A., Davies, P.A., Moss, S.J., 2011. NMDA receptor activity downregulates KCC2 resulting in depolarizing GABAA receptor–mediated currents. Nat. Neurosci. 14, 736–743.

Lee, H.H.C., Jurd, R., Moss, S.J., 2010. Tyrosine phosphorylation regulates the membrane trafficking of the potassium chloride co-transporter KCC2. Mol. Cell. Neurosci. 45, 173–9.

Lee, H.H.C., Walker, J.A., Williams, J.R., Goodier, R.J., Payne, J.A., Moss, S.J., 2007. Direct protein kinase C-dependent phosphorylation regulates the cell surface stability and activity of the potassium chloride cotransporter KCC2. J. Biol. Chem. 282, 29777–84.

Lee, I., Rao, G., Knierim, J.J., 2004. A Double Dissociation between Hippocampal Subfields: Differential Time Course of CA3 and CA1 Place Cells for Processing Changed Environments. Neuron 42, 803–815.

Lemonnier, E., Ben-Ari, Y., 2010. The diuretic bumetanide decreases autistic behaviour in five infants treated during 3 months with no side effects. Acta Paediatr. 99, 1885–1888.

Lemonnier, E., Degrez, C., Phelep, M., Tyzio, R., Josse, F., Grandgeorge, M., Hadjikhani, N., Ben-Ari, Y., 2012. A randomised controlled trial of bumetanide in the treatment of autism in children. Transl. Psychiatry 2, e202.

Lenck-Santini, P.-P., Holmes, G.L., 2008. Altered phase precession and compression of temporal sequences by place cells in epileptic rats. J. Neurosci. 28, 5053–62.

Lengyel, M., Czirják, G., Enyedi, P., n.d. Heterodimerization of TREK-1 and TREK-2 Subunits Formation of Functional Heterodimers by TREK-1 and TREK-2 Two-pore Domain Potassium Channel Subunits.

Lesage, F., 2003. Pharmacology of neuronal background potassium channels. Neuropharmacology 44, 1–7.

Lesage, F., Guillemare, E., Fink, M., Duprat, F., Lazdunski, M., Romey, G., Barhanin, J., 1996a. TWIK-1, a ubiquitous human weakly inward rectifying K+ channel with a novel structure. EMBO J. 15, 1004–11.

Lesage, F., Guillemare, E., Fink, M., Duprat, F., Lazdunski, M., Romey, G., Barhanin, J., 1996b. A pH-sensitive yeast outward rectifier K+ channel with two pore domains and novel gating properties. J. Biol. Chem. 271, 4183–7.

Leutgeb, J.K., Leutgeb, S., Moser, M.-B., Moser, E.I., 2007. Pattern separation in the dentate gyrus and CA3 of the hippocampus. Science 315, 961–6.

Lewin, N., Aksay, E., Clancy, C.E., 2012. Computational modeling reveals dendritic origins of GABA(A)-mediated excitation in CA1 pyramidal neurons. PLoS One 7, e47250.

Li, H., Khirug, S., Cai, C., Ludwig, A., Blaesse, P., Kolikova, J., Afzalov, R., Coleman, S.K., Lauri, S., Airaksinen, M.S.,

Keinänen, K., Khiroug, L., Saarma, M., Kaila, K., Rivera, C., 2007. KCC2 interacts with the dendritic cytoskeleton to promote spine development. Neuron 56, 1019–33.

Li, X.-G., Somogyi, P., Ylinen, A., Buzsáki, G., 1994. The hippocampal CA3 network: An in vivo intracellular labeling study. J. Comp. Neurol. 339, 181–208.

Li, X., Zhou, J., Chen, Z., Chen, S., Zhu, F., Zhou, L., 2008. Long-term expressional changes of Na+–K+–Cl− co-transporter 1 (NKCC1) and K+–Cl− co-transporter 2 (KCC2) in CA1 region of hippocampus following lithium-pilocarpine induced status epilepticus (PISE). Brain Res. 1221, 141–146.

Liabeuf, S., Stuhl-Gourmand, L., Gackière, F., Mancuso, R., Sanchez Brualla, I., Marino, P., Brocard, F., Vinay, L., 2017. Prochlorperazine Increases KCC2 Function and Reduces Spasticity after Spinal Cord Injury. J. Neurotrauma 34, 3397–3406.

Lillis, K.P., Kramer, M.A., Mertz, J., Staley, K.J., White, J.A., 2012. Pyramidal cells accumulate chloride at seizure onset. Neurobiol. Dis. 47, 358–366.

Llano, O., Smirnov, S., Soni, S., Golubtsov, A., Guillemin, I., Hotulainen, P., Medina, I., Nothwang, H.G., Rivera, C., Ludwig, A., 2015. KCC2 regulates actin dynamics in dendritic spines via interaction with β-PIX. J. Cell Biol. 209, 671–86.

Lopez-Pigozzi, D., Laurent, F., Brotons-Mas, J.R., Valderrama, M., Valero, M., Fernandez-Lamo, I., Cid, E., Gomez-Dominguez, D., Gal, B., Menendez de la Prida, L., 2016. Altered Oscillatory Dynamics of CA1 Parvalbumin Basket Cells during Theta-Gamma Rhythmopathies of Temporal Lobe Epilepsy. eNeuro 3.

Lorente De Nó, R., 1934. Studies on the structure of the cerebral cortex. II. Continuation of the study of the ammonic system. J. für Psychol. und Neurol. 46, 113–177.

Lothman, E.W., Stringer, J.L., Bertram, E.H., 1992. The dentate gyrus as a control point for seizures in the hippocampus and beyond. Epilepsy Res. Suppl. 7, 301–13.

Loucif, A.J.C., Saintot, P.-P., Liu, J., Antonio, B.M., Zellmer, S.G., Yoger, K., Veale, E.L., Wilbrey, A., Omoto, K., Cao, L., Gutteridge, A., Castle, N.A., Stevens, E.B., Mathie, A., 2017. GI-530159, a novel, selective, mechanosensitive two-pore-domain potassium (K_{2P}) channel opener, reduces rat dorsal root ganglion neuron excitability. Br. J. Pharmacol.

Lowenstein, D.H., Thomas, M.J., Smith, D.H., McIntosh, T.K., 1992. Selective vulnerability of dentate hilar neurons following traumatic brain injury: a potential mechanistic link between head trauma and disorders of the hippocampus. J. Neurosci. 12, 4846–53.

Ludwig, A., Uvarov, P., Pellegrino, C., Thomas-Crusells, J., Schuchmann, S., Saarma, M., Airaksinen, M.S., Rivera, C., 2011. Neurturin evokes MAPK-dependent upregulation of Egr4 and KCC2 in developing neurons. Neural Plast. 2011, 1–8.

Ma, L., Zhang, X., Zhou, M., Chen, H., 2012. Acid-sensitive TWIK and TASK two-pore domain potassium channels change ion selectivity and become permeable to sodium in extracellular acidification. J. Biol. Chem. 287, 37145–53.

MacAulay, N., Zeuthen, T., 2010. Water transport between CNS compartments: contributions of aquaporins and cotransporters. Neuroscience 168, 941–956.

MacDonald, C.J., Lepage, K.Q., Eden, U.T., Eichenbaum, H., 2011. Hippocampal "Time Cells" Bridge the Gap in Memory for Discontiguous Events. Neuron 71, 737–749.

Maglóczky, Z., Freund, T.F., 2005. Impaired and repaired inhibitory circuits in the epileptic human hippocampus. Trends Neurosci. 28, 334–340.

Mahadevan, V., Khademullah, C.S., Dargaei, Z., Chevrier, J., Uvarov, P., Kwan, J., Bagshaw, R.D., Pawson, T., Emili, A., De Koninck, Y., Anggono, V., Airaksinen, M., Woodin, M.A., 2017. Native KCC2 interactome reveals PACSIN1 as a critical regulator of synaptic inhibition. Elife 6.

Mahadevan, V., Pressey, J.C., Acton, B.A., Uvarov, P., Huang, M.Y., Chevrier, J., Puchalski, A., Li, C.M., Ivakine, E.A., Airaksinen, M.S., Delpire, E., McInnes, R.R., Woodin, M.A., 2014. Kainate receptors coexist in a functional complex with KCC2 and regulate chloride homeostasis in hippocampal neurons. Cell Rep. 7, 1762–70.

Maingret, F., Lauritzen, I., Patel, A.J., Heurteaux, C., Reyes, R., Lesage, F., Lazdunski, M., Honoré, E., 2000. TREK-1 is a heat-activated background K(+) channel. EMBO J. 19, 2483–91.

Maingret, N., Girardeau, G., Todorova, R., Goutierre, M., Zugaro, M., 2016. Hippocampo-cortical coupling mediates memory consolidation during sleep. Nat Neurosci 19, 959–964.

Makino, H., Malinow, R., 2009. AMPA receptor incorporation into synapses during LTP: the role of lateral movement and exocytosis. Neuron 64, 381–90.

Marcelin, B., Chauvière, L., Becker, A., Migliore, M., Esclapez, M., Bernard, C., 2009. h channel-dependent deficit of theta oscillation resonance and phase shift in temporal lobe epilepsy. Neurobiol. Dis. 33, 436–447.

Markkanen, M., Karhunen, T., Llano, O., Ludwig, A., Rivera, C., Uvarov, P., Airaksinen, M.S., 2014. Distribution of neuronal KCC2a and KCC2b isoforms in mouse CNS. J. Comp. Neurol. 522, 1897–1914.

Markkanen, M., Ludwig, A., Khirug, S., Pryazhnikov, E., Soni, S., Khiroug, L., Delpire, E., Rivera, C., Airaksinen, M.S., Uvarov, P., 2017. Implications of the N-terminal heterogeneity for the neuronal K-Cl cotransporter KCC2 function. Brain Res. 1675, 87–101.

Markkanen, M., Uvarov, P., Airaksinen, M.S., 2008. Role of upstream stimulating factors in the transcriptional regulation of the neuron-specific K–Cl cotransporter KCC2. Brain Res. 1236, 8–15.

Markova, O., Mukhtarov, M., Real, E., Jacob, Y., Bregestovski, P., 2008. Genetically encoded chloride indicator with improved sensitivity. J. Neurosci. Methods 170, 67–76.

Martin, M.S., Dutt, K., Papale, L.A., Dubé, C.M., Dutton, S.B., de Haan, G., Shankar, A., Tufik, S., Meisler, M.H., Baram, T.Z., Goldin, A.L., Escayg, A., 2010. Altered function of the SCN1A voltage-gated sodium channel leads to gamma-aminobutyric acid-ergic (GABAergic) interneuron abnormalities. J. Biol. Chem. 285, 9823–34.

Mathern, G.W., Kuhlman, P.A., Mendoza, D., Pretorius, J.K., 1997. Human fascia dentata anatomy and hippocampal neuron densities differ depending on the epileptic syndrome and age at first seizure. J. Neuropathol. Exp. Neurol. 56, 199–212.

McHugh, T.J., Jones, M.W., Quinn, J.J., Balthasar, N., Coppari, R., Elmquist, J.K., Lowell, B.B., Fanselow, M.S., Wilson, M.A., Tonegawa, S., 2007. Dentate gyrus NMDA receptors mediate rapid pattern separation in the hippocampal network. Science 317, 94–9.

McNaughton, N., Morris, R.G.M., 1987. Chlordiazepoxide, an anxiolytic benzodiazepine, impairs place navigation in rats. Behav. Brain Res. 24, 39–46.

McNaughton, N., Ruan, M., Woodnorth, M.-A., 2006. Restoring theta-like rhythmicity in rats restores initial learning in the Morris water maze. Hippocampus 16, 1102–1110.

Medina, I., Friedel, P., Rivera, C., Kahle, K.T., Kourdougli, N., Uvarov, P., Pellegrino, C., 2014. Current view on the functional regulation of the neuronal K(+)-Cl(-) cotransporter KCC2. Front. Cell. Neurosci. 8, 27.

Menendez de la Prida, L., Gal, B., 2004. Synaptic contributions to focal and widespread spatiotemporal dynamics in the isolated rat subiculum in vitro. J. Neurosci. 24, 5525–36.

Mercado, A., Broumand, V., Zandi-Nejad, K., Enck, A.H., Mount, D.B., 2006. A C-terminal domain in KCC2 confers constitutive K+-Cl- cotransport. J. Biol. Chem. 281, 1016–26.

Mercado, A., Gamba, G., Mount, D.B., 2004. Molecular physiology of mammalian K(+)-Cl- cotransporters. Adv. Exp. Med. Biol. 559, 29–41.

Michishita, M., Ikeda, T., Nakashiba, T., Ogawa, M., Tashiro, K., Honjo, T., Doi, K., Itohara, S., Endo, S., 2004. Expression of Btcl2, a novel member of Btcl gene family, during development of the central nervous system. Dev. Brain Res. 153, 135–142.

Miles, R., Tóth, K., Gulyás, A.I., Hájos, N., Freund, T.F., 1996. Differences between Somatic and Dendritic Inhibition in the Hippocampus. Neuron 16, 815–823.

Misgeld, U., Frotscher, M., 1986. Postsynaptic-gabaergic inhibition of non-pyramidal neurons in the guinea-pig hippocampus. Neuroscience 19, 193–206.

Mitchell, S.J., Ranck, J.B., 1980. Generation of theta rhythm in medial entorhinal cortex of freely moving rats. Brain Res. 189, 49–66.

Mitchell, S.J., Rawlins, J.N., Steward, O., Olton, D.S., 1982. Medial septal area lesions disrupt theta rhythm and cholinergic staining in medial entorhinal cortex and produce impaired radial arm maze behavior in rats. J. Neurosci. 2, 292–302.

Mizoguchi, Y., Ishibashi, H., Nabekura, J., 2003. The action of BDNF on GABA(A) currents changes from potentiating to suppressing during maturation of rat hippocampal CA1 pyramidal neurons. J. Physiol. 548, 703–9.

Mizumori, S.J.Y., Perez, G.M., Alvarado, M.C., Barnes, C.A., McNaughton, B.L., 1990. Reversible inactivation of the medial septum differentially affects two forms of learning in rats. Brain Res. 528, 12–20.

Mizuseki, K., Diba, K., Pastalkova, E., Buzsáki, G., 2011. Hippocampal CA1 pyramidal cells form functionally distinct sublayers. Nat. Neurosci. 14, 1174–81.

Moore-Hoon, M.L. and, Turner, R.J., 2000. The Structural Unit of the Secretory Na+−K+−2Cl- Cotransporter (NKCC1) Is a Homodimer.

Moore, R.Y., Halaris, A.E., 1975. Hippocampal innervation by serotonin neurons of the midbrain raphe in the rat. J. Comp. Neurol. 164, 171–183.

Mori, M., Gähwiler, B.H., Gerber, U., 2007. Recruitment of an inhibitory hippocampal network after bursting in a single granule cell. Proc. Natl. Acad. Sci. U. S. A. 104, 7640–5.

Moser, E., Moser, M.B., Andersen, P., 1993. Spatial learning impairment parallels the magnitude of dorsal hippocampal lesions, but is hardly present following ventral lesions. J. Neurosci. 13, 3916–25.

Mount, D.B., Delpire, E., Gamba, G., Hall, A.E., Poch, E., Hoover, R.S., Hebert, S.C., 1998. The electroneutral cation-chloride cotransporters. J. Exp. Biol. 201.

Mrowiec, T., Schwappach, B., 2006. 14-3-3 proteins in membrane protein transport. Biol. Chem. 387, 1227–1236.

Muñoz, A., Méndez, P., DeFelipe, J., Alvarez-Leefmans, F.J., 2007. Cation-Chloride Cotransporters and GABA-ergic Innervation in the Human Epileptic Hippocampus. Epilepsia 48, 663–673.

Nádasdy, Z., Hirase, H., Czurkó, A., Csicsvari, J., Buzsáki, G., 1999. Replay and time compression of recurring spike sequences in the hippocampus. J. Neurosci. 19, 9497–507.

Nakazawa, K., Quirk, M.C., Chitwood, R.A., Watanabe, M., Yeckel, M.F., Sun, L.D., Kato, A., Carr, C.A., Johnston, D., Wilson, M.A., Tonegawa, S., 2002. Requirement for hippocampal CA3 NMDA receptors in associative memory recall. Science 297, 211–8.

Neunuebel, J.P., Knierim, J.J., 2014. CA3 retrieves coherent representations from degraded input: direct evidence for CA3 pattern completion and dentate gyrus pattern separation. Neuron 81, 416–27.

Nokia, M.S., Gureviciene, I., Waselius, T., Tanila, H., Penttonen, M., 2017. Hippocampal electrical stimulation disrupts associative learning when targeted at dentate spikes. J. Physiol. 595, 4961–4971.

O'Keefe, J., Dostrovsky, J., 1971. The hippocampus as a spatial map. Preliminary evidence from unit activity in the freely-moving rat. Brain Res. 34, 171–175.

O'Keefe, J., Nadel, L., 1979. Précis of O'Keefe & Nadel's The hippocampus as a cognitive map. Behav. Brain Sci. 2, 487–494.

O'Kelly, I., Butler, M.H., Zilberberg, N., Goldstein, S.A.N., 2002. Forward Transport: 14-3-3 Binding Overcomes Retention in Endoplasmic Reticulum by Dibasic Signals. Cell 111, 577–588.

O'Reilly, R.C., McClelland, J.L., 1994. Hippocampal conjunctive encoding, storage, and recall: Avoiding a trade-off. Hippocampus 4, 661–682.

Okaty, B.W., Miller, M.N., Sugino, K., Hempel, C.M., Nelson, S.B., 2009. Transcriptional and electrophysiological maturation of neocortical fast-spiking GABAergic interneurons. J. Neurosci. 29, 7040–52.

Pallud, J., Le Van Quyen, M., Bielle, F., Pellegrino, C., Varlet, P., Cresto, N., Baulac, M., Duyckaerts, C., Kourdougli, N.,

Chazal, G., Devaux, B., Rivera, C., Miles, R., Capelle, L., Huberfeld, G., 2014. Cortical GABAergic excitation contributes to epileptic activities around human glioma. Sci. Transl. Med. 6, 244ra89.

Palma, E., Amici, M., Sobrero, F., Spinelli, G., Di Angelantonio, S., Ragozzino, D., Mascia, A., Scoppetta, C., Esposito, V., Miledi, R., Eusebi, F., 2006. Anomalous levels of Cl- transporters in the hippocampal subiculum from temporal lobe epilepsy patients make GABA excitatory. Proc. Natl. Acad. Sci. U. S. A. 103, 8465–8.

Parent, J.M., 2007. Adult neurogenesis in the intact and epileptic dentate gyrus. Prog. Brain Res. 163, 529–817.

Parra, P., Gulyás, A.I., Miles, R., 1998. How Many Subtypes of Inhibitory Cells in the Hippocampus? Neuron 20, 983–993.

Pasquier, D.A., Reinoso-Suarez, F., 1976. Direct projections from hypothalamus to hippocampus in the rat demonstrated by retrograde transport of horseradish peroxidase. Brain Res. 108, 165–169.

Pathak, H.R., Weissinger, F., Terunuma, M., Carlson, G.C., Hsu, F.-C., Moss, S.J., Coulter, D.A., 2007. Disrupted dentate granule cell chloride regulation enhances synaptic excitability during development of temporal lobe epilepsy. J. Neurosci. 27, 14012–22.

Patton, P.E., McNaughton, B., 1995. Connection matrix of the hippocampal formation: I. The dentate gyrus. Hippocampus 5, 245–286.

Payne, J.A., 1997. Functional characterization of the neuronal-specific K-Cl cotransporter: implications for [K+]o regulation. Am. J. Physiol. 273, C1516-25.

Payne, J.A., Rivera, C., Voipio, J., Kaila, K., 2003. Cation–chloride co-transporters in neuronal communication, development and trauma. Trends Neurosci. 26, 199–206.

Payne, J.A., Stevenson, T.J., Donaldson, L.F., 1996. Molecular characterization of a putative K-Cl cotransporter in rat brain. A neuronal-specific isoform. J. Biol. Chem. 271, 16245–52.

Pellegrino, C., Gubkina, O., Schaefer, M., Becq, H., Ludwig, A., Mukhtarov, M., Chudotvorova, I., Corby, S., Salyha, Y., Salozhin, S., Bregestovski, P., Medina, I., 2011. Knocking down of the KCC2 in rat hippocampal neurons increases intracellular chloride concentration and compromises neuronal survival. J. Physiol. 589, 2475–96.

Pentkowski, N.S., Blanchard, D.C., Lever, C., Litvin, Y., Blanchard, R.J., 2006. Effects of lesions to the dorsal and ventral hippocampus on defensive behaviors in rats. Eur. J. Neurosci. 23, 2185–2196.

Penttonen, M., Kamondi, A., Sik, A., Acsády, L., Buzsáki, G., 1997. Feed-forward and feed-back activation of the dentate gyrus in vivo during dentate spikes and sharp wave bursts. Hippocampus 7, 437–50.

PETSCHE, H., STUMPF, C., GOGOLAK, G., 1962. [The significance of the rabbit's septum as a relay station between the midbrain and the hippocampus. I. The control of hippocampus arousal activity by the septum cells]. Electroencephalogr. Clin. Neurophysiol. 14, 202–11.

Peyrache, A., Battaglia, F.P., Destexhe, A., 2011. Inhibition recruitment in prefrontal cortex during sleep spindles and gating of hippocampal inputs. Proc. Natl. Acad. Sci. U. S. A. 108, 17207–12.

Picot, M.-C., Baldy-Moulinier, M., Daurs, J.-P., Dujols, P., Crespel, A., 2008. The prevalence of epilepsy and pharmacoresistant epilepsy in adults: A population-based study in a Western European country. Epilepsia 49, 1230–1238.

Plant, L.D., 2012. A Role for K2P Channels in the Operation of Somatosensory Nociceptors. Front. Mol. Neurosci. 5, 21.

Plotkin, M.D., Kaplan, M.R., Peterson, L.N., Gullans, S.R., Hebert, S.C., Delpire, E., 1997. Expression of the Na(+)-K(+)-2Cl- cotransporter BSC2 in the nervous system. Am. J. Physiol. 272, C173-83.

Pollema-Mays, S.L., Centeno, M.V., Ashford, C.J., Apkarian, A.V., Martina, M., 2013. Expression of background potassium channels in rat DRG is cell-specific and down-regulated in a neuropathic pain model. Mol. Cell. Neurosci. 57, 1–9.

Pressey, J.C., Mahadevan, V., Khademullah, C.S., Dargaei, Z., Chevrier, J., Ye, W., Huang, M., Chauhan, A.K., Meas, S.J., Uvarov, P., Airaksinen, M.S., Woodin, M.A., 2017. A kainate receptor subunit promotes the recycling of the neuron-specific K+-Cl- co-transporter KCC2 in hippocampal neurons. J. Biol. Chem. 292, 6190–6201.

Price, G.D., Trussell, L.O., 2006. Estimate of the chloride concentration in a central glutamatergic terminal: a gramicidin perforated-patch study on the calyx of Held. J. Neurosci. 26, 11432–6.

Price, T.J., Cervero, F., de Koninck, Y., 2005. Role of cation-chloride-cotransporters (CCC) in pain and hyperalgesia. Curr. Top. Med. Chem. 5, 547–55.

Puskarjov, M., Ahmad, F., Kaila, K., Blaesse, P., 2012. Activity-dependent cleavage of the K-Cl cotransporter KCC2 mediated by calcium-activated protease calpain. J. Neurosci. 32, 11356–64.

Puskarjov, M., Ahmad, F., Khirug, S., Sivakumaran, S., Kaila, K., Blaesse, P., 2015. BDNF is required for seizure-induced but not developmental up-regulation of KCC2 in the neonatal hippocampus. Neuropharmacology 88, 103–109.

Puskarjov, M., Seja, P., Heron, S.E., Williams, T.C., Ahmad, F., Iona, X., Oliver, K.L., Grinton, B.E., Vutskits, L., Scheffer, I.E., Petrou, S., Blaesse, P., Dibbens, L.M., Berkovic, S.F., Kaila, K., 2014. A variant of KCC2 from patients with febrile seizures impairs neuronal Cl- extrusion and dendritic spine formation. EMBO Rep. 15, 723–9.

Rajan, S., Preisig-Müller, R., Wischmeyer, E., Nehring, R., Hanley, P.J., Renigunta, V., Musset, B., Schlichthörl, G., Derst, C., Karschin, A., Daut, J., 2002. Interaction with 14-3-3 proteins promotes functional expression of the potassium channels TASK-1 and TASK-3. J. Physiol. 545, 13–26.

Ren, D., 2011. Sodium leak channels in neuronal excitability and rhythmic behaviors. Neuron 72, 899–911.

Represa, A., Jorquera, I., le gal la Salle, G., Ben-Ari, Y., 1993. Epilepsy induced collateral sprouting of hippocampal mossy fibers: Does it induce the development of ectopic synapses with granule cell dendrites? Hippocampus 3, 257–268.

Rheims, S., Holmgren, C.D., Chazal, G., Mulder, J., Harkany, T., Zilberter, T., Zilberter, Y., 2009. GABA action in immature neocortical neurons directly depends on the availability of ketone bodies. J. Neurochem. 110, 1330–1338.

Rinehart, J., Maksimova, Y.D., Tanis, J.E., Stone, K.L., Hodson, C.A., Zhang, J., Risinger, M., Pan, W., Wu, D., Colangelo, C.M., Forbush, B., Joiner, C.H., Gulcicek, E.E., Gallagher, P.G., Lifton, R.P., 2009. Sites of regulated phosphorylation that control K-Cl cotransporter activity. Cell 138, 525–36.

Rinke, I., Artmann, J., Stein, V., 2010. ClC-2 voltage-gated channels constitute part of the background conductance and assist chloride extrusion. J. Neurosci. 30, 4776–86.

Rivera, C., Li, H., Thomas-Crusells, J., Lahtinen, H., Viitanen, T., Nanobashvili, A., Kokaia, Z., Airaksinen, M.S., Voipio, J., Kaila, K., Saarma, M., 2002. BDNF-induced TrkB activation down-regulates the K+-Cl- cotransporter KCC2 and impairs neuronal Cl- extrusion. J. Cell Biol. 159, 747–52.

Rivera, C., Voipio, J., Kaila, K., 2005. Two developmental switches in GABAergic signalling: the K+-Cl- cotransporter KCC2 and carbonic anhydrase CAVII. J. Physiol. 562, 27–36.

Rivera, C., Voipio, J., Payne, J.A., Ruusuvuori, E., Lahtinen, H., Lamsa, K., Pirvola, U., Saarma, M., Kaila, K., 1999. The K+/Cl− co-transporter KCC2 renders GABA hyperpolarizing during neuronal maturation. Nature 397, 251–255.

Robbe, D., Buzsáki, G., 2009. Alteration of theta timescale dynamics of hippocampal place cells by a cannabinoid is associated with memory impairment. J. Neurosci. 29, 12597–605.

Roux, L., Hu, B., Eichler, R., Stark, E., Buzsáki, G., 2017. Sharp wave ripples during learning stabilize the hippocampal spatial map. Nat. Neurosci. 20, 845–853.

Russell, J.M., 2000. Sodium-Potassium-Chloride Cotransport. Physiol. Rev. 80, 211–276.

Rust, M.B., Alper, S.L., Rudhard, Y., Shmukler, B.E., Vicente, R., Brugnara, C., Trudel, M., Jentsch, T.J., Hübner, C.A., 2007. Disruption of erythroid K-Cl cotransporters alters erythrocyte volume and partially rescues erythrocyte dehydration in SAD mice. J. Clin. Invest. 117, 1708–17.

Ruusuvuori, E., Huebner, A.K., Kirilkin, I., Yukin, A.Y., Blaesse, P., Helmy, M., Kang, H.J., El Muayed, M., Hennings, J.C., Voipio, J., Šestan, N., Hübner, C.A., Kaila, K., 2013. Neuronal carbonic anhydrase VII provides GABAergic excitatory drive to exacerbate febrile seizures. EMBO J. 32, 2275–86.

Ruusuvuori, E., Kirilkin, I., Pandya, N., Kaila, K., 2010. Spontaneous network events driven by depolarizing GABA action in neonatal hippocampal slices are not attributable to deficient mitochondrial energy metabolism. J. Neurosci.

30, 15638–42.

Saitsu, H., Watanabe, M., Akita, T., Ohba, C., Sugai, K., Ong, W.P., Shiraishi, H., Yuasa, S., Matsumoto, H., Beng, K.T., Saitoh, S., Miyatake, S., Nakashima, M., Miyake, N., Kato, M., Fukuda, A., Matsumoto, N., 2016. Impaired neuronal KCC2 function by biallelic SLC12A5 mutations in migrating focal seizures and severe developmental delay. Sci. Rep. 6, 30072.

Sakurai, Y., 2002. Coding of auditory temporal and pitch information by hippocampal individual cells and cell assemblies in the rat. Neuroscience 115, 1153–1163.

Sawada, M., Sato, M., 1975. THE EFFECT OF DIMETHYL SULFOXIDE ON THE NEURONAL EXCITABILITY AND CHOLINERGIC TRANSMISSION IN *APLYSIA* GANGLION CELLS*. Ann. N. Y. Acad. Sci. 243, 337–357.

Scharfman, H.E., 1995. Electrophysiological evidence that dentate hilar mossy cells are excitatory and innervate both granule cells and interneurons. J. Neurophysiol. 74, 179–94.

Scharfman, H.E., 1994. Synchronization of area CA3 hippocampal pyramidal cells and non-granule cells of the dentate gyrus in bicuculline-treated rat hippocampal slices. Neuroscience 59, 245–57.

Scharfman, H.E., Sollas, A.L., Berger, R.E., Goodman, J.H., 2003. Electrophysiological Evidence of Monosynaptic Excitatory Transmission Between Granule Cells After Seizure-Induced Mossy Fiber Sprouting. J. Neurophysiol. 90, 2536–2547.

Schevon, C.A., Trevelyan, A.J., Schroeder, C.E., Goodman, R.R., McKhann, G., Emerson, R.G., Emerson, R.G., 2009. Spatial characterization of interictal high frequency oscillations in epileptic neocortex. Brain 132, 3047–59.

Schlesiger, M.I., Cannova, C.C., Boublil, B.L., Hales, J.B., Mankin, E.A., Brandon, M.P., Leutgeb, J.K., Leibold, C., Leutgeb, S., 2015. The medial entorhinal cortex is necessary for temporal organization of hippocampal neuronal activity. Nat. Neurosci. 18, 1123–32.

Schlingloff, D., Káli, S., Freund, T.F., Hájos, N., Gulyás, A.I., 2014. Mechanisms of sharp wave initiation and ripple generation. J. Neurosci. 34, 11385–98.

Schomburg, E.W., Fernández-Ruiz, A., Mizuseki, K., Berényi, A., Anastassiou, C.A., Koch, C., Buzsáki, G., 2014. Theta phase segregation of input-specific gamma patterns in entorhinal-hippocampal networks. Neuron 84, 470–85.

Schuchmann, S., Schmitz, D., Rivera, C., Vanhatalo, S., Salmen, B., Mackie, K., Sipilä, S.T., Voipio, J., Kaila, K., 2006. Experimental febrile seizures are precipitated by a hyperthermia-induced respiratory alkalosis. Nat. Med. 12, 817–23.

SCOVILLE, W.B., MILNER, B., 1957. Loss of recent memory after bilateral hippocampal lesions. J. Neurol. Neurosurg. Psychiatry 20, 11–21.

Sedmak, G., Jovanov-Milošević, N., Puskarjov, M., Ulamec, M., Krušlin, B., Kaila, K., Judaš, M., 2016. Developmental Expression Patterns of KCC2 and Functionally Associated Molecules in the Human Brain. Cereb. Cortex 26, 4574–4589.

Seja, P., Schonewille, M., Spitzmaul, G., Badura, A., Klein, I., Rudhard, Y., Wisden, W., Hübner, C.A., De Zeeuw, C.I., Jentsch, T.J., 2012. Raising cytosolic Cl- in cerebellar granule cells affects their excitability and vestibulo-ocular learning. EMBO J. 31, 1217–30.

Shaffer, P.L., Goehring, A., Shankaranarayanan, A., Gouaux, E., 2009. Structure and mechanism of a Na+-independent amino acid transporter. Science 325, 1010–4.

Silayeva, L., Deeb, T.Z., Hines, R.M., Kelley, M.R., Munoz, M.B., Lee, H.H.C., Brandon, N.J., Dunlop, J., Maguire, J., Davies, P.A., Moss, S.J., 2015. KCC2 activity is critical in limiting the onset and severity of status epilepticus. Proc. Natl. Acad. Sci. U. S. A. 112, 3523–8.

Simard, C.F., Bergeron, M.J., Frenette-Cotton, R., Carpentier, G.A., Pelchat, M.-E., Caron, L., Isenring, P., 2007. Homooligomeric and Heterooligomeric Associations between K^+-Cl^- Cotransporter Isoforms and between K^+-Cl^- and Na^+-K^+-Cl^- Cotransporters. J. Biol. Chem. 282, 18083–18093.

Sipilä, S.T., Huttu, K., Voipio, J., Kaila, K., 2006. Intrinsic bursting of immature CA3 pyramidal neurons and consequent giant depolarizing potentials are driven by a persistent Na^+ current and terminated by a slow Ca^{2+}-activated K^+ current. Eur. J. Neurosci. 23, 2330–2338.

Sivakumaran, S., Cardarelli, R.A., Maguire, J., Kelley, M.R., Silayeva, L., Morrow, D.H., Mukherjee, J., Moore, Y.E., Mather, R.J., Duggan, M.E., Brandon, N.J., Dunlop, J., Zicha, S., Moss, S.J., Deeb, T.Z., 2015. Selective inhibition of KCC2 leads to hyperexcitability and epileptiform discharges in hippocampal slices and in vivo. J. Neurosci. 35, 8291–6.

Skaggs, W.E., McNaughton, B.L., Wilson, M.A., Barnes, C.A., 1996. Theta phase precession in hippocampal neuronal populations and the compression of temporal sequences. Hippocampus 6, 149–72.

Sloviter, R.S., 1987. Decreased hippocampal inhibition and a selective loss of interneurons in experimental epilepsy. Science 235, 73–6.

Somogyi, P., Klausberger, T., 2005. Defined types of cortical interneurone structure space and spike timing in the hippocampus. J. Physiol. 562, 9–26.

Sorrells, S.F., Paredes, M.F., Cebrian-Silla, A., Sandoval, K., Qi, D., Kelley, K.W., James, D., Mayer, S., Chang, J., Auguste, K.I., Chang, E.F., Gutierrez, A.J., Kriegstein, A.R., Mathern, G.W., Oldham, M.C., Huang, E.J., Garcia-Verdugo, J.M., Yang, Z., Alvarez-Buylla, A., 2018. Human hippocampal neurogenesis drops sharply in children to undetectable levels in adults. Nature 555, 377–381.

Spigelman, I., Zhang, L., Carlen, P.L., 1992. Patch-clamp study of postnatal development of CA1 neurons in rat hippocampal slices: membrane excitability and K+ currents. J. Neurophysiol. 68, 55–69.

Spruston, N., Johnston, D., 1992. Perforated patch-clamp analysis of the passive membrane properties of three classes of hippocampal neurons. J. Neurophysiol. 67, 508–29.

Squire, L.R., 1986. Mechanisms of memory. Science 232, 1612–9.

Staley, K., Smith, R., Schaack, J., Wilcox, C., Jentsch, T.J., 1996. Alteration of GABAA Receptor Function Following Gene Transfer of the CLC-2 Chloride Channel. Neuron 17, 543–551.

Staley, K.J., Mody, I., 1992. Shunting of excitatory input to dentate gyrus granule cells by a depolarizing GABAA receptor-mediated postsynaptic conductance. J. Neurophysiol. 68, 197–212.

Staley, K.J., Proctor, W.R., 1999. Modulation of mammalian dendritic GABA(A) receptor function by the kinetics of Cl- and HCO3- transport. J. Physiol. 519 Pt 3, 693–712.

Stamboulian-Platel, S., Legendre, A., Chabrol, T., Platel, J.-C., Pernot, F., Duveau, V., Roucard, C., Baudry, M., Depaulis, A., 2016. Activation of GABAA receptors controls mesiotemporal lobe epilepsy despite changes in chloride transporters expression: In vivo and in silico approach. Exp. Neurol. 284, 11–28.

Stark, E., Eichler, R., Roux, L., Fujisawa, S., Rotstein, H.G., Buzsáki, G., 2013. Inhibition-induced theta resonance in cortical circuits. Neuron 80, 1263–76.

Stark, E., Roux, L., Eichler, R., Senzai, Y., Royer, S., Buzsáki, G., 2014. Pyramidal cell-interneuron interactions underlie hippocampal ripple oscillations. Neuron 83, 467–480.

Starremans, P.G.J.F., Kersten, F.F.J., Van Den Heuvel, L.P.W.J., Knoers, N.V.A.M., Bindels, R.J.M., 2003. Dimeric architecture of the human bumetanide-sensitive Na-K-Cl Co-transporter. J. Am. Soc. Nephrol. 14, 3039–46.

Steriade, M., 2000. Corticothalamic resonance, states of vigilance and mentation. Neuroscience 101, 243–276.

Stevens, R., Cowey, A., 1973. Effects of dorsal and ventral hippocampal lesions on spontaneous alternation, learned alternation and probability learning in rats. Brain Res. 52, 203–224.

Stödberg, T., McTague, A., Ruiz, A.J., Hirata, H., Zhen, J., Long, P., Farabella, I., Meyer, E., Kawahara, A., Vassallo, G., Stivaros, S.M., Bjursell, M.K., Stranneheim, H., Tigerschiöld, S., Persson, B., Bangash, I., Das, K., Hughes, D., Lesko, N., Lundeberg, J., Scott, R.C., Poduri, A., Scheffer, I.E., Smith, H., Gissen, P., Schorge, S., Reith, M.E.A., Topf, M., Kullmann, D.M., Harvey, R.J., Wedell, A., Kurian, M.A., 2015. Mutations in SLC12A5 in epilepsy of infancy with migrating focal seizures. Nat. Commun. 6, 8038.

Strange, B.A., Witter, M.P., Lein, E.S., Moser, E.I., 2014. Functional organization of the hippocampal longitudinal axis. Nat. Rev. Neurosci. 15, 655–669.

Strange, K., Singer, T.D., Morrison, R., Delpire, E., 2000. Dependence of KCC2 K-Cl cotransporter activity on a conserved carboxy terminus tyrosine residue. Am. J. Physiol. Physiol. 279, C860–C867.

Strüber, M., Sauer, J.-F., Jonas, P., Bartos, M., 2017. Distance-dependent inhibition facilitates focality of gamma oscillations in the dentate gyrus. Nat. Commun. 8, 758.

Sullivan, D., Csicsvari, J., Mizuseki, K., Montgomery, S., Diba, K., Buzsáki, G., 2011. Relationships between hippocampal sharp waves, ripples, and fast gamma oscillation: influence of dentate and entorhinal cortical activity. J. Neurosci. 31, 8605–16.

Sun, C., Zhang, L., Chen, G., 2013. An unexpected role of neuroligin-2 in regulating KCC2 and GABA functional switch. Mol. Brain 6, 23.

Suthana, N., Haneef, Z., Stern, J., Mukamel, R., Behnke, E., Knowlton, B., Fried, I., 2012. Memory enhancement and deep-brain stimulation of the entorhinal area. N. Engl. J. Med. 366, 502–10.

Swanson, L.W., Cowan, W.M., 1979. The connections of the septal region in the rat. J. Comp. Neurol. 186, 621–655.

Talley, E.M., Solorzano, G., Lei, Q., Kim, D., Bayliss, D.A., 2001. Cns distribution of members of the two-pore-domain (KCNK) potassium channel family. J. Neurosci. 21, 7491–505.

Tamagnini, F., Scullion, S., Brown, J.T., Randall, A.D., 2014. Low concentrations of the solvent dimethyl sulphoxide alter intrinsic excitability properties of cortical and hippocampal pyramidal cells. PLoS One 9, e92557.

Tang, X., Kim, J., Zhou, L., Wengert, E., Zhang, L., Wu, Z., Carromeu, C., Muotri, A.R., Marchetto, M.C.N., Gage, F.H., Chen, G., 2016. KCC2 rescues functional deficits in human neurons derived from patients with Rett syndrome. Proc. Natl. Acad. Sci. U. S. A. 113, 751–6.

Tauck, D.L., Nadler, J. V, 1985. Evidence of functional mossy fiber sprouting in hippocampal formation of kainic acid-treated rats. J. Neurosci. 5, 1016–22.

Thind, K.K., Yamawaki, R., Phanwar, I., Zhang, G., Wen, X., Buckmaster, P.S., 2010. Initial loss but later excess of GABAergic synapses with dentate granule cells in a rat model of temporal lobe epilepsy. J. Comp. Neurol. 518, 647–67.

Thompson, S.M., Deisz, R.A., Prince, D.A., 1988. Relative contributions of passive equilibrium and active transport to the distribution of chloride in mammalian cortical neurons. J. Neurophysiol. 60, 105–24.

Torborg, C.L., Berg, A.P., Jeffries, B.W., Bayliss, D.A., McBain, C.J., 2006. TASK-like conductances are present within hippocampal CA1 stratum oriens interneuron subpopulations. J. Neurosci. 26, 7362–7.

Tornberg, J., Voikar, V., Savilahti, H., Rauvala, H., Airaksinen, M.S., 2005. Behavioural phenotypes of hypomorphic KCC2-deficient mice. Eur. J. Neurosci. 21, 1327–1337.

Tort, A.B.L., Komorowski, R.W., Manns, J.R., Kopell, N.J., Eichenbaum, H., 2009. Theta-gamma coupling increases during the learning of item-context associations. Proc. Natl. Acad. Sci. U. S. A. 106, 20942–7.

Tort, A.B.L., Kramer, M.A., Thorn, C., Gibson, D.J., Kubota, Y., Graybiel, A.M., Kopell, N.J., 2008. Dynamic cross-frequency couplings of local field potential oscillations in rat striatum and hippocampus during performance of a T-maze task. Proc. Natl. Acad. Sci. U. S. A. 105, 20517–22.

Toyoda, I., Bower, M.R., Leyva, F., Buckmaster, P.S., 2013. Early activation of ventral hippocampus and subiculum during spontaneous seizures in a rat model of temporal lobe epilepsy. J. Neurosci. 33, 11100–15.

Toyoda, I., Fujita, S., Thamattoor, A.K., Buckmaster, P.S., 2015. Unit Activity of Hippocampal Interneurons before Spontaneous Seizures in an Animal Model of Temporal Lobe Epilepsy. J. Neurosci. 35, 6600–18.

Trevelyan, A.J., 2009. The direct relationship between inhibitory currents and local field potentials. J. Neurosci. 29, 15299–307.

Trevelyan, A.J., Schevon, C.A., 2013. How inhibition influences seizure propagation. Neuropharmacology 69, 45–54.

Treves, A., Tashiro, A., Witter, M.P., Moser, E.I., 2008. What is the mammalian dentate gyrus good for? Neuroscience 154, 1155–1172.

Tyzio, R., Allene, C., Nardou, R., Picardo, M.A., Yamamoto, S., Sivakumaran, S., Caiati, M.D., Rheims, S., Minlebaev, M., Milh, M., Ferré, P., Khazipov, R., Romette, J.-L., Lorquin, J., Cossart, R., Khalilov, I., Nehlig, A., Cherubini, E., Ben-Ari, Y., 2011. Depolarizing actions of GABA in immature neurons depend neither on ketone bodies nor on

pyruvate. J. Neurosci. 31, 34–45.

Tyzio, R., Cossart, R., Khalilov, I., Minlebaev, M., Hübner, C.A., Represa, A., Ben-Ari, Y., Khazipov, R., 2006. Maternal oxytocin triggers a transient inhibitory switch in GABA signaling in the fetal brain during delivery. Science 314, 1788–92.

Tyzio, R., Nardou, R., Ferrari, D.C., Tsintsadze, T., Shahrokhi, A., Eftekhari, S., Khalilov, I., Tsintsadze, V., Brouchoud, C., Chazal, G., Lemonnier, E., Lozovaya, N., Burnashev, N., Ben-Ari, Y., 2014. Oxytocin-mediated GABA inhibition during delivery attenuates autism pathogenesis in rodent offspring. Science 343, 675–9.

Uvarov, P., Ludwig, A., Markkanen, M., Pruunsild, P., Kaila, K., Delpire, E., Timmusk, T., Rivera, C., Airaksinen, M.S., 2007. A novel N-terminal isoform of the neuron-specific K-Cl cotransporter KCC2. J. Biol. Chem. 282, 30570–6.

Uvarov, P., Ludwig, A., Markkanen, M., Rivera, C., Airaksinen, M.S., 2006. Upregulation of the neuron-specific K+/Cl- cotransporter expression by transcription factor early growth response 4. J. Neurosci. 26, 13463–73.

Uvarov, P., Ludwig, A., Markkanen, M., Soni, S., Hübner, C.A., Rivera, C., Airaksinen, M.S., 2009. Coexpression and heteromerization of two neuronal K-Cl cotransporter isoforms in neonatal brain. J. Biol. Chem. 284, 13696–704.

Uwera, J., Nedergaard, S., Andreasen, M., 2015. A novel mechanism for the anticonvulsant effect of furosemide in rat hippocampus in vitro. Brain Res. 1625, 1–8.

Vago, D.R., Kesner, R.P., 2008. Disruption of the direct perforant path input to the CA1 subregion of the dorsal hippocampus interferes with spatial working memory and novelty detection. Behav. Brain Res. 189, 273–83.

Valero, M., Averkin, R.G., Fernandez-Lamo, I., Aguilar, J., Lopez-Pigozzi, D., Brotons-Mas, J.R., Cid, E., Tamas, G., Menendez de la Prida, L., 2017. Mechanisms for Selective Single-Cell Reactivation during Offline Sharp-Wave Ripples and Their Distortion by Fast Ripples. Neuron 94, 1234–1247.e7.

Valero, M., Cid, E., Averkin, R.G., Aguilar, J., Sanchez-Aguilera, A., Viney, T.J., Gomez-Dominguez, D., Bellistri, E., de la Prida, L.M., 2015. Determinants of different deep and superficial CA1 pyramidal cell dynamics during sharp-wave ripples. Nat. Neurosci. 18, 1281–1290.

van Strien, N.M., Cappaert, N.L.M., Witter, M.P., 2009. The anatomy of memory: an interactive overview of the parahippocampal–hippocampal network. Nat. Rev. Neurosci. 10, 272–282.

Vanderwolf, C.H., 1969. Hippocampal electrical activity and voluntary movement in the rat. Electroencephalogr. Clin. Neurophysiol. 26, 407–18.

Vargas, K.J., Terunuma, M., Tello, J.A., Pangalos, M.N., Moss, S.J., Couve, A., 2008. The availability of surface GABA B receptors is independent of gamma-aminobutyric acid but controlled by glutamate in central neurons. J. Biol. Chem. 283, 24641–8.

Viitanen, T., Ruusuvuori, E., Kaila, K., Voipio, J., 2010. The K+-Cl cotransporter KCC2 promotes GABAergic excitation in the mature rat hippocampus. J. Physiol. 588, 1527–40.

Vilen, H., Eerikäinen, S., Tornberg, J., Airaksinen, M.S., Savilahti, H., 2001. Construction of gene-targeting vectors: a rapid Mu in vitro DNA transposition-based strategy generating null, potentially hypomorphic, and conditional alleles. Transgenic Res. 10, 69–80.

Vinay, L., Jean-Xavier, C., 2008. Plasticity of spinal cord locomotor networks and contribution of cation–chloride cotransporters. Brain Res. Rev. 57, 103–110.

Wang, C., Shimizu-Okabe, C., Watanabe, K., Okabe, A., Matsuzaki, H., Ogawa, T., Mori, N., Fukuda, A., Sato, K., 2002. Developmental changes in KCC1, KCC2, and NKCC1 mRNA expressions in the rat brain. Dev. Brain Res. 139, 59–66.

Wang, W., Gong, N., Xu, T.-L., 2006. Downregulation of KCC2 following LTP contributes to EPSP–spike potentiation in rat hippocampus. Biochem. Biophys. Res. Commun. 343, 1209–1215.

Wang, Y., Xu, C., Xu, Z., Ji, C., Liang, J., Wang, Y., Chen, B., Wu, X., Gao, F., Wang, S., Guo, Y., Li, X., Luo, J., Duan, S., Chen, Z., 2017. Depolarized GABAergic Signaling in Subicular Microcircuits Mediates Generalized Seizure in Temporal Lobe Epilepsy. Neuron 95, 92–105.e5.

Warmuth, S., Zimmermann, I., Dutzler, R., 2009. X-ray Structure of the C-Terminal Domain of a Prokaryotic Cation-

Chloride Cotransporter. Structure 17, 538–546.

Watanabe, M., Fukuda, A., 2015. Development and regulation of chloride homeostasis in the central nervous system. Front. Cell. Neurosci. 9, 371.

Watanabe, M., Wake, H., Moorhouse, A.J., Nabekura, J., 2009. Clustering of neuronal K+-Cl- cotransporters in lipid rafts by tyrosine phosphorylation. J. Biol. Chem. 284, 27980–8.

Wei, W., Zhang, N., Peng, Z., Houser, C.R., Mody, I., 2003. Perisynaptic localization of delta subunit-containing GABA(A) receptors and their activation by GABA spillover in the mouse dentate gyrus. J. Neurosci. 23, 10650–61.

Weng, T.-Y., Chiu, W.-T., Liu, H.-S., Cheng, H.-C., Shen, M.-R., Mount, D.B., Chou, C.-Y., 2013. Glycosylation regulates the function and membrane localization of KCC4. Biochim. Biophys. Acta - Mol. Cell Res. 1833, 1133–1146.

Wenz, M., Hartmann, A.-M., Friauf, E., Nothwang, H.G., 2009. CIP1 is an activator of the K+–Cl− cotransporter KCC2. Biochem. Biophys. Res. Commun. 381, 388–392.

Whitlock, J.R., Heynen, A.J., Shuler, M.G., Bear, M.F., 2006. Learning induces long-term potentiation in the hippocampus. Science 313, 1093–7.

Whittington, M.., Traub, R.., Kopell, N., Ermentrout, B., Buhl, E.., 2000. Inhibition-based rhythms: experimental and mathematical observations on network dynamics. Int. J. Psychophysiol. 38, 315–336.

Williams, J.R., Sharp, J.W., Kumari, V.G., Wilson, M., Payne, J.A., 1999. The neuron-specific K-Cl cotransporter, KCC2. Antibody development and initial characterization of the protein. J. Biol. Chem. 274, 12656–64.

Wilson, M.A., McNaughton, B.L., 1994. Reactivation of hippocampal ensemble memories during sleep. Science 265, 676–9.

Winson, J., 1978. Loss of hippocampal theta rhythm results in spatial memory deficit in the rat. Science 201, 160–3.

Witter, M.P., Griffioen, A.W., Jorritsma-Byham, B., Krijnen, J.L.M., 1988. Entorhinal projections to the hippocampal CA1 region in the rat: An underestimated pathway. Neurosci. Lett. 85, 193–198.

Wittner, L., Huberfeld, G., Clémenceau, S., Erőss, L., Dezamis, E., Entz, L., Ulbert, I., Baulac, M., Freund, T.F., Maglóczky, Z., Miles, R., 2009. The epileptic human hippocampal cornu ammonis 2 region generates spontaneous interictal-like activity in vitro. Brain 132, 3032–3046.

Wittner, L., Maglóczky, Z., Borhegyi, Z., Halász, P., Tóth, S., Erőss, L., Szabó, Z., Freund, T.., 2001. Preservation of perisomatic inhibitory input of granule cells in the epileptic human dentate gyrus. Neuroscience 108, 587–600.

Woo, N.-S., Lu, J., England, R., McClellan, R., Dufour, S., Mount, D.B., Deutch, A.Y., Lovinger, D.M., Delpire, E., 2002. Hyperexcitability and epilepsy associated with disruption of the mouse neuronal-specific K-Cl cotransporter gene. Hippocampus 12, 258–268.

Woodin, M.A., Ganguly, K., Poo, M., 2003. Coincident Pre- and Postsynaptic Activity Modifies GABAergic Synapses by Postsynaptic Changes in Cl− Transporter Activity. Neuron 39, 807–820.

Worrell, G.A., Parish, L., Cranstoun, S.D., Jonas, R., Baltuch, G., Litt, B., 2004. High-frequency oscillations and seizure generation in neocortical epilepsy. Brain 127, 1496–1506.

Wright, R., Newey, S.E., Ilie, A., Wefelmeyer, W., Raimondo, J. V, Ginham, R., Mcllhinney, R.A.J., Akerman, C.J., 2017. Neuronal Chloride Regulation via KCC2 Is Modulated through a GABABReceptor Protein Complex. J. Neurosci. 37, 5447–5462.

Yamada, M.K., Nakanishi, K., Ohba, S., Nakamura, T., Ikegaya, Y., Nishiyama, N., Matsuki, N., 2002. Brain-derived neurotrophic factor promotes the maturation of GABAergic mechanisms in cultured hippocampal neurons. J. Neurosci. 22, 7580–5.

Yamamoto, J., Suh, J., Takeuchi, D., Tonegawa, S., 2014. Successful Execution of Working Memory Linked to Synchronized High-Frequency Gamma Oscillations. Cell 157, 845–857.

Yeckel, M.F., Berger, T.W., 1990. Feedforward excitation of the hippocampus by afferents from the entorhinal cortex: redefinition of the role of the trisynaptic pathway. Proc. Natl. Acad. Sci. U. S. A. 87, 5832–6.

Yeo, M., Berglund, K., Augustine, G., Liedtke, W., 2009. Novel repression of Kcc2 transcription by REST-RE-1 controls developmental switch in neuronal chloride. J. Neurosci. 29, 14652–62.

Ying, Z., Babb, T.L., Comair, Y.G., Bushey, M., Touhalisky, K., 1998. Increased densities of AMPA GluR1 subunit proteins and presynaptic mossy fiber sprouting in the fascia dentata of human hippocampal epilepsy. Brain Res. 798, 239–246.

Ylinen, A., Bragin, A., Nádasdy, Z., Jandó, G., Szabó, I., Sik, A., Buzsáki, G., 1995. Sharp wave-associated high-frequency oscillation (200 Hz) in the intact hippocampus: network and intracellular mechanisms. J. Neurosci. 15, 30–46.

Zanzouri, M., Lauritzen, I., Duprat, F., Mazzuca, M., Lesage, F., Lazdunski, M., Patel, A., 2006. Membrane potential-regulated transcription of the resting K+ conductance TASK-3 via the calcineurin pathway. J. Biol. Chem. 281, 28910–8.

Zeuthen, T., MacAulay, N., 2002. Cotransporters as molecular water pumps. Int. Rev. Cytol. 215, 259–84.

Zhao, B., Wong, A.Y.C., Murshid, A., Bowie, D., Presley, J.F., Bedford, F.K., 2008. Identification of a novel di-leucine motif mediating K+/Cl− cotransporter KCC2 constitutive endocytosis. Cell. Signal. 20, 1769–1779.

Zheng, C., Bieri, K.W., Hsiao, Y.-T., Colgin, L.L., 2016. Spatial Sequence Coding Differs during Slow and Fast Gamma Rhythms in the Hippocampus. Neuron 89, 398–408.

Zhou, H.-Y., Chen, S.-R., Byun, H.-S., Chen, H., Li, L., Han, H.-D., Lopez-Berestein, G., Sood, A.K., Pan, H.-L., 2012. N-methyl-D-aspartate receptor- and calpain-mediated proteolytic cleavage of K+-Cl- cotransporter-2 impairs spinal chloride homeostasis in neuropathic pain. J. Biol. Chem. 287, 33853–64.

Zhu, L., Lovinger, D., Delpire, E., 2005. Cortical Neurons Lacking KCC2 Expression Show Impaired Regulation of Intracellular Chloride. J. Neurophysiol. 93, 1557–1568.

Zuzarte, M., Heusser, K., Renigunta, V., Schlichthörl, G., Rinné, S., Wischmeyer, E., Daut, J., Schwappach, B., Preisig-Müller, R., 2009. Intracellular traffic of the K+ channels TASK-1 and TASK-3: role of N- and C-terminal sorting signals and interaction with 14-3-3 proteins. J. Physiol. 587, 929–52.